

UNIVERSITY OF OKLAHOMA
GRADUATE COLLEGE

SHEAR PERFORMANCE OF NON-TRADITIONAL CONCRETE

A DISSERTATION
SUBMITTED TO THE GRADUATE FACULTY
in partial fulfillment of the requirements for the
Degree of
DOCTOR OF PHILOSOPHY

By
JONATHAN T. DRURY
Norman, Oklahoma
2018

SHEAR PERFORMANCE OF NON-TRADITIONAL CONCRETES

A DISSERTATION APPROVED FOR THE
SCHOOL OF CIVIL ENGINEERING AND ENVIRONMENTAL SCIENCE

BY

Dr. Jeffery Volz, Chair

Dr. Chris Ramseyer

Dr. Royce Floyd

Dr. P. Scott Harvey

Dr. Shideh Shadravan

Acknowledgements

Dr. Jeffery Volz is my advisor, my mentor, and one of my best friends. I cannot properly express how grateful I am for all he has done for me and allowed me to do. Through his guidance and encouragement, I have grown into a better researcher, educator, engineer, and person.

I would like to express my love and gratitude to my parents, Cindy and Charles, brothers, Daniel and James, and fiancée, Alexis, for their unwavering support and love.

Special thanks to Mike Schmitz. He is the reason that quality research is completed at the Fears Lab. His knowledge and experience are invaluable.

Special thanks are also to my advisory committee members, Dr. Christopher Ramseyer, Dr. Royce Floyd, Dr. P. Scott Harvey, and Dr. Shideh Shadravan, for their wisdom, guidance, and their time to review this document.

Thanks to my amazing colleagues Dan Mayen, Dr. Cameron Murray, Rex Mclauchlin, Jake Choate, Trevor Looney, Raina Coleman, Amy McDaniel, Derek Garcia, Corey Wirkman, Austin Messerli, Kodi Wallace, Brandon Schafer, Mason Moore, Kayla Buster, Grant Phillips, Maranda Leggs, Alix Bradford, and the many others who have helped me along the way.

Last but not least, I would like to thank my sponsors MoDOT, ODOT, RECAST, SPTC, Dolese Bros. Co., and the University of Oklahoma.

TABLE OF CONTENTS

ACKNOWLEDGEMENTS	iv
LIST OF TABLES	xi
LIST OF FIGURES	xiv
ABSTRACT	xxv
1. INTRODUCTION	1
1.1. BACKGROUND	1
1.2. OBJECTIVES AND SCOPE OF WORK	2
1.3. DISSERTATION OUTLINE	3
2. LITERATURE REVIEW	5
2.1. NON-TRADITIONAL CONCRETES	5
2.1.1. CEMENT-LIMITING CONCRETE	6
2.1.2. SELF-CONSOLIDATING CONCRETE	14
2.2 FACTORS EFFECTING SHEAR BEHAVIOR	15
2.3 AGGREGATE INTERLOCK	18
REFERENCES	22
PAPER	
I. SHEAR BEHAVIOR OF CEMENT-LIMITING CONCRETE PRODUCED WITH IMPROVED PARTICLE PACKING AND FIBER REINFORCEMENT	30
ABSTRACT	30
KEYWORDS	31
INTRODUCTION	31
RESEARCH SIGNIFICANCE	34
EXPERIMENTAL PROGRAM	35

TEST BEAM DESIGN	35
CONCRETE MATERIALS	35
MIXTURE PROPORTIONS.....	38
FABRICATION AND CURING OF TEST SPECIMENS.....	43
SHEAR TEST SETUP AND PROCEDURE.....	44
TEST RESULTS AND COMPARISON	44
GENERAL BEHAVIOR (CRACKING AND FAILURE MODE).....	44
COMPARISON OF TEST RESULTS WITH SHEAR PROVISIONS OF SELECTED INTERNATIONAL CODES.....	48
COMPARISON OF TEST RESULTS WITH MCFT METHOD	49
COMPARISON OF TEST RESULTS WITH FRACTURE MECHANICS APPROACH.....	50
COMPARISON OF TEST RESULTS WITH SHEAR DATABASE	52
COMPARISON OF MATERIAL PROPERTIES AND SHEAR BEHAVIOR	54
COMPARISON OF TEST RESULTS WITH RESPONSE-2000	55
STATISTICAL DATA ANALYSIS	58
PARAMETRIC TEST	58
NON-PARAMETRIC TEST.....	59
CONCLUSIONS	60
ACKNOWLEDGEMENTS	61
NOTATION	62
REFERENCES	63
II. BEAM SHEAR BEHAVIOR OF FIBER-REINFORCED SELF-CONSOLIDATING CONCRETE	66
ABSTRACT	66

KEYWORDS	67
INTRODUCTION	67
RESEARCH SIGNIFICANCE	69
EXPERIMENTAL PROGRAM.....	69
TEST BEAM DESIGN	69
CONCRETE MATERIALS	70
MIXTURE PROPORTIONS.....	72
FABRICATION AND CURING OF TEST SPECIMENS.....	74
SHEAR TEST SETUP AND PROCEDURE.....	74
TEST RESULTS AND COMPARISON	75
GENERAL BEHAVIOR (CRACKING AND FAILURE MODE).....	75
COMPARISON OF TEST RESULTS WITH SHEAR PROVISIONA OF SELECTED INTERNATIONAL CODES.....	79
COMPARISON OF TEST RESULTS WITH MCFT METHODS	80
COMPARISON OF TEST RESULTS WITH FACRTURE MECHANICS APPROACH.....	81
COMPARISON OF TEST RESULTS WITH SHEAR DATABASE.....	83
COMPARISON OF MATERIAL PROPERTIES AND SHEAR BEHAVIOR	85
COMPARISON OF TEST RESULTS WITH RESPONSE-2000	86
STATISTICAL DATA ANALYSIS	90
PARAMETRIC TEST.....	90
NON-PARAMETRIC TEST.....	91
CONCLUSIONS	92
ACKNOWLEDGEMENTS	93

NOTATION	94
REFERENCES	95
III. AGGREGATE INTERLOCK: AN IMPROVED METHOD AND A NON-TRADITIONAL CONCRETE INVESTIGATION	98
ABSTRACT	98
KEYWORDS	98
INTRODUCTION	99
RESEARCH SIGNIFICANCE	99
PUSH-OFF TEST BACKGROUND	99
EXPERIMENTAL PROGRAM.....	101
PUSH-OFF SPECIMEN DESIGN.....	101
MATERIALS AND SPECIMENS PREPARATIONS.....	104
PUSH-OFF TEST SETUP AND PROCEDURE.....	106
TEST RESULTS AND COMPARISON	107
RESULTS OF PRE-CRACKING	107
LOAD-DISPLACEMENT RESPONSES	111
COEFFICIENTS OF FRICTION.....	114
COMPARISON OF THE PROPOSED TEST	117
CONCLUSIONS	118
ACKNOWLEDGEMENTS	120
NOTATION	120
REFERENCES	121
IV. AGGREGATE INTERLOCK AND THE EFFECT OF MICRO AND MACRO SYNTHETIC FIBERS	123

ABSTRACT	123
KEYWORDS	124
INTRODUCTION	124
RESEARCH SIGNIFICANCE	125
PUSH-OFF TEST BACKGROUND	125
EXPERIMENTAL PROGRAM.....	127
PUSH-OFF SPECIMEN DESIGN.....	127
MATERIALS AND SPECIMEN PREPARATIONS	130
PUSH-OFF TEST SETUP AND PROCEDURE	132
TEST RESULTS AND COMPARISON	134
RESULTS OF PRE-CRACKING	134
LOAD-DISPLACEMENT RESPONSES	136
COEFFICIENTS OF FRICTION.....	145
COMPARISON OF THE PROPOSED TEST	148
CONCLUSIONS	150
ACKNOWLEDGEMENTS	152
NOTATION	152
REFERENCES	153
3. SUMMARY, CONCLUSIONS, AND RECOMMENDATIONS	155
3.1 SUMMARY OF RESEARCH	155
3.2. CONCLUSIONS	155
3.2.1. SHEAR BEHAVIOR OF FIBER-REINFORCED CEMENT-LIMITING CONCRETE	155
3.2.2. SHEAR BEHAVIOR OF FR-SCC	156

3.2.3. AGGREGATE INTERLOCK OF NON-TRADITIONAL CONCRETE	158
3.2.4. INFLUENCE OF FIBER ON AGGREGATE INTERLOCK.....	159
3.2.5. CORRELATION OF AGGREGATE INTERLOCK WITH BEAM SHEAR PERFORMANCE	159
3.2.6. ASSESSMENT OF NEWLY PROPOSED PUSH-OFF TEST	160
3.3. RECOMMENDATIONS	160
APPENDICES	
A - MECHANICAL PROPERTIES OF EBC.....	163
B - BEAM SHEAR TEST DATA OF EBC	166
C - STATISTICAL DATA ANALYSIS OF EBC	173
D - MECHANICAL PROPERTIES OF FR-SCC.....	176
E - BEAM SHEAR TEST DATA OF FR-SCC	180
F - STATISTICAL DATA ANALYSIS OF FR-SCC	187
G - PUSH-OFF TEST DATA OF CC.....	190
H - PUSH-OFF DATA OF EBC	210
I - PUSH-OFF DATA OF K15	230
J - SHEAR BEAM REINFORCEMENT, INSTRUMENTATION, & TEST SETUP	243
K - PUSH-OFF INSTRUMENTATION & TEST SETUP	247
L - CEMENT DATA SHEETS	254
M - FLY ASH DATA SHEETS.....	261
N - KOMPONENT® DATA SHEETS	265
O - FIBER DATA SHEETS.....	268

LIST OF TABLES

PAPER I

TABLE 1 – CEMENTITIOUS MATERIAL PROPERTIES	36
TABLE 2 – AGGREGATE PROPERTIES	36
TABLE 3 – FIBER PROPERTIES	37
TABLE 4 – ODOT CLASS AA DESIGN AND PERFORMANCE SPECIFICATIONS	38
TABLE 5 – MIXTURE DESIGNS (PER YD ³)	39
TABLE 6 – AGGREGATE GRADATION PROPORTIONS.....	42
TABLE 7 – FRESH AND HARDENED CONCRETE PROPERTIES	43
TABLE 8 – RATIOS OF EXPERIMENTAL TO CODE-PREDICTED CAPACITY	45

PAPER II

TABLE 1 – CEMENTITIOUS MATERIAL PROPERTIES	71
TABLE 2 – AGGREGATE PROPERTIES	71
TABLE 3 – FIBER PROPERTIES	72
TABLE 4 – ODOT CLASS AA DESIGN AND PERFORMANCE SPECIFICATIONS	73
TABLE 5 – MIXTURE DESIGNS (PER YD ³)	73
TABLE 6 – FRESH AND HARDENED CONCRETE PROPERTIES	74
TABLE 7 – RATIOS OF EXPERIMENTAL TO CODE-PREDICTED CAPACITY	76

PAPER III

TABLE 1 – CEMENTITIOUS MATERIAL PROPERTIES	104
TABLE 2 – AGGREGATE PROPERTIES	104
TABLE 3 – MIXTURE DESIGNS	105
TABLE 4 – MIX CHARACTERIZATIONS	106
TABLE 5 – PRE-CRACKING MATERIAL PROPERTIES	110
TABLE 6 – PEAK AND RESIDUAL SHEAR STRENGTHS AT GIVE SLIP VALUES	112
TABLE 7 – PEAK AND RESIDUAL COEFFICIENTS OF FRICTION AT GIVEN SLIP VALUES	116
TABLE 8 – PCI MAXIMUM COEFFICIENTS OF FRICTION	116

PAPER IV

TABLE 1 – CEMENTITIOUS MATERIAL PROPERTIES	130
TABLE 2 – AGGREGATE PROPERTIES	131
TABLE 3 – FIBER PROPERTIES	131
TABLE 4 – MIXTURE DESIGNS (PER YD ³)	131
TABLE 5 – MIX CHARACTERIZATIONS	132
TABLE 6 – APPARENT TENSILE AND COMPRESSIVE STRENGTH COMPARISONS	136
TABLE 7 – PEAK AND RESIDUAL SHEAR STRENGTHS AT GIVE SLIP VALUES	140
TABLE 8 – PEAK AND RESIDUAL COEFFICIENTS OF FRICTION AT GIVEN SLIP VALUES	147

TABLE 9 – PCI MAXIMUM COEFFICIENTS OF FRICTION	147
APPENDICES	
A1 – SPLITTING TENSILE STRENGTH OF EBC	165
A2 – FLEXURAL STRENGTH OF EBC.....	165
B1 – ULTIMATE SHEAR STRENGTH DATA	172
C1 – P-VALUES FOR STATISTICAL TESTS	175
D1 – SPLITTING TENSILE STRENGTH OF FR-SCC	179
D2 – FLEXURAL STRENGTH OF FR-SCC.....	179
E1 – ULTIMATE SHEAR STRENGTH DATA	186
F1 – P-VALUES FOR STATISTICAL TESTS.....	189
G1 – PRE-CRACKING DATA OF CC MIXTURES.....	191
G2 – PUSH-OFF TEST RESULTS OF CC MIXTURES	198
H1 – PRE-CRACKING DATA OF EBC MIXTURES	211
H2 – PUSH-OFF TEST RESULTS OF EBC MIXTURES	217
I1 – PRE-CRACKING DATA OF K15 MIXTURES.....	231
I2 – PUSH-OFF TEST RESULTS OF K15 MIXTURES.....	234

LIST OF FIGURES

FIGURE 2.1 – 0.45 POWER PLOT EXAMPLE.....	8
FIGURE 2.2 – IDEAL “HAYSTACK” GRADATION (INDIVIDUAL PERCENT RETAINED).....	9
FIGURE 2.3 – INDIVIDUAL PERCENT RETAINED WITH “8 TO 18” BAND ..	10
FIGURE 2.4 – AIR FORCE AGGREGATE PROPORTIONING GUIDE (SHILSTONE CHART)	12
FIGURE 2.5 – AGGREGATE INTERLOCK [11].....	18
FIGURE 2.6 – INTERNAL REINFORCEMENT METHOD [12]	19
FIGURE 2.7 – EXTERNAL REINFORCEMENT METHOD [13]	20
PAPER I	
FIGURE 1 - LOAD PATTERN, REBAR DETAIL, CROSS SECTIONS AND LOCATIONS OF INSTRUMENTATION	35
FIGURE 2 – 0.45 POWER PLOT.....	40
FIGURE 3 – INDIVIDUAL PERCENT RETAINED CHART.....	41
FIGURE 4 – SHILSTONE CHART	42
FIGURE 5 – CRACK PATTERNS OF BEAMS UPON SHEAR FAILURE.....	46
FIGURE 6 – CONTROL BEAM LOAD VS DEFLECTION PLOTS	47
FIGURE 7 – EBC1 BEAM LOAD VS DEFLECTION PLOTS	48
FIGURE 8 – EBC2 BEAM LOAD VS DEFLECTION PLOTS	48
FIGURE 9 – RATIOS OF EXPERIMENTAL TO MCFT PREDICTED CAPACITY	50

FIGURE 10 – RATIOS OF EXPERIMENTAL TO FRACTURE MECHANICS PREDICTED CAPACITY	52
FIGURE 11 – NORMALIZED SHEAR STRENGTH VS. LONGITUDINAL REINFORCEMENT RATIO	53
FIGURE 12 – NORMALIZED SHEAR STRENGTH VS. DEPTH	53
FIGURE 13 – NORMALIZED SHEAR STRENGTH VS. SHEAR SPAN TO DEPTH RATIO	54
FIGURE 14 – RATIOS OF NORMALIZED STRENGTH OF EBC TO CC	55
FIGURE 15 – RESPONSE-2000 COMPARISON TO CC EXPERIMENTAL DATA	56
FIGURE 16 – RESPONSE 2000 COMPARISON TO EBC1 EXPERIMENTAL DATA	57
FIGURE 17 – RESPONSE-2000 COMPARISON TO EBC2 EXPERIMENTAL DATA	57
PAPER II	
FIGURE 1 - LOAD PATTERN, REBAR DETAIL, CROSS SECTIONS AND LOCATIONS OF INSTRUMENTATION	70
FIGURE 2 - CRACK PATTERNS OF BEAMS UPON SHEAR FAILURE.....	77
FIGURE 3 - CONTROL BEAM LOAD VS DEFLECTION PLOTS.....	78
FIGURE 4 - K-10 BEAM LOAD VS DEFLECTION PLOTS	78
FIGURE 5 - K-15 BEAM LOAD VS. DEFLECTION PLOTS	79
FIGURE 6 - RATIOS OF EXPERIMENTAL TO MCFT PREDICTED CAPACITY	81

FIGURE 7 - RATIOS OF EXPERIMENTAL TO FRACTURE MECHANICS PREDICTED CAPACITY	82
FIGURE 8 - NORMALIZED SHEAR STRENGTH VS. LONGITUDINAL REINFORCEMENT RATIO	84
FIGURE 9 - NORMALIZED SHEAR STRENGTH VS. DEPTH.....	84
FIGURE 10 - NORMALIZED SHEAR STRENGTH VS. SHEAR SPAN TO DEPTH RATIO	85
FIGURE 11 - RATIOS OF NORMALIZED STRENGTH OF EBC TO CC.....	86
FIGURE 12 - RESPONSE 2000 COMPARISON TO CC EXPERIMENTAL DATA	88
FIGURE 13 - RESPONSE 2000 COMPARISON TO K-10 EXPERIMENTAL DATA	88
FIGURE 14 - RESPONSE 2000 COMPARISON TO K-15 EXPERIMENTAL DATA	89
PAPER III	
FIGURE 1 - REBAR DETAIL FOR PUSH-OFF SPECIMENS.....	102
FIGURE 2 - EXTERNAL STEEL REINFORCEMENT RODS AND PLATES....	103
FIGURE 3 - LOAD PATH DIAGRAM AND INSTRUMENTATION LAYOUT	103
FIGURE 4 - TYPICAL PRE-CRACK FAILURE PLANE FOR CC SPECIMENS	108
FIGURE 5 - TYPICAL PRE-CRACK FAILURE PLANE FOR EBC SPECIMENS	108

FIGURE 6 - TYPICAL PRE-CRACK FAILURE PLANE FOR K15 SPECIMENS	109
FIGURE 7 - RELATIONSHIP BETWEEN TENSILE STRENGTH AND CEMENTITIOUS CONTENT	110
FIGURE 8 - SHEAR STRESS VS. CRACK SLIP	112
FIGURE 9 - NORMAL STRESS VS. CRACK SLIP	113
FIGURE 10 - CLACK SLIP VS. CRACK OPENING	114
FIGURE 11 - RATIO OF SHEAR STRESS TO NORMAL STRESS VS. CRACK SLIP	115
FIGURE 12 - RATIO OF SHEAR STRESS TO NORMAL STRESS V.S CRACK OPENING	115
FIGURE 13 - COMPARISON TO HISTORIC EXTERNALLY REINFORCED PUSH-OFF TESTING	117
FIGURE 14 - COMPARISON TO HISTORIC INTERNALLY REINFORCED PUSH-OFF TESTING	118
PAPER IV	
FIGURE 1 - REBAR DETAIL FOR PUSH-OFF SPECIMENS	128
FIGURE 2 EXTERNAL STEEL REINFORCEMENT RODS AND PLATES	129
FIGURE 3 - LOAD PATH DIAGRAM AND INSTRUMENTATION LAYOUT	129
FIGURE 4 - SHEAR STRESS VERSUS CRACK SLIP FOR CC BASED MIXTURES	137
FIGURE 5 - SHEAR STRESS VERSUS CRACK SLIP FOR EBC BASED MIXTURES	138

FIGURE 6 - SHEAR STRESS VERSUS CRACK SLIP FOR K15 BASED MIXTURES.....	139
FIGURE 7 - SHEAR STRESS VERSUS CRACK SLIP FOR CONCRETE MIXTURES WITH AND WITHOUT MACRO-FIBERS	139
FIGURE 8 - NORMAL STRESS VERSUS CRACK SLIP FOR CC BASED MIXTURES.....	141
FIGURE 9 - NORMAL STRESS VERSUS CRACK SLIP FOR EBC BASED MIXTURES.....	141
FIGURE 10 - NORMAL STRESS VERSUSU CRACK SLIP FOR K15 BASED MIXTURES.....	142
FIGURE 11 - CRACK SLIP VERSUS CRACK OPENING FOR CC BASED MIXTURES.....	143
FIGURE 12 - CRACK SLIP VERSUS CRACK OPENING FOR EBC BASED MIXTURES.....	143
FIGURE 13 - CRACK SLIP VERSUS CRACK OPENING FOR K15 BASED MIXTURES.....	144
FIGURE 14 - RATIO OF SHEAR TO NORMAL STRESS VERSUS CRACK SLIP FOR CC BASED MIXTURES	145
FIGURE 15 - RATIO OF SHEAR TO NORMAL STRESS VERSUS CRACK SLIP FOR EBC BASED MIXTURES	146
FIGURE 16 - RATIO OF SHEAR TO NORMAL STRESS VERSUS CRACK SLIP FOR K15 BASED MIXTURES.....	146

FIGURE 17 - COMPARISON TO HISTORIC EXTERNALLY REINFORCED PUSH-OFF TESTING	149
FIGURE 18 - COMPARISON TO HISTORIC INTERNALLY REINFORCED PUSH-OFF TESTING	150
APPENDICIES	
A1 - DEVELOPMENT OF COMPRESSIVE STRENGTH OF CC AND EBC	164
B1 - CONTROL BEAM LOAD VS DEFLECTION PLOTS.....	167
B2 - EBC1 BEAM LOAD VS DEFLECTOIN PLOTS.....	168
B3 - EBC2 BEAM LOAD VS DEFLECTION PLOTS.....	168
B4 - CC-1 SHEAR FAILURE	169
B5 - CC-2 SHEAR FAILURE	169
B6 - CC-3 SHEAR FAILURE	169
B7 - EBC1-1 SHEAR FAILURE.....	170
B8 - EBC1-2 SHEAR FAILURE.....	170
B9 - EBC1-3 SHEAR FAILURE.....	170
B10 - EBC2-1 SHEAR FAILURE.....	171
B11 - EBC2-2 SHEAR FAILURE.....	171
B12 - EBC2-3 SHEAR FAILURE.....	171
D1 - DEVELOPMENT OF COMPRESSIVE STRENGTH OF CC	177
D2 - DEVELOPMENT OF COMPRESSIVE STRENGTH OF K10.....	178
D3 - DEVELOPMENT OF COMPRESSIVE STRENGTH OF K15.....	178
E1 - CONTROL BEAM LOAD VS DEFLECTION PLOTS.....	181
E2 - K10 BEAM LOAD VS DEFLECTOIN PLOTS.....	182

E3 - K15 BEAM LOAD VS DEFLECTION PLOTS	182
E4 - CC-1 SHEAR FAILURE.....	183
E5 - CC-2 SHEAR FAILURE.....	183
E6 - CC-3 SHEAR FAILURE.....	183
E7 - 4-K10 SHEAR FAILURE	184
E8 - 5-K10 SHEAR FAILURE	184
E9 - 6-K10 SHEAR FAILURE	184
E10 - 4-K15 SHEAR FAILURE	185
E11 - 5-K15 SHEAR FAILURE	185
E12 - 6-K15 SHEAR FAILURE	185
G1 - TOP VIEW OF PRE-CRACKED CC-1	192
G2 - SIDE VIEW OF PRE-CRACKED CC-1	192
G3 - TOP VIEW OF PRE-CRACKED CC-2	193
G4 - SIDE VIEW OF PRE-CRACKED CC-2.....	193
G5 - TOP VIEW OF PRE-CRACKED CC-3	194
G6 - SIDE VIEW OF PRE-CRACKED CC-3	194
G7 - TOP VIEW OF PRE-CRACKED CC1-1	195
G8 - SIDE VIEW OF PRE-CRACKED CC1-1	195
G9 - TOP VIEW OF PRE-CRACKED CC1-2	196
G10 - SIDE VIEW OF PRE-CRACKED CC1-2.....	196
G11 - TOP VIEW OF PRE-CRACKED CC1-3	197
G12 - SIDE VIEW OF PRE-CRACKED CC1-3	197
G13 - SHEAR STRESS VERSUS SLIP FOR CC	199

G14 - SHEAR STRESS VERSUS SLIP FOR CC1	199
G15 - SHEAR STRESS VERSUS SLIP FOR CC2	200
G16 - RATIO VERSUS SLIP FOR CC	200
G17 - RATIO VERSUS SLIP FOR CC1	201
G18 - RATIO VERSUS SLIP FOR CC2	201
G19 - TOP VIEW OF FAILED CC-1	202
G20 - SIDE VIEW OF FAILED CC-1	202
G21 - TOP VIEW OF FAILED CC-3	203
G22 - SIDE VIEW OF FAILED CC-3	203
G23 - TOP VIEW OF FAILED CC1-1	204
G24 - SIDE VIEW OF FAILED CC1-1	204
G25 - TOP VIEW OF FAILED CC1-2	205
G26 - SIDE VIEW OF FAILED CC1-2	205
G27 - TOP VIEW OF FAILED CC1-3	206
G28 - SIDE VIEW OF FAILED CC1-3	206
G29 - TOP VIEW OF FAILED CC2-1	207
G30 - SIDE VIEW OF FAILED CC2-1	207
G31 - TOP VIEW OF FAILED CC2-2	208
G32 - SIDE VIEW OF FAILED CC2-2	208
G33 - TOP VIEW OF FAILED CC2-3	209
G34 - SIDE VIEW OF FAILED CC2-3	209
H1 - TOP VIEW OF PRE-CRACKED EBC-1	212
H2 - SIDE VIEW OF PRE-CRACKED EBC-1	212

H3 - TOP VIEW OF PRE-CRACKED EBC-2.....	213
H4 - SIDE VIEW OF PRE-CRACKED EBC-2.....	213
H5 - TOP VIEW OF PRE-CRACKED EBC-3.....	214
H6 - SIDE VIEW OF PRE-CRACKED EBC-3.....	214
H7 - TOP VIEW OF PRE-CRACKED EBC1-1	215
H8 - SIDE VIEW OF PRE-CRACKED EBC1-1.....	215
H9 - TOP VIEW OF PRE-CRACKED EBC1-3	216
H10 - SIDE VIEW OF PRE-CRACKED EBC1-3.....	216
H11 - SHEAR STRESS VERSUS SLIP FOR EBC	218
H12 - SHEAR STRESS VERSUS SLIP FOR EBC1	218
H13 - SHEAR STRESS VERSUS SLIP FOR EBC2	219
H14 - RATIO VERSUS SLIP FOR EBC	219
H15 - RATIO VERSUS SLIP FOR EBC1	220
H16 - RATIO VERSUS SLIP FOR EBC2	220
H17 - TOP VIEW OF FAILED EBC-1	221
H18 - SIDE VIEW OF FAILED EBC-1	221
H19 - TOP VIEW OF FAILED EBC-2	222
H20 - SIDE VIEW OF FAILED EBC-2	222
H21 - TOP VIEW OF FAILED EBC-3	223
H22 - SIDE VIEW OF FAILED EBC-3	223
H23 - TOP VIEW OF FAILED EBC1-1	224
H24 - SIDE VIEW OF FAILED EBC1-1	224
H25 - TOP VIEW OF FAILED EBC1-2	225

H26 - SIDE VIEW OF FAILED EBC1-2	225
H27 - TOP VIEW OF FAILED EBC1-3	226
H28 - SIDE VIEW OF FAILED EBC1-3	226
H29 - TOP VIEW OF FAILED EBC2-1	227
H30 - SIDE VIEW OF FAILED EBC2-1	227
H31 - TOP VIEW OF FAILED EBC2-2	228
H32 - SIDE VIEW OF FAILED EBC2-2	228
H33 - TOP VIEW OF FAILED EBC2-3	229
H34 - SIDE VIEW OF FAILED CC2-3.....	229
I1 - TOP VIEW OF PRE-CRACKED K15-2	232
I2 - SIDE VIEW OF PRE-CRACKED K15-2	232
I3 - TOP VIEW OF PRE-CRACKED K15-3	233
I4 - SIDE VIEW OF PRE-CRACKED K15-3	233
I5 - SHEAR STRESS VERSUS SLIP FOR K15	234
I6 - SHEAR STRESS VERSUS SLIP FOR K15F.....	235
I7 - RATIO VERSUS SLIP FOR K15	235
I8 - RATIO VERSUS SLIP FOR K15F.....	236
I9 - TOP VIEW OF FAILED K15-1	236
I10 - SIDE VIEW OF FAILED K15-1.....	237
I11 - TOP VIEW OF FAILED K15-2	237
I12 - SIDE VIEW OF FAILED K15-2.....	238
I13 - TOP VIEW OF FAILED K15-3	238
I14 - SIDE VIEW OF FAILED K15-3.....	239

I15 - TOP VIEW OF FAILED K15F-1	239
I16 - SIDE VIEW OF FAILED K15F-1	240
I17 - TOP VIEW OF FAILED K15F-2.....	240
I18 - SIDE VIEW OF FAILED K15F-2	241
I19 - TOP VIEW OF FAILED K15F-3.....	241
I20 - SIDE VIEW OF FAILED K15F-3	242
J1 - COMPLETED REBAR CAGES.....	244
J2 - COMPLETED REBAR CAGE.....	244
J3 - STRAIN GUAGE ADHERED TO LONGITUDINAL REINFORCEMENT..	245
J4 - COMPLETED STRAIN GAUGE INSTALLATION.....	245
J5 - WIRE POTENTIOMETER SETUP.....	246
J6 - SIMPLY SUPPORTED THIRD-POINT BEAM SETUP	246
K1 - NEOPRENE BASE PADS AND WEDGE FOR PRE-CRACKING	248
K2 - NEOPRENE BASE PADS AND WEDGE FOR PRE-CRACKING	248
K3 - FRONT VIEW OF PRE-CRACKING SETUP	249
K4 - PRE-CRACKING SETUP	249
K5 - FIRST STEP IN ASSEMBLING EXTERNAL REINFORCEMENT	250
K6 - SECOND STEP IN ASSEMBLING EXTERNAL REINFOCEMENT.....	250
K7 - HAND TIGHTENING EXTERNAL REINFORCING NUTS	251
K8 - PRE-STRESSING THE SPECIMEN WITH 200 TO 300 PSI.....	251
K9 - CENTERING SPECIMEN AND ATTACHING INSTRUMENTATION	252
K10 - PUSH-OFF TEST SETUP AND INSTRUMENTATION	253

Abstract

Concrete is the second most consumed material in the world, second only to water. Concrete has been around in different forms for centuries, and science and technology continually push the previously believed limits. Two such types of concrete are self-consolidating concrete (SCC) and cement-limiting concrete. While each is vastly different from the other, they present similar problems to designers and engineers. Practitioners have implemented new technologies such as fiber reinforcement to combat issues with these concretes, but the overall behavior and internal mechanism of these concretes are not thoroughly understood. This study investigated the shear behavior of seven different concrete types: conventional concrete with micro-fibers, conventional concrete with micro-fibers and macro-fibers, cement-limiting concrete, cement-limiting concrete with micro-fibers, cement-limiting concrete with micro-fibers and macro-fibers, SCC, SCC with macro-fibers, and compared their behavior to the behavior of conventional concrete. Additionally, a newly proposed push-off test method was developed, investigated, and compared to historic methods.

The experimental programs consisted of 15 full-scale shear beams without shear reinforcement in the test regions (3 with conventional concrete, 6 with cement-limiting concrete, and 6 with SCC), 24 push-off specimens (3 for each of the eight concrete mixtures investigated), and many small-scale specimens to capture the fresh and hardened properties of the concrete mixtures. The shear beams were tested under a simply supported four-point loading condition.

Results of this study showed that fiber-reinforced concrete has more variable performance, but that fiber reinforcement can mitigate the negative performance aspects

of SCC and cement-limiting concrete. It was shown that micro-fibers amplified the cohesion performance of existing concrete matrixes, but that macro-fiber tend to govern the performance of a concrete mixture. It was shown than that the optimized gradation of the cement-limiting concrete provided the highest aggregate interlock, but that aggregate interlock is not the best predictor of shear transfer performance between two concrete surfaces. Lastly, this study showed that the proposed push-off test is not only an acceptable method for analyzing aggregate interlock, but it is an improvement due to the ability to obtain more data from it, improved quality control, simplified analysis, and repeatability of the outcomes.

1. INTRODUCTION

1.1. BACKGROUND

Concrete is the second most consumed material in the world, second only to water. Concrete has been around in different forms for centuries, and science and technology continually push the previously believed limits. Two such types of concrete are self-consolidating concrete (SCC) and cement-limiting concrete. While each is vastly different from the other, they present similar problems to designers and engineers. Practitioners have implemented new technologies such as fiber reinforcement to combat issues with these concretes, but the overall behavior and internal mechanics of these concretes are not thoroughly understood. The studies described in the following papers intended to investigate the shear behavior of seven different concrete types: conventional concrete with micro-fibers, conventional concrete with micro-fibers and macro-fibers, cement-limiting concrete, cement limiting concrete with micro-fibers, cement-limiting concrete with micro-fibers and macro-fibers, SCC, SCC with macro-fibers, and compared their behavior to the behavior of conventional concrete. Additionally, a newly proposed push-off test method will be investigated and compared to historic methods.

Recent trends in the construction industry have led the way for faster, cheaper, and “greener” practices. Towards this end, SCC was developed to improve construction times and reduce overall costs. SCC is a highly workable concrete that can flow under its own weight without segregation, and thus it reduces construction times and labor cost. SCC has many advantages when compared to conventional concrete: decreased labor and equipment costs during concrete placement; improved consolidation potential;

increased production rates of both cast-in-place and precast elements; and improved finish and appearance of concrete surfaces. However, SCC tends to have detrimental effects associated with it such as increased creep and shrinkage, potential decreased bond strength, and potential decreased shear strength.

Focusing more on needing cheaper⁵ and “greener” practices, cement-limiting concrete is being developed to reduce the cost and reduce the carbon footprint of concrete. Cement-limiting concrete is made primarily in two ways: replacing cement content with supplementary cementitious material, and decreasing the overall cementitious content in a concrete mixture. While decreasing the cementitious content in concrete makes sense financially and in regard to making concrete “greener”, it causes two major problems: decreased workability leading to slower construction times and poorer finishes; and decreased cohesion in the matrix leading to reduced tensile and flexural strengths.

1.2. OBJECTIVES AND SCOPE OF WORK

There are three main objectives of this research: evaluate the shear and aggregate interlock performances of two non-traditional concretes – SCC and cement-limiting concrete – and determine if there is a correlation between these two engineering properties and evaluate the effectiveness and applicability of a newly proposed test method for push-off testing. The SCC test program included shear beams and push-off specimens constructed with an SCC mix design that used macro synthetic fibers and an expansive cement material called Komponent®. The SCC was originally designed for use as a repair material for bridge elements. The cement-limiting test program included shear beams and push-off specimens constructed with an improved

particle packing and fiber-reinforced mix. The aggregate gradation was optimized by adding an intermediate material to the commonly used limestone and sand aggregates in Oklahoma and was optimized using three different methods proposed for aggregate optimization.

The following scope of work was implemented in an effort to reach these goals:

1. Review applicable literature;
2. Develop a research plan;
3. Develop and characterize applicable mixture designs;
4. Design, construct, and test full-scale beam shear specimens;
5. Compare beam shear results with design standards, shear database, and standard design methods;
6. Develop, design, construct, and test push-off specimens;
7. Compare push-off test results with design standards and past research;
8. Evaluate correlation between push-off data and shear strength;
9. Summarize findings and develop conclusions and recommendations; and
10. Prepare this dissertation in order to document the information obtained during this study.

1.3. DISSERTATION OUTLINE

This dissertation includes three parts along with appendices. The first part gives a brief introduction to the subject area and explains the need for the current research study. The first part also presents the objectives and scope of work of the study, as well as a detailed literature review to establish the state-of-the-art on the proposed topic. The second part presents four manuscripts submitted for journal paper publication

discussing the beam shear and aggregate interlock performance of SCC and cement-limiting concrete. The third part summarizes the findings and conclusions of this study and proposes future research. The appendices include the detailed test data from the research study.

2. LITERATURE REVIEW

The following section serves to supplement the literature reviews covered in each of the four manuscripts. The four concepts outlined in more detail are a review of two non-traditional concretes – self-consolidating concrete (SCC) and cement-limiting concrete – a review of the factors effecting shear behavior of concrete, and a review of aggregate interlock. Along with the expanded literature reviews, a list of all references from this literature review and for the manuscripts is provided at the end of this section.

2.1. NON-TRADITIONAL CONCRETES

Concrete is a non-homogenous composite material consisting of two basic parts: the aggregate and the cement paste. The combination of it being both a composite material and non-homogenous makes understanding it in a scientific, or “basic principles” manner extremely difficult, if not impossible. This is where engineering plays an important role. Engineers must use experimental data to develop understanding of materials. This method works well if the material in question conforms to some standards. When a material falls outside these standards, the rules may not apply. This is the basic problem that most concrete researchers wrestle with. If a researcher develops a new concrete, they must either fully classify its behavior in all plausible scenarios, or assure that it behaves in a manner such that the current design and analysis methods can be applied.

It is important to note that the cement paste and the aggregate each play vital roles in the behavior of concrete. The aggregate serves the role of a rigid filler material, while the paste serves the role of bonding the system together. It is the paste that allows the system to resist tension forces. It is because of this ability to resist not only

compression forces that concrete can be used in so many applications. However, cement also plays two major negative roles in concrete. Cement production produces many unwanted emissions and is responsible for much of the cost of the concrete. For every ton of cement produced, nearly one ton of carbon dioxide (CO₂) is also produced [1]. To limit the effect of concrete on the environment, researchers have been attempting to limit the cement content in concrete, and there are many approaches.

2.1.1. Cement-Limiting Concrete. Cement-limiting concrete is designed to reduce the financial and environmental impact of concrete. The cement content of concrete can be reduced in two ways: reducing the overall cementitious material in a concrete mix and using supplementary cementitious material to replace some of the cement.

2.1.1.1. Aggregate Optimization. The first method to reduce the amount of cement in a concrete mixture is to limit the void space between the aggregate particles, and this is referred to as aggregate optimization. An aggregate gradation is considered optimized when its particle distribution is manipulated in a way that minimizes the void spaces present in a given volume. A common phrase to describe that state of minimized voids is the maximum packing density. Aggregate optimization is achieved by blending multiple aggregate sources, and considering the combined gradation of all aggregate particles present. As aggregate sources are not uniform in shape, size, distribution, etc., determining the portion of each source that yields the optimized gradation is a difficult task. Many methods have been proposed for determining the optimized aggregate blend.

2.1.1.1.1. 0.45 Power Maximum Density Curve. The 0.45 power curve is a method commonly used to assess asphalt aggregate gradations [2, 3]. It is a visual method that plots the total percentage of aggregate passing each sieve size on the

vertical axis paired with the opening size of that sieve raised to the power of 0.45 on the horizontal axis. Once the data is plotted, an optimum line, or “maximum density line” is drawn from the origin to the intersection of the 100 percent passing line and the first sieve to retain aggregate. Straight lines are then drawn from the origin to the intersection of the 100 percent passing line and one sieve size larger and one sieve size smaller than the first sieve to retain aggregate.

James M. Shilstone is credited with promoting its usage for concrete aggregate gradations, and he proposed that the optimum gradation should follow the optimum line and remain inside the envelope drawn until the #16 sieve, at which point the curve would drop below the envelope. Figure 2.1 is an example of a recycled concrete aggregate (RCA) gradation plotted and assessed by the 0.45 power method. The coarse portion of the curve strays marginally from the optimum line. Also, there are too many fines in the gradation, as can be seen by the gradation curve never getting under the optimum line for sieves below the #16.

To determine the optimum curve for this method, the equation 2-1 was developed [3]:

$$\text{Eqn. 2-1} \quad P = \left(\frac{d}{D}\right)^n$$

P = amount of material finer than size “d”

d = size of the particle group in question

D = largest particle size

n = exponent governing the distribution of sizes

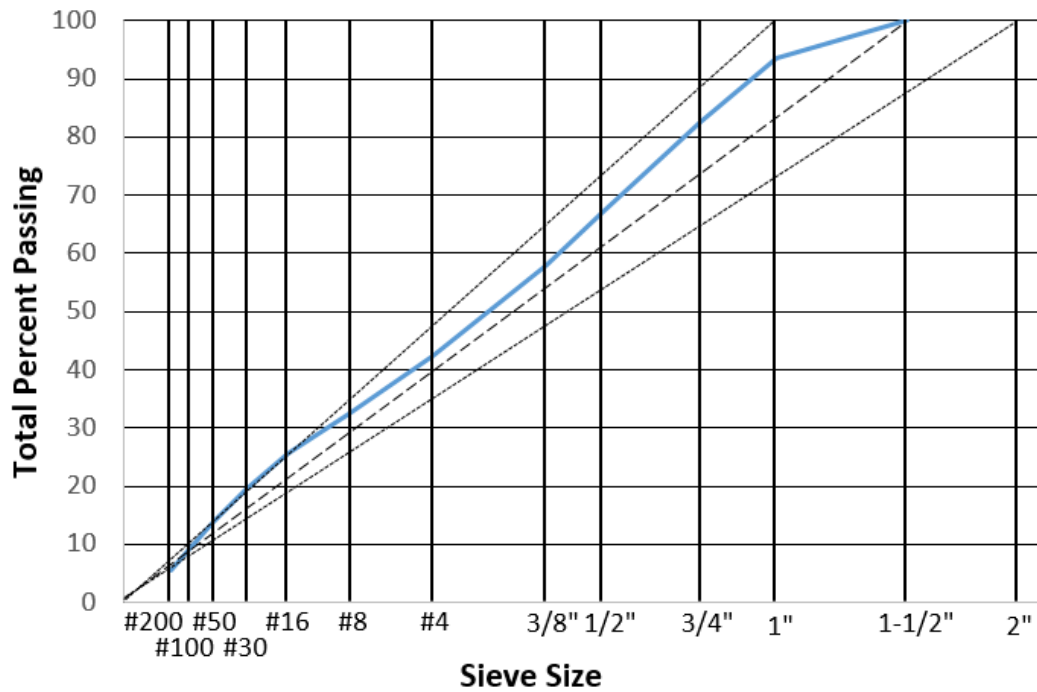


Figure 2.1 – 0.45 Power Plot Example

Equation 2-1 applies for any power factor deemed to govern the optimum distribution of sizes. To apply the equation to the 0.45 power maximum density curve, set the variable “n” equal to 0.45. To use this method, the user can either start with the equation or chart for desired and acceptable values for total percent passing for each sieve. From there, they would need to run a sieve analysis for a combined gradation, and attempt to minimize the variance between the desired curve and the actual curve by adding new, specific sized, aggregate portions.

2.1.1.1.2. Individual Percent Retained. Shilstone and Shilstone Jr. advocated for the evaluation of the gradation on the basis of volume rather than the previously traditional method basis of weight [4]. This is the same approach as presented in the above method. However, in this method, the gradation is presented in terms of the

individual percent retained on each sieve. When analyzed in this method, the combined aggregate should follow the desired “haystack” shape, as shown in Figure 2.2 [5].

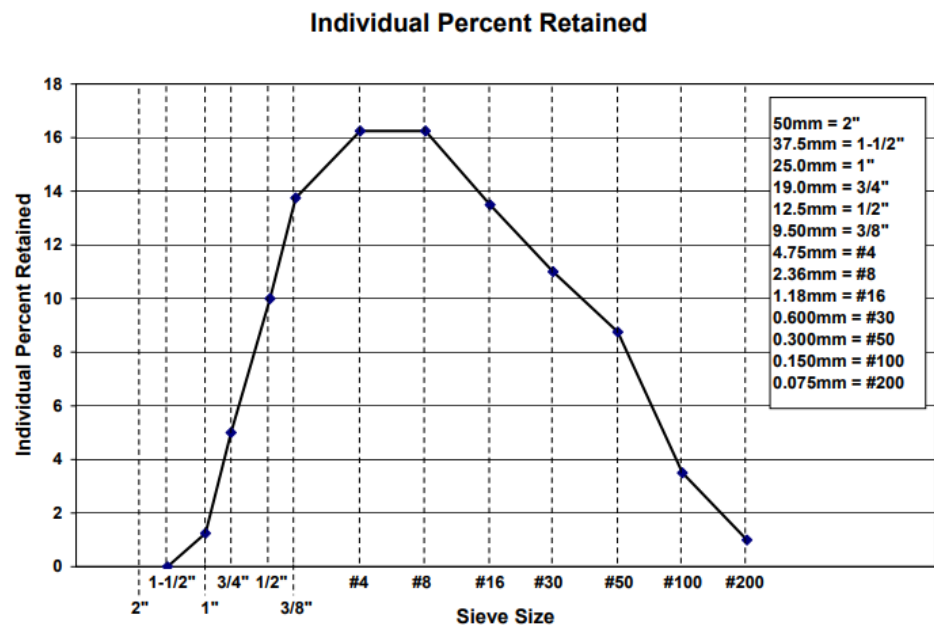


Figure 2.2 – Ideal “haystack” gradation (Individual Percent Retained)

To assess the acceptability of an aggregate gradation and force the gradation into the desired “haystack” shape, an “8 to 18” band was developed. The idea behind the band is to keep the individual percent retained between 8 and 18 percent for the sieves between the No. 30 sieve and one sieve size below the nominal maximum size, and to keep all individual percent retained values below 18 percent. The band is defined with 8 points that are dependent on the nominal maximum size for the aggregate. An example of an aggregate plotted with its “8 to 18” band is shown in Figure 2.3.

This method is possibly easier for a user to use to locate the problem areas within an aggregate gradation. It is obvious if an individual sieve size has too much or too little material if the curve passes outside the bounds of the “8 to 18” band. Research has shown that it is important that there are no major peaks or valleys between the 3/8”

sieve and the lowest specified sieve size. If there are points slightly outside the bounds of the “8 to 18” band, but the curve has a gradual trend, the gradation may be adequate [2].

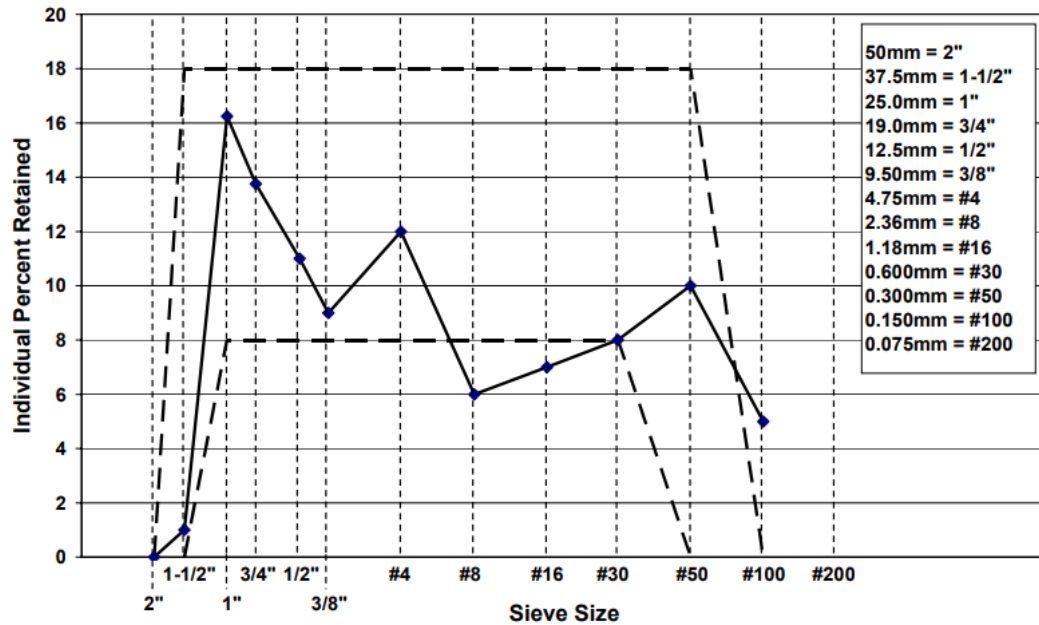


Figure 2.3 – Individual Percent Retained with “8 to 18” Band

2.1.1.1.3. Shilstone Chart. Shilstone and Shilstone Jr. developed this method which again is a visual method of characterizing the quality of the aggregate gradation [4]. This method differs from the previous methods in that it attempts to determine the workability of a concrete mix. It does so by recognizing that cement present in the concrete mixture affects the workability, and accounts for it. The first factor, the coarseness factor, is calculated by using the following equation.

$$\text{Eqn. 2-2} \quad CF = \frac{Q}{R} \times 100$$

CF = coarseness factor

Q = cumulative percent of the material retained on the 3/8" sieve

R = cumulative percent of the material retained on the No. 8 sieve

The second factor needed to assess the quality of the aggregate was the workability factor. An original equation was published in the 1987 report. However, the equation was improved over further investigation by the researchers, and in 1997 the updated version was set to be calculated by equation 2-3 [6]. The updated equation uses the original factor and adds to it a variable accounting for the cement present in the system. The updated equation is presented below.

$$\text{Eqn. 2-3} \quad WF = W + \left(\frac{2.5(C-564)}{94} \right)$$

W = cumulative percent passing the No. 8 sieve

C = cementitious material content of the mix (lb/yd³)

The 94 in the above equation represents the weight of a standard sack of cement. The 564 represents the weight of cement in the defined standard mix which uses six sacks of cement per cubic yard. Such a mix is commonly referred to as a 6-sack mix. The 2.5 factor comes from the common volumetric relationship between a sack of cement and the percent of the aggregate in the absolute volume of the mix.

After calculating the coarseness factor and the workability factor, a point can be plotted on the Shilstone chart that the authors developed. The chart has coarseness factors along the x axis in descending order and ranging from 100 to 0, and the workability factors along the y axis in ascending order and ranging from 20 to 45. The plot area is divided up into 5 major zones. Figure 2.4 is a representative Shilstone chart prepared by the Air Force [2].

The zones are typically labeled by roman numerals and defined as follows:

I – Coarse Gap Graded, II – Well Graded (1-1/2” to 3/4”), III - Well Graded (Minus 3/4”) or Excessive Intermediate Sizes, IV – Sandy, V – Rocky. Zone II is desired zone

for most concrete application. By using this method, a concrete mix designer can evaluate the overall workability of their proposed mix, and parametrically re-design their mix to achieve the desired workability, with only knowing the amount of cement present in the system and the combined gradation of the aggregate.

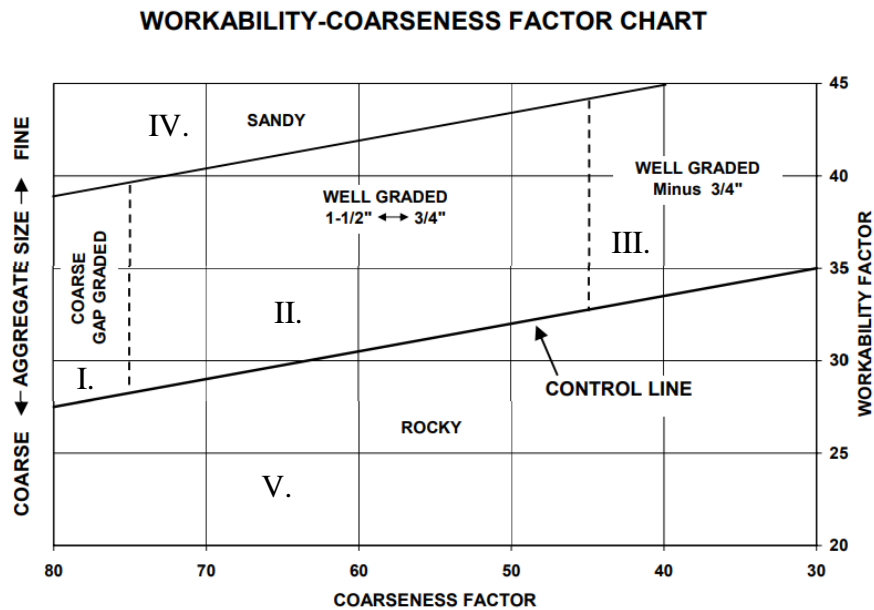


Figure 2.4 – Air Force Aggregate Proportioning Guide (Shilstone Chart)

2.1.1.2. Cement Replacement. The second method of limiting the cement in a given concrete mixture is replacing some portion of the cement with a supplementary cementitious material (SCM). This method has been widely studied, and is utilized in some manner in every state within the United States. The major benefit to this method over using solely aggregate optimization is that a user can maintain the total cementitious content within the concrete mixture while also reducing the amount of cement. This is a benefit for the reason laid out earlier: the cementitious material provides the concrete the ability to transfer tension forces. Also, there is a direct correlation between cement content and concrete strength [7].

That correlation between cement content and concrete strength also leads to concerns about replacing cement with SCMs. This is because the hydration process is different for each cementitious material. The cement hydration process is the reaction initiated when cement and moisture are combined in the presence of heat. For cement, there are two primary products of hydration: calcium silica hydrate (CSH) and calcium hydroxide (CH) or lime. CSH is a dense and strong compound that provides all the desirable properties to the hardened cement paste. CH alternatively is a weak and porous compound that is detrimental to the hardened cement paste.

The hydration process for SCMs differs slightly from that of cement. SCMs require moisture, heat and CH to initiate hydration. The major product of the hydration is CSH. In other words, adding SCMs to a traditional concrete mixture would reduce the CH in the system and increase the CSH. The cement paste will be denser and stronger. SCMs come primarily from either natural pozzolans or from the byproducts of industrial processes. Some typical SCMs that come from byproducts consist of the following: fly ash, slag cement and silica fume. These byproducts each have their own unique properties, but they share at least one common property; they require little to no extra energy to produce their powder form. This fact is why it is more environmentally friendly to replace cement in a concrete mixture with SCMs. The energy and emissions associated with producing the SCMs are tied to the original industrial process. For example, if 25% of the cement in a concrete mixture is replaced with fly ash, the emissions from the cementitious materials, the primary source of emissions, is cut by 25%. (This assumes that the transportation emissions are equal for both the fly ash and cement.)

With the obvious efficiency in mitigating environmental damage, much work has been done in this line of research. The drawback of using these SCMs is that there is often a time delay in the growth of the concrete micro-structure, and thus in the gain of strength, durability, etc. This time delay is due to the pozzolanic reaction's need for cement hydration byproducts. For example, the cement interacts with moisture; the hydration reaction occurs: CSH and CH are formed; CH (the hydration byproduct) reacts with the pozzolans and moisture; more CSH is formed. In some applications, this “delayed gratification” is acceptable. However, in many applications it is not. Clients are constantly demanding improved quality without any sacrifices. It is also worth noting that, varying the chemical reactions that create the hardened paste can have a major impact on the micro-structure makeup and therefore the behavior of the concrete.

2.1.2. Self-Consolidating Concrete. “Self-consolidating concrete, also known as self-compacting concrete (SCC), is a highly flowable, non-segregating concrete that spreads into place, fills formwork, and encapsulates even the most congested reinforcement, all without any mechanical vibration” [8]. It can be developed with many different methods, but there are common components between most SCC mixes: increase paste volumes, increased paste fluidity, increased fine aggregate volumes and reduced coarse aggregate sizes.

An SCC mix has two important plastic properties: flowability and stability. The mixes need to be sufficiently stable to prevent segregation and excessive bleeding, while also being flowable enough to completely fill any formwork or congested area. To achieve the flowability, high-range water reducers (HRWR) are used. These chemicals allow the concrete to flow without interfering with the water-to-cement ratio

(w/c), which is the best indicator of concrete strength. To achieve stability, viscosity modifying admixtures can be added. Alternatively, fine particles, typically in the form of mineral admixtures, can be added to the mixture.

This non-traditional concrete has many obvious benefits: reduced labor cost, improved consolidation, decreased concrete placement time, improved pumpability, etc. However, the general makeup of the fresh and hardened concretes varies drastically from traditional concrete. Due to that, much research must be done to understand the behavior of SCC. Notably, with increase paste volumes, creep and shrinkage issues may be more prevalent and shear strengths may be reduced.

2.2. FACTORS AFFECTING SHEAR BEHAVIOR

Concrete shear behavior is the focus of this proposed study. Concrete shear behavior is governed by the presence of reinforcement, the aggregate properties, the location and direction of loading on the member and the tensile strength of the concrete. Some of these factors are directly accounted for in shear design equations, and some are not.

Reinforcement, commonly in the form of steel rebar, can be utilized in either or both of two primary roles: web reinforcement and longitudinal reinforcement. Web reinforcement, often in the form of stirrups, is used to provide shear resistance to concrete beams and to ensure flexural failures occur. Flexural failures are desirable, because they are more ductile and slow when compared to shear failures which are sudden and violent. Web reinforcement is typically placed in the beams at standard spacing and orientated transversely to the longitudinal reinforcement. Usually small sized rebar (#3 or #4 sized bars) is used and bent into either a closed or open U-shape

Reinforcement has very little effect prior to the formation of cracks in the concrete. However, after cracking, web reinforcement enhances the beam in the following ways [9]:

- The stirrups crossing the crack help in resisting shear force.
- The stirrups restrict the growth of the cracks and reduce their penetration farther in the compression zone.
- The stirrups oppose widening of the cracks, which helps to maintain aggregate interlock within the concrete.
- The presence of stirrups provides extra restraint against the splitting of concrete along the longitudinal bars due to their confinement effect.

The longitudinal reinforcement is installed in the beams to increase the flexural capacity of the member. However, it does affect the shear behavior. The reinforcement resists shear cracks through dowel action. When the longitudinal reinforcement ratio (ρ_L), which is a ratio of the area of longitudinal reinforcement to the cross-sectional area of the beam, is small, flexural cracks extend higher into the beam and open wider. When the cracks are wide, shear force transfer is reduced or even removed entirely.

The aggregate size, strength and density all affect the shear behavior. While aggregate is traditionally thought of as filler material, it also tends to be denser and stronger than cement paste. Stronger and denser aggregates increase the average compressive strength of the concrete, and therefore increase the tensile strength of the concrete. Also, larger aggregate sizes improve shear strength of concrete by increasing the roughness of the crack surface, allowing higher shear stresses to be transferred [10].

The loading on the beam can greatly affect the shear behavior of the member. If axial compression loads are present, beam shear strength is seen to increase, and if axial tension loads are present, the beam shear strength is seen to decrease [10]. For loads transverse to the beam, there is a relationship that must be considered called the shear span to depth ratio (a/d). The shear span (a) is the distance from the face of the support to the load. The depth (d) is the distance from the top face of the beam to the centroid of the longitudinal steel. For a/d ratios larger than 2.5, there is no noticeable effect on the shear performance of the beam. This type of loading is commonly referred to as slender beam behavior. However, for a/d ratios smaller than 2.5, the load transfer mechanism inside the beam changes. Some of the load is carried directly to the support through compressive forces. This type of behavior is commonly referred to as deep beam behavior. For deep beams, the initial diagonal cracking develops suddenly along almost the entire length of the test region [10].

The tensile strength of concrete (f_{ct}) also affects the shear behavior. Concrete has a relatively low tensile strength, and tends to crack diagonally between load points. While tensile strength is directly linked to shear strength, concrete compressive strength (f'_c) is more commonly used to compute beam shear strength. This is because tensile testing is difficult to conduct, and the relationship between the two is well understood for traditional concrete.

As non-traditional concretes have drastically different mixture compositions when compared to traditional concretes, researchers must evaluate all aspects of their behavior. The author could find no published research on the structural performance of cement-limiting concrete made with optimized gradations. Richardson noted that some

states DOT's allow a reduction in the minimum cement content of up to half a sack per yard when optimized gradations are used, but they did not cite research to back up their allowing this [2]. For these reasons, the behavior of this material needs to be better understood if it is to be used in structural applications.

For SCC, there is a limited amount of shear beam data, and the conclusions from the researchers vary from claiming a reduced shear capacity to a slightly increased shear capacity [11, 12, 13, 14, 15, 16, 17, 18]. Due to the material variations between each mix, and the inherent variability of shear testing, more data is needed on this topic.

2.3. AGGREGATE INTERLOCK

As was stated previously, aggregate plays a key role in the shear behavior of concrete, especially when reinforcement is not present. Coarser aggregate helps to provide a rougher crack surface, which increases concrete tensile strength and surface friction. Conversely, in SCC, smaller, and often rounder aggregates, are thought to reduce these effects. Aggregate interlock is the load transfer from one face of a crack to the other by contact between exposed aggregate particles, as shown in Figure 2.5.

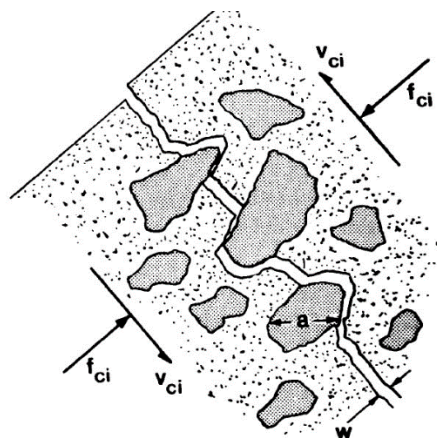


Figure 2.5 – Aggregate Interlock [19]

This behavior is known to occur on all concrete crack surfaces when the cracks are sufficiently small. Another term for this load transfer is shear friction. The first

researcher to publish research on this topic was Hanson in 1960 [20]. Hanson was working in the pre-cast concrete industry and saw the need to understand the behavior of the connections between pre-cast and cast-in-place concrete. He designed some laboratory tests to simulate such behavior. In the mid 1960's, Birkeland and Birkeland also performed similar tests on pre-cast elements [21]. The laboratory tests that were performed consisted of push-off and pull-off tests. Their specimens were constructed to force the load path to run through a desired plane of concrete which had reinforcement crossing the path tangentially, as shown in Figure 2.6. The reinforcement provided the required normal force to contain the cracked concrete and allow the two planes to resist shearing through friction forces. There must be a normal force perpendicular to the crack face to keep the concrete from simply splitting into two.

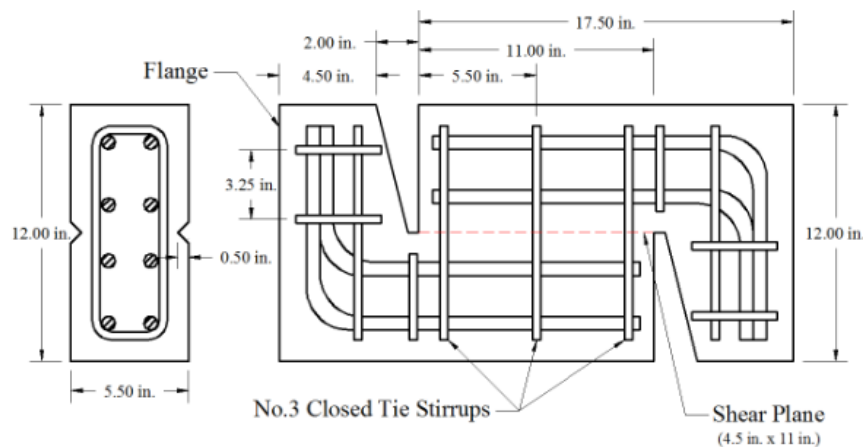


Figure 2.6 – Internal Reinforcement Method [12]

Many other researchers performed similar tests to analyze the shear friction of concrete in both monolithic scenarios and cold-joint scenarios [22, 23, 19]. The difference between monolithic and cold-joint scenarios are the exposed crack surfaces. Monolithic scenarios allow for more irregular surfaces and both cracked and un-cracked aggregate particles along the surface. Thus, to better understand the role of aggregate

interlock in the load transfer between crack surfaces, researchers had to adapt the original test methods. Specimens were made, and external reinforcement was used to provide the required normal force as shown in Figure 2.7 [24].

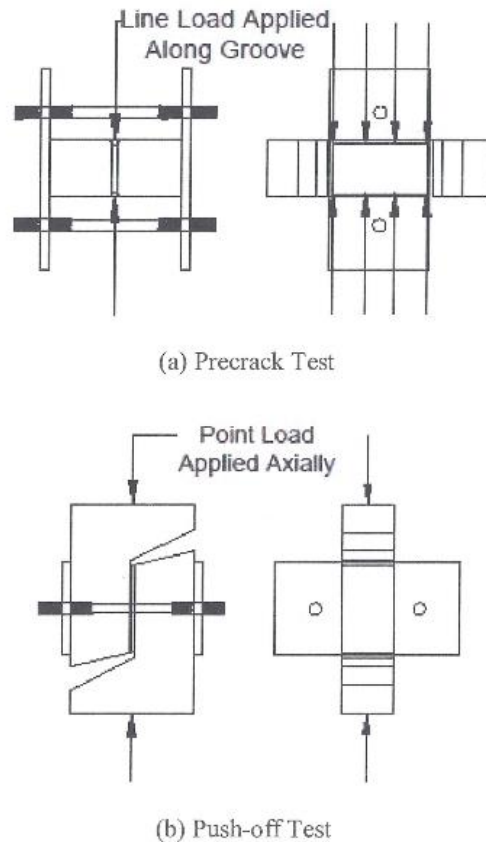


Figure 2.7 – External Reinforcement Method [13]

There is no standardized test for shear friction or for aggregate interlock. Due to that, the author is proposing a new method of conducting the test after reviewing the literature on the topic. Many of the previous specimens were very heavy, with all weighing at least 70 pounds. Also, either internal reinforcement or external reinforcement was used and attached to the specimen from the beginning of testing until the end. This adds a lot of weight and complicates the pre-cracking step. The use of internal reinforcement was more convenient but made the desired property unable to be

precisely measured. If the specimens were pre-cracked along their desired failure planes, that load was recorded, but the surface could not be inspected and analyzed. The author is proposing using external reinforcement but attaching it after first pre-cracking the specimens. This will allow for the collection of more and better data of the tensile strength of the concrete. After the crack is made, the reinforcement will be attached, and the test will be run as was previously run with the external reinforcement method. The crack will be monitored along with the load and the slip between the two crack surfaces. It is believed that this approach will lead to improved results.

REFERENCES

- [1] L. Hanle, K. Jayaraman and J. Smith, "CO2 Emissions Profile of the U.S. Cement Industry," U.S. Environmental Protection Agency, Washington D.C., 2012.
- [2] D. N. Richardson, "Aggregate Gradation Optimization - Literature Search," Missouri Department of Transportation, 2005, 2005.
- [3] A. N. Talbot and F. E. Richart, "The Strength of Concrete and Its Relation to the Cement, Aggregate, and Water," University of Illinois at Urbana Champaign, College of Engineering. Engineering Experiment Station., Urbana, IL, 1923.
- [4] J. M. Shilstone and J. M. Shilstone Jr., "Practical Concrete Mixture Proportioning Technology," Shilstone Software Co., Reference Manual, 1987.
- [5] J. M. Shilstone , "Concrete Mixture Optimization," *Concrete International* 12(6), pp. 33-39, 1990.
- [6] J. M. Shilstone and J. M. Shilstone Jr., "Concrete Mix Analysis - Interpreting the Coarseness Factor Chart," Shilstone Software Co., Newsletter., 1997.
- [7] PCA, "Cement & Concrete Basics FAQs," 29 November 2017. [Online]. Available: <http://www.cement.org/cement-concrete-applications/cement-and-concrete-basics-faqs>.
- [8] NRMCA, "Self-Consolidating Concrete," 29 November 2017. [Online]. Available: <http://www.selfconsolidatingconcrete.org/>.
- [9] A. H. Nilson, D. Darwin and D. W. Dolan, Design of Concrete Structures (13th Ed.), McGraw Hill, 2004.
- [10] J. K. Wight and J. G. MacGregor, Reinforced Concrete: Mechanics and Design, Upper Saddle River, NJ: Pearson Education, Inc., 2012.
- [11] Y. Choulli, A. R. Mari and A. Cladera, "Shear behavior of full-scale prestressed i-beams made with self compacting concrete," *Materials and Structures*, vol. 41, no. 1, pp. 131-141, 2007.
- [12] E. Cuenca, P. Serna and M. J. Pelufo, "Structural Behavior of Self-Compacting and Fiber Reinforced Concrete Under Shear Loading," in

Evolution and Trends in Design, Analysis and Construction of Shell and Spatial Structures, Valencia, Spain, 2009.

- [13] P. L. Domone, "A review of the hardened mechanical properties of self-compacting concrete," *Cement and Concrete Composites*, vol. 29, no. 1, pp. 1-12, 2007.
- [14] T. Greenough and M. Nehdi, "Shear Behavior of Fiber-Reinforced Self-Consolidating Concrete Slender Beams," *ACI Materials Journal*, vol. 105, no. 5, p. 468, 2008.
- [15] A. Hassan, K. Hossain and M. Lachemi, "Strength, Cracking and Deflection Performance of Large-Scale Self-Consolidating Concrete Beams Subjected to Shear Failure," *Engineering Structures*, vol. 32, no. 5, pp. 1262-1271, 2010.
- [16] P. Helincks, V. Boel, W. De Corte, G. De Schutter and P. Desnerck, "Structural Behaviour of Powder-Type Self-Compacting Concrete: Bond Performance and Shear Capacity," *Engineering Structures*, vol. 48, pp. 121-132, 2013.
- [17] T. Labonte and H. R. Hamilton III, "Self-Consolidating Concrete (SCC) Structural Investigation," Florida Department of Transportation, Gainesville, FL, 2005.
- [18] C.-H. Lin and J.-H. Chen, "Shear Behavior of Self-Consolidating Concrete Beams," *ACI Structural Journal*, vol. 109, no. 3, pp. 307-315, 2012.
- [19] F. J. Vecchio and M. P. Collins, "The Modified Compression-Field Theory for Reinforced Concrete Elements Subjected to Shear," *ACI Journal*, vol. 83, no. 2, pp. 219-231, 1986.
- [20] N. W. Hanson, "Precast-Prestressed Concrete Bridges 2: Horizontal Shear Connections," *Journal of the Research and Development Division*, vol. 2, no. 2, pp. 38-58, 1960.
- [21] P. W. Birkeland and H. W. Birkeland, "Connections in Precast Concrete Construction," *ACI Journal*, vol. 63, no. 3, pp. 345-368, 1966.
- [22] D. M. Shaw, "Direct Shear Transfer of Lightweight Aggregate Concretes with Non-Monolithic Interface Conditions," Missouri University of Science and Technology, Rolla, MO, 2013.

- [23] J. Walraven, F. Jerome and P. Arjan, "Influence of Concrete Strength and Load History on the Shear Friction Capacity of Concrete Members," *PCI Journal*, vol. 32, no. 1, pp. 66-84, 1987.
- [24] E. B. Sells, J. J. Myers and J. S. Volz, "Aggregate Interlock Push-Off Test Results of Self-Consolidating Concrete (SCC) for Use in Infrastructure Elements," in *New Developments in Structural Engineering and Construction*, 2013.
- [25] E. B. Sells, "Self-Consolidating Concrete for Infrastructure Elements Shear Characteristics," Missouri University of Science and Technology, Rolla, MO, 2012.
- [26] H. Okamura, "Self Compacting High Performance Concrete - Ferguson Lecture for 1996," *Concrete International*, vol. 19, no. 7, pp. 50-54, 1997.
- [27] K. Ozawa, K. Maekawa and H. Okamura, "Development of the High Performnace Concrete," *Proceedings of JSI*, vol. 11, no. 1, pp. 699-704, 1989.
- [28] E. K. Rice, "Shrinkage-Compensating Concrete". USA Patent 5,846,316, 12 Sep. 1996.
- [29] S. Rolsa, J. Ambroisea and J. Peraa, "Effects of different viscosity agents on the properties of self-leveling concrete," *Cement and Concrete Research*, vol. 29, no. 2, pp. 261-266, 1999.
- [30] "Self-Compacting Concrete," in *1st International RILEM Symposium*, Stockholm, Sweened, 1999.
- [31] E. P. Koehler, D. W. Fowler, E. H. Foley, G. J. Rogers, S. Watanachet and M. J. Jung, "Self-Consolidating Concrete for Precast Structural Applications: Mixture Proportions, Workability, and Early-Age Hardened Properties," Center for Transportation Research at The University of Taxas at Austin, Austin, TX, 2007.
- [32] F. Kassimi and K. H. Khayat, "Effect of fiber and admixture types on restrained shrinkage cracking of self-consolidating concrete," in *Proceedings of the Fifth North American Conference on the Design and Use of Self-Consolidating Concrete*, Chicago, IL, 2013.
- [33] A. A. A. Hassan, K. M. A. Hossain and M. Lachemi, "Behavior of full-scale self-consolidating concrete beams in shear," *Cement and Concrete Composites*, vol. 30, no. 7, pp. 588-596, 2008.

- [34] O. J. Gasteble and I. M. May, "Fracture Mechanics Model Applied to Shear Failure of Reinforced Concrete Beams without Stirrups," *ACI Structural Journal*, vol. 131, no. 12, pp. 184-190, 2001.
- [35] S. Xu, X. Zhang and H. W. Reinhardt, "Shear Capacity Prediction of Reinforced Concrete Beams without Stirrups Using Fracture Mechanics Approach," *ACI Structural Journal*, vol. 109, no. 5, pp. 705-714, 2012.
- [36] K. H. Reineck, D. A. Kuchma, K. S. Kim and S. Marx, "Shear Database for Reinforced Concrete Members without Shear Reinforcement," *ACI Structural Journal*, vol. 100, no. 2, pp. 240-249, 2003.
- [37] P. Dayaratnam and R. Ranganathan, "Statistical Analysis of Strength of Concrete," *Building and Environment*, vol. 11, pp. 145-152, 1976.
- [38] J. Butlin, *Our Common Future*. World Commission on Environmental and Development, London: Oxford University Press, 1987.
- [39] U.S. Geological Survey, "Mineral Commodities Summaries," 2017.
- [40] P. Mehta and P. Monteiro, *Concrete: Microstructure, Properties, and Materials*, Third ed., New York: McGraw-Hill, 2006, p. 659.
- [41] L. Lam, Y. Wong and C. Poon, "Effect of Fly Ash and Silica Fume on Compressive and Fracture Behaviors of Concrete," *Cement and Concrete Research*, vol. 28, no. 2, pp. 271-283, February 1998.
- [42] R. Siddique, "Performance characteristics of high-volume Class C fly ash concrete," *Cement and Concrete Research*, vol. 34, no. 3, pp. 487-493, March 2004.
- [43] P. K. Mehta, "High-Performance, High-Volume Fly Ash Concrete for Sustainable Development," in *Proceedings of the International Workshop on Sustainable Development & Concrete Technology*, Beijing, China, 2004.
- [44] S. Sadati, M. Arezoumandi, K. H. Khayat and J. S. Volz, "Shear performance of reinforced concrete beams incorporating recycled concrete aggregate and high-volume fly ash," *Journal of Cleaner Production*, vol. 115, pp. 284-293, March 2016.
- [45] A. H. Mattock, J. A. Hofbeck and I. O. Ibrahim, "Shear Transfer in Reinforced Concrete," *ACI Journal*, vol. 66, no. 2, pp. 119-128, 1969.

- [46] A. H. Mattock and N. M. Hawkins, "Shear Transfer in Reinforced Concrete - Recent Research," *PCI Journal*, vol. 17, no. 2, pp. 55-75, 1972.
- [47] C. M. Wirkman, "Performance of Fiber-Reinforced Self-Consolidating Concrete for Repair of Bridge Sub-Structures," The University of Oklahoma, Norman, OK, 2016.
- [48] K. S. Wallace, "Performance of Fiber-Reinforced Eco-Friendly Concrete for Bridge Structures," The University of Oklahoma, Norman, OK, 2016.
- [49] J. C. Walraven and J. Stroband, "Shear Friction in High-Strength Concrete," in *SP-149, American Concrete Institute International Conference*, Singapore, 1994.
- [50] F. J. Vecchio and D. Lai, "Crack Shear-Slip in Reinforced Concrete Elements," *Journal of Advanced Concrete Technology*, vol. 2, no. 3, pp. 289-300, 2004.
- [51] C. A. Ortega, "Shear and Fracture Behavior of High-Volume Fly Ash Reinforced Concrete for Sustainable Construction," Missouri University of Science and Technology, Rolla, MO, 2012.
- [52] M. Lachemi, K. Hossain and V. Lambros, "Shear Resistance of Self-Consolidating Concrete Beams - Experimental Investigations," *Canadian Journal of Civil Engineering*, vol. 32, no. 6, pp. 1103-1113, 2005.
- [53] A. Hassan, K. Hossain and M. Lachemi, "Behavior of Full-Scale Self-Consolidating Concrete Beams in Shear," *Cement and Concrete Composites*, vol. 30, no. 7, pp. 588-596, 2008.
- [54] R. Mast, "Auxiliary Reinforcement in Concrete Connections," *ASCE Journal of the Structural Division Proceedings*, vol. 94, no. ST6, pp. 1485-1504, 1968.
- [55] J. A. Hofbeck, I. O. Ibrahim and A. H. Mattock, "Shear Transfer in Reinforced Concrete," *ACI Journal*, vol. 66, no. 2, pp. 119-128, 1969.
- [56] A. H. Mattock and N. M. Hawkins, "Shear Transfer in Reinforced Concrete - Recent Research," *PCI Journal*, vol. 17, no. 2, pp. 55-75, 1972.
- [57] T. Paulay, R. Park and M. H. Phillips, "Horizontal Construction Joints in Cast-In-Place Reinforced Concrete," *American Concrete Institute Special Publications*, vol. SP 42, pp. 599-616, 1974.

- [58] A. H. Mattock, L. Johal and C. H. Chow, "Shear Transfer in Reinforced Concrete With Moment or Tension Acting Across the Shear Plane," *PCI Journal*, vol. 20, no. 4, pp. 76-93, 1975.
- [59] A. H. Mattock, W. K. Li and T. C. Wang, "Shear Transfer in Lightweight Reinforced Concrete," *PCI Journal*, vol. 21, no. 1, pp. 20-39, 1976.
- [60] F. A. Shaikh, "Proposed Revisions to Shear Friction Provisions," *PCI Journal*, vol. 23, no. 2, pp. 12-21, 1978.
- [61] T. T. Hsu, S. T. Mau and B. Chen, "Theory of Shear Transfer Strength of Reinforced Concrete," *ACI Structural Journal*, vol. 84, no. 2, pp. 149-160, 1987.
- [62] G. C. Hoff, "High Strength Lightweight Aggregate Concrete for Arctic Applications - Part 3: Structural Parameters," *American Concrete Institute Special Publication*, no. SP 136, pp. 175-246, 1992.
- [63] A. H. Mattock, "Shear Friction and High-Strength Concrete," *ACI Structural Journal*, vol. 98, no. 1, pp. 50-59, 2001.
- [64] L. F. Kahn and A. D. Mitchell, "Shear Friction Tests with High-Strength Concrete," *ACI Structural Journal*, vol. 99, no. 1, pp. 98-103, 2002.
- [65] J. A. Tanner, "Calculating Shear Friction Using Effective Coefficient of Friction," *PCI Journal*, vol. 53, no. 3, pp. 114-120, 2008.
- [66] K. A. Harries, Zeno and Shahrooz, "Toward an Improved Understanding of Shear-Friction Behavior," *ACI Structural Journal*, vol. 109, no. 6, pp. 835-844, 2012.
- [67] M. Berndt, "Properties of sustainable concrete containing fly ash, slag and recycled concrete aggregate," *Construction and Building Materials*, vol. 23, no. 7, pp. 2606-2613, July 2009.
- [68] E. C. Bentz, Sectional Analysis of Reinforced Concrete Members, University of Toronto, 2000.
- [69] Z. P. Bazant and Q. Yu, "Design Against Size Effect on Shear Strength of Reinforced Concrete Beams without Stirrups: I, Formulation," *Journal of Structural Engineering*, vol. 131, no. 12, pp. 1877-1885, 2005.

- [70] B. Barragain, R. Gettu, L. Agullu and R. Zerbio, "Shear Failure of Steel Fiber-Reinforced Concrete Based on Push-Off Tests," *ACI Materials Journal*, vol. 103, no. 4, pp. 251-257, 2006.
- [71] M. Arezoumandi, J. S. Volz, C. A. Ortega and J. J. Myers, "Effect of total cementitious content on shear strength of high-volume fly ash concrete beams," *Materials & Design*, vol. 46, pp. 301-309, April 2013.
- [72] M. Arezoumandi and J. S. Volz, "Effect of fly ash replacement level on the shear strength of high-volume fly ash concrete beams," *Journal of Cleaner Production*, vol. 59, pp. 120-130, November 2013.
- [73] M. Arezoumandi, M. H. Wolfe and J. S. Volz, "A comparative study of the bond strength of reinforcing steel in high-volume fly ash concrete and conventional concrete," *Construction and Building Materials*, vol. 40, pp. 919-924, March 2013.
- [74] ACI Committee 318, Building Code Requirements for Structural Concrete (ACI 318-14) and Commentary, American Concrete Institute, 2014.
- [75] ASTM C469-14, Standard Test Method for Static Modulus of Elasticity and Poisson's Ratio of Concrete in Compression, ASTM International, 2014.
- [76] ASTM C496-17, Standard Test Method for Splitting Tensile Strength of Cylindrical Concrete Specimens, ASTM International, 2017.
- [77] ASTM C78-18, Standard Test Method for Flexural Strength of Concrete, ASTM International, 2018.
- [78] ASTM C39-18, Standard Test Method for Compressive Strength of Cylindrical Concrete Specimens, ASTM International, 2018.
- [79] JSCE, "Standard Specifications for Concrete Structures," Japan Society of Civil Engineers, 2007.
- [80] Oklahoma Department of Transportation Transportation Commission, "Standard Specifications," 2009.
- [81] ASTM C150-18, Standard Specification for Portland Cement, ASTM International, 2018.
- [82] ASTM A615-16, Standard Specification for Deformed and Plain Carbon-Steel Bars for Concrete Reinforcement, ASTM International, 2016.

- [83] ASTM C33-18, Standard Specification for Concrete Aggregates, ASTM International, 2018.
- [84] ASTM C618-17, Standard Specification for Coal Fly Ash and Raw or Calcined Pozzolan for Use in Concrete, ASTM International, 2017.
- [85] ACI Committee 445, "Recent Approaches to Shear Design of Structural Concrete," American Concrete Institute, Farmington Hills, MI, 1999.
- [86] IStructE, "Manual for the design of concrete building structures to Eurocode 2," The Institution of Structural Engineers, 2006.
- [87] AASHTO, "LRFD Bridge Design Specifications," American Association of State Highway and Transportation Officials, 2015.
- [88] CSA, "Concrete Materials and Methods of Concrete Construction/Methods of Test for Concrete," CSA Group, 2004.
- [89] ACI 318-11, "Building Code Requirements for Structural Concrete and Commentary," The American Concrete Institute, 2011.
- [90] American Concrete Institute, ACI Concrete Terminology, Farmington Hills, MI, 2018.

Paper

I. Shear Behavior of Cement-Limiting Concrete Produced with Improved Particle Packing and Fiber Reinforcement

Jonathan T. Drury and Jeffery S. Volz

Abstract

An experimental investigation was conducted to evaluate the mechanical properties and shear behavior of large-scale beams constructed with cement-limiting concrete made with improved particle packing. This study included two cement-limiting mixtures, Eco-Bridge-Crete 1 (EBC1) and Eco-Bridge-Crete 2 (EBC2), and one conventional concrete (CC) mixture. The two cement-limiting concrete mixtures differ from each other based on the type and amount of fibers present: EBC1 had 0.5 lb/yd³ of micro-fibers, EBC2 had 0.5 lb/yd³ of micro-fibers and 3.0 lb/yd³ of macro-fibers. The study consisted of 9 beams with identical reinforcement for every beam. The experimental data was compared to the shear provisions for both U.S. and international design codes. Furthermore, the shear performance of the beams was evaluated based on fracture mechanics approaches, Modified Compression Field Theory (MCFT), a shear database of CC beams, material properties testing, and Response-2000. Finally, statistical data analyses were performed to evaluate whether there were any statistically significant differences between the performance of the cement limiting concrete and CC beams.

Results of this study show that the basic mechanical properties of both EBC1 and EBC2 correlate well to their comparative beam shear performances, but not as closely when compared to the CC. However, the crack morphology and stresses in the

longitudinal bars showed that the presence of fibers and reduced cementitious materials had an impact on the internal stresses of the test region in all cases. The average normalized shear strengths of EBC1 and EBC2 were 7% and 10% stronger, respectively, than CC, but statistical analysis showed that the three concrete mixtures performed without significant differences between each other. This statistical correlation shows that the current design approaches may be acceptable for experimental concrete similar to those used in this study.

Keywords

Mechanical Properties; Cement-Limiting; Shear Behavior; Particle Packing; Aggregate Optimization; Beam(s)

Introduction

Sustainability, as defined by the United Nations (U.N.) World Commission on Environment and Development, is “development that meets the needs of the present without compromising the ability of future generations to meet their own needs” [1]. Sustainable development was a new idea when it was presented in 1987, but it is at the forefront of our society today, and it is a hot topic in concrete research.

Concrete, the most consumed man-made material in the world, uses a significant amount of nonrenewable resources and the concrete industry generates large amounts of carbon dioxide (CO²) emissions. The United States Geological Survey (USGS) reported that world total production of cement was approximately 4.6 billion tons (4.2 billion metric tons) in 2016 [2], and that nearly equal amounts of CO² emissions were generated.

Even with all these negative effects, the demand for concrete is expected to grow to approximately 18 billion tons (16 billion metric tons) per year by 2050 [3]. As a result, researchers have been investigating methods to mitigate the environmental and economic impacts of concrete.

The main contributor to both the environmental and economic impact of concrete is the cement. To reduce the amount of cement in a given concrete mixture, two methods have been proposed: optimizing the aggregate gradation and utilizing supplementary cementitious materials.

Much research has been done on both the fresh and hardened properties of concrete containing supplementary cementitious materials. Lam et al. investigated the compressive and fracture behavior of concrete containing both fly ash and silica fume [4]. In their study, they found that the high-volume fly ash exhibited slight decreases in tensile strength when compared to portland cement concrete and poorer fracture behavior. They also found that the negative effects of the fly ash could be offset by small additions of silica fume.

Siddique performed small scale testing on concrete containing 40, 45 and 50% fly ash replacements [5]. The testing showed a decrease in hardened and durability properties at 28 days, but those properties continued to improve significantly up to one year of age. From those studies, they recommended that concrete with up to 50% fly ash replacements could be used in producing precast elements.

Mehta investigated the use of high-volume fly ash concrete to produce high-performance concrete [6]. He noted that fly ash has improved workability, and that can be used to reduce the water-to-cementitious material ratio, which yields improved

strength and performance. While the slower strength gain and setting times can be problematic, the long-term property gains and improved dimensional stability may offset those negative effects.

Berndt researched sustainable concrete which was made with fly ash, slag and recycled concrete aggregate [7]. The metric he used to increase sustainability was a reduction in environmental impact. He replaced large percentages of portland cement (up to 70%) with these supplementary cementitious materials. In his study, he found that replacements of 50% fly ash produced poor material and durability performance, but that replacements of 50% slag showed quality results.

Arezoumandi et al. investigated the concrete-to-rebar bond performance of concrete containing at least 50% fly ash and compared them to the performance of portland cement concrete and a robust database [8]. They tested pull-out specimens and full-scale beams. That study showed that the high-volume fly ash concrete showed no detrimental behavior when considering bond and load-deformation behavior.

Arezoumandi et al. investigated the shear performance of high-volume fly ash concrete beams [9]. The high-volume fly ash concrete was produced with 70% fly ash replacements, two different cementitious content levels and three different longitudinal reinforcement ratios. Their fly ash beam performances were compared to portland cement concrete, international design codes, a large shear database and statistical analyses. They reported that there was no statistical difference between the differing levels of cementitious content and that the current codes conservatively predict the capacity of the high-volume fly ash beams.

Arezoumandi and Volz investigated the impact of differing levels of fly ash replacements on the shear performance of reinforced concrete beams [10]. They compared 50% and 70% replacement levels of fly ash with three different longitudinal reinforcement ratios. Their results were compared to portland cement concrete beams and differing methods of analysis. They found that the 70% fly ash concrete exhibited the best shear performance and that the control concrete exhibited the worst.

Sadati et al. investigated the shear performance of reinforced concrete made with recycled concrete aggregate and high volumes of fly ash [11]. Their study compared 24 full-scale beams with variables including longitudinal reinforcement ratio, amount of recycled concrete aggregate and amount of fly ash. They compared their results using international design codes, differing methods of analysis and a large shear database. They found that, on average, 50% replacements of either fly ash or recycled concrete aggregate showed improved shear performance, and that the mixtures containing 50% replacements of each showed slightly reduced shear performance.

While there has been research into shear performance of concrete with large quantities of supplementary cementitious materials, there is little to no published research investigating shear performance of concrete mixtures with improved aggregate gradations. For this reason, the current study was performed.

Research Significance

Based on a review of the existing literature, there is a lack of full scale shear testing of specimens constructed with cement-limiting concrete. Without this background, there is no quantitative basis for implementing cement limiting concrete in structural design. Consequently, the authors developed a testing plan to evaluate the

shear strength of specimens constructed with cement limiting concrete as a function of the percentage and type of fibers added to the mixture. Fibers were added to the concrete mixtures to improve durability and thus sustainability of the cement limiting concrete.

Experimental Program

Test Beam Design

Nine beams (three beams for each concrete mixture) were constructed without shear reinforcement in the test region and were designed with reinforcement ratios of 1.98% to preclude flexural failure and satisfy the minimum longitudinal reinforcement requirements of ACI 318 [12]. All the beams tested in this study had a rectangular cross-section with a width of 12 in. (305 mm), a height of 18 in. (457 mm), a shear span to depth ratio greater than 3.0 and 6 No. 7 (22 mm) longitudinal reinforcement bars within the tension zone of the beam section (Fig. 1).

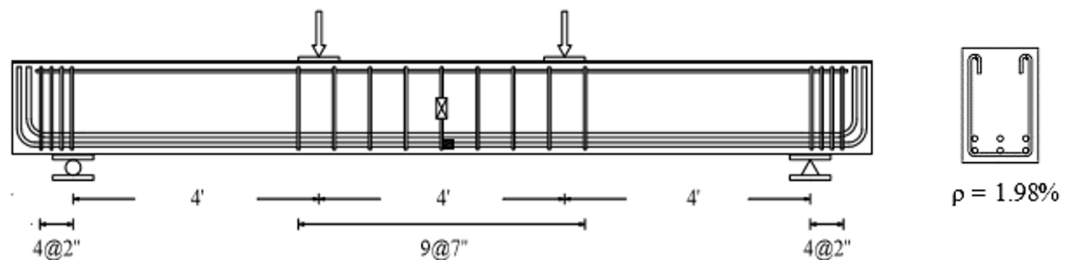


Figure 1 - Load pattern, rebar detail, cross section and location of instrumentation

Concrete Materials

There were two cementitious materials used in this study. The primary cementitious material was a Type I/II portland cement from Ash Grove Cement Company (Chanute, KS) which conformed to ASTM C-150 [13] specifications for both Type I and Type II cements. The secondary cementitious material used in this study was a Class C fly ash from Headwaters Resources (Jeffery Plant, St. Mary's, KS) which

conformed to ASTM C-618 [14] specifications. A detailed summary of test results for the properties of the cementitious materials is given in Table 1.

Table 1 – Cementitious material properties

Property	Type I/II Cement	Class C fly ash
Fineness (+325 mesh), %	—	10.3
Air permeability, ft ² /lb	1939	—
Specific gravity	3.11	2.72
Loss on ignition, %	2.4	0.67
Silica, %	20.8	31.9
Aluminum oxide, %	3.8	20.4
Ferric oxide, %	3	5.9
Sulfur trioxide, %	2.9	3.0
Calcium oxide, %	63.9	28.3
Magnesium oxide, %	1.9	7.2

Note: 1 ft²/lb = 2.05 cm²/g

There were three aggregate sources used in this study. The primary coarse aggregate was a crushed limestone from the Dolese Bros. Co. Davis Quarry (Davis, OK) which conformed to ASTM C-33 [15] specification for a size #57. The secondary coarse aggregate was a 3/8" chipped limestone from Metro Materials (Norman, OK). The fine aggregate used was a concrete sand from Dolese Bros. Co. East Sand Plant (Oklahoma City, OK) which conformed to ASTM C-33 [15]. A detailed summary of the properties of the aggregate is given in Table 2.

Table 2 - Aggregate properties

Property	#57	3/8" chip	Concrete sand
Specific gravity, oven-dry	2.69	2.67	2.65
Dry-rodded unit weight, lb/ft ³	101	95	—
Absorption, %	0.86	1.01	0.7
LA abrasion, % loss	26	22	—

Note: 1 lb/ft³ = 16 kg/m³

Two different fibers were used in this study. One fiber was a polypropylene micro-fiber from BASF (Florham Park, NJ) called MasterFiber M 100. Each of the M 100 fibers had a negligible absorption, measured approximately 0.75 in. (19 mm) in

length and approximately 0.00047 in. (0.012 mm) in thickness and had a design tensile strength of 70 ksi (482 MPa). The second fiber was a polypropylene macro-fiber from BASF (Florham Park, NJ) called MasterFiber MAC Matrix. Each of the MAC matrix fibers had a negligible absorption, measured approximately 2.1 in. (53 mm) in length and approximately 0.03 in. (0.8 mm) in thickness and had a design tensile strength of 85 ksi (586 MPa). A detailed summary of the fiber properties supplied by the manufacturer is given in Table 3.

The rebar used in this study was all ASTM A615 [16] Grade 60 (414 MPa). All of the bars were from the same heat of steel, used the same deformation pattern and met the requirements of ASTM A615 [16]. The longitudinal bars were sampled and tested in tension to determine their properties. Testing showed that the bars had an average yield strength of 78 ksi (537 MPa), an average ultimate strength of 109 ksi (751 MPa) and an average modulus of elasticity of 28,600 ksi (197,000 MPa).

Table 3 – Fiber properties

Property	MasterFiber M 100	MasterFiber MAC Matrix
Specific gravity	0.91	0.91
Absorption	Nil	Nil
Tensile strength, ksi	70	85
Nominal length, in.	0.75	2.1
Nominal diameter, in.	0.00047	0.03
Material	Polypropylene	Polypropylene

Notes: 1 in. = 25.4 mm; 1 ksi = 6.89 MPa

There were two admixtures used in this study. A high-range water reducer (HRWR) was selected from BASF (Florham Park, NJ). The HRWR, called MasterGlenium 7920, was selected because of its high usage in the region, improved potency and ability to maintain workability benefits longer than its competition. The air entraining admixture (AEA) was also selected from BASF (Florham Park, NJ). The

AEA, called MasterAir AE 90, was selected due to its high usage in the region and its excellent performance record.

Mixture Proportions

This research was focused on structural concrete for bridge applications in Oklahoma. As such, the conventional concrete (CC) mixture was designed to comply with Oklahoma DOT (ODOT) design and performance specifications for Class AA concrete, which is required for superstructure concrete. The performance and design specification for an ODOT Class AA concrete are listed in Table 4. Many possible CC mixtures were tested, and the CC mixture selected had the proportions as listed in Table 5. This mixture was used to construct control specimens to serve as baseline comparisons to the Eco-Bridge-Crete (EBC) mixtures.

Table 4 – ODOT Class AA design and performance specifications

Min. cementitious content (lb/yd ³)	Air content* (%)	w/cm	Slump ^{*†} (in.)	Min. 28-day strength ^{**} (psi)
564	6.5 ± 1.5	0.25-0.44	2 ± 1	4,000

*Values are based on ASTM C231

*Values are based on ASTM C143

**Values are based on ASTM C39

†Slump range only applies for concrete made without admixtures

Notes: 1 in. = 25.4 mm; 1 lb/yd³ = 0.593 kg/m³; 1 psi = 0.00689 MPa; 1 lb/in = 175.1 N/m

The EBC mixtures were designed to conform to the performance specifications of the ODOT Class AA but have a reduced cementitious material content. Knowing that reducing the cementitious materials and holding all other mixture constituent ratios constant would lead to a reduction in shear performance, shear improvements had to be made. Two improvements were implemented. First, the aggregate gradations were optimized to provide maximum packing density. Improved packing density is believed to improve aggregate interlock, which is one of the components of shear resistance for

concrete. Second, fibers were added to the concrete. Three aggregate optimization approaches were used simultaneously in order to achieve the best result: the 0.45 power maximum density curve, the individual percent retained chart and the Shilstone chart.

Table 5 – Mixture designs (per yd³)

	CC	EBC1	EBC2
Type I/II cement	470	414	414
Class C fly ash	118	103	103
w/cm	0.4	0.4	0.4
#57 limestone, lb	1857	989	989
3/8" chip, lb	—	565	565
Concrete sand, lb	1323	1415	1415
Micro-fiber, lb	—	0.5	0.5
Macro-fiber, lb	—	—	3
HRWR, fl oz	26.7	36.19	36.19
AEA, fl oz	4.40	2.59	2.59

Notes: 1 lb = 0.454 kg; 1 fl oz = 29.5 mL

The 0.45 power maximum density curve is a method commonly used to assess asphalt gradations [17, 18]. It is a visual method that plots the total percent of aggregate passing each sieve size on the vertical axis paired with the opening size of that sieve raised to the 0.45 power on the horizontal axis. The “optimum gradation” is then based on a line drawn from the origin of the plot to the intersection of the 100 percent passing line and the first sieve to retain aggregate. This line is considered the maximum density line. An envelope of acceptable ranges of gradations is then developed by drawing two lines connecting the origin and the intersection of the 100 percent passing line and one sieve larger and one sieve smaller than the first sieve to retain aggregate. It is important to note that the gradation being evaluated is a combination of all aggregate sources used. Figure 2 shows how the selected gradations fit within the 0.45 power plot maximum density curve method.

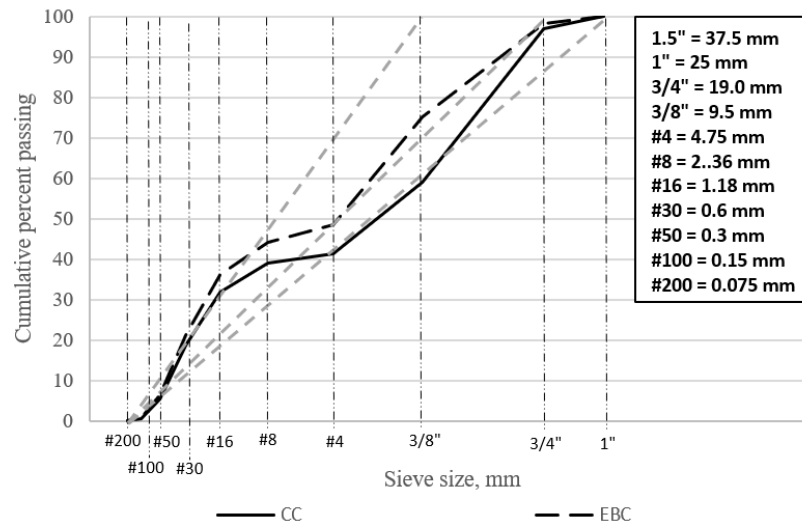


Figure 2 – 0.45 power plot

The individual percent retained chart was originally designed to evaluate combined concrete aggregate gradations [19, 20]. This method varies from the 0.45 power plot method in that the curve plotted represents the individual percent passing each sieve on the vertical axis plotted against the opening of each associated sieve size on the horizontal axis. The ideal curve for this method would look like a “haystack”. To assess the acceptability of an aggregate gradation and force the gradation into the desired “haystack” shape, an “8 to 18” band was developed. This band was intended to keep the individual percent retained on each sieve between the No. 30 sieve and one size below the nominal maximum size between 8 and 18 percent. The band is defined with 8 points that are dependent on the nominal maximum size (NMS) for the aggregate. This method is believed to make locating problematic areas in the gradation easier to locate. Figure 3 shows how the selected gradations fit within the individual percent retained chart.

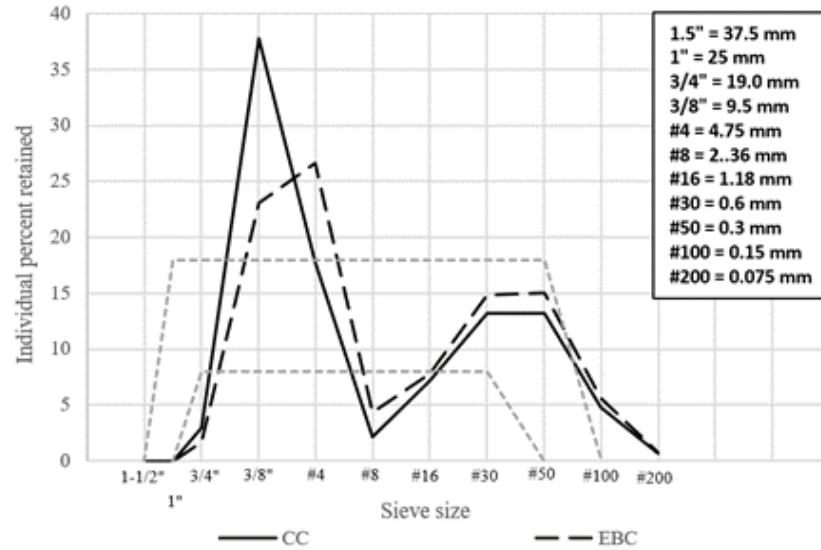


Figure 3 – Individual percent retained chart

The Shilstone chart is the only method used to directly assess the workability of a concrete mixture [21]. It does so by accounting for the impact of a given amount of cement paste in each mixture. The Shilstone chart is again a graphical representation of two variables. The horizontal axis represents what Shilstone and Shilstone Jr. termed the coarseness factor, CF. The coarseness factor is a ratio of the cumulative percent retained on the 3/8 in. sieve (Q) to the cumulative percent retained on the No. 8 sieve (R). The vertical axis represents what Shilstone and Shilstone Jr. termed the workability factor (WF). The workability factor is a function of the cumulative percent passing the No. 8 sieve (W) and the cementitious material content of the mix (C), as shown in Eqns. 1 and 2.

$$CF = \frac{Q}{R} \times 100 \quad \text{Eqn. 1}$$

$$WF = W + \left(\frac{2.5(C-564)}{94} \right) \quad \text{Eqn. 2}$$

The Shilstone chart has 5 predetermined zones which represent the expected behavior of concrete mixtures which fall within them: Zone I-coarse gap graded, Zone

II-well graded for 1-1/2 in. to 3/4 in. (38 mm to 19mm) NMS, Zone III-well graded for smaller than 3/4 in. (19 mm) NMS or excessive intermediate sizes, Zone IV-sandy and Zone V-rocky. For the concrete in this study, Zone II was the optimum area for the data to plot within. Table 6 shows the selected aggregate percentages for each source, and Fig. 4 shows how the selected gradations fit within the Shilstone chart.

Table 6 – Aggregate gradation proportions

Aggregate source	CC	EBC
#57 limestone	60%	35%
3/8" limestone chip	—	20%
concrete sand	40%	45%

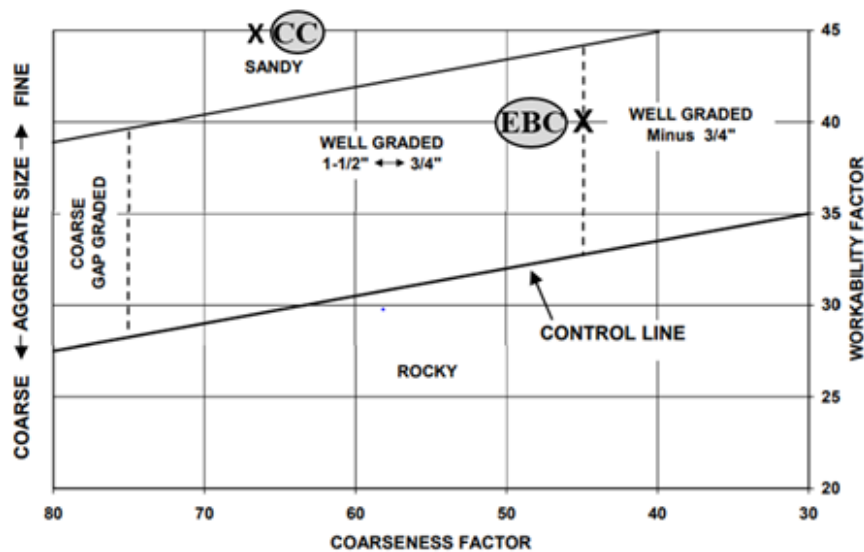


Figure 4 – Shilstone chart

Multiple iterations of gradations were tested in order to achieve the most optimized blend. With all the trial gradations, there was difficulty increasing the #8 size particles. This difficulty is common with commercially available aggregates. By adding the 3/8 in. aggregate, particle packing and workability was improved. While the selected gradation did not meet the criteria for all three methods, it did move towards the acceptable criteria for all, and it met the criteria for the Shilstone chart. The selected

gradation showed the best workability in laboratory testing, which is why it was selected for the next phase.

All three concrete mixtures were delivered by the local Dolese Bros. Co. ready mix plant (Norman, OK). The purpose of using a concrete supplier was to validate the EBC concept in actual concrete production runs, and to maintain the consistency of large batch operations. The mixture proportions for all three mixtures is given in Table 5, and the fresh and hardened concrete properties are given in Table 7.

Fabrication and Curing of Test Specimens

The specimens were constructed and tested in the Donald G. Fears Structural Engineering Laboratory at the University of Oklahoma. After casting, the beam specimens and the quality control/quality assurance companion cylinders [22, 23, 24] and beams [25] were covered with wet burlap and then plastic sheeting for 3 days. After 3 days, all beams and cylinders were removed from their formwork, and were covered with wet burlap and plastic sheeting for the remainder of 7 days. After 7 days, the beams and cylinders were stored in a semi-controlled environment until they were tested at an age of 28 days.

Table 7 – Fresh and hardened concrete properties

Property	CC	EBC1	EBC2
Slump, in.	6	3	5.2
Air content, %	6	7.2	6.3
Unit weight, lb/ft ³	144	141	143
Compressive strength [†] , psi	4,750	4,440	4,810
Modulus of elasticity [†] , ksi	4,250	3,600	4,050
Split cylinder strength [†] , psi	352	365	392
Modulus of rupture [‡] , psi	835	676	712

[†] Values represent an average of three cylinders (ASTM C39, ASTM C469 and ASTM C496)

[‡] Values represent an average of three beams (ASTM C78)

Notes: 1 in. = 25.4 mm; 1 lb/ft³ = 16 kg/m³; 1 psi = 0.00689 MPa; 1 lb/in = 175.1 N/m

Shear Test Setup and Procedure

A load frame was assembled and equipped with a 300 kip (1330 kN), double action hydraulic cylinder intended to apply load to a spreader beam, which was used to transfer the load from the ram into two equal point loads. The shear beams were simply supported with a pin at one end and a roller at the other, each located 1 ft (300 mm) from their respective ends of the beam. The load points and reaction points were located symmetrically with 4 ft (1,200 mm) between each. String potentiometers and strain gauges were used to measure the deflection at midspan of the beam and strain in longitudinal reinforcement. The string potentiometers were attached to the beam at mid-height. The strain gauges were installed on the lower layer of the bottom longitudinal reinforcement at midspan (maximum flexural moment location). Figure 1 shows both the beam loading pattern and the locations of the instrumentation. The load was applied in a quasi-static method in 5 kip (22 kN) intervals. After reaching each successive load step, cracks were marked, and the load was noted. Load, deflection and strain in the reinforcement was monitored until the beam reached failure.

Test Results and Comparison

General Behavior (Cracking and Failure Mode)

Table 8 summarizes the compressive strength of the concrete at the time of testing, shear forces at failure, V_{test} , as well as $V_{\text{test}}/V_{\text{code}}$ for the following codes: ACI 318 [12], AASHTO [26], CSA [27], Eurocode 2 [28] and JSCE [29].

Table 8 – Ratios of experimental to code-predicted capacity

Beam		Cylinder (psi)	V _{test} (kip)	AASHTO	ACI 11-3	ACI 11-5	CSA	Eurocode 2	JSCE
CC	1	4750	32.5	0.92	1.30	0.99	1.40	1.49	0.79
	2		29.5	0.81	1.18	0.90	1.27	1.35	0.71
	3		28.2	0.76	1.13	0.86	1.22	1.29	0.68
			Average	0.83	1.20	0.92	1.30	1.38	0.73
			COV, %	9.9	7.3	7.3	7.2	7.5	7.8
EBC1	1	4440	34.9	1.04	1.44	1.09	1.56	1.63	0.86
	2		32.6	0.95	1.35	1.02	1.46	1.53	0.81
	3		25.7	0.7	1.06	0.80	1.15	1.20	0.64
			Average	0.90	1.28	0.97	1.39	1.45	0.77
			COV, %	19.6	15.5	15.6	15.4	15.5	15.0
EBC2	1	4810	30.1	0.82	1.19	0.91	1.29	1.37	0.73
	2		35.5	1.02	1.41	1.08	1.52	1.62	0.85
	3		34.1	0.97	1.35	1.04	1.46	1.55	0.82
			Average	0.94	1.32	1.01	1.42	1.46	0.80
			COV, %	11.1	8.6	8.8	8.4	8.8	7.8

Note: 1 psi = 0.00689 Mpa; 1 kip = 4.448 kN

In terms of crack morphology and crack progression, the behavior of EBC1 and EBC2 differed from that of CC. Both EBC mixtures developed their first cracks at lower loads than CC and their crack patterns were more irregular. That behavior can be attributed to the reduction in paste, the improved aggregate profile and the presence of fibers. All the beams failed in shear and it occurred when the inclined flexure-shear crack penetrated to the compression zone of the beam near the loading plate, as observed in Fig. 5. None of the longitudinal reinforcement reached yield during testing, as expected, based upon data collected from the attached strain gauges.

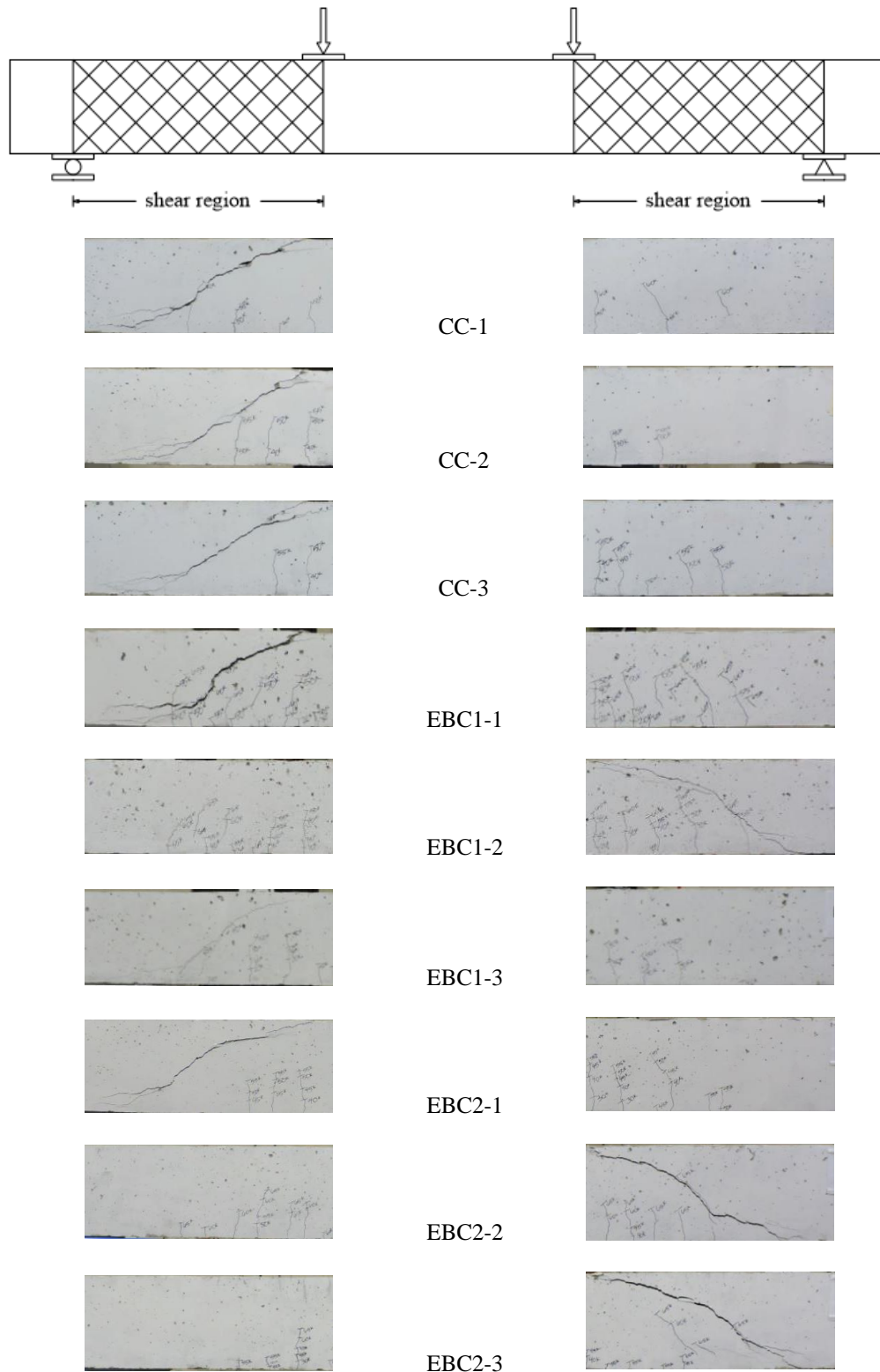


Figure 5 – Crack patterns of beams upon shear failure

Figures 6, 7, and 8 show the load-deflection behavior for each beam from all three mixtures, CC, EBC1, and EBC2, respectively. EBC1 and CC both displayed bi-linear load-deflection behavior with a reduction in the slope of their curves after first developing flexural cracks. Both mixtures displayed similar slopes prior to and after first cracking. They both immediately lost the majority of their load carrying capacity upon reaching their ultimate loads. EBC2 displayed a linear load-deflection behavior throughout the test until ultimate load was reached but displayed plasticity at near ultimate loads. That linearity of the load-deflection response and plasticity must be attributed to the presence of macro-fibers, which functioned like shear reinforcement in the test region.

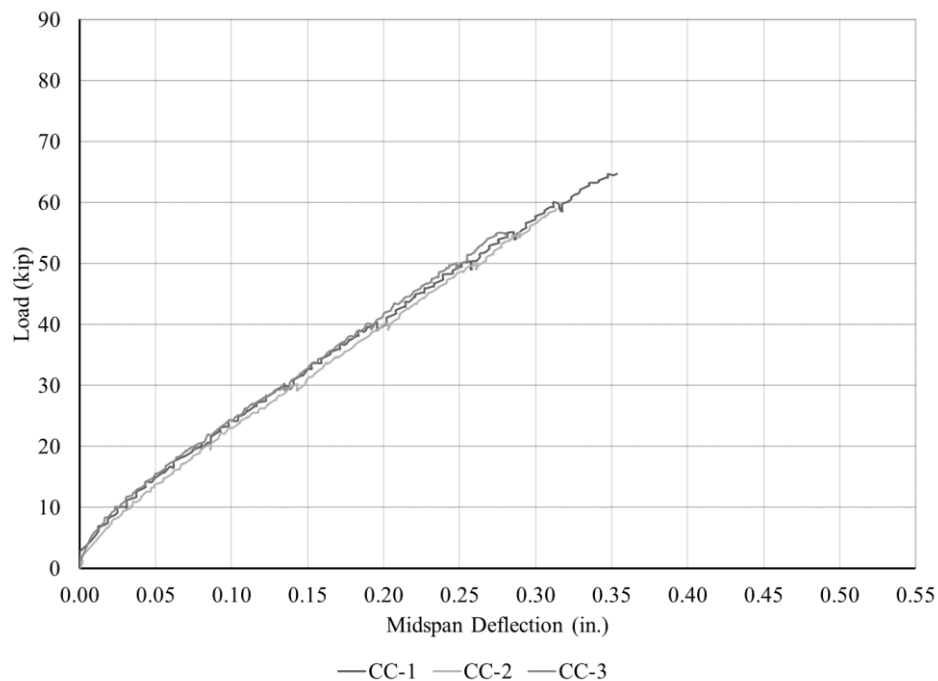


Figure 6 – Control beam load vs deflection plots

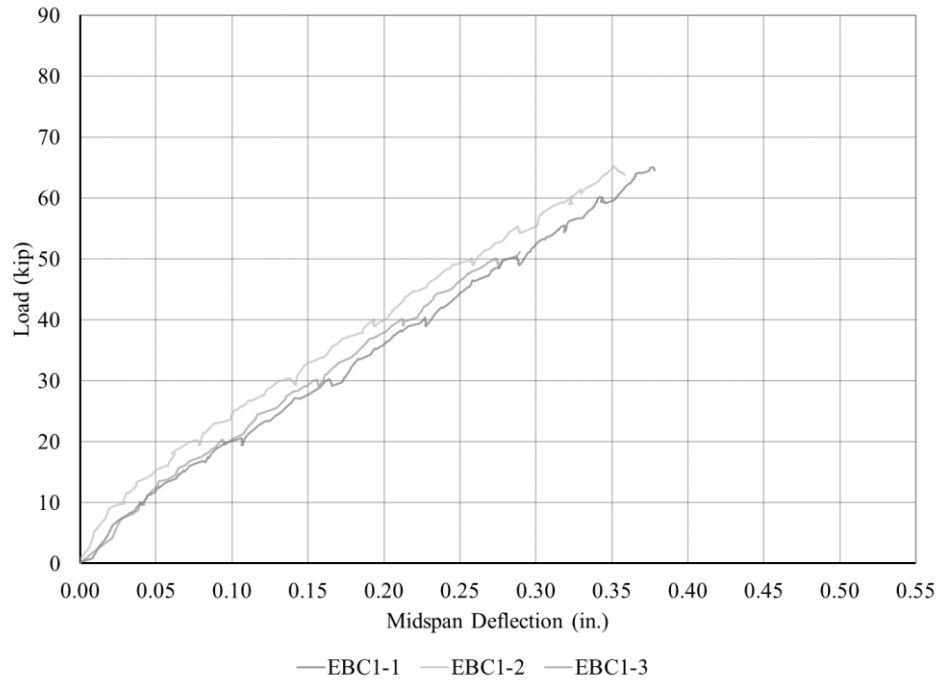


Figure 7 – EBC1 beam load vs deflection plots

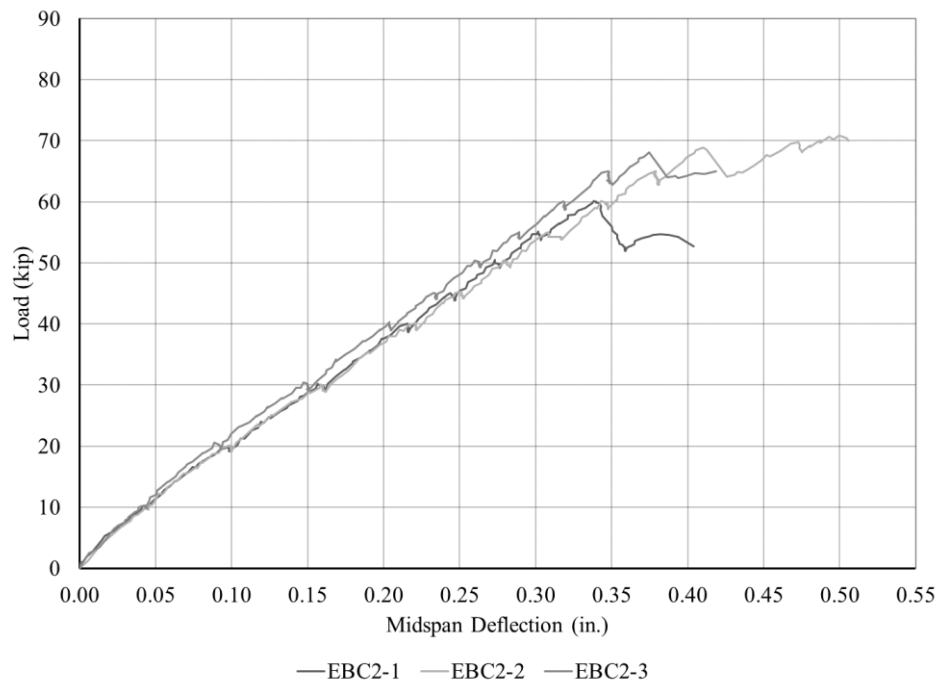


Figure 8 – EBC2 beam load vs deflection plots

Comparison of Test Results with Shear Provisions of Selected International Codes

In the following section, the experimental shear strengths of the beams are compared with the shear provisions of selected international provisions [12, 27, 29, 26,

28]. Table 8 presents the ratio of experimental to code-predicted capacity ($V_{\text{test}}/V_{\text{code}}$) for each of the selected design standards. In general, for a given standard, the ratios for the EBC2 beams are the largest and the ratios for the CC beams are the smallest.

The shear provisions of AASHTO [26] and JSCE [29] are unconservative for every beam in the study. Overall, the ratios from all design codes range from 0.68 to 1.49 for the CC beams, 0.64 to 1.63 for the EBC1 beams and 0.73 to 1.62 for the EBC2 beams. The shear provision of JSCE [29] has the lowest coefficient of variation (COV) and AASHTO [26] has the highest COV. The Eurocode 2 [28] and JSCE [29] show the most and least conservative results for the beams of this study, respectively. With regards to the ratios that fell below 1.0 – an unconservative result – it is important to note that the majority of standards do not allow sections without stirrups unless the factored shear force is significantly less than the concrete capacity in shear. This result has also been reported by other researchers [30].

The increase in shear strength of the EBC1 beams may be attributed to the improved aggregate profile which may increase the aggregate interlock potential, as the micro-fibers are primarily used to minimize crack widths at lower loads. The EBC2 beams appear to have benefited from the combination of improved aggregate interlock and the presence of macro-fibers.

Comparison of Test Results with MCFT Method

The Modified Compression Field Theory (MCFT) was developed by researchers at the University of Toronto [31]. Several codes have incorporated simplified versions of the MCFT including AASHTO [26] and CSA [27]. For this reason, the following section presents the shear strength of the specimens based on the MCFT methods.

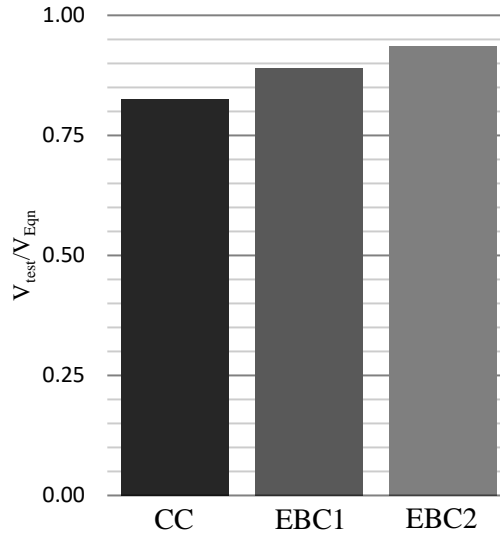


Figure 9 – Ratios of experimental to MCFT predicted capacity

Figure 9 shows that, in general, the MCFT overestimates the shear strength of the beams in this investigation (17% on average for CC, 11% on average for EBC1 and 6% on average for EBC2). Similar to the shear provisions from the design codes, the MCFT method predicts the highest strength for EBC2 and the lowest strength for CC.

Comparison of Test Results with Fracture Mechanics Approach

Researchers have attempted to predict the shear behavior of reinforced concrete members which have no stirrups using fracture mechanics [30, 32, 33]. Bazant and Yu [30] proposed Eqn. 3. Gasteble and May [32] proposed Eqn. 4 which was based on failure being triggered by a splitting crack propagating to the longitudinal reinforcement (Mode I fracture energy). Xu et al. [33] proposed Eqn. 5 which is based on failure being triggered by the loss of bond of the longitudinal reinforcement from the adhered concrete by overcoming the bond fracture resistance (Mode II fracture energy). The International Federation for Structural Concrete (fib) uses Eqn. 6, which is also based on fracture mechanics.

$$V_c = 10\rho^{3/8} \left(1 + \frac{d}{a}\right) \sqrt{\frac{f'_c}{1 + \frac{d}{f'_c 3800 \sqrt{da}}}} b_w d \quad \text{Eqn. 3 (in., psi)}$$

$$V_c = \frac{1.109}{\sqrt{H}} \left(\frac{H}{a}\right)^{1/3} \rho^{1/6} (1 - \sqrt{\rho})^{2/3} f'_c{}^{0.35} \sqrt{E_s} b_w d \quad \text{Eqn. 4 (m, MPa)}$$

$$V_c = \frac{1.018}{\sqrt{d}} \left(\frac{d}{a}\right)^{1/3} \rho^{1/6} (1 - \sqrt{\rho})^{2/3} (0.0255 f'_c + 1.024) b_w d \quad \text{Eqn. 5 (m, MPa)}$$

$$V_c = 150 \left(1 + \sqrt{\frac{0.2}{d}}\right) \left(\frac{3d}{a}\right)^{1/3} (100\rho)^{1/3} f'_c{}^{1/3} b_w d \quad \text{Eqn. 6 (m, MPa)}$$

Figure 10 compares $V_{\text{test}}/V_{\text{Eqn}}$ for the four fracture mechanics approaches noted. The Bazant and Yu equation is the only equation that does not conservatively estimate the shear capacity of the beams tested in this study. The $V_{\text{test}}/V_{\text{Eqn}}$ ratio for Bazant and Yu, Gastebled and May, Xu et al. and the fib equations range from 0.70 to 0.95, 1.00 to 1.36, 1.03 to 1.40 and 0.98 to 1.33 respectively. Figure 10 shows the average $V_{\text{test}}/V_{\text{Eqn}}$ ratio for each concrete type. This approach of predicting the shear performance of reinforced concrete without stirrups shows to be best calibrated based on the limited results from this study. Furthermore, this comparison shows that, similar to the design code shear strength comparisons, the ratios ($V_{\text{test}}/V_{\text{Eqn}}$) for the CC beams are lower than the EBC1 beams and the EBC2 beams. Most importantly, the fracture mechanics approaches appear to be applicable for cement limiting and fiber reinforced concrete.

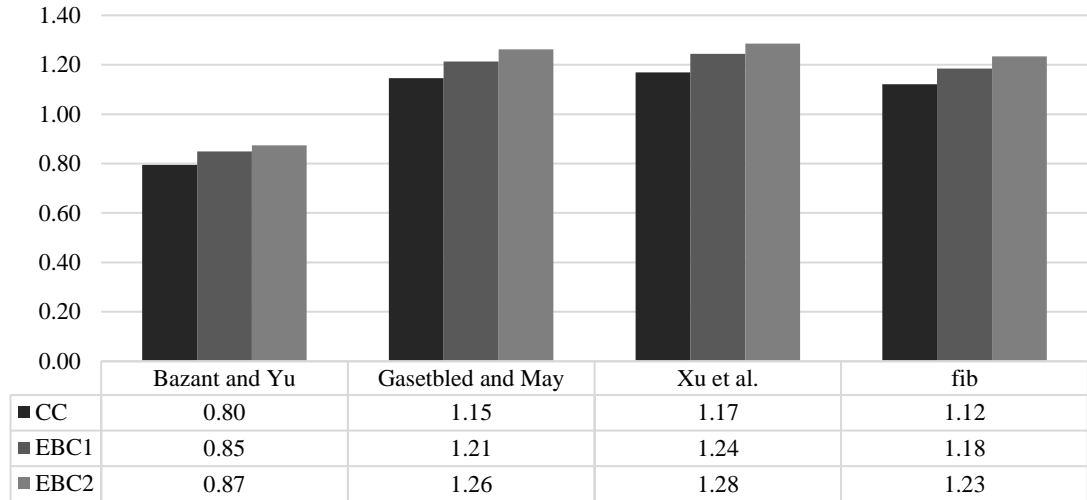


Figure 10 – Ratios of experimental to fracture mechanics predicted capacity

Comparison of Test Results with Shear Database

The shear performance of concrete has been shown to be impacted the most by four key parameters: d – the depth of the member, which impacts the size effect; a/d – the shear span ratio; f'_c – the compressive strength of the concrete; ρ – the longitudinal reinforcement ratio [34]. To evaluate the effect of the aforementioned parameters on the shear strength of the beams, the results of this study are compared with the wealth of shear test data available in the literature [34].

Figures 11, 12 and 13 present the normalized shear stress (shear stress divided by the square root of the compressive strength) versus ρ , d and a/d , respectively. The normalization of the data based on the square root of the compressive strength was selected because that is the relationship most commonly used in shear design equations [12, 27, 26]. Given the significant scatter of the database, it is difficult to draw definitive conclusions on the current test values. However, the data seems to indicate that the CC and EBC tests results fall well within the spread of the existing beam data. These results show that the shear stress at failure for all beams tested were in a

relatively tight group near the center third of the data, and that on average, the EBC2 beams were stronger than the EBC1 and CC beams.

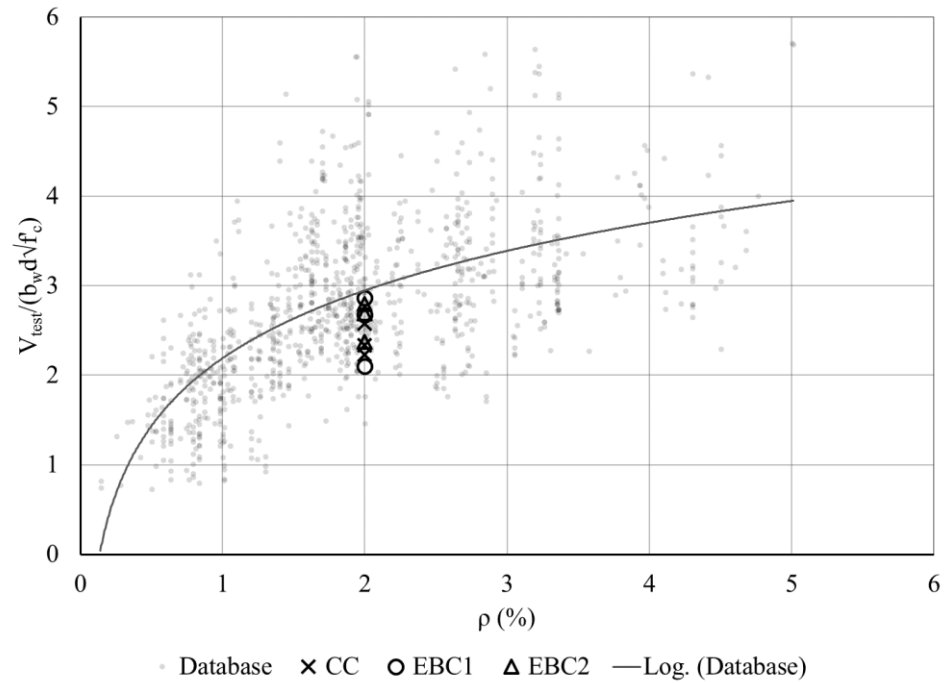


Figure 11 – Normalized shear strength vs. longitudinal reinforcement ratio

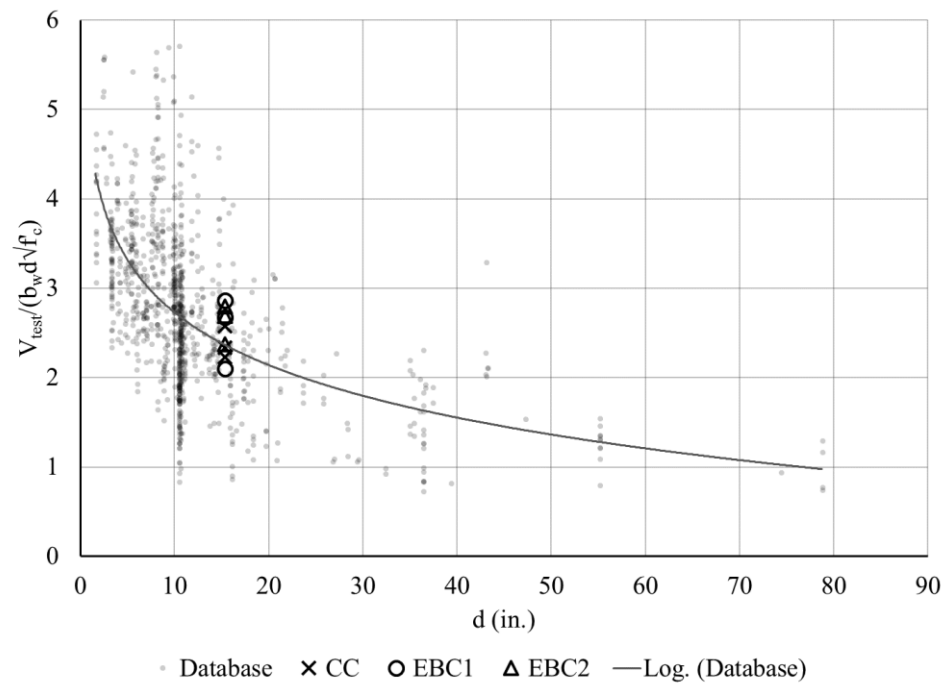


Figure 12 – Normalized shear strength vs. depth

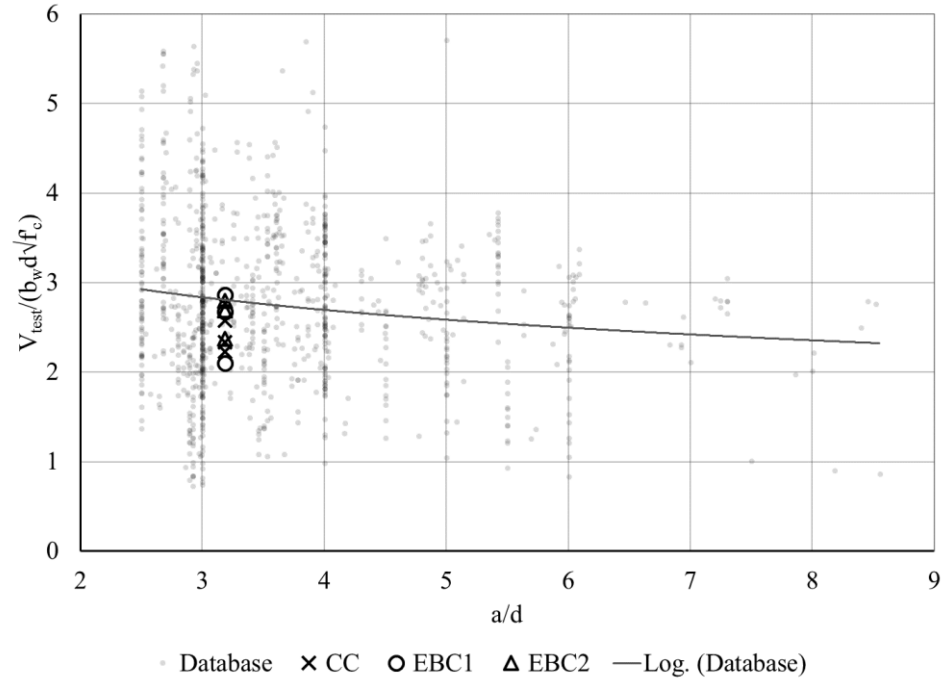


Figure 13 – Normalized shear strength vs. shear span to depth ratio

Comparison of Material Properties and Shear Behavior

Previous research [35] has shown that splitting tensile strength and flexural strength are important parameters affecting the shear strength of concrete. For this reason, the following section compares the relationship between these parameters and the shear strengths for the three mixtures studied in this investigation. To compare the material properties and shear strengths of the CC and EBC beams, the test results have been normalized to reflect the compressive strengths. ACI 318 [12] uses the square root of the compressive strength of concrete to determine the splitting tensile strength, flexural strength and shear strength of beams. Figure 14 shows the ratio of EBC to CC for the normalized splitting tensile strength, flexural strength and shear strength.

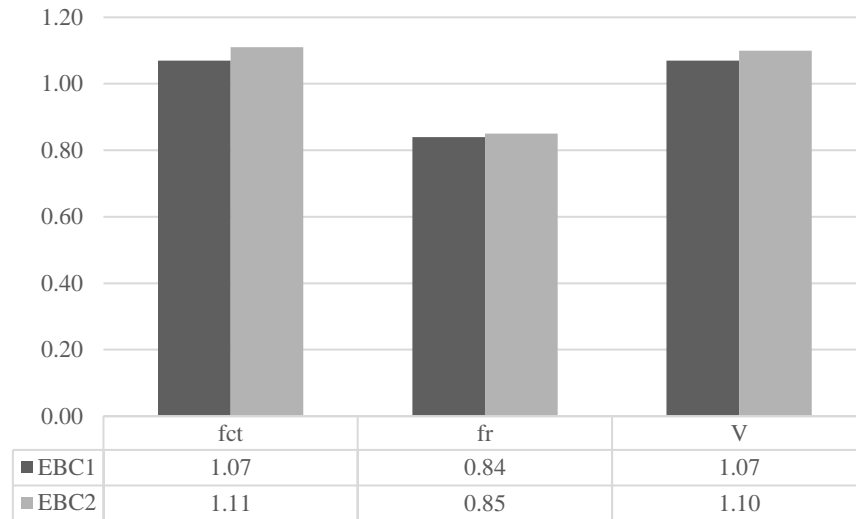


Figure 14 – Ratios of normalized strength of EBC to CC

Mixture EBC1 showed increased splitting tensile strength, decreased flexural strength and increased shear strength at 7%, 16% and 7%, respectively, relative to the CC. Mixture EBC2 also showed similar increased splitting tensile strength, decreased flexural strength and increased shear strength at 11%, 15% and 10%, respectively, relative to the CC. Based on this comparison, it would appear that splitting tensile strength shows the best correlation to shear strength.

Comparison of Test Results with Response-2000

Response-2000 is a sectional analysis program used to calculate the strength and ductility of reinforced concrete members which was developed by Dr. Evan Bentz during his doctoral studies at the University of Toronto [36]. It uses the modified compression field theory to simultaneously consider all possible two-dimensional loading configurations (shear, moment and axial load). The output of the program is a full load-deformation response, member crack diagram and detailed analysis of the failure mechanism.

Response-2000 was used to predict the response of the CC beams as well as the EBC beams. Figures 15, 16 and 17 show the comparison of the average shear versus deflection plots for the CC, EBC1 and EBC2 beams paired with their corresponding Response-2000 predicted behavior. The predicted failure mechanism, crack morphology and ultimate loads for all three concrete types were very close for all three mixtures. However, the actual load-deformation responses for all three mixtures differed from the predicted response. A deviation from the predicted was expected as Response-2000 only allows for a single input on stirrup detailing (spacing, size, strength, etc.), and the beams in this study had stirrups located in the constant moment region of the beam and above the reaction points, which would have decreased the degree of cracking and associated loss of stiffness.

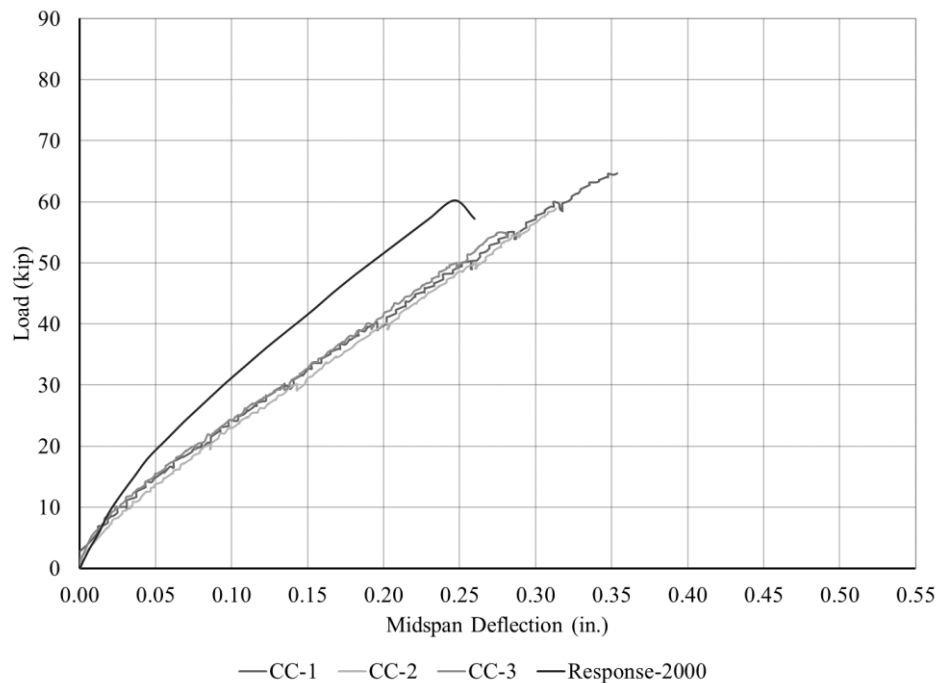


Figure 15 – Response-2000 comparison to CC experimental data

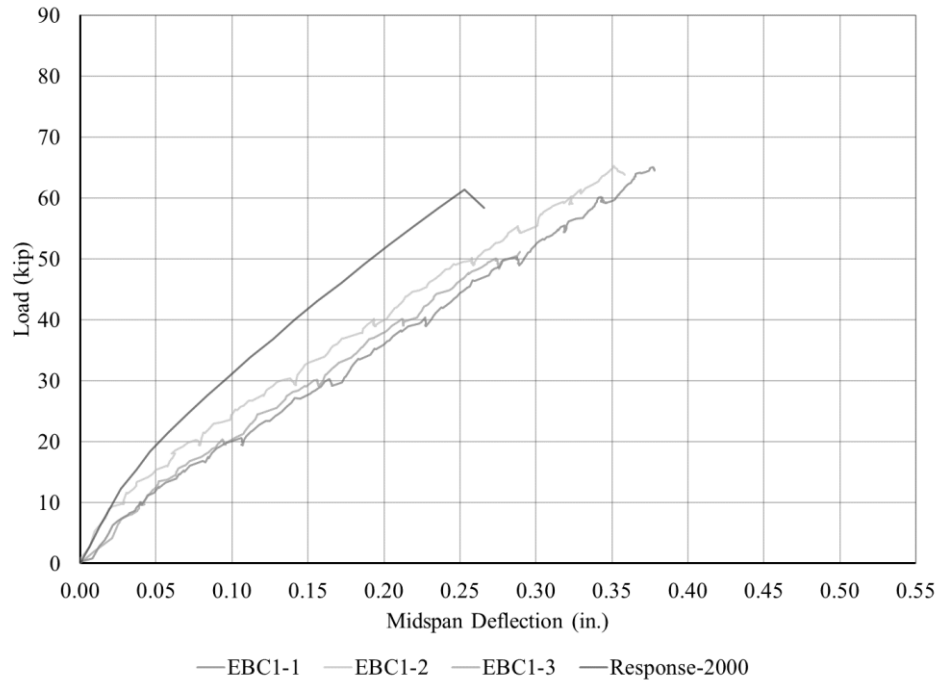


Figure 16 – Response 2000 comparison to EBC1 experimental data

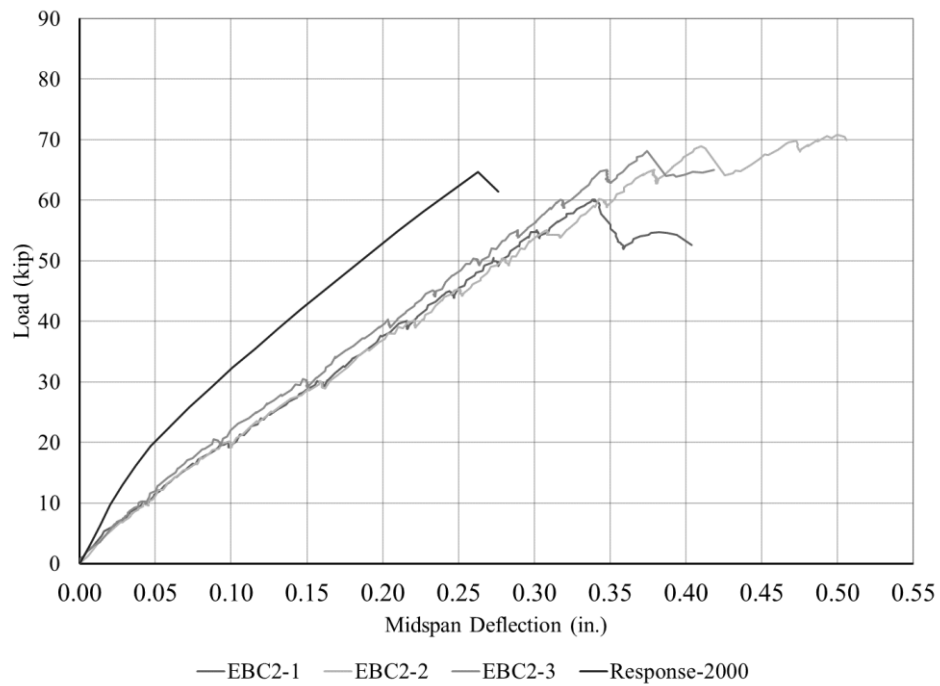


Figure 17 – Response-2000 comparison to EBC2 experimental data

When comparing the curves for each mixture, differences appeared. Both predicted EBC mixtures displayed lower load-deformation slopes than the CC mixture, and EBC2 displayed the lowest slope. This change in slope must be attributed to both

the reduced cementitious (paste) content and the presence of fibers. With reduced paste, the concrete is less able to transfer tension. This leads to increased cracking, as was observed in the tested beams. However, the cracks were thinner than those of the CC beams. For the EBC2 beams, the presence of macro-fibers worked as tensile reinforcement. This increased tensile reinforcement improved strength and increased ductility.

From these results, it appears that Response-2000 is still a viable tool to analyze the ultimate response of cement-limiting and fiber-reinforced concrete. It should be noted that the deformations and crack patterns will vary from those predicted.

Statistical Data Analysis

Statistical tests were used to evaluate whether there is any statistical difference between the normalized shear strengths of the CC and EBC beams. Both parametric and nonparametric statistical tests were performed. Again, the shear strengths were normalized based on the square root of the compressive strength, as is common in most design codes [12, 27, 26].

Parametric Test

The paired t-test is a statistical technique used to compare two population means. This test assumes that the difference between two pairs are normally distributed. If this assumption is violated, the paired t-test may not be the best test to choose. However, we assume that the natural occurring spread of concrete strength data is a normal distribution [37]. Although the previous data showed that the EBC mixtures exhibited an increase in shear strength, the assumptions made for the paired t-test are as follows:

H_{o1} : The mean of normalized shear strength of the CC beams is equal to that of the EBC1 beams.

H_{o2} : The mean of normalized shear strength of the CC beams is equal to that of the EBC2 beams.

H_{o3} : The mean of normalized shear strength of the EBC1 beams is equal to that of the EBC2 beams.

$H_{a1,2,3}$: Not H_o .

The statistical capabilities of Excel were employed to perform these statistical tests. The results of the paired t-test showed that the p-values are 0.386, 0.401 and 0.842 (>0.05) for H_{o1} , H_{o2} and H_{o3} , respectively. These confirm the null hypothesis at the 0.05 significance level. In other words, the normalized shear strengths for all three mixtures are not statistically significantly different. It is worth noting that the data shows that the correlation between the two EBC mixtures is much stronger than those of either EBC mixture to the CC mixture. This means that, while the mixtures are statistically similar, there is a noticeable difference between the mixtures. Also, this data again suggests that the current methods for analyzing concrete can be used on all the mixtures in this study.

Non-Parametric Test

Unlike the parametric tests, nonparametric tests are referred to as distribution-free test. These tests have the advantage of requiring no assumption of normality, and they usually compare medians rather than means. The Wilcoxon sign-ranked test is usually identified as a nonparametric alternative to the paired t-test. The hypotheses for this test are the same as those for the paired t-test. The Wilcoxon sign ranked test assumes that the distribution of the difference of pairs is symmetrical. This assumption

can be made because, as mentioned earlier, a normal distribution is commonly assumed for concrete strength [37], and a normal distribution is symmetric.

The p-values for the Wilcoxon sign-ranked test are 0.175, 0.175 and 0.344 (>0.05) for H_{o1} , H_{o2} and H_{o3} , respectively. These confirm the null hypothesis at the 0.05 significance level. This means that the performance of the three mixtures are not statistically significantly different. Also, there is again a stronger correlation between the two EBC mixture than to the EBC mixtures and the CC mixture. This outcome again suggests that the current methods for analyzing concrete can be used on all mixtures in this study.

Conclusions

To evaluate the shear performance of cement-limiting and fiber-reinforced concrete, three methods of optimizing aggregate gradations were investigated using commonly available materials, and differing levels of micro and macro-fibers were added to the best mixture. From there, 9 full-scale beams (3 for each mixture in the study) without shear reinforcement were constructed and tested to failure. Along with the beams, companion small-scale specimens were constructed and tested. Based on the results of this study, the following conclusions are presented:

1. The Shilstone chart was shown to be the best method tested to optimize aggregate gradations for a concrete mixture.
2. Without a commonly available aggregate source containing larger amounts of #8 size particles, it is difficult to meet the criteria for an optimized aggregate gradation using the three tested methods.

3. The problems with reduced cementitious material (weaker concrete, larger cracks, lower beam strengths) can be offset by utilizing an optimized aggregate gradation and the addition of micro- and macro-fibers.
4. In terms of crack morphology and crack progression, the EBC mixtures cracked more and at lower loads, but the cracks were less wide than those present in the CC beams.
6. In general, for a given standard, the ratios of experimental response to code-predicted capacity for the EBC2 beams are the largest, and those of the CC beams are the lowest.
7. The fracture mechanics approaches best predict the shear strengths of the beams in the study.
8. Statistical data analyses (parametric and nonparametric) indicate that there is no significant difference between the shear capacity of the EBC beams and the CC beams tested in this study.
9. The current methods for analyzing the shear capacity of concrete can be used on all mixtures in this study.

Acknowledgements

The authors gratefully acknowledge the financial and capital support provided by Dolese Bros. Co. and the National University Transportation Center at The University of Oklahoma. The conclusions and opinions expressed in this paper are those of the authors and do not necessarily reflect the official views or policies of the funding institutions.

Notation

a = shear span of beam

b_w = web width

d = distance from extreme compression fiber to centroid of longitudinal tension reinforcement

d_a = maximum aggregate size

E_s = modulus of elasticity of steel

f'_c = specified compressive strength of concrete for use in design

V_c = shear force provided by concrete

v_c = nominal shear stress provided by concrete

ρ = longitudinal reinforcement ratio

References

- [1] J. Butlin, *Our Common Future*. World Commission on Environmental and Development, London: Oxford University Press, 1987.
- [2] U.S. Geological Survey, "Mineral Commodities Summaries," 2017.
- [3] P. Mehta and P. Monteiro, *Concrete: Microstructure, Properties, and Materials*, Third ed., New York: McGraw-Hill, 2006, p. 659.
- [4] L. Lam, Y. Wong and C. Poon, "Effect of Fly Ash and Silica Fume on Compressive and Fracture Behaviors of Concrete," *Cement and Concrete Research*, vol. 28, no. 2, pp. 271-283, February 1998.
- [5] R. Siddique, "Performance characteristics of high-volume Class C fly ash concrete," *Cement and Concrete Research*, vol. 34, no. 3, pp. 487-493, March 2004.
- [6] P. K. Mehta, "High-Performance, High-Volume Fly Ash Concrete for Sustainable Development," in *Proceedings of the International Workshop on Sustainable Development & Concrete Technology*, Beijing, China, 2004.
- [7] M. Berndt, "Properties of sustainable concrete containing fly ash, slag and recycled concrete aggregate," *Construction and Building Materials*, vol. 23, no. 7, pp. 2606-2613, July 2009.
- [8] M. Arezoumandi, M. H. Wolfe and J. S. Volz, "A comparative study of the bond strength of reinforcing steel in high-volume fly ash concrete and conventional concrete," *Construction and Building Materials*, vol. 40, pp. 919-924, March 2013.
- [9] M. Arezoumandi, J. S. Volz, C. A. Ortega and J. J. Myers, "Effect of total cementitious content on shear strength of high-volume fly ash concrete beams," *Materials & Design*, vol. 46, pp. 301-309, April 2013.
- [10] M. Arezoumandi and J. S. Volz, "Effect of fly ash replacement level on the shear strength of high-volume fly ash concrete beams," *Journal of Cleaner Production*, vol. 59, pp. 120-130, November 2013.
- [11] S. Sadati, M. Arezoumandi, K. H. Khayat and J. S. Volz, "Shear performance of reinforced concrete beams incorporating recycled concrete aggregate and high-volume fly ash," *Journal of Cleaner Production*, vol. 115, pp. 284-293, March 2016.

- [12] ACI 318-11, "Building Code Requirements for Structural Concrete and Commentary," The American Concrete Institute, 2011.
- [13] ASTM C150-18, Standard Specification for Portland Cement, ASTM International, 2018.
- [14] ASTM C618-17, Standard Specification for Coal Fly Ash and Raw or Calcined Pozzolan for Use in Concrete, ASTM International, 2017.
- [15] ASTM C33-18, Standard Specification for Concrete Aggregates, ASTM International, 2018.
- [16] ASTM A615-16, Standard Specification for Deformed and Plain Carbon-Steel Bars for Concrete Reinforcement, ASTM International, 2016.
- [17] A. N. Talbot and F. E. Richart, "The Strength of Concrete and Its Relation to the Cement, Aggregate, and Water," University of Illinois at Urbana Champaign, College of Engineering. Engineering Experiment Station., Urbana, IL, 1923.
- [18] D. N. Richardson, "Aggregate Gradation Optimization - Literature Search," Missouri Department of Transportation, 2005, 2005.
- [19] J. M. Shilstone and J. M. Shilstone Jr., "Practical Concrete Mixture Proportioning Technology," Shilstone Software Co., Reference Manual, 1987.
- [20] J. M. Shilstone , "Concrete Mixture Optimization," *Concrete International* 12(6), pp. 33-39, 1990.
- [21] J. M. Shilstone and J. M. Shilstone Jr., "Concrete Mix Analysis - Interpreting the Coarseness Factor Chart," Shilstone Software Co., Newsletter., 1997.
- [22] ASTM C39-18, Standard Test Method for Compressive Strength of Cylindrical Concrete Specimens`, ASTM International, 2018.
- [23] ASTM C469-14, Standard Test Method for Static Modulus of Elasticity and Poisson's Ratio of Concrete in Compression, ASTM International, 2014.
- [24] ASTM C496-17, Standard Test Method for Splitting Tensile Strength of Cylindrical Concrete Specimens, ASTM International, 2017.
- [25] ASTM C78-18, Standard Test Method for Flexural Strength of Concrete, ASTM International, 2018.

- [26] AASHTO, "LRFD Bridge Design Specifications," American Association of State Highway and Transportation Officials, 2015.
- [27] CSA, "Concrete Materials and Methods of Concrete Construction/Methods of Test for Concrete," CSA Group, 2004.
- [28] IStructE, "Manual for the design of concrete building structures to Eurocode 2," The Institution of Structural Engineers, 2006.
- [29] JSCE, "Standard Specifications for Concrete Structures," Japan Society of Civil Engineers, 2007.
- [30] Z. P. Bazant and Q. Yu, "Design Against Size Effect on Shear Strength of Reinforced Concrete Beams without Stirrups: I, Formulation," *Journal of Structural Engineering*, vol. 131, no. 12, pp. 1877-1885, 2005.
- [31] F. J. Vecchio and M. P. Collins, "The Modified Compression-Field Theory for Reinforced Concrete Elements Subjected to Shear," *ACI Journal*, 1986.
- [32] O. J. Gasteble and I. M. May, "Fracture Mechanics Model Applied to Shear Failure of Reinforced Concrete BEams without Stirrups," *ACI Structural Journal*, vol. 131, no. 12, pp. 184-190, 2001.
- [33] S. Xu, X. Zhang and H. W. Reinhardt, "Shear Capacity Prediction of Reinforced Concrete BEams without Stirrups Using Fracture Mechanics Approach," *ACI Structural Journal*, vol. 109, no. 5, pp. 705-714, 2012.
- [34] K. H. Reineck, D. A. Kuchma, K. S. Kim and S. Marx, "Shear Database for Reinforced Concrete Members without Shear Reinforcement," *ACI Structural Journal*, vol. 100, no. 2, pp. 240-249, 2003.
- [35] ACI Committee 445, "Recent Approaches to Shear Design of Structural Concrete," American Concrete Institute, Farmington Hills, MI, 1999.
- [36] E. C. Bentz, Sectional Analysis of Reinforced Concrete Members, University of Toronto, 2000.
- [37] P. Dayaratnam and R. Ranganathan, "Statistical Analysis of Strength of Concrete," *Building and Environment*, vol. 11, pp. 145-152, 1976.

II. Beam Shear Behavior of Fiber-Reinforced Self-Consolidating Concrete

Jonathan T. Drury and Jeffery S. Volz

Abstract

An experimental investigation was conducted to evaluate the mechanical properties and shear behavior of large-scale beams constructed with fiber-reinforced self-consolidating concrete (FR-SCC) with variable amounts of expansive cement. This study included two FR-SCC mixtures, one having a 10 percent replacement of cement with Komponent® (K10) and one having a 15 percent replacement of cement with Komponent® (K15), and one conventional concrete (CC) mixture. The study consisted of 9 beams with identical reinforcement for every beam. The experimental data was then compared to shear provisions for both U.S. and international design codes. Furthermore, the shear performance of the beams was evaluated based on fracture mechanics approaches, Modified Compression Field Theory (MCFT), a shear database of CC beams, materials properties testing and Response-2000. Finally, statistical data analyses were performed to evaluate whether there were any statistically significant differences between the performance of the FR-SCC and CC beams.

Results of this study show that, for FR-SCC, the splitting tensile strength correlates well to the shear strength, and that modulus of rupture is a poor indicator of shear strength. Also, concrete crack morphology and stresses in the longitudinal bars showed that the presence of fibers had an impact on the internal stresses of the test region in all cases. The average normalized shear strength of K10 matched that of CC and K15 was 7% weaker than CC. Statistical analysis showed strong correlations between CC and K10 and weak correlations between K15 and K10 as well as between

K15 and CC. This statistical correlation, along with the other findings, shows that fiber reinforced concrete creates problems when using current design methods to predict performance. Fracture mechanics approaches and MCFT were shown to predict concrete behavior well for all three concrete mixtures.

Keywords

Concrete; Fiber-Reinforced; Self-Consolidating; Shear; Beam(s); Mechanical Properties; Komponent

Introduction

Self-consolidating concrete (SCC) is a relatively new construction material. In 1986, Professor Okamura conceived the idea to combat issues of limited skilled labor in the Japanese precast industry [1]. He envisioned a concrete material that could use the advancements in chemical admixtures to consolidate under its own weight, thereby eliminating the need for skilled workers to properly consolidate the concrete. In 1988 the first useable version of SCC was created, and the first high profile application of SCC was the in the anchor blocks for the Akashi Kaikyo Bridge [2].

It was observed early on that shrinkage was a problem that must be resolved to use SCC successfully [3, 4, 5]. While shrinkage is always an issue in concrete, the increased paste volumes of SCCs allows for the potential of more detrimental shrinkage. Shrinkage can lead to unsightly cracks in pavements, but in structural applications, more catastrophic problems can arise. For this reason, researchers have and still do investigate the shrinkage problem in SCC [6].

Kassimi and Khayat investigated the shrinkage problem and possible mitigation techniques [7]. They investigated 13 different mixtures of concrete and mortar using

different fibers, shrinkage reducers and expansive agents. The fibers were intended to both reduce cracks from forming and restraining them if they would form. The shrinkage reducers and expansive agents were intended to help volumetrically stabilize the mixtures, and thus eliminate shrinkage cracks. They concluded that their best solution came from a mixture with steel fibers and an expansive agent.

Other researchers have also investigated the benefits of combining fiber reinforced concrete (FRC) and SCC [8]. They termed this new concrete fiber-reinforced, self-consolidating concrete (FR-SCC). This research has primarily been focused on the fresh and hardened properties of SCC and FR-SCC, as they have both been found to be useful in repairing damaged concrete structures. Many of the researchers have focused on steel fibers, as the initial research showed that steel outperformed synthetic fibers. From that research, the American Concrete Institute (ACI) included provisions for allowing discrete steel fibers to take the place of minimum transverse reinforcement. However, steel fibers can be more difficult to work with and are more expensive.

Of the limited research into the structural performances of SCC and FR-SCC, again many have primarily investigated the use of steel fibers. The reporting on SCC is scattered as many researchers have stated that there is a reduction in shear and flexural strengths, and many have also stated the opposite [5, 9, 10, 11, 12]. This is not completely unexpected as SCC is a new material with a range of possible configurations and its behavior is very dependent on material properties and qualities.

This scatter in the current data proves that there is a need for more structural testing of FR-SCC, and especially those containing synthetic fibers. Based on the earlier

findings, it is apparent that expansive agents may play a key role in the overall performance of FR-SCC. For these reasons, the current study was performed.

Research Significance

Based on a review of the existing literature, there is a lack of full scale shear testing of specimens constructed with fiber-reinforced, self-consolidating concrete (FR-SCC). Without this background, there is no quantitative basis for implementing FR-SCC in structural design. Consequently, the authors developed a testing plan to evaluate the shear strength of specimens constructed with FR-SCC as a function of the percentage of expansive agent added to the mixture. Fibers were added to the concrete mixtures to improve the shear performance commonly lost when using rounded aggregate with self-consolidating concrete (SCC). The expansive agent was added to improve dimensional stability of the concrete, rebar bond and engagement of the fibers.

Experimental Program

Test Beam Design

Nine beams (three beams for each concrete mixture) were constructed without shear reinforcement in the test region and were designed with reinforcement ratios of 1.98% to preclude flexural failure and satisfy the minimum longitudinal reinforcement requirements of ACI 318 [13]. All the beams tested in this study had a rectangular cross-section with a width of 12 in. (305 mm), a height of 18 in. (457 mm), a shear span to depth ratio greater than 3.0 and 6 No. 7 (22 mm) longitudinal reinforcement bars within the tension zone of the beam section (Fig. 1).

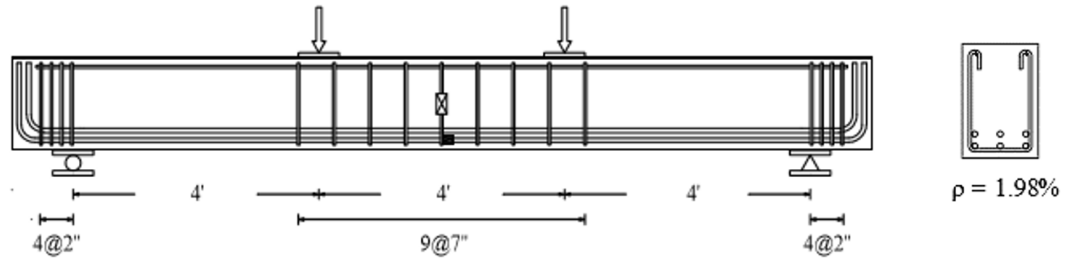


Figure 1 - Load pattern, rebar detail, cross section and location of instrumentation

Concrete Materials

There were three cementitious materials used in this study. The primary cementitious material was a Type I/II portland cement from Ash Grove Cement Company (Chanute, KS) which conformed to ASTM C-150 [14] specifications for both Type I and Type II cements. The second cementitious material used in this study was a Class C fly ash from Headwaters Resources (Jeffery Plant, St. Mary's, KS) which conformed to ASTM C-618 [15] specifications. The third cementitious material used in this study was a proprietary expansive cement called Komponent® from CTS Manufacturing Corp (Cypress, CA). Komponent® is an expansive calcium sulfoaluminate (CSA) cement-based additive that is used to produced ASTM C845 Type K Shrinkage Compensating cement. A detailed summary of the test results for the properties of the cement and fly ash is given in Table 1.

There were three aggregate sources used in this study. The coarse aggregate used for the conventional concrete was crushed limestone from the Dolese Bros Co Davis Quarry (Davis, OK) which conformed to ASTM C-33 [16] specifications for a size #57. The coarse aggregate for the FR-SCC was a 3/8" pea gravel from Metro Materials (Norman, OK). The fine aggregate used in all three concrete mixtures was a concrete sand from Dolese Bros Co. East Sand Plant (Oklahoma City, Oklahoma)

which conformed to ASTM C-33. A detailed summary of the properties of the aggregates is given in Table 2.

Table 1 – Cementitious material properties

Property	Type I/II Cement	Class C fly ash
Fineness (+325 mesh), %	—	10.3
Air permeability, ft ² /lb	1939	—
Specific gravity	3.11	2.72
Loss on ignition, %	2.4	0.67
Silica, %	20.8	31.9
Aluminum oxide, %	3.8	20.4
Ferric oxide, %	3	5.9
Sulfur trioxide, %	2.9	3.0
Calcium oxide, %	63.9	28.3
Magnesium oxide, %	1.9	7.2

Note: 1 ft²/lb = 2.05 cm²/g

Table 2 - Aggregate properties

Property	#57	3/8" pea gravel	Concrete sand
Specific gravity, oven-dry	2.69	2.59	2.65
Dry-rodded unit weight, lb/ft ³	101	105	—
Absorption, %	0.86	0.72	0.7
LA abrasion, % loss	26	22	—
Mohr's hardness	3.5 - 4	3 – 3.5	—

Note: 1 lb/ft³ = 16 kg/m³

The fibers used in this study were a polypropylene macro-fiber from BASF (Florham, NJ) called MasterFiber MAC Matrix. The fibers had a length of 2.1 in. (19 mm) and a diameter of approximately 0.03 in. (0.8 mm). A detailed summary of the fibers properties given by the manufacturer is given in Table 3.

The reinforcing steel used in this study was all ASTM A615 [17] Grade 60 (414 MPa). All of the bars were from the same heat of steel, used the same deformation pattern and met the requirements of ASTM A615 [17]. The longitudinal bars were sampled and tested in tension to determine their properties. Testing showed that the bars had an average yield strength of 78 ksi (537 MPa), an average ultimate strength of 109 ksi (751 MPa) and an average modulus of elasticity of 28,600 ksi (197,000 MPa).

Table 3 – Fiber properties

Property	MasterFiber MAC Matrix
Specific gravity	0.91
Absorption	Nil
Tensile strength, ksi	85
Nominal length, in.	2.1
Nominal diameter, in.	0.03
Material	Polypropylene

Notes: 1 in. = 25.4 mm; 1 ksi = 6.89 MPa

There were two admixtures used in this study. A high-range water reducer (HRWR) was selected from BASF (Florham Park, NJ). The HRWR, called MasterGlenium 7920, was selected because of its high usage in the region, improved potency and ability to maintain workability benefits longer than its competition. The air entraining admixture (AEA) was also selected from BASF (Florham Park, NJ). The AEA, called MasterAir AE 90, was selected due to its high usage in the region and its excellent performance record.

Mixture Proportions

This research was focused on structural concrete for bridge applications in Oklahoma. As such, the conventional concrete (CC) mixture was designed to comply with Oklahoma Department of Transportation (ODOT) design and performance specifications for Class AA concrete, which is required for superstructure concrete. The performance and design specification for an ODOT Class AA concrete are listed in Table 4. A variety of possible CC mixtures were tested, and the CC mixture selected had the proportions as listed in Table 5. This mixture was used to construct control specimens to serve as baseline comparisons to the FR-SCC mixtures.

Table 4 – ODOT Class AA design and performance specifications

Min. cementitious content (lb/yd ³)	Air content* (%)	w/cm	Slump ^{**†} (in.)	Min. 28-day strength ^{**} (psi)
564	6.5 ± 1.5	0.25-0.44	2 ± 1	4,000

* Values are based on ASTM C231

* Values are based on ASTM C143

** Values are based on ASTM C39

† Slump range only applies for concrete made without admixtures

Notes: 1 in. = 25.4 mm; 1 lb/yd³ = 0.593 kg/m³; 1 psi = 0.00689 MPa; 1 lb/in = 175.1 N/m

The FR-SCC mixtures were designed to conform to most of the performance specifications of the ODOT Class AA with slump being the exception. This exception is due to the ODOT specification making no reference to SCC. To achieve quality flow properties, the 3/8" pea gravel was used. Many SCC mixtures were tested until a stable slump flow of 30 ± 2 in. (760 ± 50 mm) was achieved. This high slump flow was targeted with the knowledge that the slump flow would be reduced with the addition of the fibers.

Table 5 – Mixture designs (per yd³)

	CC	K10	K15
Type I/II cement	470	451	413
Class C fly ash	118	224	224
Komponent®	—	76	113
w/cm	0.4	0.39	0.39
#57 limestone, lb	1857	—	—
3/8" pea gravel, lb	—	1223	1223
Concrete sand, lb	1323	1401	1401
Macro-fiber, lb	—	7.7	7.7
HRWR, fl oz	26.7	67.6	67.6
AEA, fl oz	4.4	8.3	8.3
Citric acid, g	—	117	176

Notes: 1 lb = 0.454 kg; 1 fl oz = 29.5 mL

Note: CC and SCC mixtures have different level of cementitious material

With the pea gravel having a smooth surface and low absorption, a reduction in shear performance was expected. Fibers were added to overcome the detrimental effects

of the use of pea gravel and control shrinkage cracking. With the selected SCC mixture, fibers were added, and the slump flow was again measures. The target slump flow for the FR-SCC was 28 ± 2 in. (710 ± 50 mm). The selected FR-SCC mixture proportions are detailed in Table 5. The fresh and hardened properties are shown in Table 6.

Fabrication and Curing of Test Specimens

The specimens were constructed and tested in the Donald G. Fears Structural Engineering Laboratory at the University of Oklahoma. After casting, the beam specimens and the quality control/quality assurance companion cylinders [18, 19, 20] and beams [21] were covered with wet burlap and then plastic sheeting for 3 days. After 3 days, all beams and cylinders were removed from their formwork, and were covered with wet burlap and plastic sheeting for the remainder of 7 days. After 7 days, the beams and cylinders were stored in a semi-controlled environment until they were tested at an age of 28 days.

Table 6 – Fresh and hardened concrete properties

Property	CC	K10	K15
Slump or slump flow, in.	6	32	30
Air content, %	6	9.0	10.5
Unit weight, lb/ft ³	144	123	139
Compressive strength [†] , psi	4,750	4,740	6,010
Modulus of elasticity [†] , ksi	4,250	3,952	4,081
Split cylinder strength [†] , psi	352	406	511
Modulus of rupture [‡] , psi	835	559	549

[†] Values represent an average of three cylinders (ASTM C39, ASTM C469 and ASTM C496)

[‡] Values represent an average of three beams (ASTM C78)

Notes: 1 in. = 25.4 mm; 1 lb/ft³ = 16 kg/m³; 1 psi = 0.00689 MPa; 1 lb/in = 175.1 N/m

Shear Test Setup and Procedure

A load frame was assembled and equipped with a 300 kip (1330 kN), double action hydraulic cylinder intended to apply load to a spreader beam, which was used to

transfer the load from the ram into two equal point loads. The shear beams were simply supported with a pin at one end and a roller at the other, each located 1 ft (300 mm) from their respective ends of the beam. The load points and reaction points were located symmetrically with 4 ft (1,200 mm) between each. String potentiometers and strain gauges were used to measure the deflection at midspan of the beam and strain in the longitudinal reinforcement. The string potentiometers were attached to the beam at mid-height. The strain gauges were installed on the lower layer of the bottom longitudinal reinforcement at midspan (maximum flexural moment location). Figure 1 shows both the beam loading pattern and the locations of the instrumentation. The load was applied in a quasi-static method in 5 kip (22 kN) intervals. After reaching each successive load step, cracks were marked, and the load was noted. Load, deflection and strain in the reinforcement was monitored until the beam reached failure.

Test Results and Comparison

General Behavior (Cracking and Failure Mode)

Table 7 summarizes the compressive strength of the concrete at the time of testing, shear forces at failure, V_{test} , as well as V_{test}/V_{code} for the following codes: ACI 318 [13], AASHTO [22], CSA [23], Eurocode 2 [24] and JSCE [25].

In terms of crack morphology and crack progression, the behavior of the FR-SCC beams differed vastly from that of the CC beams. The FR-SCC beams had smaller crack widths and a more irregular crack pattern. That behavior can most likely be attributed to the presence of fibers. All the beams failed in shear and it occurred when the inclined flexure-shear crack penetrated to the compression zone of the beam near the loading plate, as observed in Fig. 2. A major difference between the ultimate

failure behavior of the FR-SCC and CC beams was that after the failure crack was formed in the FR-SCC beams, the fibers provided an increased strength as well as added plastic behavior. None of the longitudinal reinforcement reached yield during testing, as expected, based upon data collected from the attached strain gauges.

Table 7 – Ratios of experimental to code-predicted capacity

Beam		Cylinder (psi)	V _{test} (kip)	AASHT O	ACI 11-3	ACI 11-5	CSA	Eurocod e 2	JSCE
CC	1	4750	32.5	0.92	1.30	0.99	1.40	1.49	0.79
	2		29.5	0.81	1.18	0.90	1.27	1.35	0.71
	3		28.2	0.76	1.13	0.86	1.22	1.29	0.68
			Average	0.83	1.20	0.92	1.30	1.38	0.73
			COV, %	9.9	7.3	7.3	7.2	7.5	7.8
	K10	1	4460	30.8	0.96	1.27	0.96	1.37	1.44
2		26.6		0.80	1.10	0.83	1.18	1.24	0.66
3		30.0		0.93	1.24	0.94	1.34	1.40	0.74
		Average	0.90	1.20	0.91	1.30	1.53	0.72	
		COV, %	9.5	7.5	7.7	7.9	1.4	7.3	
K15		1	5910	32.8	0.91	1.18	0.92	1.27	1.40
	2	29.8		0.80	1.07	0.84	1.15	1.27	0.67
	3	29.2		0.78	1.04	0.82	1.13	1.24	0.65
			Average	0.83	1.10	0.86	1.18	1.46	0.69
			COV, %	8.4	6.7	6.2	6.4	5.8	6.9

Note: 1 psi = 0.00689 Mpa; 1 kip = 4.448 kN

Figures 3, 4, and 5 show the load-deflection behavior for each beam from all three mixtures, CC, K10, and K15, respectively. The CC beams displayed a traditional bi-linear load-deflection behavior with a reduced slope of their curves after developing the first flexural cracks, and total failure occurred after reaching the ultimate load. The K10 and K15 beams, on the other hand, displayed a nearly linear load-deflection behavior from first loading up to the ultimate loads. Also, the FR-SCC beams maintained approximately 80% of their load carrying capacity after reaching their ultimate load. The linearity observed in the load-deflection response is most likely

attributed to the presence of the macro-fibers, which function like shear reinforcement in the test region.

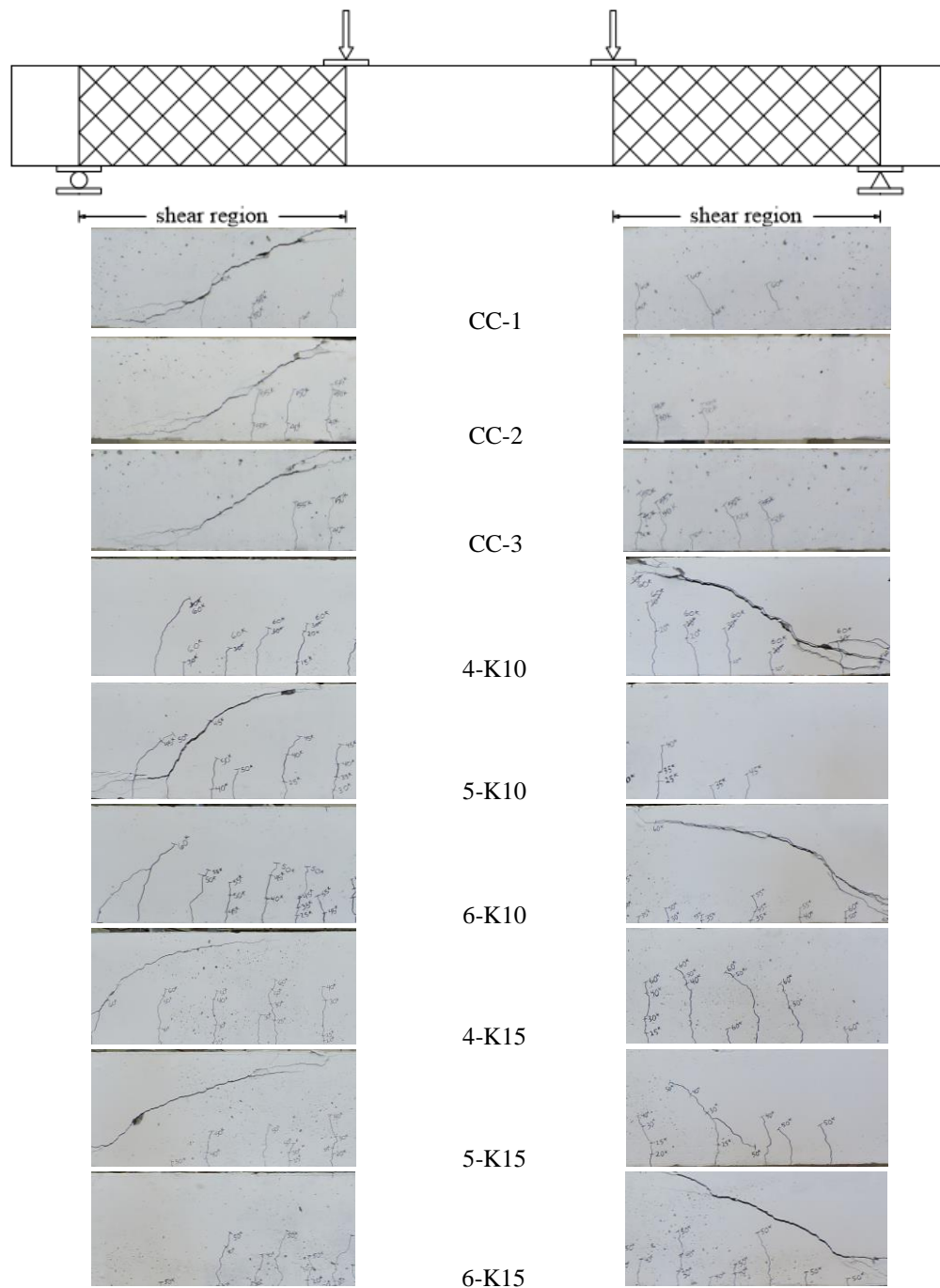


Figure 2 – Crack patterns of beams upon shear failure

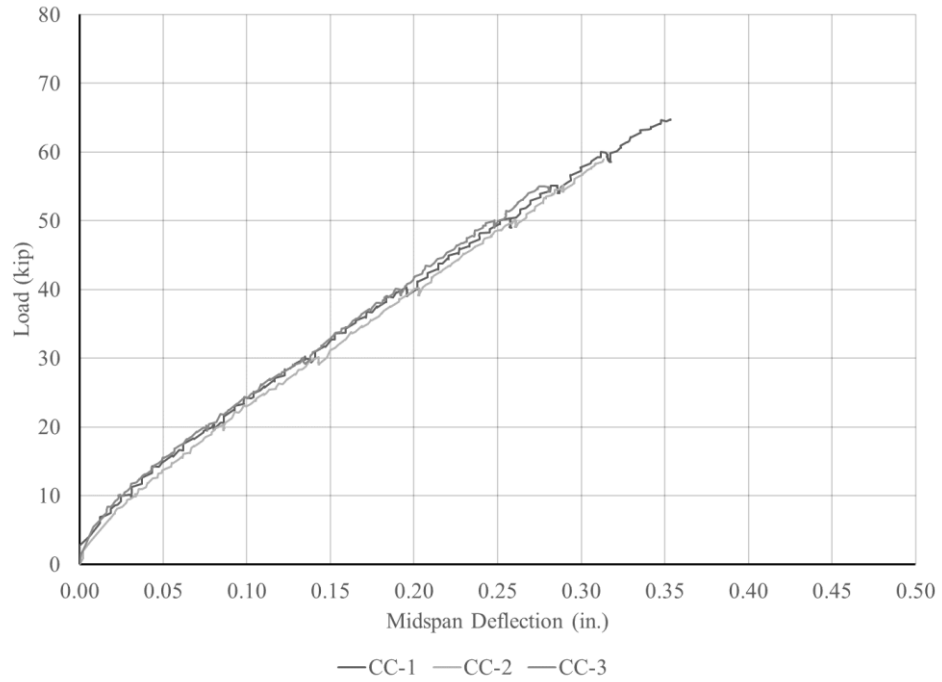


Figure 3 – Control beam load vs deflection plots

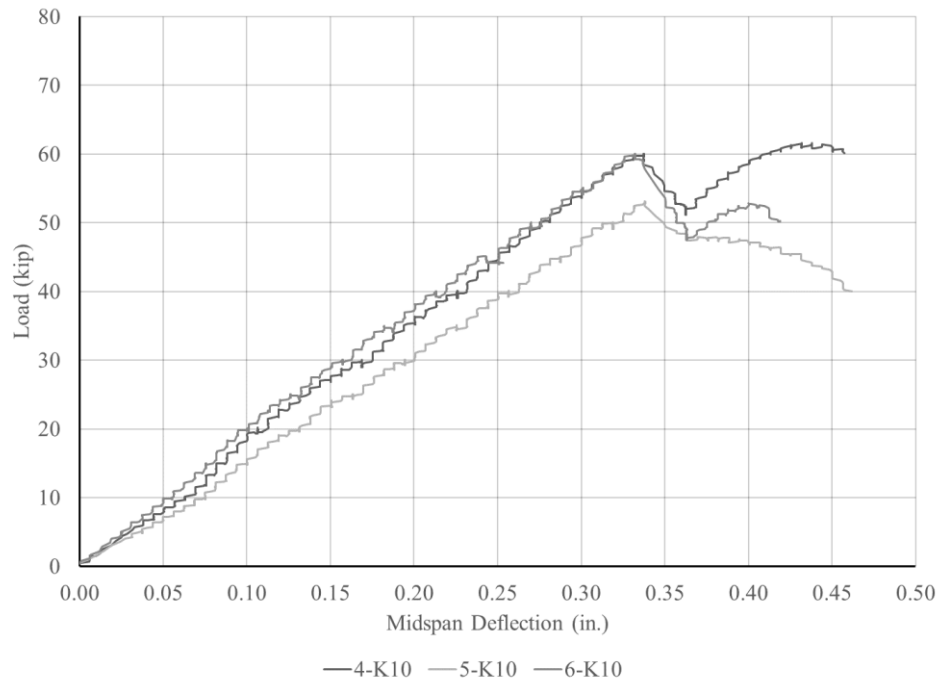


Figure 4 – K-10 beam load vs deflection plots

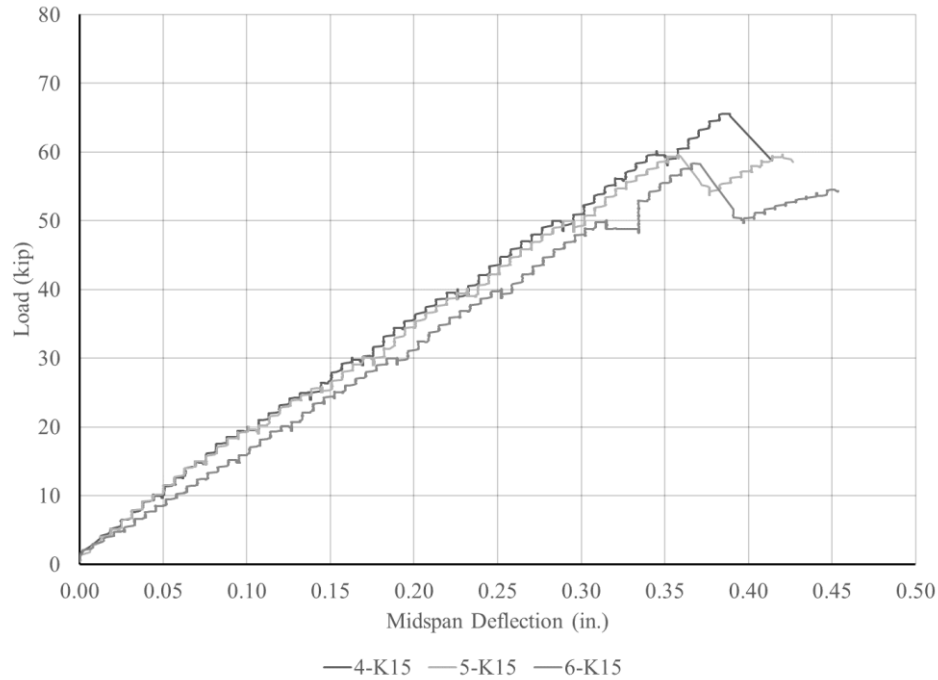


Figure 5 – K-15 beam load vs deflection plots

Comparison of Test Results with Shear Provisions of Selected International Codes

In the following section, the experimental shear strengths of the beams are compared with the shear provisions of selected international provisions [13, 23, 25, 22, 24]. Table 7 presents the ratio of experimental to code-predicted capacity ($V_{\text{test}}/V_{\text{code}}$) for each of the selected design standards. In general, for a given standard, the ratios for the CC beams are the largest and the ratios for the K15 beams are the smallest.

The shear provisions of AASHTO [22], ACI 318 11-5 [13] and JSCE [25] are unconservative for every beam in the study (i.e., ratios less than 1.0). Overall, the ratios from all design codes range from 0.68 to 1.49 for the CC beams, 0.66 to 1.44 for the K10 beams and 0.65 to 1.40 for the K15 beams. Also, the average ratio from all design codes was 1.06 for the CC beams, 1.06 for the K10 beams and 0.99 for the K15 beams. The shear provisions of the Eurocode 2 [24] had the lowest coefficient of variation (COV) and AASHTO [22] had the highest COV. The Eurocode 2 [24] and JSCE [25]

show the most and least conservative results for the beams of this study, respectively. With regards to the ratios that fell below 1.0 – an unconservative result – it is important to note that the majority of standards do not allow sections without stirrups unless the factored shear force is significantly less than the concrete capacity in shear. This result has also been reported by other researchers [26].

While the K15 beams showed an unconservative prediction on average and the K10 beams showed similar ratios to those of the CC beams, it is of note that the fibers present in the concrete affect the compressive strength and shear strength proportionally different than do traditional concrete constituents. However, it is noteworthy that, SCC can perform as well in shear when long fibers are added to the mix.

Comparison of Test Results with MCFT Method

The Modified Compression Field Theory (MCFT) was developed by researchers at the University of Toronto [27]. Several codes have incorporated simplified versions of the MCFT including AASHTO [22] and CSA [23]. For this reason, the following section presents the shear strength of the specimens based on the MCFT methods.

Figure 6 shows that, in general, the MCFT overestimates the shear strength of the beams in this investigation (17% on average for CC, 10% on average for K10 and 17% on average for K15). Unlike the shear provisions from the design codes, the MCFT method predicts similar strengths for CC and K15 and lower strengths for K10.

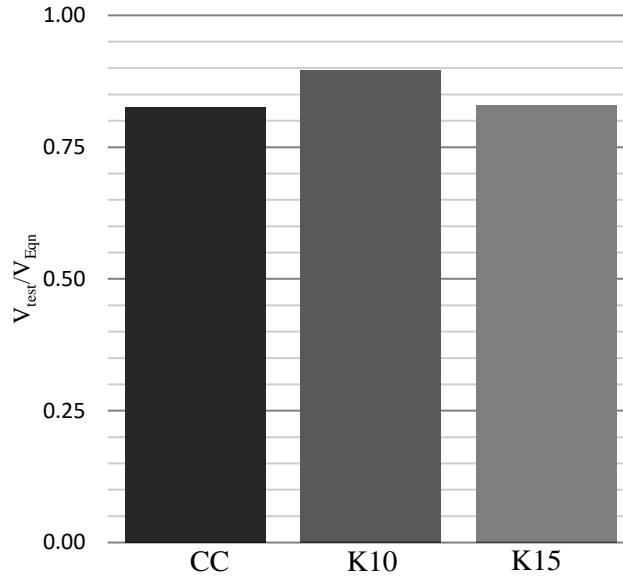


Figure 6 – Ratios of experimental to MCFT predicted capacity

Comparison of Test Results with Fracture Mechanics Approach

Researchers have attempted to predict the shear behavior of reinforced concrete members which have no stirrups using a fracture mechanics approach [26, 28, 29]. Bazant and Yu [26] proposed Eqn. 1, Gasteble and May [28] proposed Eqn. 2, which was based on failure being triggered by a splitting crack propagating to the longitudinal reinforcement (Mode I fracture energy). Xu et al. [29] proposed Eqn. 3, which is based on failure being triggered by the loss of bond of the longitudinal reinforcement from the adhered concrete by overcoming the bond fracture resistance (Mode II fracture energy). The International Federation for Structural Concrete (fib) uses Eqn. 4, which is also based on a fracture mechanics approach.

$$V_c = 10\rho^{3/8} \left(1 + \frac{d}{a}\right) \sqrt{\frac{f'_c}{1 + \frac{d}{f'_c 3800 \sqrt{da}}}} b_w d \quad \text{Eqn. 1 (in., psi)}$$

$$V_c = \frac{1.109}{\sqrt{H}} \left(\frac{H}{a}\right)^{1/3} \rho^{1/6} (1 - \sqrt{\rho})^{2/3} f'_c{}^{0.35} \sqrt{E_s} b_w d \quad \text{Eqn. 2 (m, MPa)}$$

$$V_c = \frac{1.018}{\sqrt{d}} \left(\frac{d}{a} \right)^{1/3} \rho^{1/6} (1 - \sqrt{\rho})^{2/3} (0.0255 f'_c + 1.024) b_w d \quad \text{Eqn. 3 (m, MPa)}$$

$$V_c = 150 \left(1 + \sqrt{\frac{0.2}{d}} \right) \left(\frac{3d}{a} \right)^{1/3} (100\rho)^{1/3} f'_c{}^{1/3} b_w d \quad \text{Eqn. 4 (m, MPa)}$$

Figure 7 compares the average $V_{\text{test}}/V_{\text{Eqn}}$ for the four fracture mechanics approaches noted. The Bazant and Yu equation is the only equation that does not conservatively estimate the shear capacity of the beams tested in this study. The $V_{\text{test}}/V_{\text{Eqn}}$ ratio for Bazant and Yu, Gasetbled and May, Xu et al. and the fib equations range from 0.69 to 0.86, 1.03 to 1.24, 1.02 to 1.26 and 1.01 to 1.21, respectively. This approach of predicting the shear performance of reinforced concrete without stirrups shows to be best calibrated based on the limited results from this study. Furthermore, this comparison shows that, similar to the design code shear strength comparisons, the ratios ($V_{\text{test}}/V_{\text{Eqn}}$) for the K10 beams and CC beams are similar, and those for the K15 beams are almost 10% lower. Most importantly, the fracture mechanics approaches appear to be applicable for fiber-reinforced concrete.

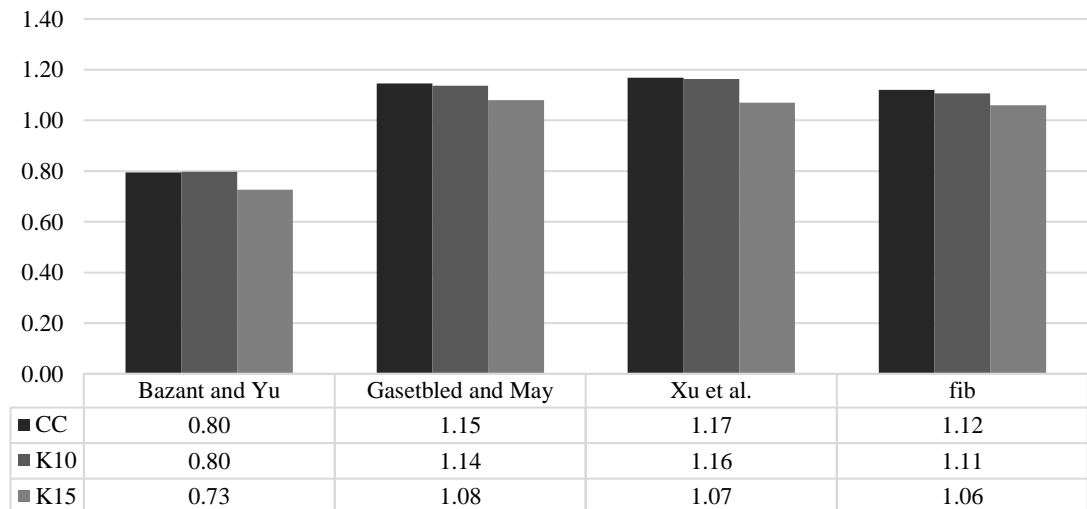


Figure 7 – Ratios of experimental to fracture mechanics predicted capacity

Comparison of Test Results with Shear Database

The shear performance of concrete has been shown to be impacted the most by four key parameters: d – the depth of the member, which impacts the size effect; a/d – the shear span ratio; f'_c – the compressive strength of the concrete; ρ – the longitudinal reinforcement ratio [30]. To evaluate the effect of the aforementioned parameters on the shear strength of the beams, the results of this study are compared with the wealth of shear test data available in the literature [30].

Figures 8, 9 and 10 present the normalized shear stress (shear stress divided by the square root of the compressive strength) versus ρ , d and a/d , respectively. The normalization of the data based on the square root of the compressive strength was selected because that is the relationship most commonly used in shear design equations [13, 23, 22]. Given the significant scatter of the database, it is difficult to draw definitive conclusions on the current test values. However, the data seems to indicate that the CC and FR-SCC tests results fall well within the spread of the existing beam data. These results show that the shear stress at failure for all beams tested were in a relatively tight group near the center third of the data, and that on average, the K15 beams were weaker than the CC and K10 beams.

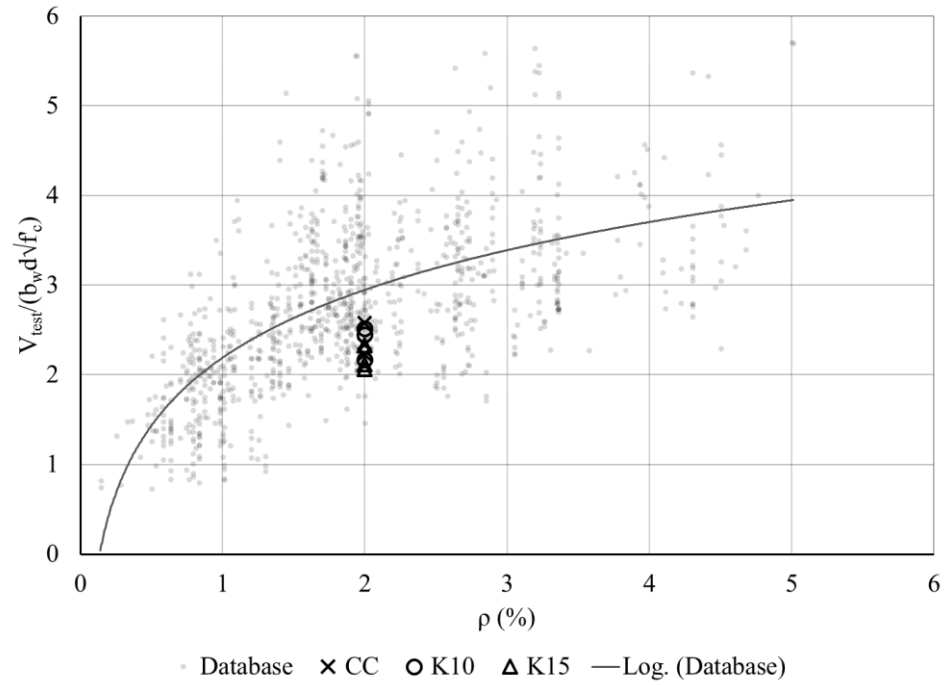


Figure 8 – Normalized shear strength vs. longitudinal reinforcement ratio

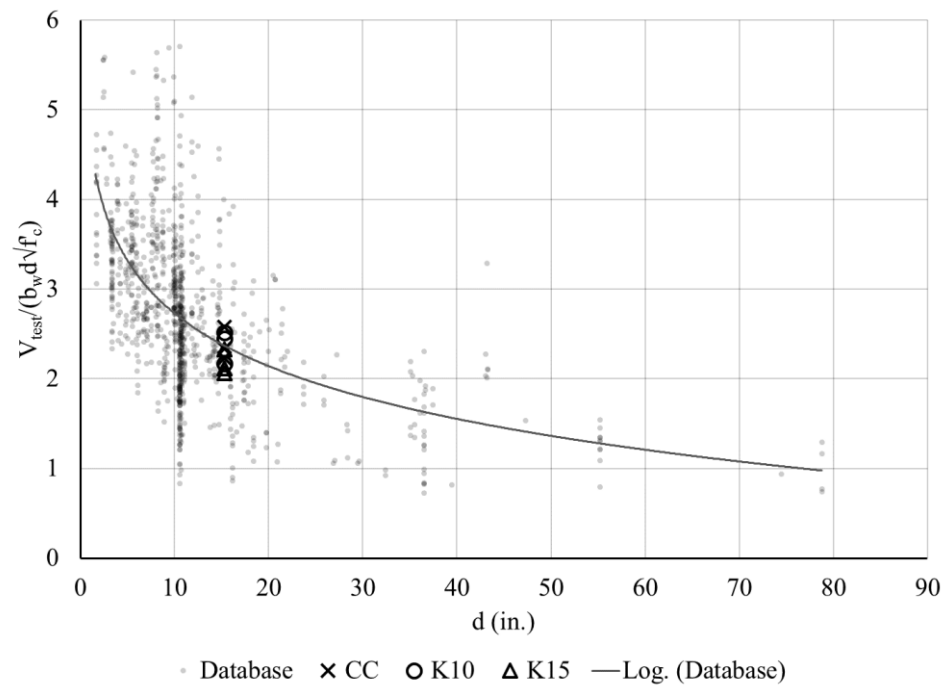


Figure 9 – Normalized shear strength vs. depth

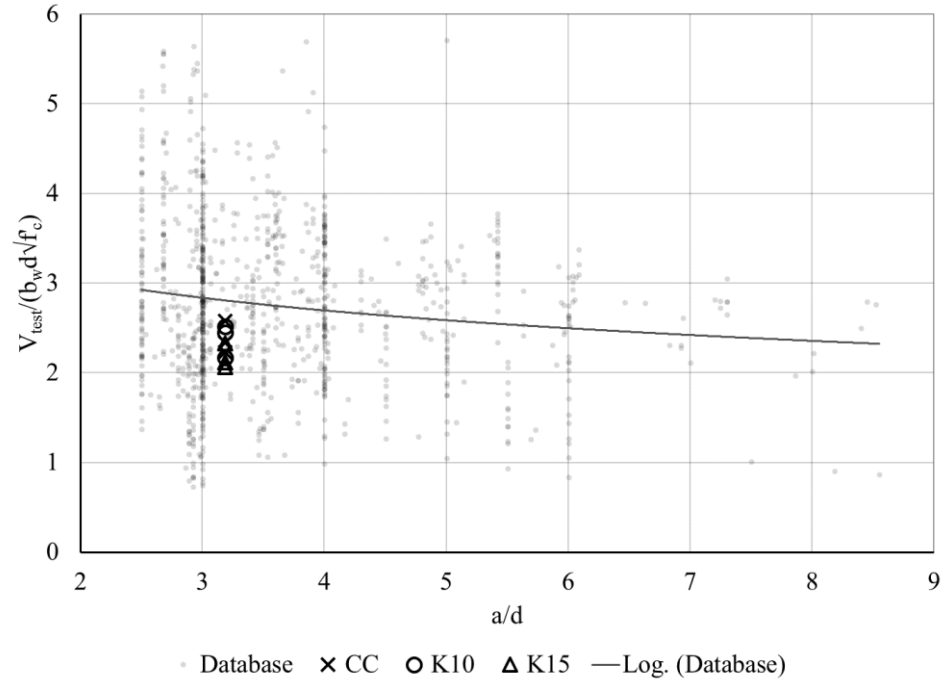


Figure 10 – Normalized shear strength vs. shear span to depth ratio

Comparison of Material Properties and Shear Behavior

Previous research [31] has shown that splitting tensile strength and flexural strength are important parameters affecting the shear strength of concrete. For this reason, the following section compares the relationship between these parameters and the shear strengths for the three mixtures studied in this investigation. To compare the material properties and shear strengths of the CC and FR-SCC beams, the test results have been normalized to reflect the compressive strengths. ACI 318 [13] uses the square root of the compressive strength of concrete to determine the splitting tensile strength, flexural strength and shear strength of beams. Figure 11 shows the ratio of FR-SCC to CC for the normalized splitting tensile strength, flexural strength and shear strength.

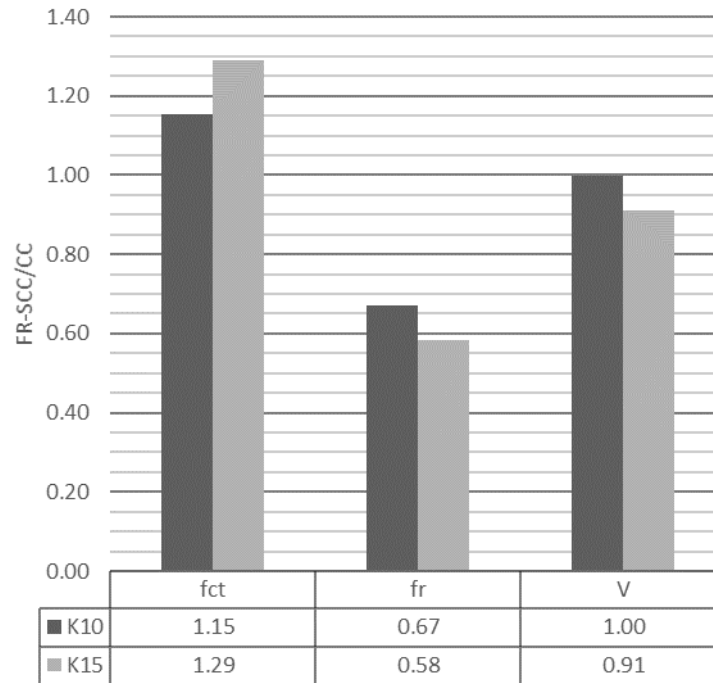


Figure 11 – Ratios of normalized strength of EBC to CC

This data shows increased splitting tensile strength, decreased flexural strength and equivalent shear strength at 15%, 33% and 0%, respectively, for mixture K10 relative to mixture CC. Also, it shows increased splitting tensile strength, decreased flexural strength and decreased shear strength at 29%, 42% and 9%, respectively, for mixture K15 relative to mixture CC. Based on this experimental data, modulus of rupture is a poor predictor of shear strength and splitting tensile strength shows a reasonable correlation for the K10 mixture but a poor correlation for the K15 mixture.

Comparison of Test Results with Response-2000

Response-2000 is a sectional analysis program used to calculate the strength and ductility of reinforced concrete members which was developed by Dr. Evan Bentz during his doctoral studies at the University of Toronto [32]. It uses the modified compression field theory to simultaneously consider all possible two-dimensional loading configurations (shear, moment and axial load). The output of the program is a

full load-deformation response, member crack diagram and detailed analysis of the failure mechanism.

Response-2000 was used to predict the response of the CC beams as well as the FR-SCC beams. Figures 12, 13 and 14 show the comparison of the average shear versus deflection plots for the CC, K10 and K15 beams paired with their corresponding Response-2000 predicted behavior. The predicted failure mechanism and crack morphology were very accurate for all three mixtures. The predicted failure loads for the CC, K10 and K15 mixtures were 10%, 12% and 17% over-predicted, respectively. Also, the predicted maximum deflection for the CC, K10 and K15 mixtures were approximately 25%, 60% and 50% under-predicted, respectively. A potential deviation from the test results was expected as Response-2000 only allows for a single input on stirrup detailing (spacing, size, strength, etc.), and the beams in this study had stirrups located in the constant moment region of the beam and above the reaction points, which would have decreased the degree of cracking and associated loss of stiffness. Also, the presence of fibers skews the traditional strength relationships as well as provides increased ductility.

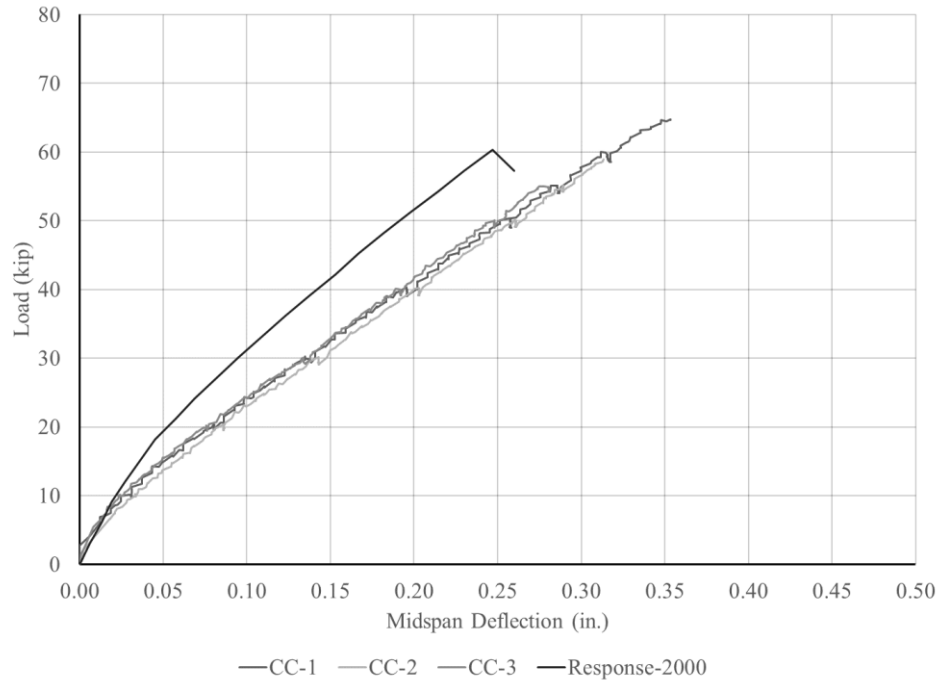


Figure 12 – Response-2000 comparison to CC experimental data

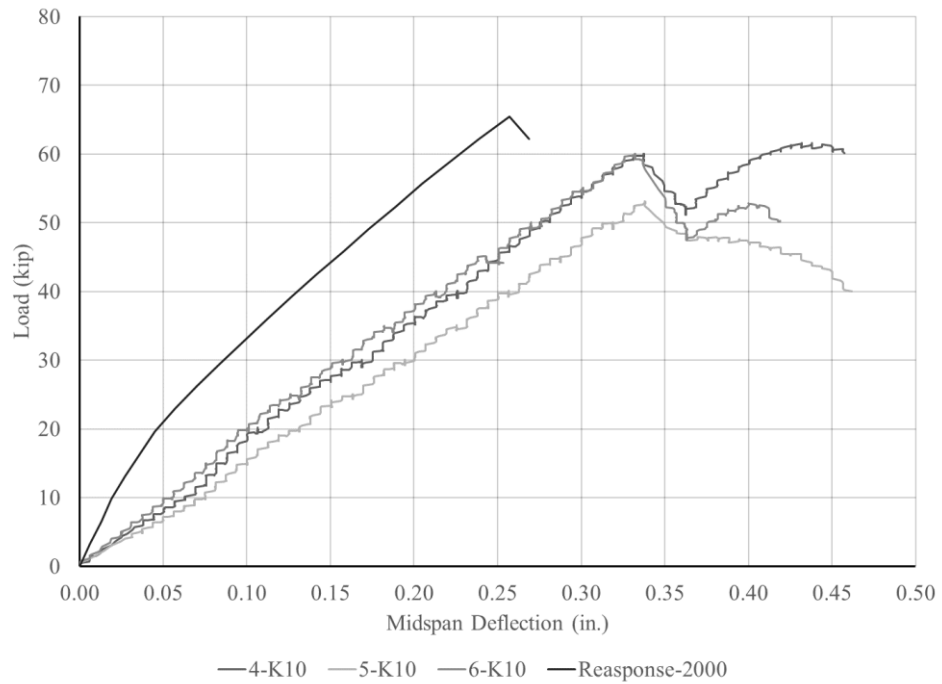


Figure 13 – Response 2000 comparison to K-10 experimental data

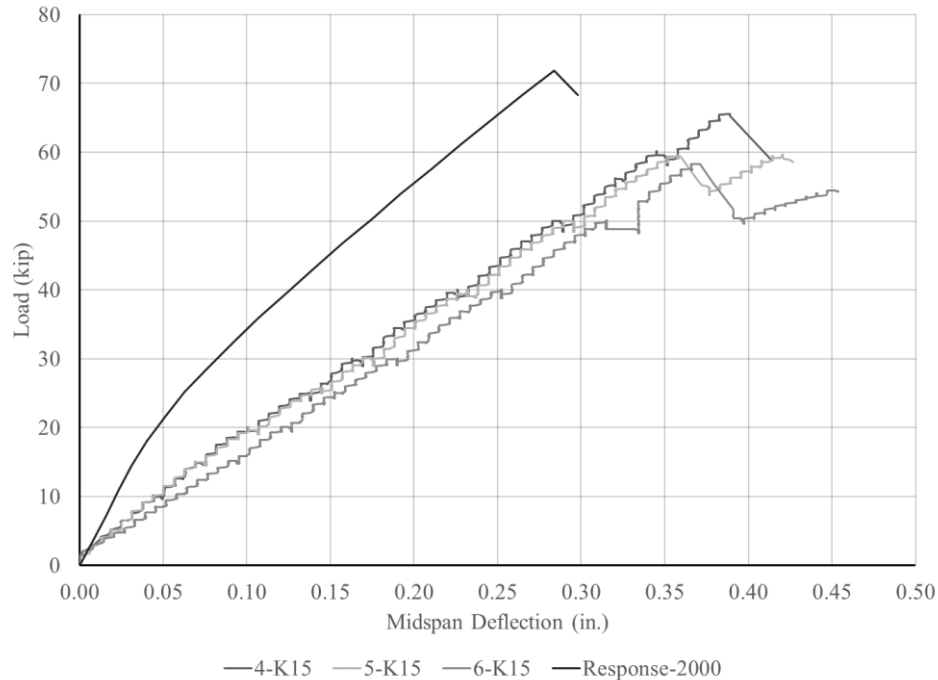


Figure 14 – Response-2000 comparison to K-15 experimental data

When comparing the curves for each mixture, differences appeared. The difference between predicted load-deformation curves to experimental was smallest for the CC beams and largest for the K15 beams. The main difference was that the predicted behaviors were bi-linear, and the experimental nearly linear, more so for the FR-SCC specimens. The predicted behavior also showed fewer and more regular cracks, and a sudden failure upon reaching the failure load. As was discussed earlier, this was not the case for the FR-SCC specimens. The FR-SCC beams cracked more irregularly and sustained load after the failure crack formed. The irregular crack morphology and ductility was due to the presence of fibers.

From these results, it appears that Response-2000 is less reliable at predicting member responses for FR-SCC than it is for conventional concrete. However, it does use a MCFT method to predict the ultimate strength, and that has been shown to be an effective method to predict FR-SCC beam strengths.

Statistical Data Analysis

Statistical tests were used to evaluate whether there is any statistical difference between the normalized shear strengths of the CC and FR-SCC beams. Both parametric and nonparametric statistical tests were performed. Again, the shear strengths were normalized based on the square root of the compressive strength, as is common in most design codes [13, 23, 22].

Parametric Test

The paired t-test is a statistical technique used to compare two population means. This test assumes that the difference between two pairs are normally distributed. If this assumption is violated, the paired t-test may not be the best test to choose. However, it is generally assumed that the natural occurring spread of concrete strength data is a normal distribution [33]. Although the previous data showed that the K10 beams behaved similar to the CC beams, and the K15 beams exhibited a decrease in shear strength compared to the CC beams, the assumptions made for the paired t-test are as follows:

H_{o1} : The mean of normalized shear strength of the CC beams is equal to that of the K10 beams.

H_{o2} : The mean of normalized shear strength of the CC beams is equal to that of the K15 beams.

H_{o3} : The mean of normalized shear strength of the K10 beams is equal to that of the K15 beams.

$H_{a1,2,3}$: Not H_o .

The statistical capabilities of Excel were employed to perform these statistical tests. The results of the paired t-test showed that the p-values are 0.991, 0.011 and 0.15 for H_{o1} , H_{o2} and H_{o3} , respectively. This data confirms the null hypothesis for H_{o1} and H_{o3} and does not confirm the null hypothesis for H_{o2} , at the 0.05 significance level. In other words, when comparing the shear performances for the CC and K10 mixtures, the two are strongly correlated. When comparing the shear performances for the K10 and K15 mixtures, the two are weakly correlated. When comparing the shear performances for the CC and K15 mixtures, they are significantly different. This correlates well with the observed differences between the different mixtures and their structural performances. This again suggests that there is a need to better understand and evaluate FR-SCC, as it behaves vastly differently from conventional concrete.

Non-Parametric Test

Unlike the parametric tests, nonparametric tests are referred to as distribution-free tests. These tests have the advantage of requiring no assumption of normality, and they usually compare medians rather than means. The Wilcoxon sign-ranked test is usually identified as a nonparametric alternative to the paired t-test. The hypotheses for this test are the same as those for the paired t-test. The Wilcoxon sign ranked test assumes that the distribution of the difference of pairs is symmetrical. This assumption can be made because, as mentioned earlier, a normal distribution is commonly assumed for concrete strength [33], and a normal distribution is symmetric.

The p-values for the Wilcoxon sign-ranked test are 0.894, 0.082 and 0.082 for H_{o1} , H_{o2} and H_{o3} , respectively. These confirm the null hypothesis for H_{o1} , H_{o2} and H_{o3} at the 0.05 significance level. This means that the CC and K10 mixtures are strongly

correlated, mixtures K10 and K15 are weakly correlated and that mixtures CC and K15 are weakly correlated. This outcome again suggests that FR-SCC may be more variable than conventional concrete.

Conclusions

To evaluate the shear performance of FR-SCC, a highly workable SCC mixture was designed, and synthetic macro-fibers were added to the mixture. Two research mixtures were created with differing levels of Komponent®. From there, 9 full-scale beams (3 for each mixture in the study) without shear reinforcement were constructed and tested to failure. Along with the beams, companion small-scale specimens were constructed and tested. Based on the results of this study, the following conclusions are presented:

1. While synthetic fibers are not currently allowed to be considered as minimum shear reinforcement, it is proven that they act similar to shear reinforcement.
2. By not treating the fibers as part of the structural system, and instead as part of the concrete mixture, the conventional relationships between strength parameters do not hold well.
3. The qualitative data and observances from this research show that fiber-reinforced concrete has more variability in regard to fresh and hardened properties.
4. The current code methods for calculating shear strength appear to be as adequate for FR-SCC as they are for conventional concrete, but they are less exact.
5. The detrimental effects caused by SCC and rounded aggregates can be offset by the addition of fibers.

6. The data suggests that compressive strength is not an effective method to predict the shear performance of structural members fabricated with fiber-reinforced concrete.
7. The shear strength of both FR-SCC mixtures may have been governed by the performance of the fibers, as the shear crack was opened and sustaining load.
8. In terms of crack morphology and crack progression, the FR-SCC beams had more cracks and smaller crack openings when compared to the CC beams.
9. The fracture mechanics approaches best predicted the shear strengths of the beams for all three concrete mixtures.
10. Statistical data analyses (parametric and nonparametric) indicate that there is a strong correlation between the CC and weaker FR-SCC shear test data, and that the relationship is much weaker for stronger FR-SCC.

Acknowledgements

The authors gratefully acknowledge the financial and capital support provided by Dolese Bros. Co. and the National University Transportation Center at the University of Oklahoma. The conclusions and opinions expressed in this paper are those of the authors and do not necessarily reflect the official views or policies of the funding institutions.

Notation

a = shear span of beam

b_w = web width

d = distance from extreme compression fiber to centroid of longitudinal tension reinforcement

d_a = maximum aggregate size

E_s = modulus of elasticity of steel

f'_c = specified compressive strength of concrete for use in design

V_c = shear force provided by concrete

v_c = nominal shear stress provided by concrete

ρ = longitudinal reinforcement ratio

References

- [1] H. Okamura, "Self Compacting High Performance Concrete - Ferguson Lecture for 1996," *Concrete International*, vol. 19, no. 7, pp. 50-54, 1997.
- [2] K. Ozawa, K. Maekawa and H. Okamura, "Development of the High Performnace Concrete," *Proceedings of JSI*, vol. 11, no. 1, pp. 699-704, 1989.
- [3] E. K. Rice, "Shrinkage-Compensating Concrete". USA Patent 5,846,316, 12 Sep. 1996.
- [4] S. Rolsa, J. Ambroisea and J. Peraa, "Effects of different viscosity agents on the properties of self-leveling concrete," *Cement and Concrete Research*, vol. 29, no. 2, pp. 261-266, 1999.
- [5] "Self-Compacting Concrete," in *1st International RILEM Sympossium*, Stockholm, Sweened, 1999.
- [6] E. P. Koehler, D. W. Fowler, E. H. Foley, G. J. Rogers, S. Watanachet and M. J. Jung, "Self-Consolidating Concrete for Precast Structural Applications: Mixture Proportions, Workability, and Early-Age Hardened Properties," Center for Transportation Research at The University of Taxas at Austin, Austin, TX, 2007.
- [7] F. Kassimi and K. H. Khayat, "Effect of fiber and admixture types on restrained shrinkage cracking of self-consolidating concrete," in *Proceedings of the Fifth North American Conference on the Design and Use of Self-Consolidating Concrete*, Chicago, IL, 2013.
- [8] T. Greenough and M. Nehdi, "Shear Behavior of Fiber-Reinforced Self-Consolidating Concrete Slender Beams," *ACI Materials Journal*, vol. 105, no. 5, p. 468, 2008.
- [9] A. A. A. Hassan, K. M. A. Hossain and M. Lachemi, "Behavior of full-scale self-consolidating concrete beams in shear," *Cement and Concrete Composites*, vol. 30, no. 7, pp. 588-596, 2008.
- [10] Y. Choulli, A. R. Mari and A. Cladera, "Shear behavior of full-scale prestressed i-beams made with self compacting concrete," *Materials and Structures*, vol. 41, no. 1, pp. 131-141, 2007.
- [11] T. Labonte and H. R. Hamilton III, "Self-Consolidating Concrete (SCC) Structural Investigation," Florida Department of Transportation, Gainesville, FL, 2005.

- [12] P. L. Domone, "A review of the hardened mechanical properties of self-compacting concrete," *Cement and Concrete Composites*, vol. 29, no. 1, pp. 1-12, 2007.
- [13] ACI 318-11, "Building Code Requirements for Structural Concrete and Commentary," The American Concrete Institute, 2011.
- [14] ASTM C150-18, Standard Specification for Portland Cement, ASTM International, 2018.
- [15] ASTM C618-17, Standard Specification for Coal Fly Ash and Raw or Calcined Pozzolan for Use in Concrete, ASTM International, 2017.
- [16] ASTM C33-18, Standard Specification for Concrete Aggregates, ASTM International, 2018.
- [17] ASTM A615-16, Standard Specification for Deformed and Plain Carbon-Steel Bars for Concrete Reinforcement, ASTM International, 2016.
- [18] ASTM C39-18, Standard Test Method for Compressive Strength of Cylindrical Concrete Specimens`, ASTM International, 2018.
- [19] ASTM C469-14, Standard Test Method for Static Modulus of Elasticity and Poisson's Ratio of Concrete in Compression, ASTM International, 2014.
- [20] ASTM C496-17, Standard Test Method for Splitting Tensile Strength of Cylindrical Concrete Specimens, ASTM International, 2017.
- [21] ASTM C78-18, Standard Test Method for Flexural Strength of Concrete, ASTM International, 2018.
- [22] AASHTO, "LRFD Bridge Design Specifications," American Association of State Highway and Transportation Officials, 2015.
- [23] CSA, "Concrete Materials and Methods of Concrete Construction/Methods of Test for Concrete," CSA Group, 2004.
- [24] IStructE, "Manual for the design of concrete building structures to Eurocode 2," The Institution of Structural Engineers, 2006.
- [25] JSCE, "Standard Specifications for Concrete Structures," Japan Society of Civil Engineers, 2007.

- [26] Z. P. Bazant and Q. Yu, "Design Against Size Effect on Shear Strength of Reinforced Concrete Beams without Stirrups: I, Formulation," *Journal of Structural Engineering*, vol. 131, no. 12, pp. 1877-1885, 2005.
- [27] F. J. Vecchio and M. P. Collins, "The Modified Compression-Field Theory for Reinforced Concrete Elements Subjected to Shear," *ACI Journal*, 1986.
- [28] O. J. Gasteble and I. M. May, "Fracture Mechanics Model Applied to Shear Failure of Reinforced Concrete BEams without Stirrups," *ACI Structural Journal*, vol. 131, no. 12, pp. 184-190, 2001.
- [29] S. Xu, X. Zhang and H. W. Reinhardt, "Shear Capacity Prediction of Reinforced Concrete BEams without Stirrups Using Fracture Mechanics Approach," *ACI Structural Journal*, vol. 109, no. 5, pp. 705-714, 2012.
- [30] K. H. Reineck, D. A. Kuchma, K. S. Kim and S. Marx, "Shear Database for Reinforced Concrete Members without Shear Reinforcement," *ACI Structural Journal*, vol. 100, no. 2, pp. 240-249, 2003.
- [31] ACI Committee 445, "Recent Approaches to Shear Design of Structural Concrete," American Concrete Institute, Farmington Hills, MI, 1999.
- [32] E. C. Bentz, Sectional Analysis of Reinforced Concrete Members, University of Toronto, 2000.
- [33] P. Dayaratnam and R. Ranganathan, "Statistical Analysis of Strength of Concrete," *Building and Environment*, vol. 11, pp. 145-152, 1976.

III. Aggregate Interlock: An Improved Method and a Non-Traditional Concrete Investigation

Jonathan T. Drury and Jeffery S. Volz

Abstract

After reviewing the literature on push-off testing, it was determined that the data and reporting were inconsistent and scattered, and that if an improved method could be found, it may lead to a standardized test method. An experimental study was conducted on a proposed improved test method to determine its validity and the shear characteristics of non-traditional concrete. Three types of concrete were evaluated: a self-consolidating concrete (SCC) with pea gravel, a cement-limiting and optimized-aggregate concrete with limestone, and a conventional concrete with limestone. The experimentally obtained push-off data was compared to hardened properties of the mixtures, the mix designs, and to historic data.

This study showed that the coefficient of friction obtained from the ratio of shear stress to normal stress is a good indicator of aggregate interlock, but a poor indicator of shear performance. When comparing the experimentally obtained test data to previous methods, it was shown that the proposed method of push-off testing not only allowed the researchers to obtain more data, but the data was more reproducible and fit the trendline for historic data extremely well.

Keywords

aggregate, interlock, push-off, non-traditional, concrete, shear

Introduction

Shear behavior of concrete is a complex phenomenon not completely understood, but researchers believe that there are three main mechanisms that govern it: tensile strength of the cementitious matrix, the presence of reinforcement, and aggregate interlock. The first two are well understood and have standardized tests to determine their influence, but aggregate interlock is not well understood.

The objective of this study is to present an improved push-off test setup, as well as to better understand the impact of aggregate interlock in conventional and non-traditional concrete. To this end, push-off tests were performed on three concrete mixtures: a conventional concrete produced with limestone coarse aggregate (CC), an optimized-aggregate and cement-limiting concrete (EBC), and a self-consolidating concrete (SCC) produced with pea gravel (K15). The experimentally obtained load-slip relationships were investigated.

Research Significance

The fundamental knowledge of shear failure in concrete is essential for structural design, and aggregate interlock plays an important role in shear behavior. Analyzing different concrete types helps to obtain more general knowledge. To provide consistency in determining this behavior, testing should be standardized. The test method presented provides significant improvement on existing push-off testing.

Push-Off Test Background

Aggregate interlock, one of three main shear transfer mechanisms inside reinforced concrete, has been the focus of research for over 50 years [1]. The research started due to a need to understand the impact friction played in structural connections

of precast elements. The first tests were designed to simply gather data for specific design connections, and it was focused on surface friction, and not directly on aggregate interlock.

Subsequent researchers extended the ideas of Hanson and applied them to better understanding shear behavior in concrete elements. This research led to defining the term aggregate interlock as “the effect of portions of aggregate particles from one side of a joint or crack in concrete protruding into recesses in the other side of the joint or crack so as to transfer load in shear and maintain alignment” [2]. The research has seen many different test setups [3, 4, 5, 6, 7], but the basic principles are consistent: create a weak plane to force concrete failure, provide a normal force perpendicular to the failure plane, provide a force parallel to and in line with the failure plane, monitor loads and displacements.

The two major difference between test setups have been in the method of providing normal force. The first method to provide normal force was through internal reinforcement perpendicular to and through the failure plane. The concrete would bond to the reinforcement, and the reinforcement would act as a crack inhibitor. To monitor the level of force containing the crack, strain in the reinforcement was recorded. This method was an obvious choice, as it modeled shear steel in reinforced concrete elements, however it had major drawbacks. In attempting to monitor the behavior of aggregate interlock, the reinforcement was corrupting the data by providing crack slip resistance. Researchers presented methods to refine the data, but this was still not presenting a clear picture of the shear behavior of the concrete alone.

The second method to provide normal force was through external reinforcement. This was obtained through externally mounted confinement. To monitor the level of force containing the crack, strain in the confining members was recorded. This method was an improvement on the previous method, as it allowed only the concrete interface to resist shear forces. Another benefit of this second method was that it allowed investigation of the crack surface after the test was completed. By visually inspecting the failed surfaces, researchers could better understand the mechanisms resisting shear.

Experimental Program

Push-Off Specimen Design

The specimens for this research were based on previous externally reinforced members. The main difference in the proposed test method and previous research was that the concrete specimens were cracked without any perpendicular normal forces present. The specimens were cracked in this manner to provide a means of visual inspection of the failure plane prior to as well as after push-off testing. The specimen geometry is detailed in Figure 1. The push-off specimens were designed with a 7.5 in. (190 mm) by 4.0 in. (100 mm) failure surface. The outside dimensions of the specimens were 10.0 in (255 mm) by 18.0 in. (460 mm). The slots that separate the monolithic specimen into two halves protruded 5.25 in. (135 mm) into the specimen and were trapezoidal with exterior widths of 1.5 in. (40 mm) and interior widths of 0.5 in. (15 mm). A triangular 0.5 in. (15 mm) wide by 0.25 in. (5 mm) deep groove was cast into opposite faces of the specimen to create the desired reduced sized failure surface.

Reinforcement was installed in the specimens to prevent failures other than through the desired plane. The reinforcement was constructed using #3 (metric #10)

size grade 40 (metric grade 280) deformed steel bars. P-shaped cages were constructed to provide 1.0 in. (25 mm) cover around the edges of each half of the specimen, and no steel within 3.0 in. (75 mm) of the failure surface. The cages were constructed with two layers, and again formed with 1.0 in. (25 mm) cover from the rebar to any concrete surface. The reinforcement detail is displayed in Figure 1. For clarity, the reinforcement is only drawn for one half of the symmetric specimen.

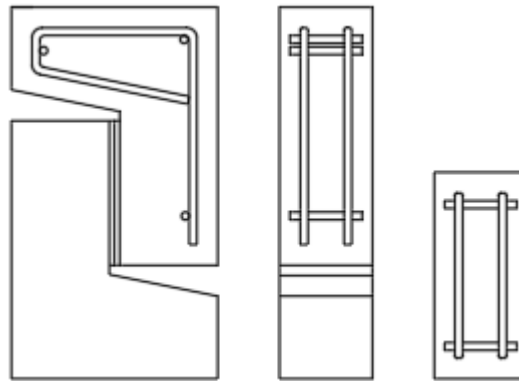


Figure 1 – Rebar detail for push-off specimens

High-strength steel rods and plates were used to produce the external reinforcement and wedges for pre-cracking the specimens. The rods were 0.5 in. (15 mm) diameter and sufficiently long to properly install a washer and nut on each end. The confining plates were 0.75 in (20 mm) thick, 8.0 in (200 mm) wide and 12.0 in (300 mm) long. Holes were drilled into the plates to create 0.5 in. (15 mm) clearance between the rods and the specimen. The wedges were 0.75 in. (20 mm) thick, 4.0 in (100 mm) wide, 8.0 in. (200 mm) long and had one long edge machined down to create a 60° angle point. The point was set to a smaller angle than the groove angle (90°) to create a line load in the groove instead of a distributed load. Drawings of the steel pieces are shown in Figure 2.

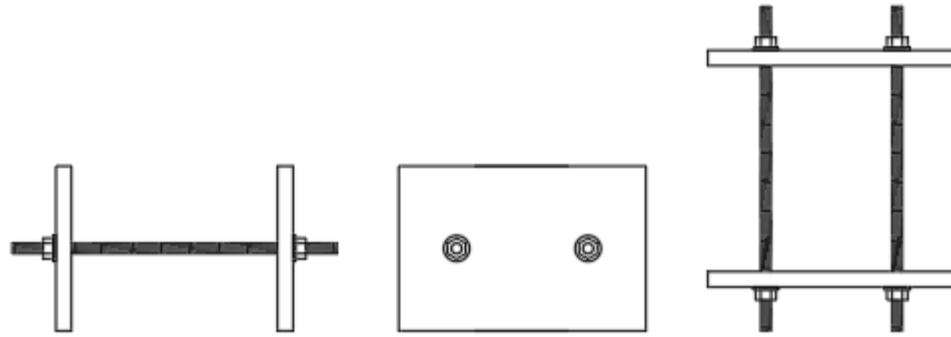


Figure 2 – External steel reinforcement rods and plates

The load path and instrumentation for the push-off test is detailed in Figure 3.

One strain gauge was installed on each threaded rod. The rod strains were used to monitor the compressive normal force being applied perpendicularly to the failure plane. One linear variable differential transformer (LVDT) was installed on the face of each specimen to monitor the opening of the crack width. The crack slip was monitored via an LVDT magnetically mounted to the moving crosshead of the testing machine. Angles were epoxied to the same face of the specimen to provide contact points for tips of the LVDTs.

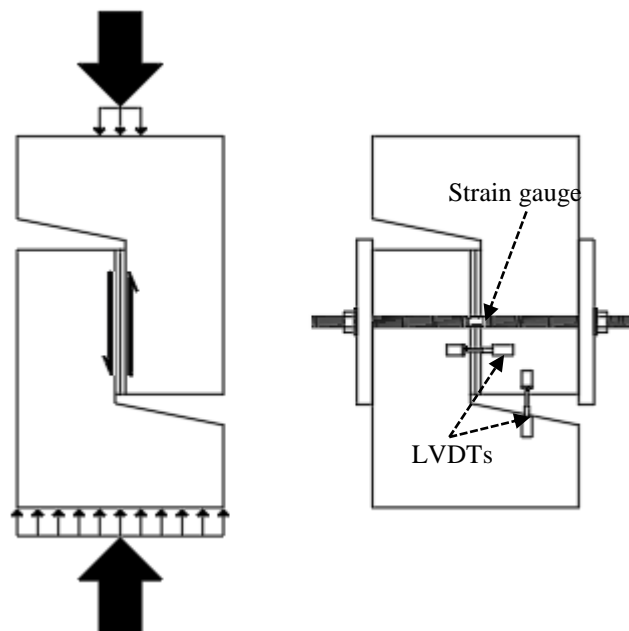


Figure 3 – Load path diagram and instrumentation layout

Materials and Specimen Preparations

The three mix designs investigated in this study were developed for previous research [8, 9]. They were designed for use as structural concrete per the performance specifications of the Oklahoma Department of Transportation (ODOT) [10]. The cementitious material properties, aggregate properties, and mix designs are detailed in Tables 1, 2, and 3, respectively. A third cementitious material was used in this study, but it was a proprietary expansive cement called Komponent® from CTS Manufacturing Corp (Cypress, CA). Komponent® is an expansive calcium sulfoaluminate (CSA) cement-based additive that is used to produce ASTM C845 Type K Shrinkage Compensating cement. Due to it being proprietary, it is not detailed in Table 1.

Table 1 – Cementitious material properties

Property	Type I/II Cement	Class C fly ash
Fineness (+325 mesh), %	—	10.3
Air permeability, ft ² /lb	1939	—
Specific gravity	3.11	2.72
Loss on ignition, %	2.4	0.67
Silica, %	20.8	31.9
Aluminum oxide, %	3.8	20.4
Ferric oxide, %	3	5.9
Sulfur trioxide, %	2.9	3.0
Calcium oxide, %	63.9	28.3
Magnesium oxide, %	1.9	7.2

Note: 1 ft²/lb = 2.05 cm²/g

Table 2 – Aggregate properties

Property	#57	3/8" chip	3/8" pea gravel	Concrete sand
Specific gravity, oven-dry	2.69	2.67	2.59	2.65
Dry-rodded unit weight, lb/ft ³	101	95	105	—
Absorption, %	0.86	1.01	0.72	0.7
LA abrasion, % loss	26	22	22	—
Mohr's hardness	3.5 - 4	3.5 - 4	3 - 3.5	—

Note: 1 lb/ft³ = 16 kg/m³

Table 3 – Mix designs

	CC	EBC	K15
Type I/II cement	470	414	413
Class C fly ash	118	103	224
Komponent®	—	—	113
w/cm	0.4	0.4	0.39
#57 limestone, lb	1857	989	—
3/8" chip, lb	—	565	—
3/8" pea gravel, lb	—	—	1223
Concrete sand, lb	1323	1415	1401
HRWR, fl oz	26.7	36.2	67.6
AEA, fl oz	4.40	2.59	8.3
Citric acid, g	—	—	176

Notes: 1 lb = 0.454 kg; 1 fl oz = 29.5 mL

The specimens were cast by carefully placing concrete into the form to maintain the rebar in its desired locations. Tamping rods and mallets were used to consolidate the specimens. Once the concrete had stiffened enough to hold the shape of the groove, a grooving tool was used to shape and center the groove on the open side of the specimen form. Cast specimens were covered with wet burlap and plastic sheeting to cure for 7 days. After 7 days, the concrete was left to cure in a controlled room at 50% RH and 72°F (22.2°C). Companion cylinder specimens were cast along with each batch of push-off specimens, and they were cured alongside the push-off specimens. Also, a full characterization of each concrete mix was performed to determine the 28-day properties per ASTM standards [10, 11, 12, 13]. The mix characterization data is presented in Table 4.

Table 4 – Mix characterizations

Property	CC	EBC	K15
Slump or slump flow, in.	6	32	30
Air content, %	6	9.0	10.5
Unit weight, lb/ft ³	144	123	139
Compressive strength [†] , psi	6,385	6,425	5,530
Modulus of elasticity [†] , ksi	4,250	3,600	3,950
Split cylinder strength [†] , psi	525	525	480
Modulus of rupture [‡] , psi	560	620	700

[†] Values represent an average of three cylinders (ASTM C39, ASTM C469 and ASTM C496)

[‡] Values represent an average of three beams (ASTM C78)

Notes: 1 in. = 25.4 mm; 1 lb/ft³ = 16 kg/m³; 1 psi = 0.00689 MPa; 1 lb/in = 175.1 N/m

Push-Off Test Setup and Procedure

To pre-crack the specimens, high-density neoprene pads were used to restrain the bottom wedge from slipping as well as to protect the cracked specimen halves from damage after being cracked. Each specimen was installed into the testing machine and cracked with a wedge applying a line load to each side of the failure plane. The loads were applied slowly, and immediately removed once the crack was formed. The peak load required to crack each specimen was recorded. The specimen halves were then inspected and photographed to characterize the pre-test (post-cracking) surfaces. For specimens that cracked, but did not separate, care was taken to prevent damage while handling them prior to installing the external reinforcement.

After inspecting the pre-cracked specimens, the two halves were carefully seated together, and the external reinforcement was placed on the specimen. The threaded rods were then tensioned to provide 200 to 300 psi (1.4 to 2.1 MPa) of compression onto the failure plane. The confined specimen was then centered in the testing machine, and the LVDTs were installed onto the specimen. At this point, the bar strains were noted, and the gauges were zeroed. A small steel plate was placed between the top surface of the

specimen and the top crosshead to better concentrate the load. The load was then slowly applied parallel to the failure surface, and the instrumentation readouts were monitored. The test was stopped when either an LVDT was extended or compressed to its extreme limit or a rod strain was such that the rods were approaching yielding. It was desired to open each crack width past 0.045 in. (1.1 mm) as well as to push each crack slip past 0.325 in. (8.3 mm) based on previous research.

Once a criterion was met to signal stopping the test, the load was immediately removed from the testing machine, and the threaded rods were de-tensioned and removed. The two halves of the push-off specimen were then again inspected and photographed.

Test Results and Comparison

Results of Pre-Cracking

All three of the CC specimens cracked in half during pre-cracking. In all three tests, the surfaces of the failure plane showed that nearly all aggregate crossing the plane fractured along the plane. The average load required to crack the CC specimens was 9567 lb (4340 kg). The average compression strength from the three companion cylinders was 5500 psi (37.9 MPa). Figure 4 is a photo of a typical pre-crack failure plane for the CC specimens.

All three of the EBC specimens cracked in half during pre-cracking. In all three tests, the surfaces of the failure plane showed that nearly all aggregate crossing the plane fractured along the plane. The reduced paste volume compared to the CC mixture was evident. The average load required to crack the EBC specimens was 8753 lb (3970 kg). The average compression strength from the three companion cylinders was 5900

psi (40.7 MPa). Figure 5 is a photo of a typical pre-crack failure plane for the EBC specimens.

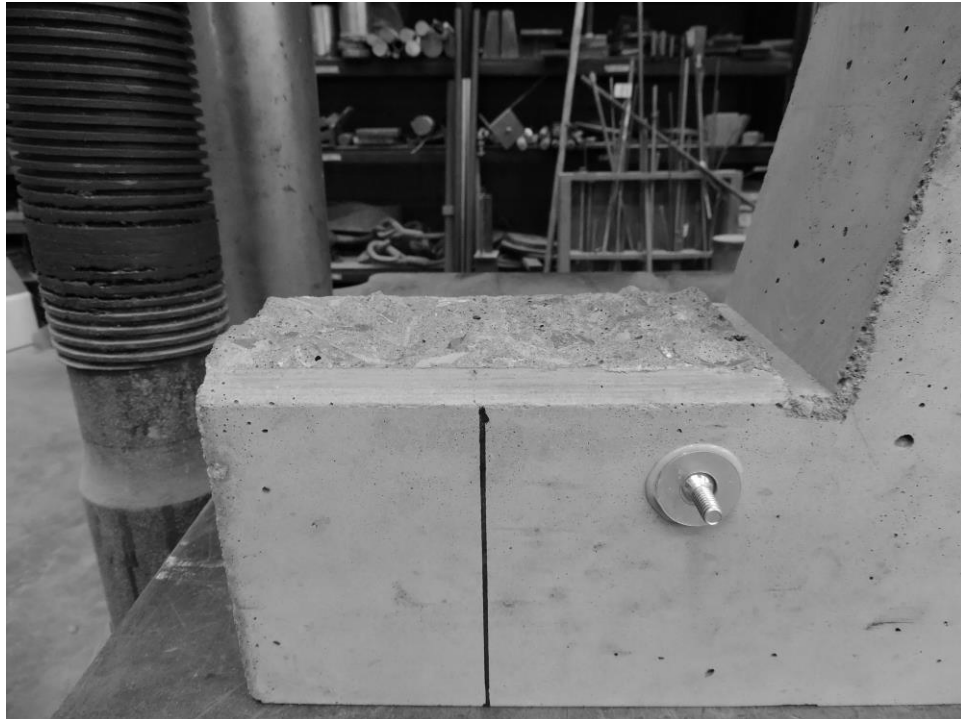


Figure 4 – Typical pre-crack failure plane for CC specimens



Figure 5 – Typical pre-crack failure plane for EBC specimens

Two of the three K15 specimens cracked in half during pre-cracking, and one cracked, but did not separate in two. In the two tests that permitted failure plane inspection, it was noted that many of the aggregate particles crossing the plane fractured along the plane, but that some de-bonded and remained intact. It was evident that there was an increased paste volume compared to the CC mixture. The average load required to crack the K15 specimens was 11744 lb (5327 kg). The average compression strength from the three companion cylinders was 5900 psi (40.7 MPa). Figure 6 is a photo of a typical pre-failure plane for the K15 specimens.

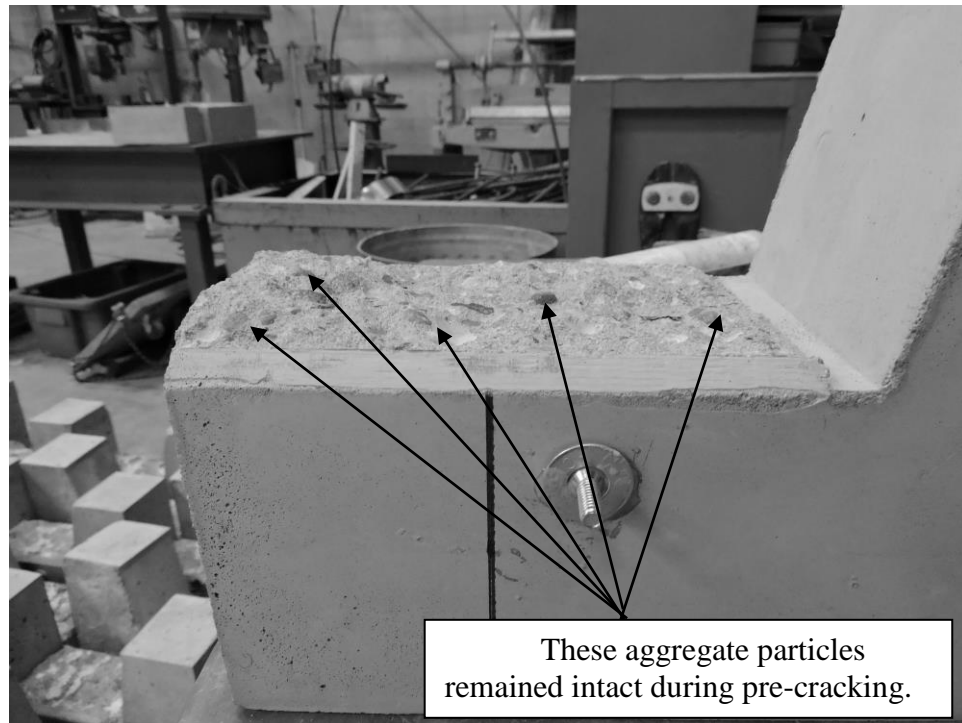


Figure 6 – Typical pre-crack failure plane for K15 specimens

The apparent tensile strength, f_{ct}^* , was calculated for each mixture by dividing the pre-cracking load by the failure plane area. The apparent tensile strength is compared to the splitting tensile strength in Table 4. As can be seen in the table, the two

correlate well. Also presented in Table 4 is the comparison between the apparent tensile strength to the compressive strength and the cementitious content.

Table 5 – Pre-cracking material properties

Concrete Mixture	f_{ct} (psi)	f_{ct}^* (psi)	f_c (psi)	f_{ct}^*/f_c	$f_{ct}^*/(f_c)^{1/2}$	Cementitious Content (pcf)	$f_{ct}^*/\text{cementitious content}$
CC	350	340	5500	0.062	4.61	588	0.58
EBC	340	315	5880	0.053	4.08	517	0.61
K15	400	420	5890	0.071	5.46	750	0.56

Note: 1 psi = 0.00689 Mpa, 1 pcf = 16 kg/m³

The apparent tensile strengths trend well when compared with the cementitious content, and to illustrate that further the data is plotted in Figure 7. This trend is to be expected, as the cementitious paste in a concrete mixture provides cohesion, and aggregate provides rigidity and filler.

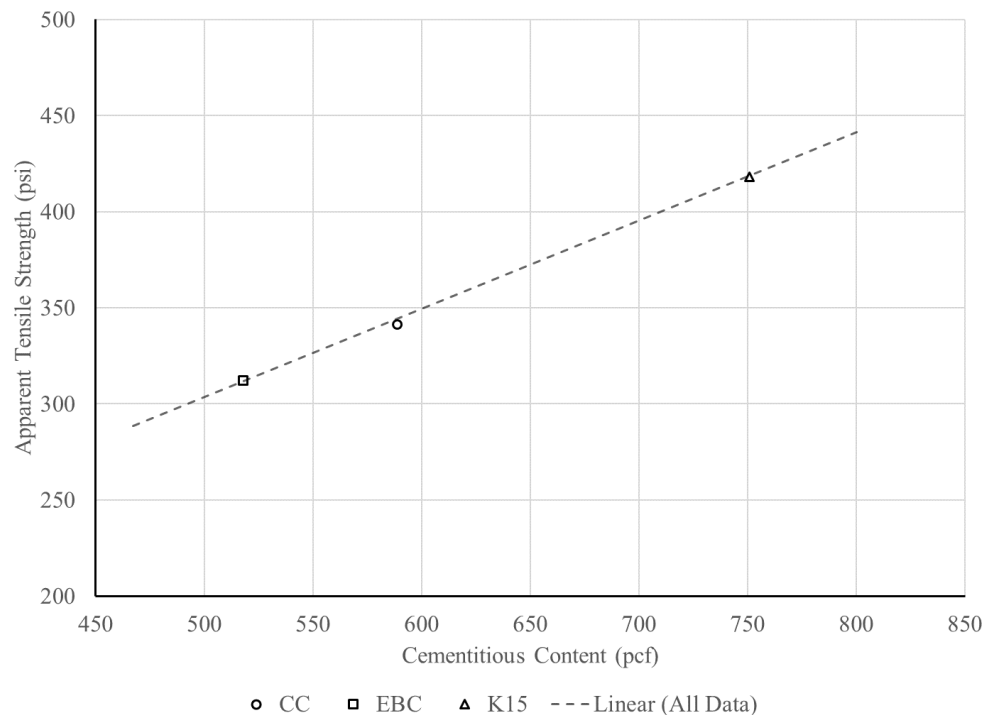


Figure 7 – Relationship between tensile strength and cementitious content

Load-Displacement Responses

The push-off test determines the ability of a pre-cracked failure plane to transfer shear. For that reason, the first trend that is of note is the shear stress-displacement response. The shear stress development for all three mixtures had similar trends: the shear stresses increased rapidly at first, a point was reached when the peak interface friction was overcome, then the shear stresses leveled off.

Figure 8 is a plot of the shear stress versus the crack slip. Each curve on the plot is an average of at least two push-off test results. The tests were pushed past a slip limit of 0.325 in. (8.3 mm), and the average points were calculated at intervals of 0.025 in. (0.64 mm). The plot shows that K15 was able to resist the largest shear forces while EBC resisted the smallest shear forces. Also noteworthy on the plot, EBC exhibited a consistent shear stress resistance once peaking, but both CC and K15 exhibited substantial gains in shear stress resistance throughout the slipping of the crack. This appears to be a setback of reducing the cement content and optimizing the aggregate gradation for the EBC mixture. The failure plane is smoother than its comparable CC mixture, and that reduction in paste as well as roughness provides less shear resistance after surpassing the peak interface friction.

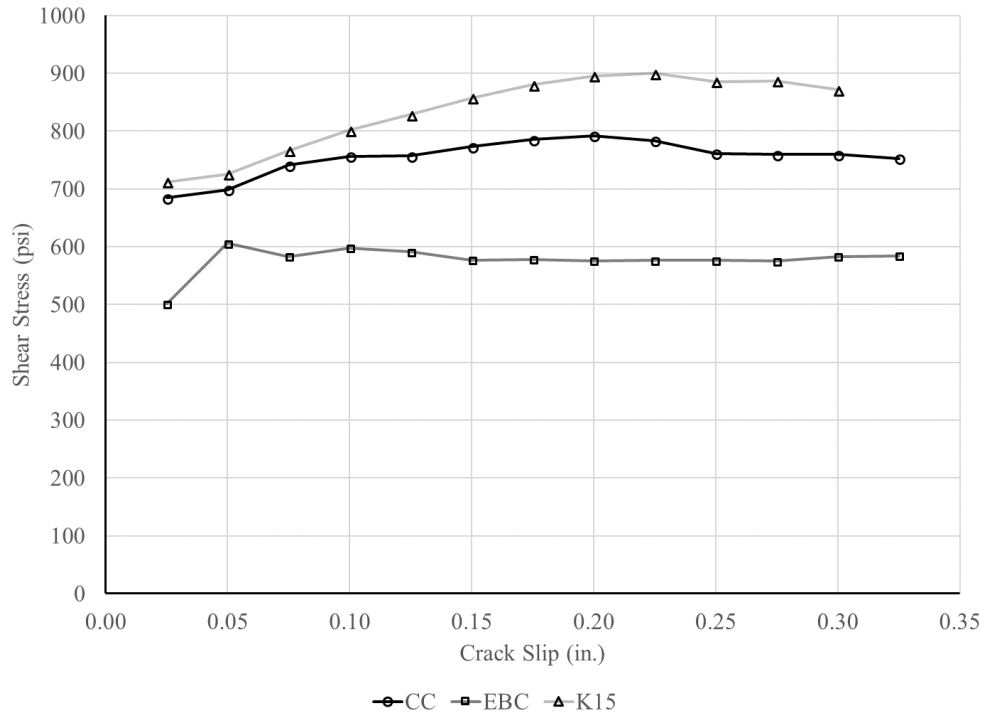


Figure 8 – Shear stress vs. crack slip

Another helpful means of presenting the shear stress data is residual shear strength. The residual shear strength is defined as the shear strength present in the system at a given slip limit. Table 5 presents the peak shear strength as well as residual shear strengths at given slip limits.

Table 6 – Peak and residual shear strengths at given slip values

Concrete Mixture	Peak Shear Strength (psi)	Residual Shear Strength (psi)		
		0.10 in.	0.20 in.	0.30 in.
CC	793	757	793	760
EBC	606	598	576	583
K15	900	802	895	872

Note: 1 psi = 0.00689 MPa, 1 in. = 25.4 mm

As shear stress is generated along the failure plane, the imperfection in the surface must either shear off or the crack must widen. Any opening of the crack will lead to an increased normal force. Figure 9 is a plot of the normal stress versus the crack slip. Each curve on the plot is an average of at least two push-off test results. The plot

shows that EBC generated the smallest normal stresses and that K15 generated the largest normal stresses. This is consistent with the shear vs. slip behavior as well as the surface roughness for all three mixtures.

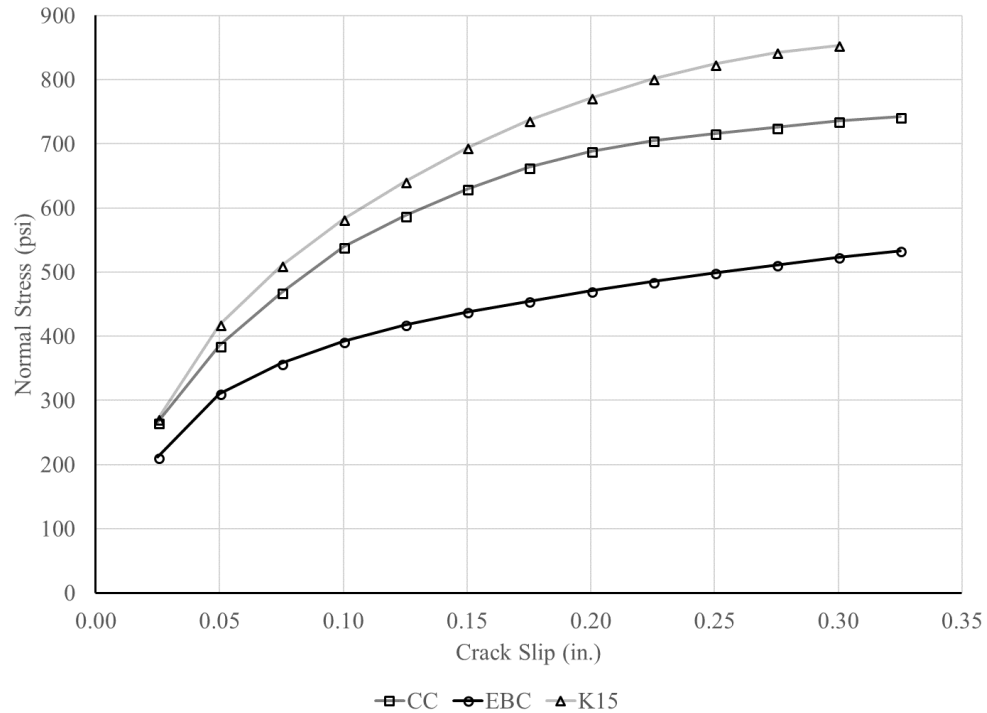


Figure 9 – Normal Stress vs. Crack Slip

To fully illustrate the crack slip and crack width opening relationship, Figure 10 plots crack slip versus crack opening for all three mixtures. This plot again shows that the optimized aggregate in EBC tends to slip more for a given crack opening. CC and K15 displayed similar slip versus opening tendencies. As can be seen from the load-displacement responses, K15 provides the greatest shear resistance, and EBC provides the weakest shear resistance.

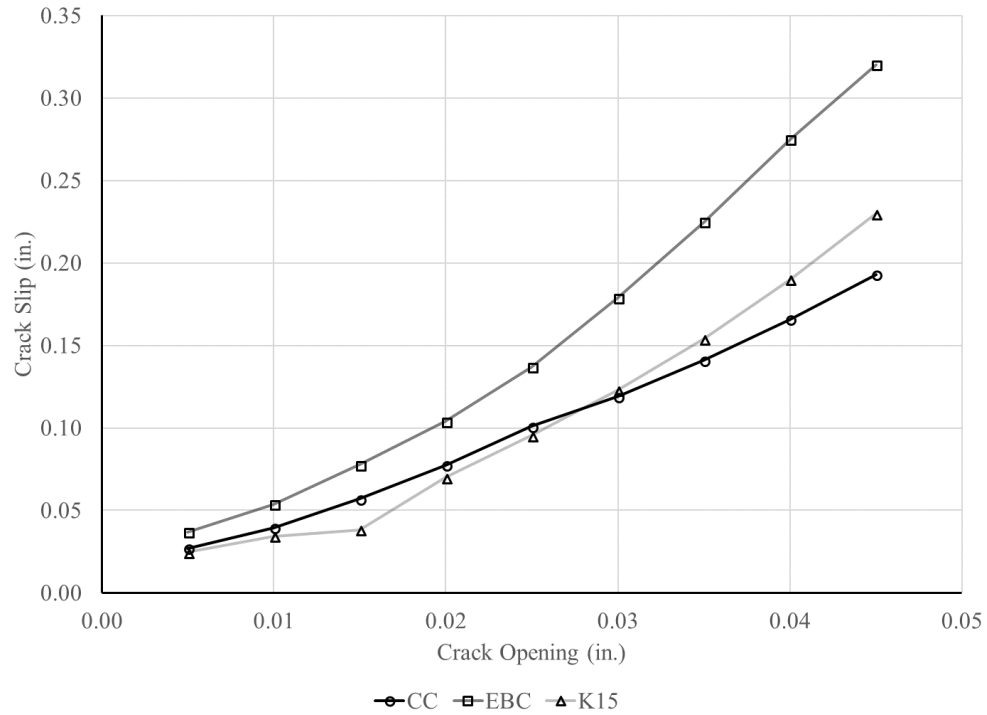


Figure 10 – Crack Slip vs. Crack Opening

Coefficients of Friction

The coefficient of friction of concrete is complex because it involves terms for both the cohesion of the concrete and the roughness of the failure surface. However, the coefficient of friction for a push off test is simpler because there is no cohesion over the cracked surface, and the equation simplifies to the ratio of the shear stress divided by the normal stress. Figures 11 and 12 are plots of the ratio of shear stress to normal stress versus crack slip and crack opening, respectively.

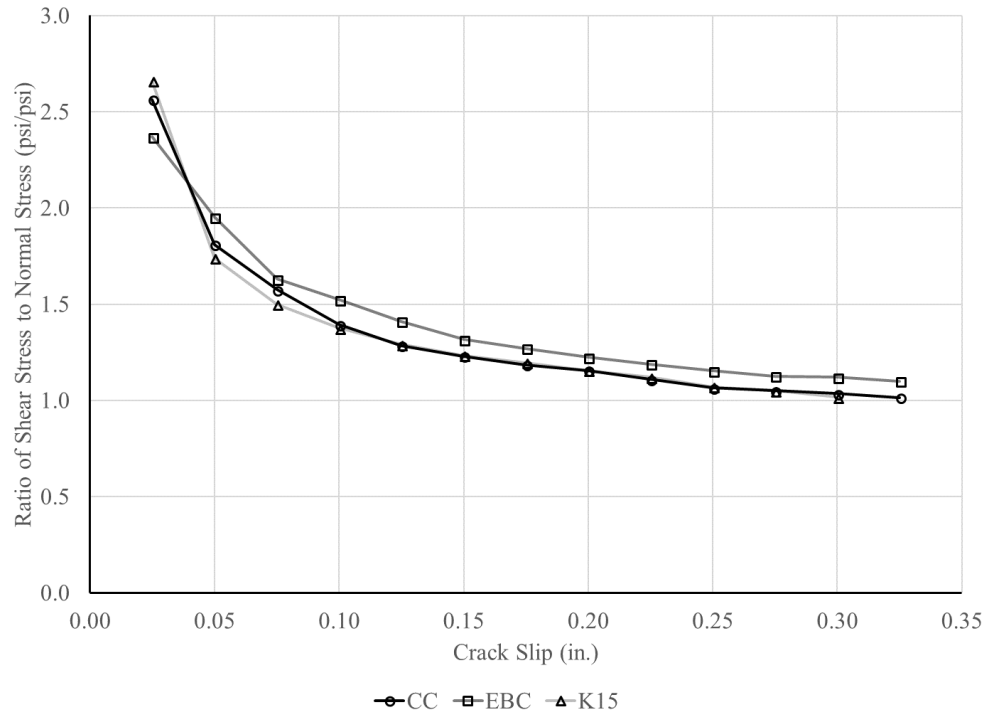


Figure 11 – Ratio of Shear Stress to Normal Stress vs. Crack Slip

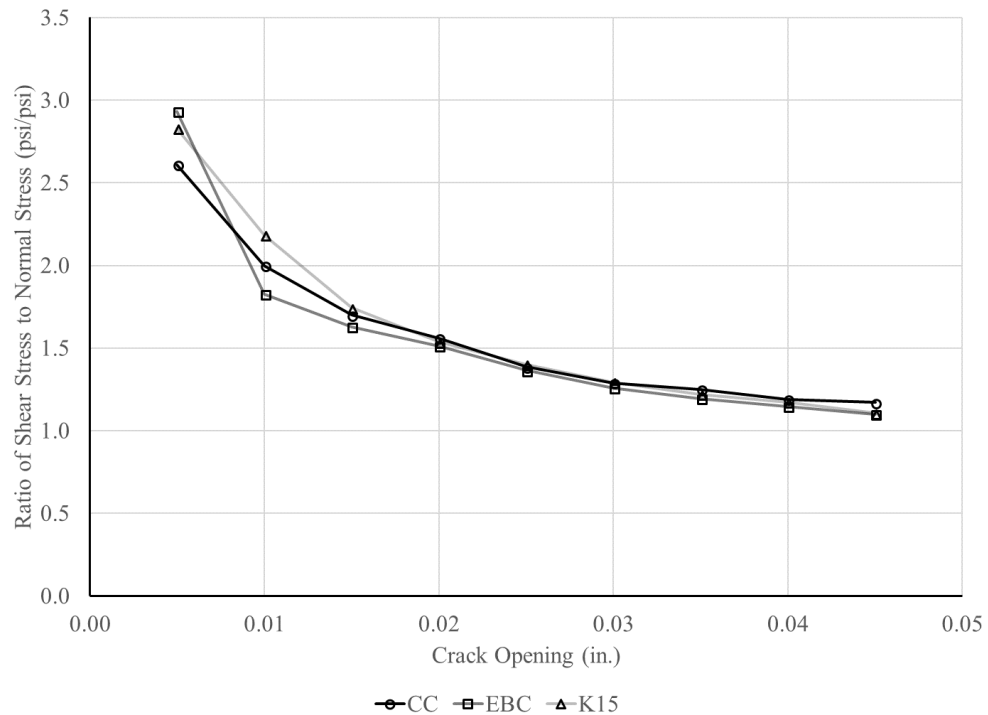


Figure 12 – Ratio of Shear Stress to Normal Stress vs. Crack Opening

As with the residual shear strength, it may be helpful to present the residual friction coefficient for a given displacement. The peak friction coefficients and the

residual friction coefficients at given slip limits are presented in Table 6. Note that the peak coefficients may be larger than the plotted values. That is because the average peaks did not all occur at the same slip values plotted.

Table 7 – Peak and residual coefficients of friction at given slip values

Concrete Mixture	Peak Coefficient of Friction	Residual Coefficient of Friction		
		0.25 in.	0.50 in.	0.75 in.
CC	2.89	2.57	1.81	1.58
EBC	3.22	2.37	1.95	1.63
K15	3.01	2.66	1.74	1.50

Note: 1 in. = 25.4 mm

To put these friction coefficients into perspective, it is important to compare these values to common friction coefficients. The PCI Handbook 6th Edition presents maximum effective coefficients of friction for different surface considerations [7]. Table 7 presents the 4 cases along with their coefficients. Based on the code values for coefficients of friction, the experimental data correlates well with previous data. All of the experimental coefficients fall between the table values for the “concrete to hardened concrete, with roughened surface” and “concrete to concrete’ cast monolithically.” As code values must represent conservative values, this correlation is excellent.

Table 8 – PCI maximum coefficients of friction

Case	Crack Interface Condition	Max Coefficient of Friction
1	Concrete to concrete, cast monolithically	3.4
2	Concrete to hardened concrete, with roughened surface	2.9
3	Concrete placed against hardened concrete not intentionally roughened	2.2
4	Concrete to steel	2.4

Based on the friction coefficient data alone, one could determine that EBC provides the greatest resistance to shear. This data however is misleading. EBC does

provide the highest friction coefficient, but it does not provide the greatest shear resistance. The friction coefficient is a better representation of the ability of a mixture to provide aggregate interlock. However, the nature of the angular and brittle aggregate is to shatter when stressed too far. The less packed limestone in CC and the rounded pea gravel in K15 allowed those mixtures to open the cracks and provide better maintained shear strength.

Comparison of the Proposed Test

To submit this new test as an improvement on existing methods, it is important to compare data from past research. However, since this is not a standardized test method, researchers have chosen to focus on different results. Presented in Figure 13 is a comparison between this study and historic data on push-off testing with external reinforcement [15]. Note, the previous test methods differed from the proposed method by attaching the external reinforcement prior to pre-cracking. While the two methods are slightly different, the side-by-side comparison shows that they generate similar data. A better comparison would be to compare load and displacement data directly, but these researchers only presented these plots to compare their data to historic data [15].

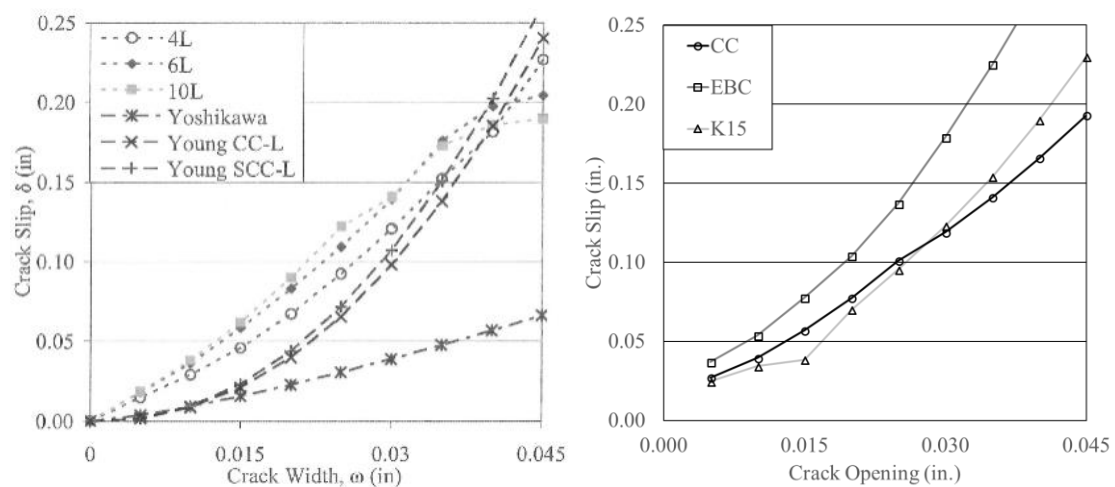


Figure 13 – Comparison to historic externally reinforced push-off testing

Presented in Figure 14 is a comparison between this study and historic data on push-off testing with internal reinforcement [7]. Note, these test methods differed from the proposed method by using internal bars crossing the failure plane to provide the normal force to the shearing surfaces. These researchers presented all of their data, so a better comparison can be made. The plotted data strongly suggests that the proposed method not only is an acceptable method to acquire data on aggregate interlock and shear, but it is an improvement. While the sample size is small, the data is more consistent and reproducible. For this reason, and the many other presented, this method is proposed as a new standard for aggregate interlock testing.

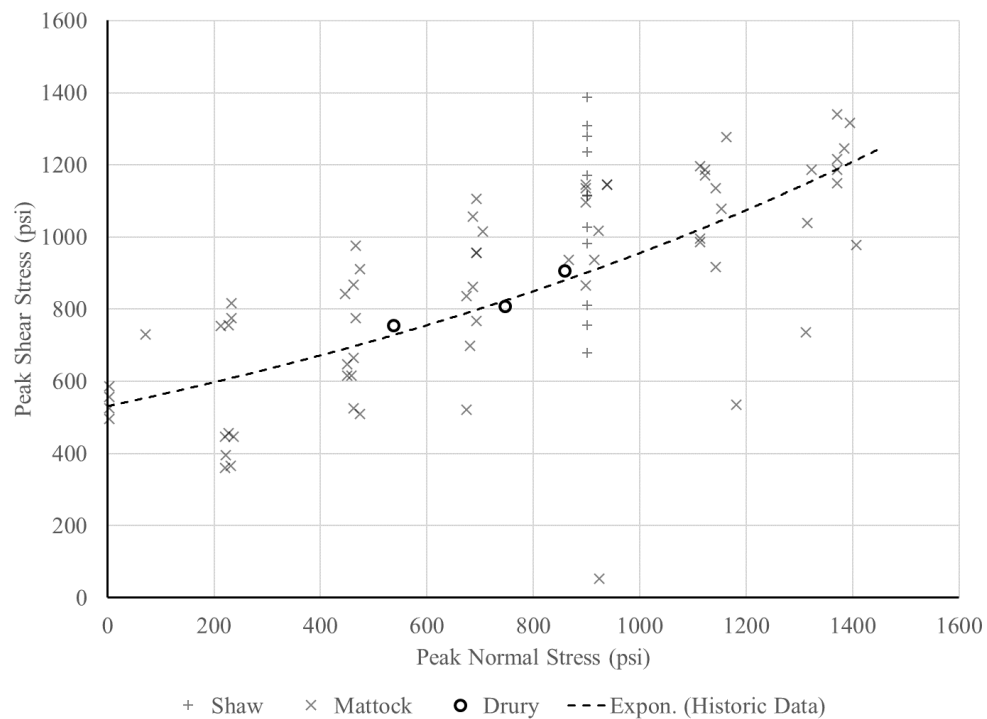


Figure 14 – Comparison to historic internally reinforced push-off testing

Conclusions

To improve understanding of aggregate interlock in both conventional and non-traditional concrete, three different concrete mixtures were characterized and tested using a proposed improved push-off test. The push-off specimens were analyzed prior

to pre-cracking, after pre-cracking, and after the completion of the push-off test. Based on the results of this study, the following conclusions are presented.

1. The proposed push-off test shows excellent correlation to past push-off testing methods and has been proven to be more reproducible.
2. The proposed push-off test is suggested as a replacement to other push-off tests due to the elimination of errors and the improved quality control.
3. The proposed push-off test allows the researcher to obtain before and after data on the failure surface. This data may allow future researchers to expand the knowledge of shear friction and aggregate interlock.
4. The existing means of determining aggregate interlock of a mixture, the ratio of shear stress to normal stress, presents relative information. This ratio alone is not adequate for determining the shear resistance characteristics of a mixture.
5. There is strong correlation between the cement content and apparent tensile strength of the specimens. Also, there is a strong correlation between splitting tensile strength and the apparent tensile strength of the mixtures. Pre-cracking an unreinforced member may be able to supplement performing splitting tensile tests.
6. K15, the SCC mix produced with pea gravel, exhibited the strongest apparent tensile strength and shear strength, and EBC, the cement-limiting and optimized aggregate mix, exhibited the weakest apparent tensile strength and shear strength.
7. EBC exhibited the highest friction coefficient, which represents aggregate interlock performance, and the CC exhibited the lowest friction coefficient.

Acknowledgements

The authors gratefully acknowledge the financial and capital support provided by Dolese Bros. Co. and the National University Transportation Center at The University of Oklahoma. The conclusions and opinions expressed in this paper are those of the authors and do not necessarily reflect the official views or policies of the funding institutions.

Notation

f_c = Compressive strength

f_{ct} = Splitting tensile strength

f_{ct}^* = Apparent tensile strength

References

- [1] N. W. Hanson, "Precast-Prestressed Concrete Bridges 2: Horizontal Shear Connections," *Journal of the Research and Development Division*, vol. 2, no. 2, pp. 38-58, 1960.
- [2] American Concrete Institute, *ACI Concrete Terminology*, Farmington Hills, MI, 2018.
- [3] A. H. Mattock, J. A. Hofbeck and I. O. Ibrahim, "Shear Transfer in Reinforce Concrete," *ACI Journal*, vol. 66, no. 2, pp. 119-128, 1969.
- [4] A. H. Mattock and N. M. Hawkins, "Shear Transfer in Reinforced Concrete - Recent Research," *PCI Journal*, vol. 17, no. 2, pp. 55-75, 1972.
- [5] B. Barragain, R. Gettu, L. Agullu and R. Zerbio, "Shear Failure of Steel Fiber-Reinforced Concrete Based on Push-Off Tests," *ACI Materials Journal*, vol. 103, no. 4, pp. 251-257, 2006.
- [6] E. B. Sells, "Self-Consolidating Concrete for Infrastructure Elements Shear Characteristics," Missouri University of Science and Technology, Rolla, MO, 2012.
- [7] D. M. Shaw, "Direct Shear Transfer of Lightweight Aggregate Concretes with Non-Monolithic Interface Conditions," Missouri University of Science and Technology, Rolla, MO, 2013.
- [8] C. M. Wirkman, "Performance of Fiber-Reinforced Self-Consolidating Concrete for Repair of Bridge Sub-Structures," The University of Oklahoma, Norman, OK, 2016.
- [9] K. S. Wallace, "Performance of Fiber-Reinforced Eco-Friendly Concrete for Bridge Structures," The University of Oklahoma, Norman, OK, 2016.
- [10] Oklahoma Department of Transportation Transportation Commission, "Standard Specifications," 2009.
- [11] ASTM C39-18, Standard Test Method for Compressive Strength of Cylindrical Concrete Specimens, ASTM International, 2018.
- [12] ASTM C469-14, Standard Test Method for Static Modulus of Elasticity and Poisson's Ratio of Concrete in Compression, ASTM International, 2014.

- [13] ASTM C496-17, Standard Test Method for Splitting Tensile Strength of Cylindrical Concrete Specimens, ASTM International, 2017.
- [14] ASTM C78-18, Standard Test Method for Flexural Strength of Concrete, ASTM International, 2018.
- [15] E. B. Sells, J. J. Myers and J. S. Volz, "Aggregate Interlock Push-Off Test Results of Self-Consolidating Concrete (SCC) for Use in Infrastructure Elements," in *New Developments in Structural Engineering and Construction* , 2013.
- [16] J. C. Walraven and J. Stroband, "Shear Friction in High-Strength Concrete," in *SP-149, American Concrete Institute International Conference*, Singapore, 1994.
- [17] F. J. Vecchio and D. Lai, "Crack Shear-Slip in Reinforced Concrete Elements," *Journal of Advanced Concrete Technology*, vol. 2, no. 3, pp. 289-300, 2004.
- [18] J. Walraven, F. Jerome and P. Arjan, "Influence of Concrete Strength and Load History on the Shear Friction Capacity of Concrete Members," *PCI Journal*, vol. 32, no. 1, pp. 66-84, 1987.

IV. Aggregate Interlock and the Effect of Micro and Macro Synthetic Fibers

Jonathan T. Drury and Jeffery S. Volz

Abstract

As concrete professionals continually push the limits of concrete performance, they regularly experiment with the constituents used to produce concrete. From this, fiber reinforcement has become regularly implemented. It is clear that the overall performance of fiber reinforced concrete is superior in many ways when compared to plain concrete. However, data on the internal mechanics of fiber reinforced concrete has not been heavily investigated. Based on this, an experimental study was designed to investigate the aggregate interlock performance of concrete with and without fiber reinforcement present. A proposed improvement on the commonly used push-off tests was used to investigate aggregate interlock. The experimentally obtained load-slip relationships were investigated, and the improved push-off test was compared to historic data.

Eight different concrete mixtures were investigated: a conventional concrete with limestone (CC), CC with the addition of micro-fibers (CC1), CC1 with the addition of macro-fibers (CC2), a cement-limiting and optimized-aggregate concrete (EBC), EBC with the addition of micro-fibers (EBC1), EBC1 with the addition of macro-fibers (EBC2), a self-consolidating concrete (SCC) produced with pea gravel (K15), and K15 with the addition of macro-fibers (K15F).

This study showed that the addition of micro-fibers improved cohesion of the concrete and allowed for greater maintained shear resistance throughout the test. However, when macro-fibers were added to the concrete, the behavior of the specimens

improved at times and decreased at times. The behavior of the macro-fibers were shown to govern the behavior of the concrete, as the data converged upon a given shear strength.

Keywords

aggregate, interlock, push-off, non-traditional, concrete, shear, synthetic, fiber(s), micro, macro

Introduction

Traditional concrete constituents fall into three categories: cementitious material, aggregate, and water. Concrete has great longevity when used efficiently in compression but using it in other applications requires the need for a new constituent, tension reinforcement. This discovery led to the invent of reinforced concrete. Reinforced concrete has greatly improved the behavior of plain concrete, but problems still arise in regions between segments of reinforcement. To combat this, fiber reinforced concrete is being developed. Fiber reinforced concrete minimizes the distance between tension reinforcement inside the concrete and provides a randomized reinforcement orientation to provide reinforcement in many more directions than traditional reinforcement.

While shear behavior of traditional concrete is a complex phenomenon not completely understood, researchers believe there are three main mechanisms that govern it: tensile strength of the cementitious matrix, presence of reinforcement, and aggregate interlock. Fiber reinforced concrete presents a major issue for these three-piece models because fibers influence all three mechanisms.

The objective of this study is to understand the influence of fibers on aggregate interlock and, to a greater extent, the shear behavior of concrete. To this end, an improved method for push-off testing was performed on eight different concrete mixtures with three specimens tested for each. The mixtures were a conventional concrete (CC), CC with the addition of micro-fibers (CC1), CC1 with the addition of macro-fibers (CC2), a cement-limiting and optimized-aggregate concrete (EBC), EBC with the addition of micro-fibers (EBC1), EBC1 with the addition of macro-fibers (EBC2), a self-consolidating concrete (SCC) produced with pea gravel (K15), and K15 with the addition of macro-fibers (K15F). The experimentally obtained load-slip relationships were investigated, and the improved push-off test was compared to historic data.

Research Significance

The fundamental knowledge of shear failure in concrete is essential for structural design, and aggregate interlock plays an important role in shear behavior. The influence on this behavior of fiber reinforcement must be understood to utilize fiber-reinforced concrete in structural applications. This paper expands knowledge of fiber reinforced concrete by investigating non-metallic fibers.

Push-Off Test Background

Aggregate interlock, one of three main shear transfer mechanisms inside reinforced concrete, has been the focus of research for over 50 years [1]. The research started due to a need to understand the impact friction played in structural connections of precast elements. The first tests were designed to simply gather data for specific

design connections, and it was focused on surface friction, and not directly on aggregate interlock.

Subsequent researchers extended the ideas of Hanson and applied them to better understanding shear behavior in concrete elements. This research led to defining the term aggregate interlock as “the effect of portions of aggregate particles from one side of a joint or crack in concrete protruding into recesses in the other side of the joint or crack so as to transfer load in shear and maintain alignment” [2]. The research has seen many different test setups [3, 4, 5, 6, 7], but the basic principles are consistent: create a weak plane to force concrete failure, provide a normal force perpendicular to the failure plane, provide a force parallel to and in line with the failure plane, monitor loads and displacements.

The two major difference between test setups have been in the method of providing normal force. The first method to provide normal force was through internal reinforcement perpendicular to and through the failure plane. The concrete would bond to the reinforcement, and the reinforcement would act as a crack inhibitor. To monitor the level of force containing the crack, strain in the reinforcement was recorded. This method was an obvious choice, as it modeled shear steel in reinforced concrete elements, however it had major drawbacks. In attempting to monitor the behavior of aggregate interlock, the reinforcement was corrupting the data by providing crack slip resistance. Researchers presented methods to refine the data, but this was still not presenting a clear picture of the shear behavior of the concrete alone.

The second method to provide normal force was through external reinforcement. This was obtained through externally mounted confinement. To monitor the level of

force containing the crack, strain in the confining members was recorded. This method was an improvement on the previous method, as it allowed only the concrete interface to resist shear forces. Another benefit of this second method was that it allowed investigation of the crack surface after the test was completed. By visually inspecting the failed surfaces, researchers could better understand the mechanisms resisting shear.

Experimental Program

Push-Off Specimen Design

The specimens for this research were based on previous externally reinforced members. The main difference in the proposed test method and previous research was that the concrete specimens were cracked without any perpendicular normal forces present. The specimens were cracked in this manner to provide a means of visual inspection of the failure plane prior to as well as after push-off testing. The specimen geometry is detailed in Figure 1. The push-off specimens were designed with a 7.5 in. (190 mm) by 4.0 in. (100 mm) failure surface. The outside dimensions of the specimens were 10.0 in (255 mm) by 18.0 in. (460 mm). The slots that separate the monolithic specimen into two halves protruded 5.25 in. (135 mm) into the specimen and were trapezoidal with exterior widths of 1.5 in. (40 mm) and interior widths of 0.5 in. (15 mm). A triangular 0.5 in. (15 mm) wide by 0.25 in. (5 mm) deep groove was cast into opposite faces of the specimen to create the desired reduced sized failure surface.

Reinforcement was installed in the specimens to prevent failures other than through the desired plane. The reinforcement was constructed using #3 (metric #10) size grade 40 (metric grade 280) deformed steel bars. P-shaped cages were constructed to provide 1.0 in. (25 mm) cover around the edges of each half of the specimen, and no

steel within 3.0 in. (75 mm) of the failure surface. The cages were built with two layers, and again built with 1.0 in. (25 mm) cover from the rebar to any concrete surface. The reinforcement detail is displayed in Figure 1. For clarity, the reinforcement is only drawn for one half of the symmetric specimen.

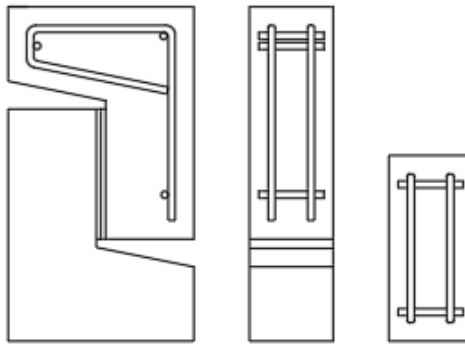


Figure 1 – Rebar detail for push-off specimens

High-strength steel rods and plates were used to produce the external reinforcement and wedges for pre-cracking the specimens. The rods were 0.5 in. (15 mm) diameter and sufficiently long to properly install a washer and nut on each end. The confining plates were 0.75 in (20 mm) thick, 8.0 in (200 mm) wide and 12.0 in (300 mm) long. Holes were drilled into the plates to create 0.5 in. (15 mm) clearance between the rods and the specimen. The wedges were 0.75 in. (20 mm) thick, 4.0 in (100 mm) wide, 8.0 in. (200 mm) long and had one long edge machined down to create a 60° angle point. The point was set to a smaller angle than the groove angle (90°) to create a line load in the groove instead of a distributed load. Drawings of the steel pieces are shown in Figure 2.

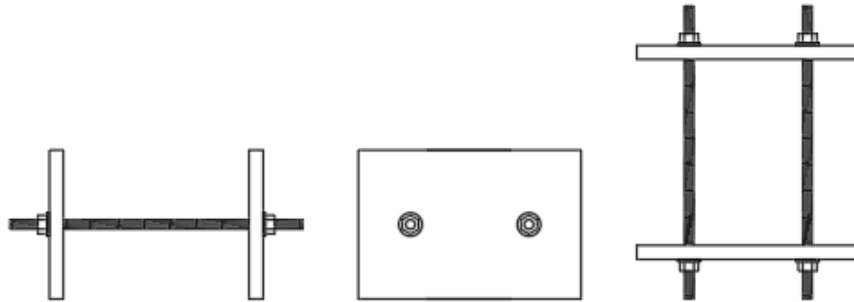


Figure 2 – External steel reinforcement rods and plates

The load path and instrumentation for the push-off test is detailed in Figure 3.

One strain gauge was installed on each threaded rod. The rod strains were used to monitor the compressive normal force being applied perpendicularly to the failure plane. One linear variable differential transformer (LVDT) was installed on the face of each specimen to monitor the opening of the crack width. The crack slip was monitored via an LVDT magnetically mounted to the moving crosshead of the testing machine. Angles were epoxied to the same face of the specimen to provide contact points for tips of the LVDTs.

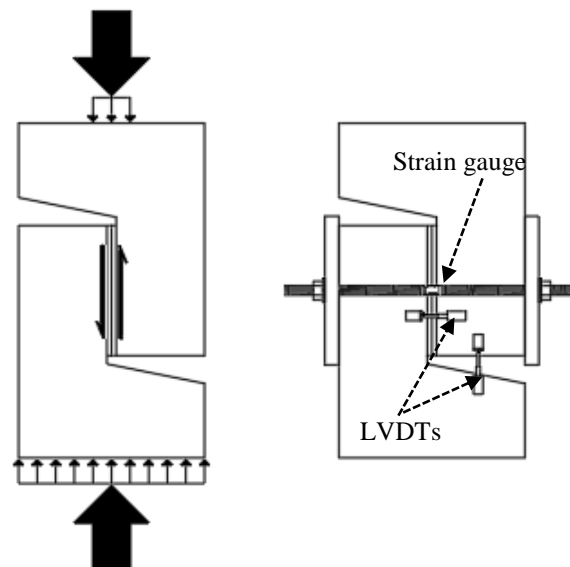


Figure 3 – Load path diagram and instrumentation layout

Materials and Specimen Preparations

The three mix designs investigated in this study were developed for previous research [8, 9]. They were designed for use as structural concrete per the performance specifications of the Oklahoma Department of Transportation (ODOT) [10]. The cementitious material properties, aggregate properties, fiber properties, and mix designs are detailed in Tables 1, 2, 3, and 4, respectively. A third cementitious material was used in this study, but it was a proprietary expansive cement called Komponent® from CTS Manufacturing Corp (Cypress, CA). Komponent® is an expansive calcium sulfoaluminate (CSA) cement-based additive that is used to produce ASTM C845 Type K Shrinkage Compensating cement. Due to it being proprietary, it is not detailed in Table 1.

Table 1 – Cementitious material properties

Property	Type I/II Cement	Class C fly ash
Fineness (+325 mesh), %	—	10.3
Air permeability, ft ² /lb	1939	—
Specific gravity	3.11	2.72
Loss on ignition, %	2.4	0.67
Silica, %	20.8	31.9
Aluminum oxide, %	3.8	20.4
Ferric oxide, %	3	5.9
Sulfur trioxide, %	2.9	3.0
Calcium oxide, %	63.9	28.3
Magnesium oxide, %	1.9	7.2

Note: 1 ft²/lb = 2.05 cm²/g

Table 2 – Aggregate properties

Property	#57	3/8" chip	3/8" pea gravel	Concrete sand
Specific gravity, oven-dry	2.69	2.67	2.59	2.65
Dry-rodded unit weight, lb/ft ³	101	95	105	—
Absorption, %	0.86	1.01	0.72	0.7
LA abrasion, % loss	26	22	22	—
Mohr's hardness	3.5 - 4	3.5 - 4	3 - 3.5	—

Note: 1 lb/ft³ = 16 kg/m³

Table 3 – Fiber properties

Property	MasterFiber M 100	MasterFiber MAC Matrix
Specific gravity	0.91	0.91
Absorption	Nil	Nil
Tensile strength, ksi	70	85
Nominal length, in.	0.75	2.1
Nominal diameter, in.	0.00047	0.03
Material	Polypropylene	Polypropylene

Notes: 1 in. = 25.4 mm; 1 ksi = 6.89 MPa

Table 4 – Mix designs (per yd³)

	CC	CC1	CC2	EBC	EBC1	EBC2	K15	K15F
Type I/II cement	470	470	470	414	414	414	413	413
Class C fly ash	118	118	118	103	103	103	224	224
Komponent®	—	—	—	—	—	—	113	113
w/cm	0.4	0.4	0.4	0.4	0.4	0.4	0.39	0.39
#57 limestone, lb	1857	1857	1857	989	989	989	—	—
3/8" chip, lb	—	—	—	565	565	565	—	—
3/8" pea gravel, lb	—	—	—	—	—	—	1223	1223
Concrete sand, lb	1323	1323	1323	1415	1415	1415	1401	1401
Micro-fibers, lb	—	0.5	0.5	—	0.5	0.5	—	—
Macro-fibers, lb	—	—	3.0	—	—	3.0	—	3.0
HRWR, fl oz	26.7	26.7	26.7	36.2	36.2	36.2	67.6	67.6
AEA, fl oz	4.40	4.40	4.40	2.59	2.59	2.59	8.3	8.3
Citric acid, g	—	—	—	—	—	—	176	176

Notes: 1 lb = 0.454 kg; 1 fl oz = 29.5 mL

The specimens were cast by carefully placing concrete into the form to maintain the rebar in its desired locations. Tamping rods and mallets were used to consolidate the specimens. Once the concrete had stiffened enough to hold the shape of the groove, a

grooving tool was used to shape and center the groove on the open side of the specimen. Cast specimens were covered with wet burlap and plastic sheeting to cure for 7 days. After 7 days, the concrete was left to cure in a controlled room at 50% RH and 72°F (22.2°C). Companion cylinder specimens were cast along with each batch of push-off specimens, and they were cured alongside the push-off specimens. Also, a full characterization of each concrete mix was performed to determine the 28-day properties per ASTM standards [10, 11, 12, 13]. The mix characterization data is presented in Table 5.

Table 5 – Mix characterizations

Property	CC	CC1	CC2	EBC	EBC1	EBC2	K15	K15F
Slump or slump flow, in.	6	—	—	4	—	—	30	—
Air content, %	6.0	—	—	9.0	—	—	10.5	—
Unit weight, lb/ft ³	144	—	—	143	—	—	139	—
Compressive strength [†] , psi	6,385	8,500	9,250	6,425	6,400	6,520	5,530	6,010
Modulus of elasticity [†] , ksi	4,250	4,200	4,310	3,600	3,640	4,050	3,950	4,080
Split cylinder strength [†] , psi	525	610	650	525	540	565	480	511
Modulus of rupture [‡] , psi	560	690	721	620	676	712	700	549

[†]Values represent an average of three cylinders (ASTM C39, ASTM C469 and ASTM C496)

[‡]Values represent an average of three beams (ASTM C78)

Notes: 1 in. = 25.4 mm; 1 lb/ft³ = 16 kg/m³; 1 psi = 0.00689 MPa; 1 lb/in = 175.1 N/m

Push-Off Test Setup and Procedure

To pre-crack the specimens, high-density neoprene pads were used to restrain the bottom wedge from slipping as well as to protect the cracked specimen halves from damage after being cracked. Each specimen was installed into the testing machine and cracked with a wedge applying a line load to each side of the failure plane. The loads were applied slowly, and immediately removed once the crack was formed. The peak

load required to crack each specimen was recorded. The specimen halves were then inspected and photographed to characterize the pre-test (post-cracking) surfaces. For specimens that cracked, but did not separate, care was taken to prevent damage while handling them prior to installing the external reinforcement.

After inspecting the pre-cracked specimens, the two halves were carefully seated together, and the external reinforcement was placed on the specimen. The threaded rods were then tensioned to provide 200 to 300 psi (1.4 to 2.1 MPa) of compression onto the failure plane. The confined specimen was then centered in the testing machine, and the LVDTs were installed onto the specimen. At this point, the bar strains were noted, and the gauges were zeroed. A small steel plate was placed between the top surface of the specimen and the top crosshead to better concentrate the load. The load was then slowly applied parallel to the failure surface, and the instrumentation readouts were monitored. The test was stopped when either an LVDT was extended or compressed to its extreme limit or a rod strain was such that the rods were approaching yielding. It was desired to open each crack width past 0.045 in. (1.1 mm) as well as to push each crack slip past 0.325 in. (8.3 mm) based on previous research.

Once a criterion was met to signal stopping the test, the load was immediately removed from the testing machine, and the threaded rods were de-tensioned and removed. The two halves of the push-off specimen were then again inspected and photographed.

Test Results and Comparison

Results of Pre-Cracking

The first method to analyze the pre-cracking behavior of the eight mixtures was visual inspection. For all three CC specimens, pre-cracking caused the specimens to break into two pieces along the desired failure plane. There was minimal debris generated during this step, and nearly all aggregate crossing the plane was fractured along the plane. For all three CC1 specimens, pre-cracking again caused the specimens to break into two pieces along the desired failure plane. There was less debris generated during this step, and again nearly all aggregate crossing the plane was fractured along the plane. The influence of micro-fibers appeared to hold the cementitious matrix together. For all three CC2 specimens, pre-cracking did not cause the specimens to break into two pieces. The failure plane was visible, but the macro-fibers appeared to hold the specimens together.

For all three EBC specimens, pre-cracking caused the specimens to break into two pieces along the desired failure plane. There was minimal debris generated during this step, and nearly all aggregate crossing the plane was fractured along the plane. Two of the EBC1 specimens broke into two pieces during pre-cracking, and one did not. Of the two that broke into two, less debris was generated compared to EBC, and again nearly all aggregate crossing the plane was fractured along the plane. Again, the micro-fibers appeared to hold the cementitious matrix together better than when no micro-fibers were present. For all three EBC2 specimens, the pre-cracking did not cause the specimens to break into two pieces. The failure plane was visible, but the macro-fibers appeared to hold the specimens together.

Two of the K15 specimens broke into two pieces during pre-cracking, and one did not. Of the two that broke into two, some of the aggregate fractured along the failure plane, but many de-bonded and remained intact. Again, there was not much debris generated during pre-cracking. For all three K15F specimens, pre-cracking did not cause the specimens to break into two pieces. The failure plane was visible, but the macro-fibers appeared to hold the specimens together.

The quantitative data from testing all eight mixtures in pre-cracking is given in Table 6. The apparent tensile strength was calculated using Equation 1.

$$f_t^* = \frac{P}{A} \quad \text{Eqn. 1}$$

P = Applied shear force

A = Surface area of the failure surface

To understand the influence of the addition of fibers, the change in properties correlated to the change in fibers is also presented in Table 6. Also, the ratio of apparent tensile strength to compressive strength was calculated and presented as well. From this data, micro-fibers appear to yield a greater improvement on tensile strength than compressive strength. Macro-fibers however don't appear to have a consistent effect on the tensile or compressive behavior of the concrete mixtures.

Table 6 – Apparent tensile and compressive strength comparisons

Concrete Mixture	Apparent Tensile Strength (psi)	% Change	Compressive Strength (psi)	% Change	Ratio of Tensile to Compressive	% Change
CC	342	---	5501	---	0.062	---
CC1	480	40	6683	21	0.072	16
CC2	476	-1	8254	24	0.058	-20
EBC	313	---	5878	---	0.053	---
EBC1	331	6	5945	1	0.056	5
EBC2	373	13	6120	3	0.061	9
K15	419	---	5890	---	0.071	---
K15F	366	-13	7113	21	0.051	-28

Note: 1 psi = 0.00689 MPa

Load-Displacement Responses

The push-off test determines the ability of a pre-cracked failure plane to transfer shear. For that reason, the first trend that is of note is the shear stress-displacement response. Figure 4 is a plot of the shear stress versus the crack slip for the CC based mixtures. The plot shows that the addition of micro and macro-fibers improved the shear strength of the concrete. Also shown is that the fibers continued to improve the shear resistance of the mixture throughout the duration of the test whereas the mixture containing no fibers peaked on shear resistance at around 0.20 in (mm) of slip.

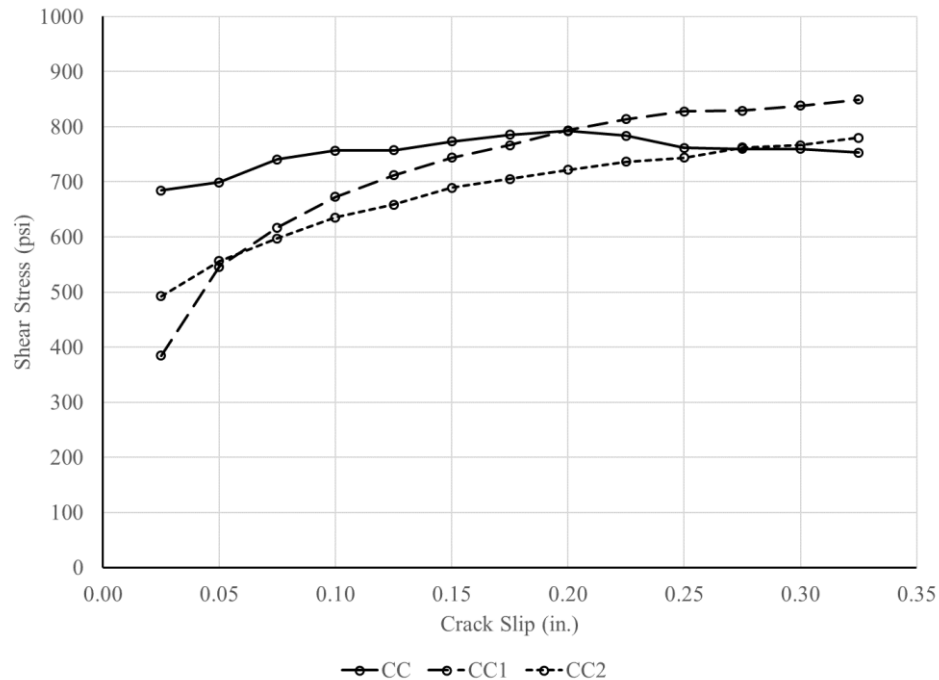


Figure 4 – Shear stress versus crack slip for CC based mixtures

Figure 5 is a plot of the shear stress versus the crack slip for the EBC based mixtures. The plot shows again that the addition of both micro and macro-fibers improved the shear strength of the concrete. However, while the micro-fibers continued to improve the shear resistance throughout the duration of the test, the micro-fiber concrete reached peak shear resistance at around 2.0 in. (mm) of slip. Mixture EBC, which contained no fibers, peaked on shear resistance at around 0.05 in. (mm).

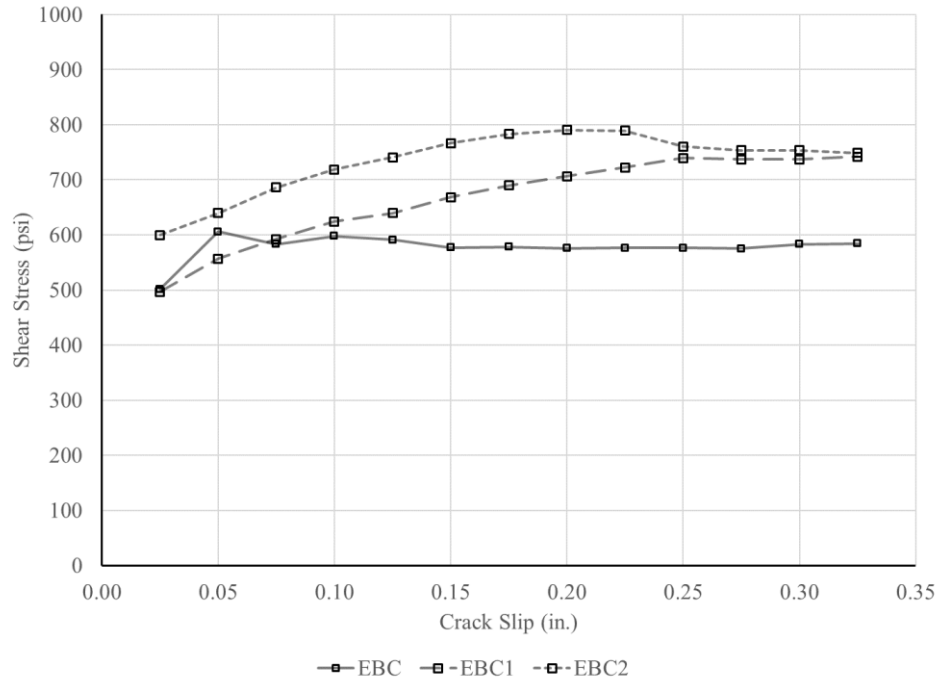


Figure 5 – Shear stress versus crack slip for EBC based mixtures

Figure 6 is a plot of the shear stress versus the crack slip for the mixtures K15 and K15F. The plot shows that the addition of macro-fibers to the concrete caused a reduction in the shear resistance. This behavior is in line with the apparent tensile strength from the pre-cracking. However, the correlation between the two tests does not help to explain why tensile strength and shear strength are reduced with the addition of fibers.

To gain a better picture of the behavior of the macro-fiber reinforced concrete, only the mixtures containing no fibers and those containing macro-fibers were plotted in Figure 7. As can be seen from Figure 7, the shear strength for macro-fiber reinforced concrete appears to converge. This behavior suggests that the shear strength of concrete containing macro-fibers is likely governed by the performance of those fibers.

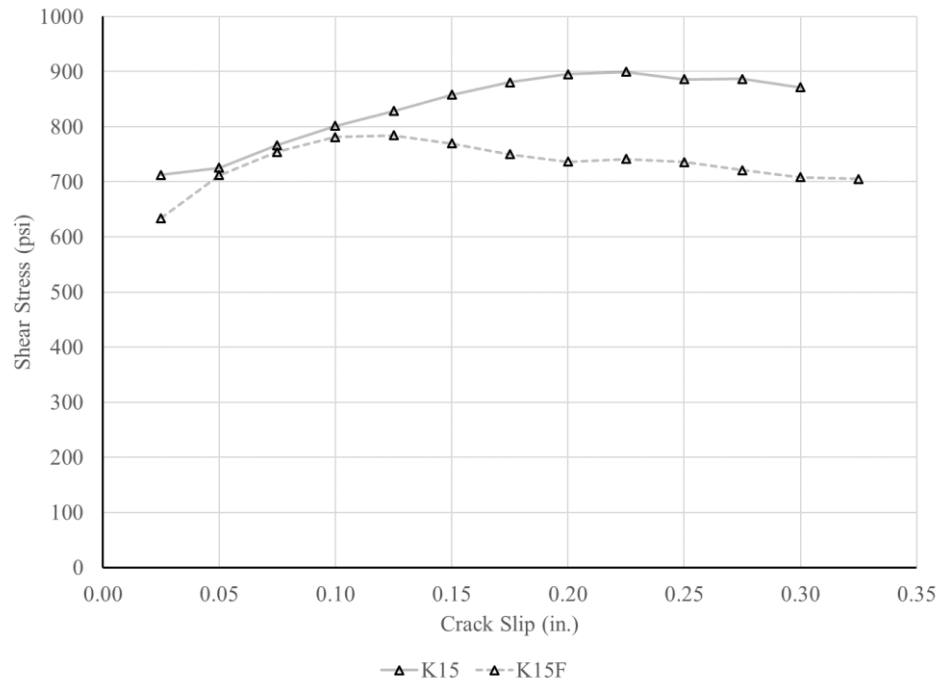


Figure 6 – Shear stress versus crack slip for K15 based mixtures

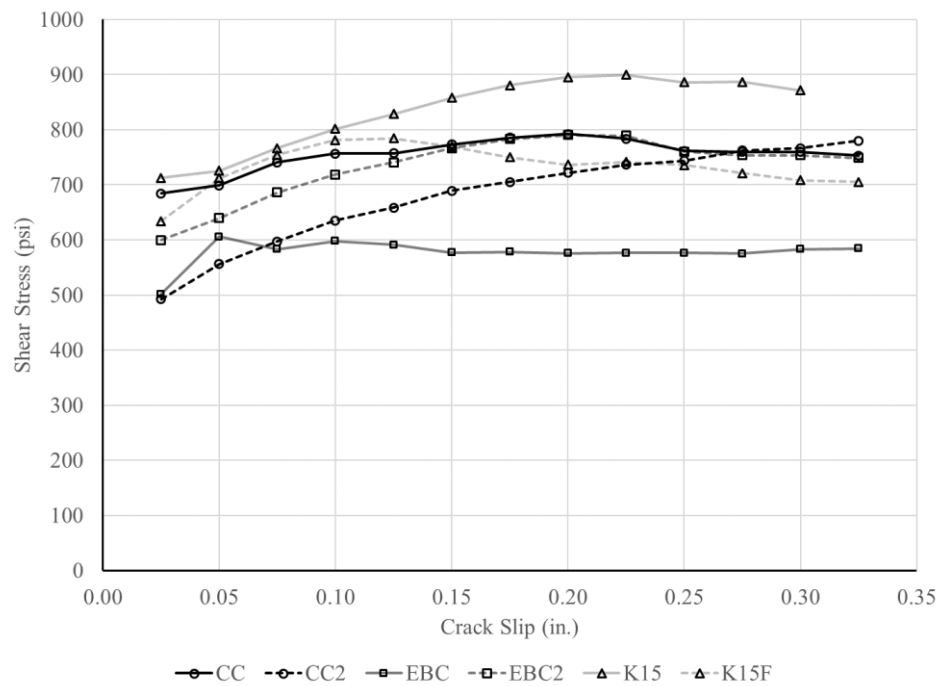


Figure 7 – Shear stress versus crack slip for concrete mixtures with and without macro-fibers

Another helpful means of presenting the shear stress data is residual shear strength. The residual shear strength is defined as the shear strength present in the

system at a given slip limit. Table 7 presents the peak shear strength as well as residual shear strengths at given slip limits. This further illustrates the relative plateauing of the non-fiber mixtures (CC, EBC, and K15) and the continued improvement in shear strength with fibers for CC and EBC. The K15 mixtures again show the decrease in shear strength which may be more a function of the pea gravel and fiber interaction.

Table 7 – Peak and residual shear strengths at given slip values

Concrete Mixture	Peak Shear Strength (psi)	Residual Shear Strength (psi)		
		0.10 in.	0.20 in.	0.30 in.
CC	793	757	793	760
CC1	849	673	793	838
CC2	780	635	722	766
EBC	606	598	576	583
EBC1	742	624	706	737
EBC2	791	719	791	753
K15	900	802	895	872
K15F	784	781	736	708

Note: 1 psi = 0.00689 MPa, 1 in. = 25.4 mm

As shear stress is generated along the failure plane, the imperfection in the surface must either shear off or the crack must widen. Any opening of the crack will lead to an increased normal force. Figures 8, 9, and 10, respectively, are plots of the normal stress versus the crack slip for each of the three base mixture types. Each curve on the plot is an average of at least two push-off test results.

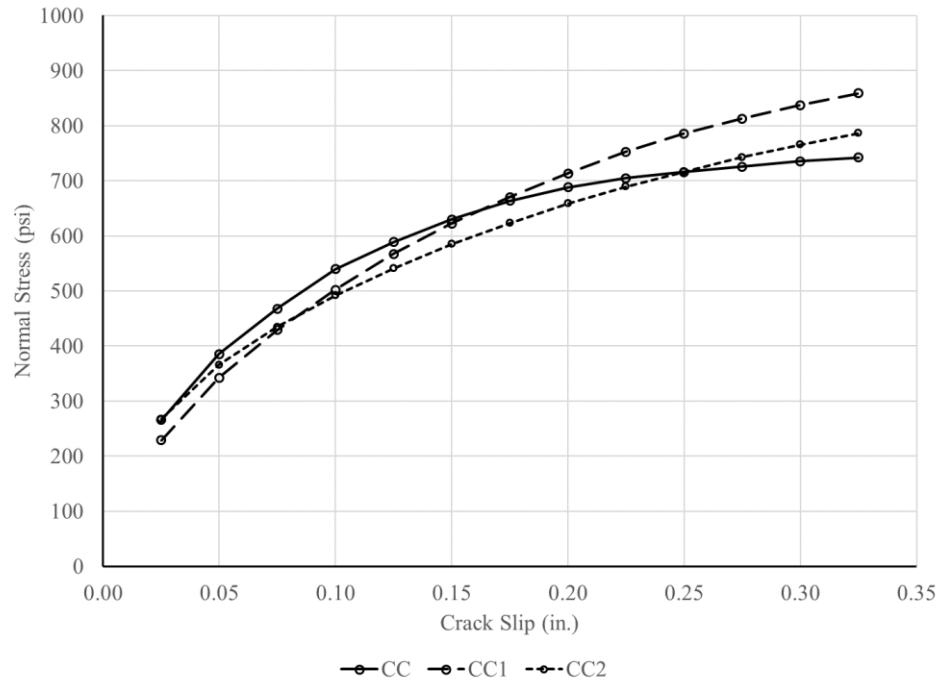


Figure 8 – Normal stress versus crack slip for CC based mixtures

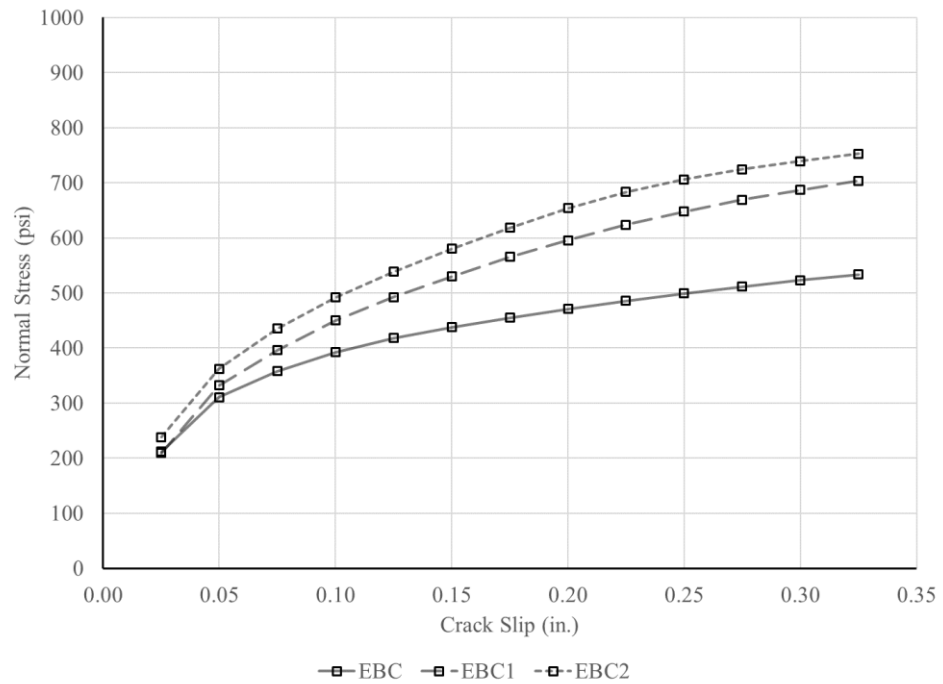


Figure 9 – Normal stress versus crack slip for EBC based mixtures

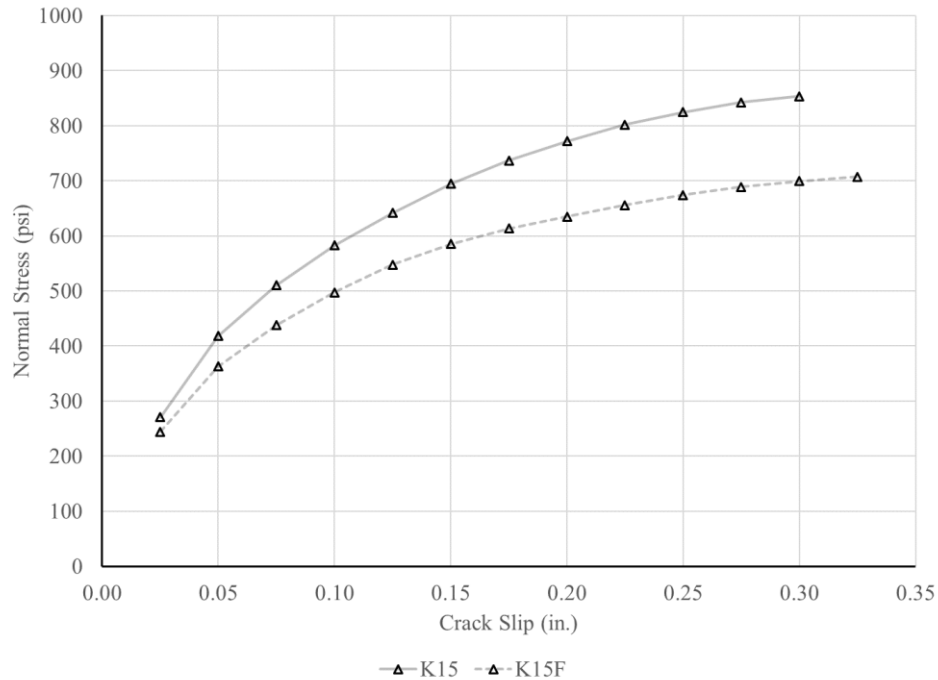


Figure 10 – Normal stress versus crack slip for K15 based mixtures

The plots show similar behavior to the shear stress versus slip data. Again, in the CC and EBC based mixtures, the presence of synthetic fibers increase the stresses generated from push-off testing, but in the K15 based mixtures, fibers decreased the stresses generated. As was stated before, normal stresses generated during the test are due to the two non-true failure surfaces pushing each other apart when they are being forced to slide next to each other. To fully illustrate the crack slip and crack width opening relationship, Figures 11, 12, and 13, respectively, plot crack slip versus crack opening for all three mixture types.

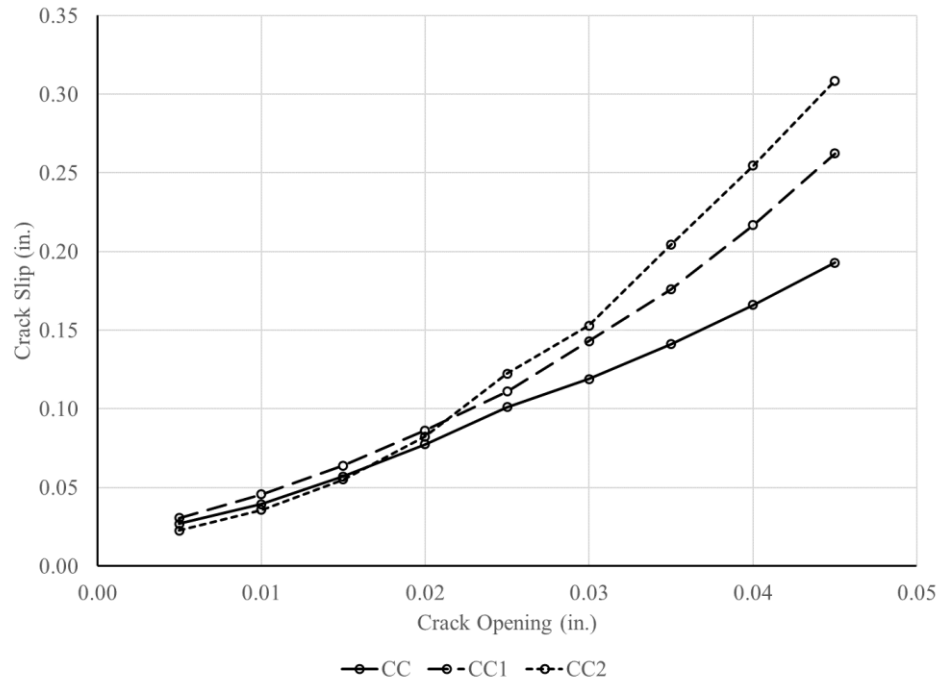


Figure 11 – Crack slip versus crack opening for CC based mixtures

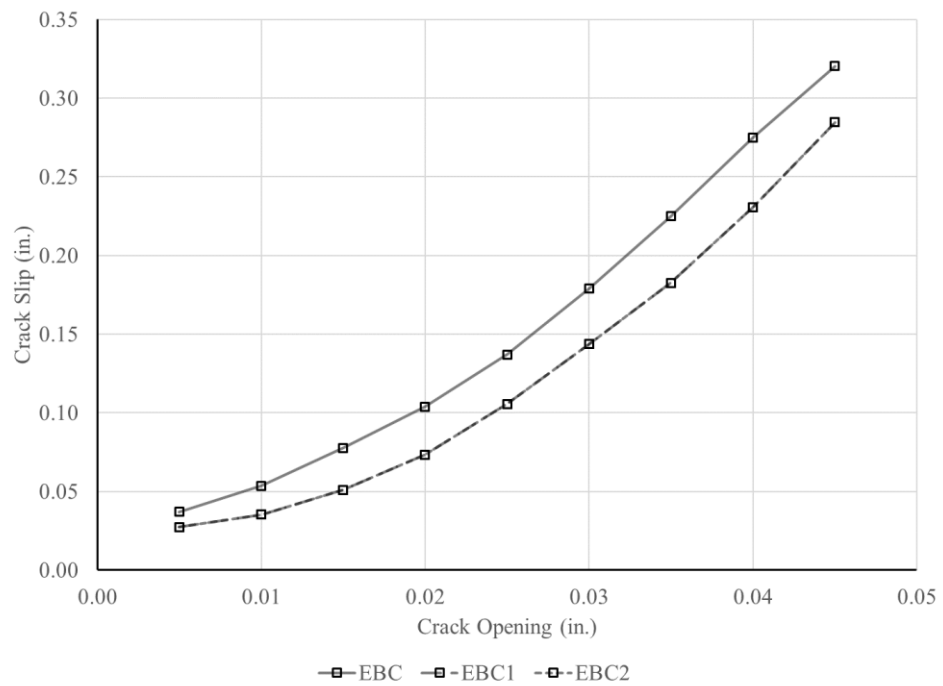


Figure 12 – Crack slip versus crack opening for EBC based mixtures

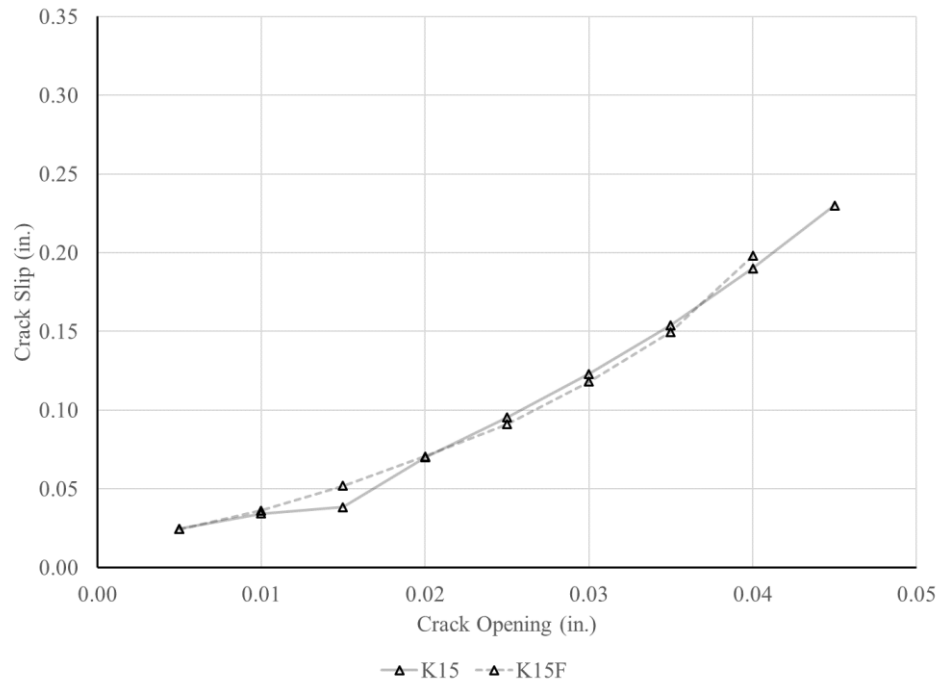


Figure 13 – Crack slip versus crack opening for K15 based mixtures

These plots show that the influence of fibers again have both positive and negative effects on influencing a crack's tendency to widen. In CC based mixtures and K15 based mixtures, the presence of fibers is shown to hold cracks together better, which is shown by reduced or maintained crack openings for a given crack slip value. However, the EBC based mixtures exhibited larger crack widths for a given crack slip. This may be due to the reduced cement paste. By reducing the paste, the bond between fibers, paste, and aggregate is weaker. Also, the smooth surfaces of the EBC specimens were more roughened more by the addition of fibers than the more roughened surfaces of the CC and K15 specimens.

Coefficients of Friction

The coefficient of friction of concrete is complex because it involves terms for both the cohesion of the concrete and the roughness of the failure surface. However, the coefficient of friction for a push off test is simpler because there is no cohesion over the cracked surface, and the equation simplifies to the ratio of the shear stress divided by the normal stress. Figures 14, 15, and 16, respectively, are plots of the ratio of shear stress to normal stress versus crack slip for all three mixture types.

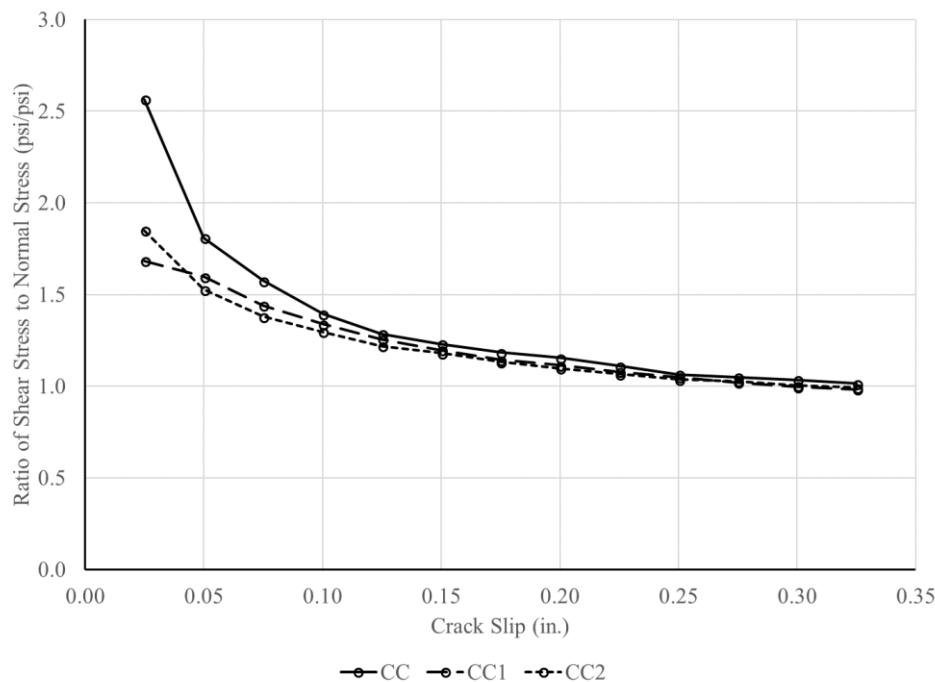


Figure 14 – Ratio of shear to normal stress versus crack slip for CC based mixtures

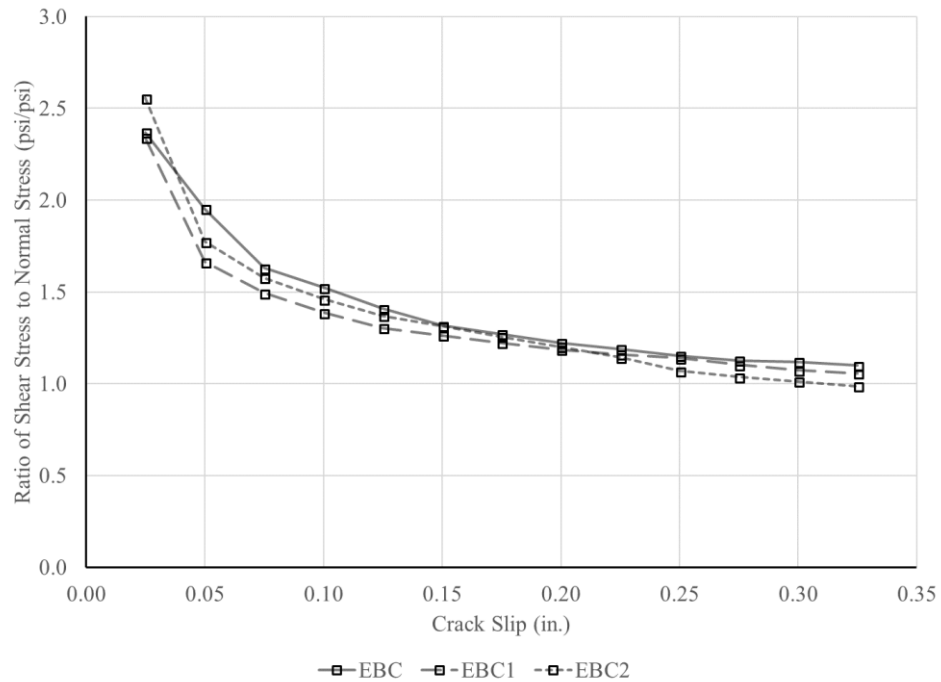


Figure 15 – Ratio of shear to normal stress versus crack slip for EBC based mixtures

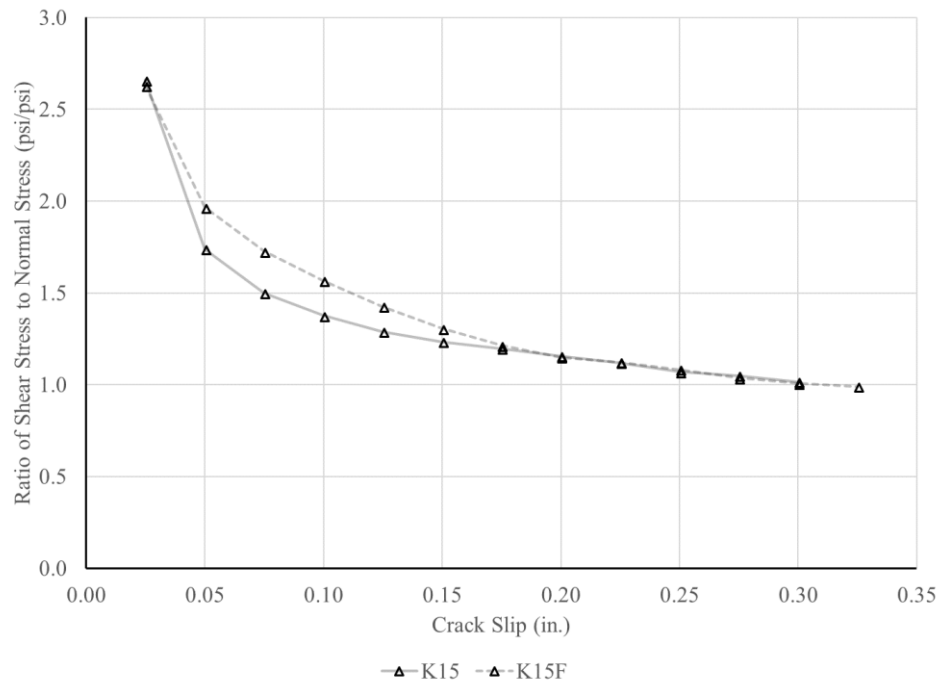


Figure 16 – Ratio of shear to normal stress versus crack slip for K15 based mixtures

As with the residual shear strength, it may be helpful to present the residual friction coefficient for a given displacement. The peak friction coefficients and the

residual friction coefficients at given slip limits are presented in Table 8. Note that the peak coefficients may be larger than the plotted values. That is because the average peaks did not all occur at the same slip values plotted.

Table 8 – Peak and residual coefficients of friction at given slip values

Concrete Mixture	Peak Coefficient of Friction	Residual Coefficient of Friction		
		0.025 in.	0.050 in.	0.075 in.
CC	2.89	2.57	1.81	1.58
CC1	1.93	1.68	1.60	1.44
CC2	2.08	1.85	1.53	1.38
EBC	3.22	2.37	1.95	1.63
EBC1	2.49	2.34	1.66	1.49
EBC2	2.98	2.56	1.77	1.58
K15	3.01	2.66	1.74	1.50
K15F	2.81	2.63	1.97	1.73

Note: 1 in. = 25.4 mm

To put these friction coefficients into perspective, it is important to compare these values to common friction coefficients. The PCI Handbook 6th Edition presents maximum effective coefficients of friction for different surface considerations [7].

Table 9 presents the 4 cases along with their coefficients.

Table 9 – PCI maximum coefficients of friction

Case	Crack Interface Condition	Max Coefficient of Friction
1	Concrete to concrete, cast monolithically	3.4
2	Concrete to hardened concrete, with roughened surface	2.9
3	Concrete placed against hardened concrete not intentionally roughened	2.2
4	Concrete to steel	2.4

Based on the code values for coefficients of friction, the experimental data for concrete without fibers correlates well with previous data. The CC, EBC, and K15 coefficients fall between the table values for the “concrete to hardened concrete, with roughened surface” and “concrete to concrete’ cast monolithically.” This is a good sign,

as code values are intentionally conservative. However, when fibers are added to the concrete, the coefficients fall well below the values given in the code. This is a problem for two reasons. Firstly, if the concrete performance is not in line with the design codes, then designs are not conservative and run the risk endangering lives. This is unacceptable. Secondly, as the shear strength data showed, micro fibers always showed an improved performance over their non-fiber concrete counterparts. This would suggest that this method of determining shear friction potential to be flawed.

Comparison of the Proposed Test

To submit this new test as an improvement on the existing methods, it is important to compare data from past research. However, since this is not a standardized test method, researchers have chosen to focus on different results. Presented in Figure 17 is a comparison between this study and historic data on push-off testing with external reinforcement. Note, the previous test methods differed from the proposed method by attaching the external reinforcement prior to pre-cracking. While the two methods are slightly different, the side-by-side comparison shows that they generate similar data. A better comparison would be to compare load and displacement data directly, but these researchers only presented these plots to compare their data to historic data [15].

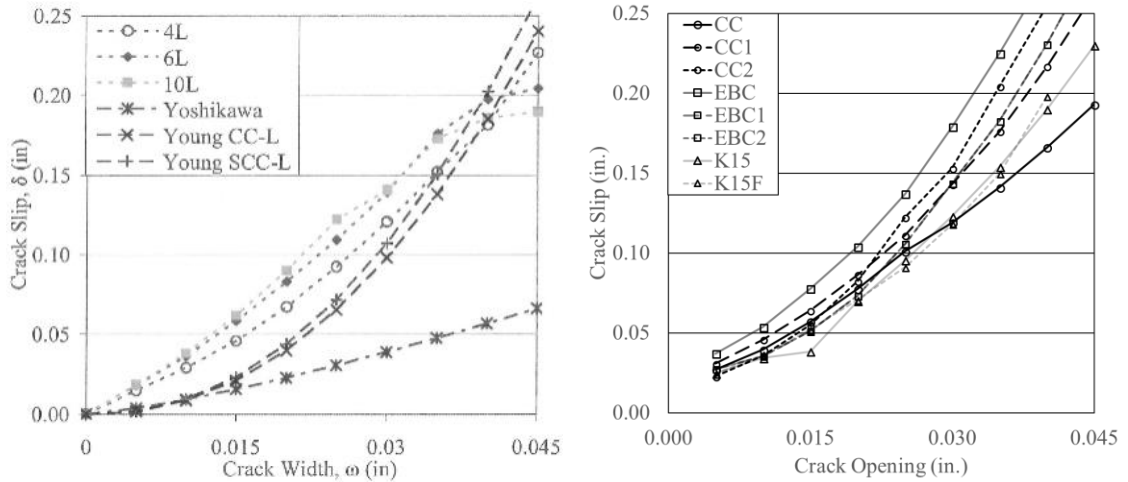


Figure 17 – Comparison to historic externally reinforced push-off testing

Presented in Figure 18 is a comparison between this study and historic data [7] on push-off testing with internal reinforcement. Note, this test methods differed from the proposed method by using internal bars crossing the failure plane to provide the normal force to the shearing surfaces. These researchers presented their data, allowing for a better comparison to be made. The plotted data strongly suggests that the proposed method not only is an acceptable method to acquire data on aggregate interlock and shear, but it is an improvement. While the sample size is small, the data is more consistent and reproducible. For this reason, and the many other presented, this method is proposed.

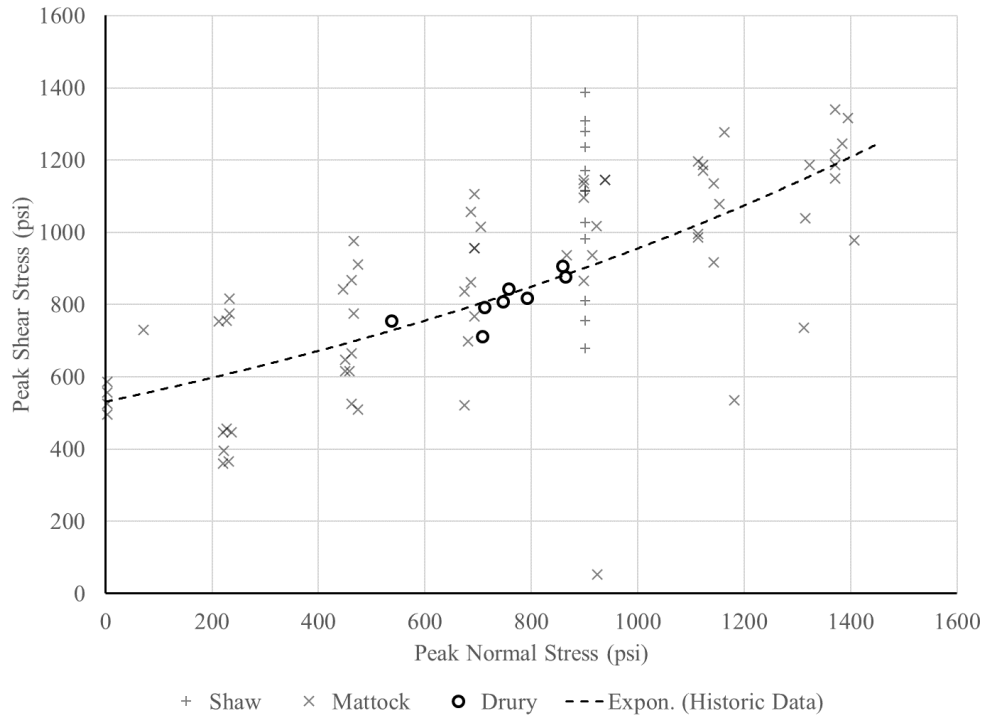


Figure 18 – Comparison to historic internally reinforced push-off testing

A main reason this test is more reproducible is that it was designed to eliminate sources of error that are present in past methods. By moving the reinforcement from inside the specimen to the outside of the specimen, errors arising from poor bonding of the internal reinforcement to poor placement of the reinforcement to the unknown interactive effects of the internal reinforcement can be eliminated. By cracking the specimens prior to attaching the external reinforcement, the actual failure surface can be determined, the aggregate particles and surface can be inspected, and better quality control can be assured. For all of these reasons, this test method is highly recommended for future studies.

Conclusions

To better understand the effect of fiber reinforcement on aggregate interlock and shear resistance of concrete, three basic concrete types were investigated. For each concrete type, different fibers were added to produce similar concrete that could be

directly compared. Push-off testing was performed, and the specimens were analyzed prior to pre-cracking, after pre-cracking, and after the completion of the push-off test.

Based on the results of this study, the following conclusions are presented.

1. Micro-fibers were shown to improve all strength properties of the concrete by improving the cohesion of the matrix.
2. Macro-fibers were shown to improve the small-scale material properties but had mixed effects on the push off specimens.
3. The shear performance of macro-fiber concrete was shown to be governed by the shear performance of the fibers themselves.
4. While fibers have been shown to improve the shear performance of reinforced concrete members, it is clear that the internal mechanics of the concrete are heavily influenced and changed with the presence of fibers.
5. The proposed push-off test shows excellent correlation to past push-off testing methods and has been proven to be more reproducible.
6. The proposed push-off test is suggested as a replacement to other push-off tests due to the elimination of errors and the improved quality control.
7. The proposed push-off test allows the researcher to obtain before and after data on the failure surface. This data may allow future researchers to expand the knowledge of shear friction and aggregate interlock.
8. The existing means of determining aggregate interlock of a mixture, the ratio of shear stress to normal stress, presents relative information. This ratio alone is not adequate for determining the shear resistance characteristics of a mixture.

Acknowledgements

The authors gratefully acknowledge the financial and capital support provided by Dolese Bros. Co. and the National University Transportation Center at The University of Oklahoma. The conclusions and opinions expressed in this paper are those of the authors and do not necessarily reflect the official views or policies of the funding institutions.

Notation

f_c = Compressive strength

f_{ct} = Splitting tensile strength

f_{ct}^* = Apparent tensile strength

References

- [1] N. W. Hanson, "Precast-Prestressed Concrete Bridges 2: Horizontal Shear Connections," *Journal of the Research and Development Division*, vol. 2, no. 2, pp. 38-58, 1960.
- [2] American Concrete Institute, *ACI Concrete Terminology*, Farmington Hills, MI, 2018.
- [3] A. H. Mattock, J. A. Hofbeck and I. O. Ibrahim, "Shear Transfer in Reinforce Concrete," *ACI Journal*, vol. 66, no. 2, pp. 119-128, 1969.
- [4] A. H. Mattock and N. M. Hawkins, "Shear Transfer in Reinforced Concrete - Recent Research," *PCI Journal*, vol. 17, no. 2, pp. 55-75, 1972.
- [5] B. Barragain, R. Gettu, L. Agullu and R. Zerbio, "Shear Failure of Steel Fiber-Reinforced Concrete Based on Push-Off Tests," *ACI Materials Journal*, vol. 103, no. 4, pp. 251-257, 2006.
- [6] E. B. Sells, "Self-Consolidating Concrete for Infrastructure Elements Shear Characteristics," Missouri University of Science and Technology, Rolla, MO, 2012.
- [7] D. M. Shaw, "Direct Shear Transfer of Lightweight Aggregate Concretes with Non-Monolithic Interface Conditions," Missouri University of Science and Technology, Rolla, MO, 2013.
- [8] C. M. Wirkman, "Performance of Fiber-Reinforced Self-Consolidating Concrete for Repair of Bridge Sub-Structures," The University of Oklahoma, Norman, OK, 2016.
- [9] K. S. Wallace, "Performance of Fiber-Reinforced Eco-Friendly Concrete for Bridge Structures," The University of Oklahoma, Norman, OK, 2016.
- [10] Oklahoma Department of Transportation Transportation Commission, "Standard Specifications," 2009.
- [11] ASTM C39-18, Standard Test Method for Compressive Strength of Cylindrical Concrete Specimens, ASTM International, 2018.
- [12] ASTM C469-14, Standard Test Method for Static Modulus of Elasticity and Poisson's Ratio of Concrete in Compression, ASTM International, 2014.

- [13] ASTM C496-17, Standard Test Method for Splitting Tensile Strength of Cylindrical Concrete Specimens, ASTM International, 2017.
- [14] ASTM C78-18, Standard Test Method for Flexural Strength of Concrete, ASTM International, 2018.
- [15] E. B. Sells, J. J. Myers and J. S. Volz, "Aggregate Interlock Push-Off Test Results of Self-Consolidating Concrete (SCC) for Use in Infrastructure Elements," in *New Developments in Structural Engineering and Construction* , 2013.
- [16] J. C. Walraven and J. Stroband, "Shear Friction in High-Strength Concrete," in *SP-149, American Concrete Institute International Conference*, Singapore, 1994.
- [17] F. J. Vecchio and D. Lai, "Crack Shear-Slip in Reinforced Concrete Elements," *Journal of Advanced Concrete Technology*, vol. 2, no. 3, pp. 289-300, 2004.
- [18] J. Walraven, F. Jerome and P. Arjan, "Influence of Concrete Strength and Load History on the Shear Friction Capacity of Concrete Members," *PCI Journal*, vol. 32, no. 1, pp. 66-84, 1987.

3. SUMMARY, CONCLUSIONS, AND RECOMMENDATIONS

3.1. SUMMARY OF RESEARCH

The purpose of this research was to evaluate the shear and aggregate interlock performances of two non-traditional concretes – SCC and cement-limiting concrete – and determine if there is a correlation between these two engineering properties, and evaluate the effectiveness and applicability of a newly proposed test method for push-off testing. The test matrices for the two beam studies were identical. Each study included 9 full-scale beam shear specimens with no shear reinforcement located within the test region. A total of 3 beams were tested for the comparative conventional concrete and 3 beams were tested for each of the two experimental mixture designs. The test matrix for the first push-off study consisted of 9 push-off specimens (3 for each concrete mixture in the study). The test matrix for the second push-off study consisted of 24 push-off specimens (3 for each concrete mixture in the study).

This chapter contains the conclusions from the full-scale beam shear tests, the push-off tests, assessment of the shear design provisions of selected standards, and assessment of the newly proposed push-off test method. Lastly, recommendations are presented.

3.2. CONCLUSIONS

The following section summarizes the conclusions from all four studies performed for this dissertation.

3.2.1. Shear behavior of fiber-reinforced cement-limiting concrete. Based on the results of this study, the following conclusions can be made:

- The Shilstone chart was shown to be the best method tested to optimize aggregate gradations for a concrete mixture.
- Without a commonly available aggregate source containing larger amounts of #8 size particles, it is difficult to meet the criteria for an optimized aggregate gradation using the three tested methods.
- The problems with reduced cementitious material (weaker concrete, larger cracks, lower beam strengths) can be offset by utilizing an optimized aggregate gradation and the addition of micro- and macro-fibers.
- In terms of crack morphology and crack progression, the EBC mixtures cracked more and at lower loads, but the cracks were less wide than those present in the CC beams.
- In general, for a given standard, the ratios of experimental response to code-predicted capacity for the EBC2 beams are the largest, and those of the CC beams are the lowest.
- The fracture mechanics approaches best predict the shear strengths of the beams.
- Statistical data analyses (parametric and nonparametric) indicate that there is no significant difference between the shear capacity of the EBC beams and the CC beams tested in this study.
- The current methods for analyzing the shear capacity of concrete can be used on all mixtures examined in this study.

3.2.2. Shear behavior of FR-SCC. Based on the results of this study, the following conclusions can be made:

- In terms of crack morphology and crack progression, the behavior of the FR-SCC beams had more cracks and smaller crack openings when compared to the CC beams.
- By not treating the fibers as part of the structural system, and instead as part of the concrete mixture, the conventional relationships between strength parameters do not hold well.
- The qualitative data and observances from this research show that fiber-reinforced concrete has more variability in regard to fresh and hardened properties.
- The current code methods for calculating shear strength appear to be as adequate for FR-SCC as they are for conventional concrete, but they are less exact.
- The detrimental effects caused by SCC and rounded aggregates can be offset by the addition of fibers.
- The data suggests that compressive strength is not an effective method to predict the shear performance of structural members fabricated with fiber-reinforced concrete.
- The shear strength of both FR-SCC mixtures appear to be governed by the performance of the fibers.
- The fracture mechanics approaches best predicted the shear strengths of the beams for all three concrete mixtures.

- Statistical data analyses (parametric and nonparametric) indicate that there is a strong correlation between the CC and lower strength FR-SCC shear test data. However, higher strength FR-SCC had a weaker correlation.

3.2.3. Aggregate interlock of non-traditional concrete. Based on the results of this study, the following conclusions can be made:

- The existing means of determining aggregate interlock of a mixture, the ratio of shear stress to normal stress, presents relative information. This ratio alone is not adequate for determining the shear resistance characteristics of a mixture.
- There is strong correlation between the cement content and apparent tensile strength of the specimens.
- There is a strong correlation between splitting tensile strength and the apparent tensile strength of the mixtures.
- Pre-cracking an unreinforced member may be able to supplement performing splitting tensile tests.
- K15, the SCC mix produced with pea gravel, exhibited the strongest apparent tensile strength and shear strength, and EBC, the cement-limiting and optimized aggregate mix, exhibited the weakest apparent tensile strength and shear strength.
- EBC exhibited the highest friction coefficient, which represents aggregate interlock performance, and the CC exhibited the lowest friction coefficient.
- Both CC and K15 exhibited better residual shear strength.

3.2.4. Influence of fiber on aggregate interlock. Based on the results of this study, the following conclusions can be made:

- Micro-fibers were shown to improve all strength properties of the concrete by improving the cohesion of the matrix.
- Macro-fibers were shown to improve the small-scale material properties but had mixed effects on the push off specimens.
- The shear performance of macro-fiber concrete was shown to be governed by the shear performance of the fibers themselves.
- While fibers have been shown to improve the shear performance of reinforced concrete members, it is clear that the internal mechanics of the concrete are heavily influenced and changed with the presence of fibers.

3.2.5. Correlation of aggregate interlock with beam shear performance.

Based on the results of this study, the following conclusions can be made:

- In both the beam shear testing and the push-off testing, the K15 specimens with macro-fibers were the weakest, and the EBC2 specimens were the strongest. This suggests a correlation between aggregate interlock and beam shear performance.
- Fiber reinforcement is shown to reduce the effect of aggregate interlock but improve beam shear performance. This reinforces the findings that the addition of fiber reinforcement distorts the traditional relationships between internal mechanics of concrete.
- There is a correlation between the delayed peak stresses and maintained residual stresses in push-off testing with fiber reinforcement and the reduced

stress vs. strain moduli from the beam tests. This suggest a strong correlation between the behavior of push-off and beam shear testing.

3.2.6. Assessment of newly proposed push-off test. Based on the results of this study, the following conclusions can be made:

- There is no standardized test method for the push-off test, which leads to varied results between researchers.
- The proposed push-off test shows excellent correlation to past push-off testing methods and has been proven to be more reproducible.
- The proposed push-off test is suggested as a replacement to other push-off tests due to the elimination of errors and the improved quality control.
- The proposed push-off test allows the researcher to obtain before and after data on the failure surface. This data may allow future researchers to expand the knowledge of shear friction and aggregate interlock.
- The proposed method is an improvement due to the reduction in weight of the specimens, which improves safety.
- The existing means of determining aggregate interlock of a mixture, the ratio of shear stress to normal stress, presents relative information. This ratio alone is not adequate for determining the shear resistance characteristics of a mixture.

3.3. RECOMMENDATIONS

Based on the conclusions stated in the previous sections, the following recommendations for future research were developed:

- Test beam shear specimens for mixtures CC1, CC2, EBC, and K15 to further flesh out the correlations between aggregate interlock and beam shear.
- Investigate the effect of depth of section, shear span to depth ratio, compressive strength of concrete, and aggregate size on the shear strength of FR-SCC and cement-limiting and aggregate-optimized concrete.
- Investigate cyclic load behavior of FR-SCC and cement-limiting and aggregate-optimized concrete.
- Compile more historic push-off data and compare the results of those tests to the data from this study.
- Perform push-off testing on mixtures from historic studies, and compare the finding from each study.
- Investigate the push-off performance of FR-SCC made with crushed stone aggregate.
- Investigate the relationship between aggregate interlock and aggregate soundness tests.
- Investigate the influence of fiber orientation on the outcomes of push-off testing.

APPENDICES

APPENDIX A – MECHANICAL PROPERTIES OF EBC

MECHANICAL PROPERTIES OF EBC

The following section includes the results and discussion on the compressive strength, tensile splitting strength, and flexural strength of the CC and EBC mixtures.

COMPRESSIVE STRENGTH

Results of the compressive strength tests of the CC, EBC1, and EBC2 mixtures at 1, 3, 7, 14, 21, and 28 days are presented in Figure A1. Each data point represents the average of three replicate specimens tested in accordance with ASTM C39 using 4in.x8in. cylindrical specimens. The compressive strength of EBC1 was always lower than CC, and the compressive strength of EBC2 was similar to CC throughout.

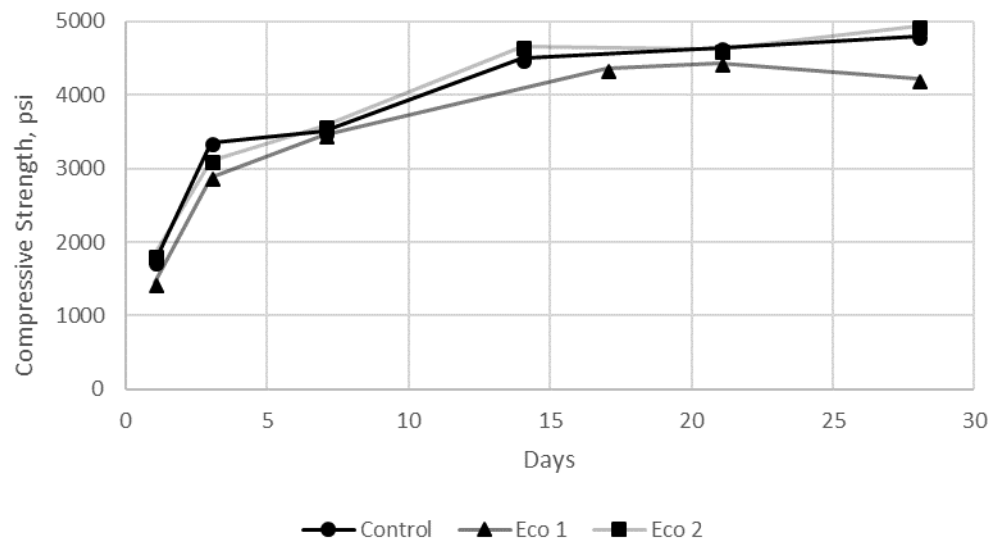


Figure A1 – Development of compressive strength of CC and EBC

TENSILE SPLITTING STRENGTH

Results of the splitting tensile strength testing are presented in Table A1. Each data entry represents the average three replicate specimens tested in accordance with ASTM C496. The values are normalized by dividing by the square root of compressive strength. For all three mixtures, the normalized values fall above the ACI 318 predicted

values. Both EBC mixtures recorded larger normalized strengths, and EBC2 recorded the largest normalized strength.

Table A1 – Splitting tensile strength of EBC

Mixture	f'_c	f_{ct}	$f_{ct}/\sqrt{f'_c}$
CC	4750	352	5.1
EBC1	4440	365	5.5
EBC2	4810	392	5.7

FLEXURAL STRENGTH

Results of the flexural strength testing are presented in Table A2. Each data entry represents the average of three replicate specimens tested in accordance with ASTM C78. The values are also normalized by dividing by the square root of compressive strength. For all three mixture, the normalized values fall above the ACI 318 predicted values. Both EBC mixtures recorded smaller normalized strengths, and EBC1 recorded the smallest normalized strength.

Table A2 – Flexural strength of EBC

Mixture	f'_c	f_r	$f_r/\sqrt{f'_c}$
CC	4750	835	12.1
EBC1	4440	676	10.1
EBC2	4810	712	10.3

APPENDIX B – BEAM SHEAR TEST DATA OF EBC

BEAM SHEAR TEST DATA OF EBC

LOAD-DEFLECTION DATA

Three beams were tested for each of the three concrete mixtures investigated. All of the beams tested failed in shear. Based on the data collected, none of the longitudinal reinforcement yielded, as was expected. Figures B1 through B3 show the load-deflection plots for each beam. EBC2 exhibited similar load-deflection behavior to CC. EBC2 exhibited similar behavior to CC until the ultimate load was reached, but exhibited plasticity at near ultimate loads. Figures B4 through B12 show each beam after failure had been reached.

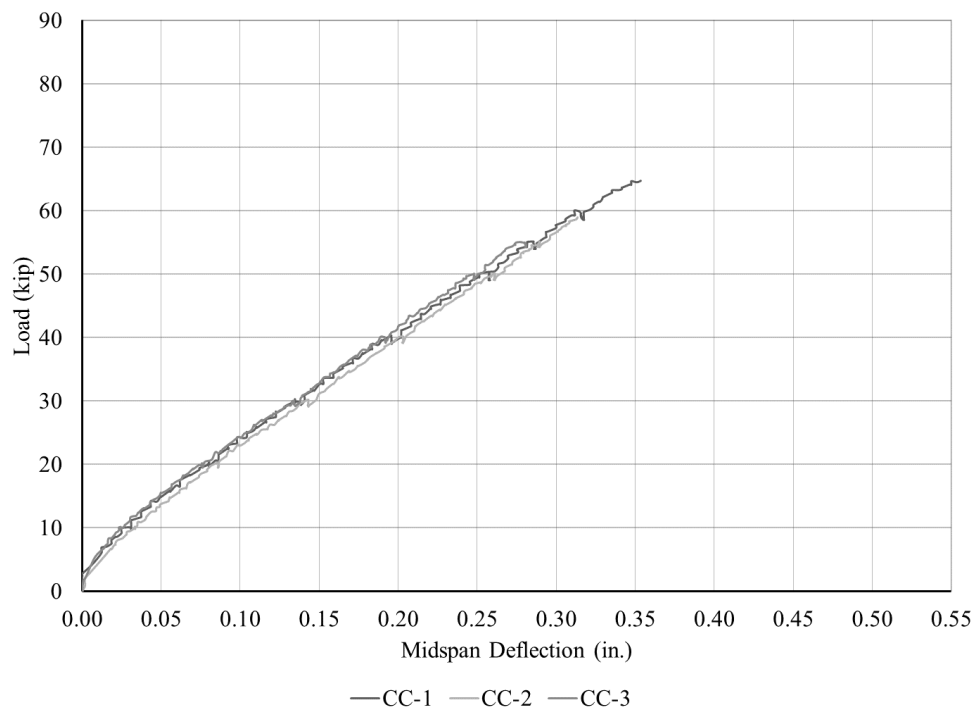


Figure B1 – Control beam load vs deflection plots

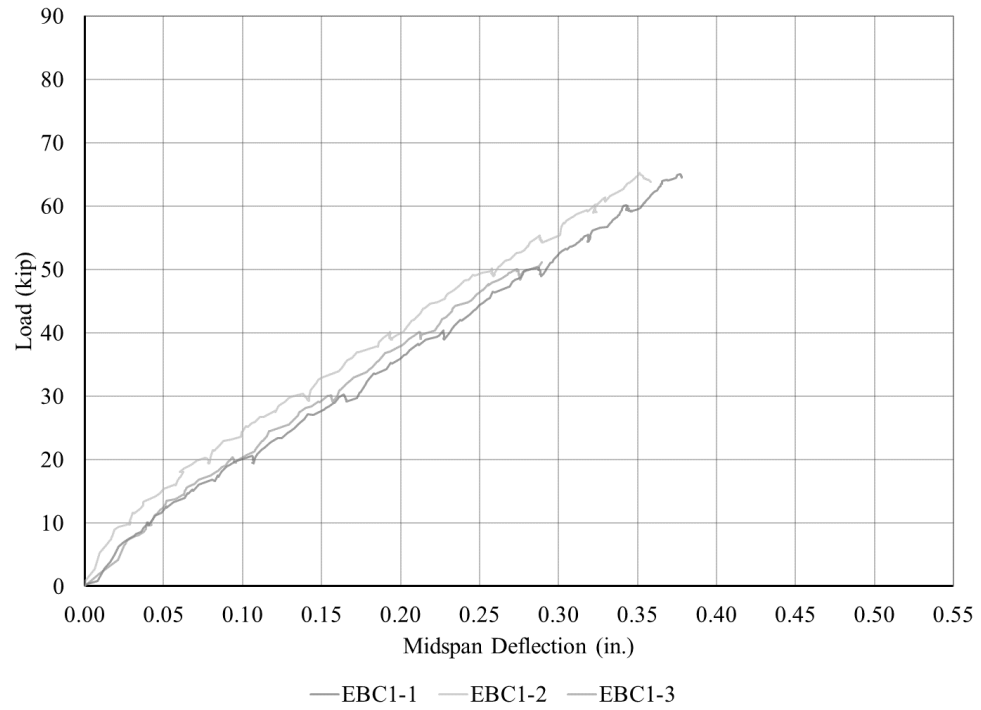


Figure B2 – EBC1 beam load vs deflection plots

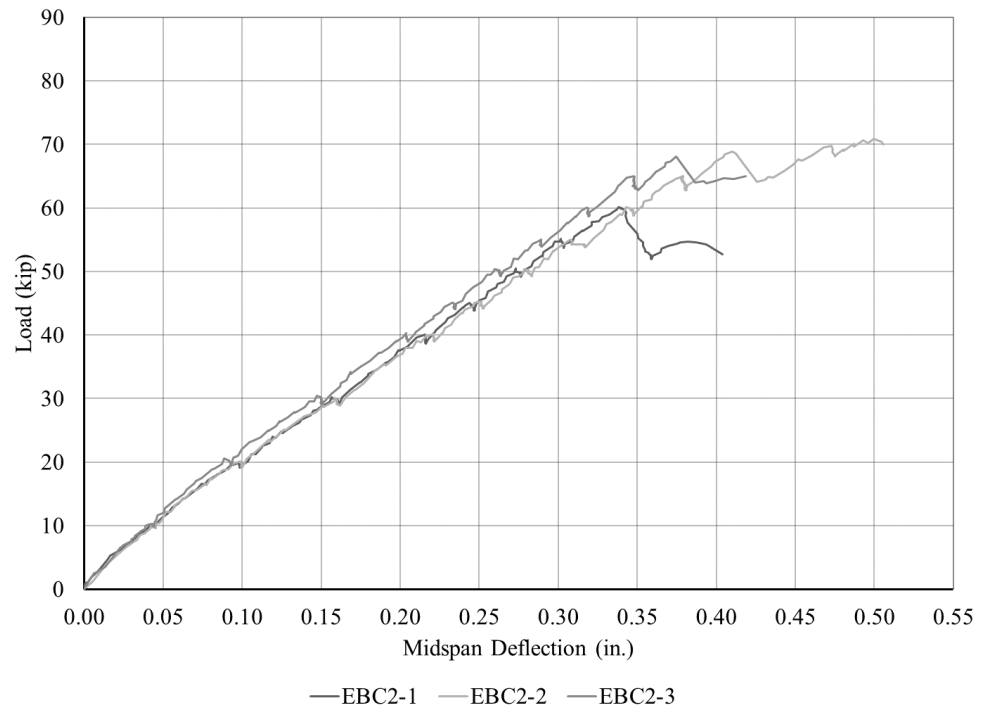


Figure B3 – EBC2 beam load vs deflection plots

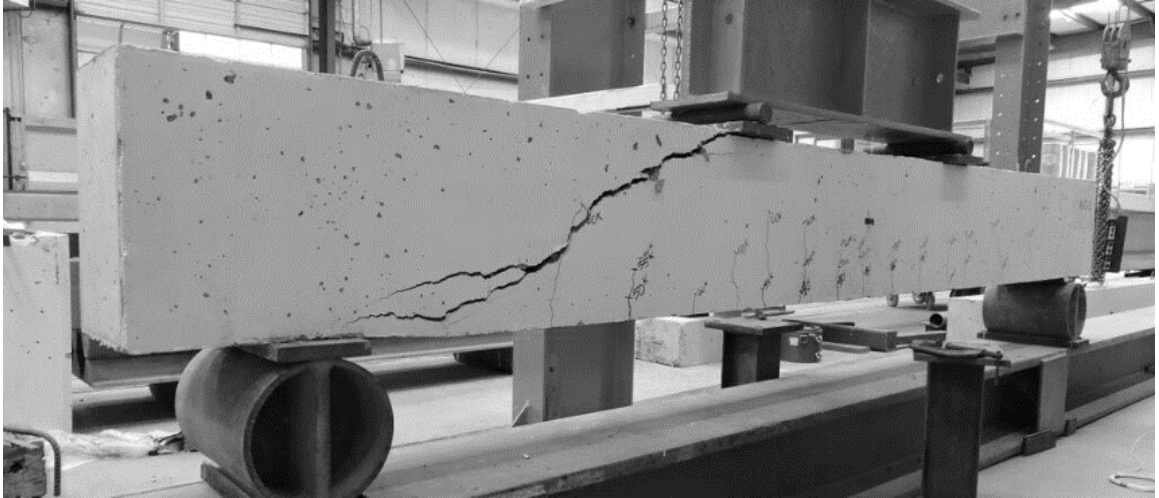


Figure B4 – CC-1 shear failure

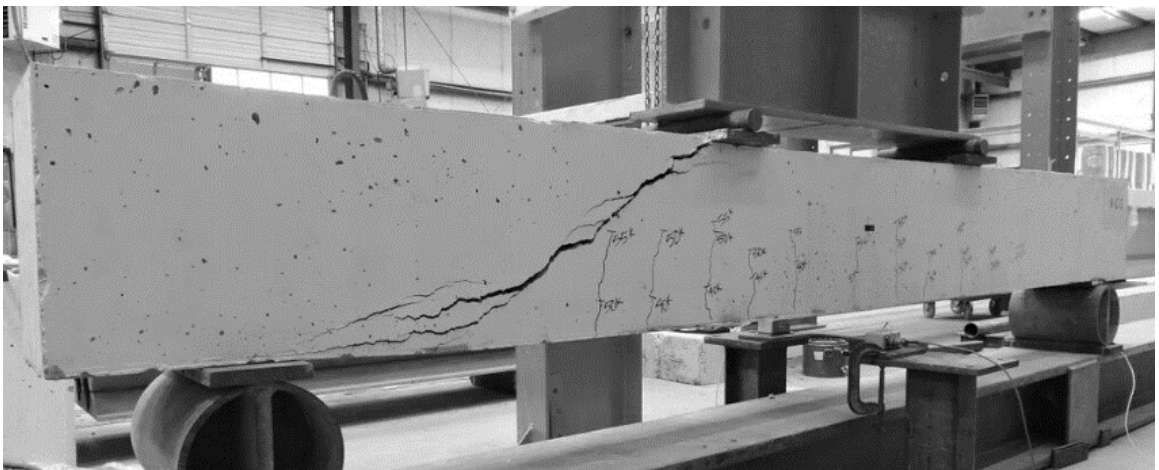


Figure B5 – CC-2 shear failure



Figure B6 – CC-3 shear failure

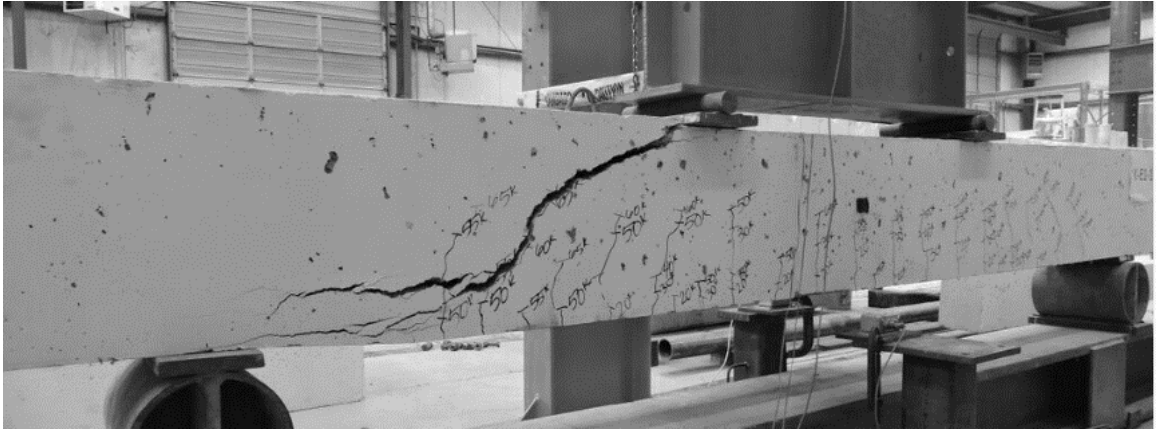


Figure B7 – EBC1-1 shear failure

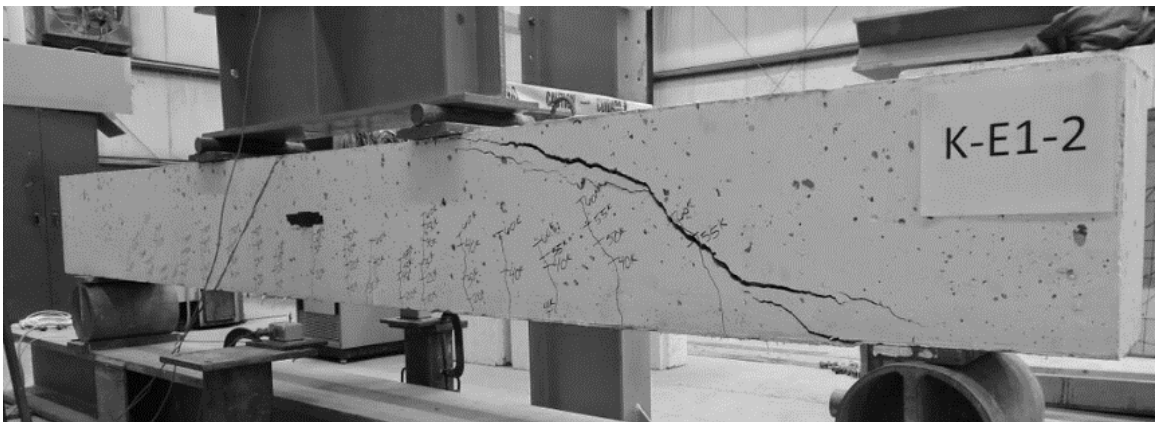


Figure B8 – EBC1-2 shear failure

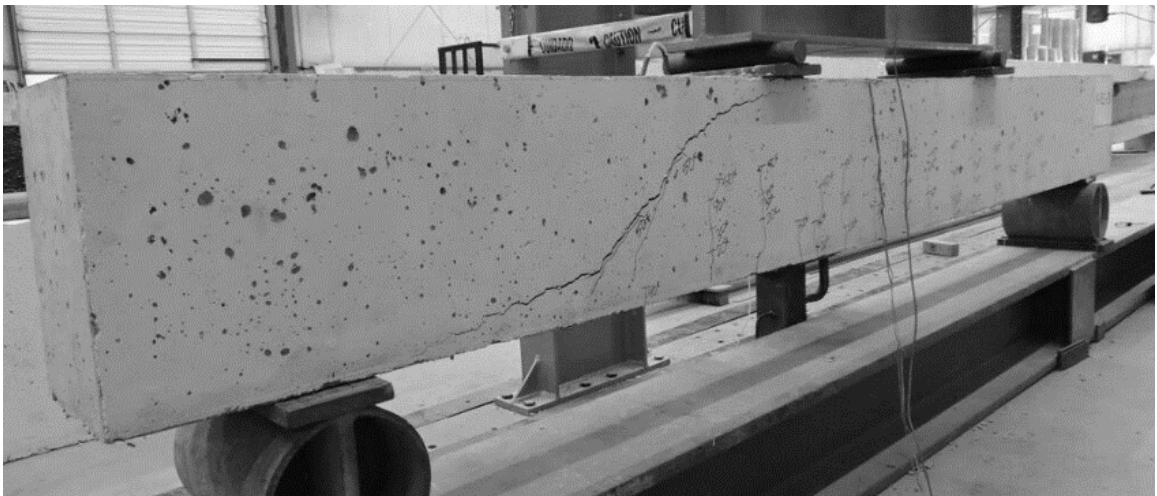


Figure B9 – EBC1-3 shear failure

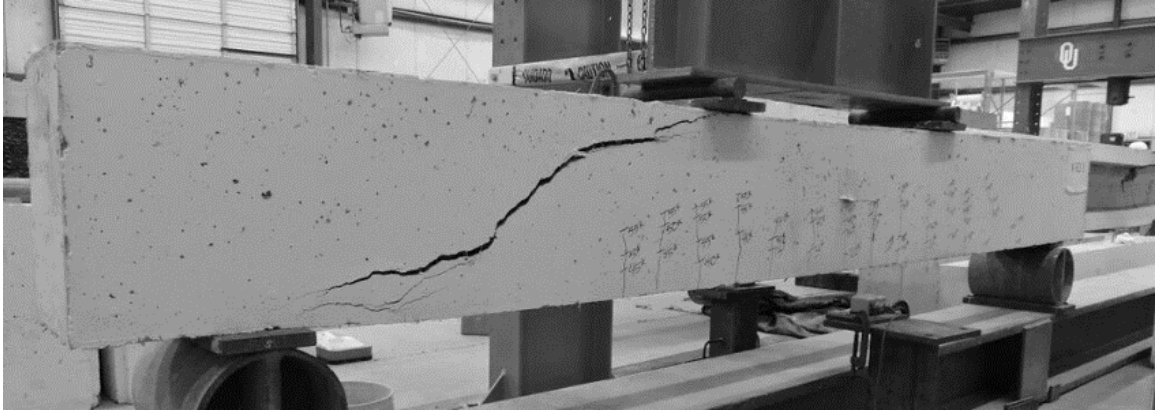


Figure B10 – EBC2-1 shear failure

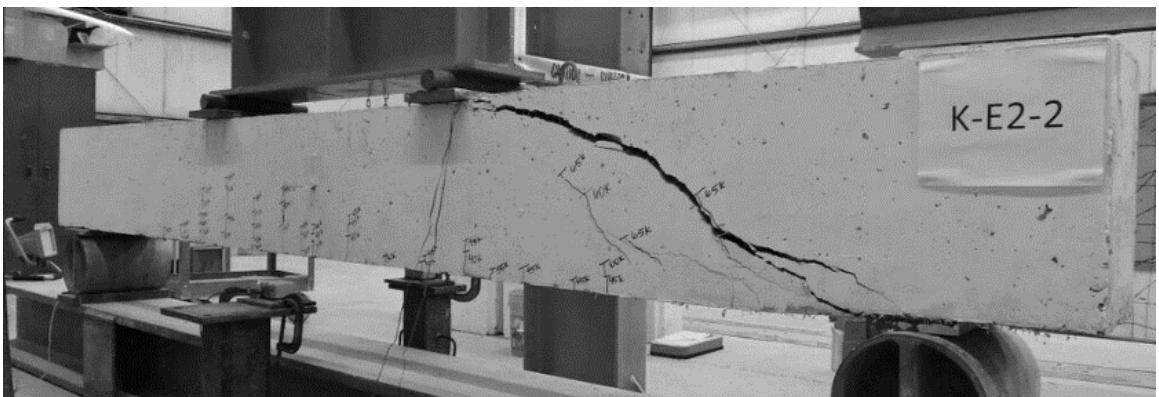


Figure B11 – EBC2-2 shear failure

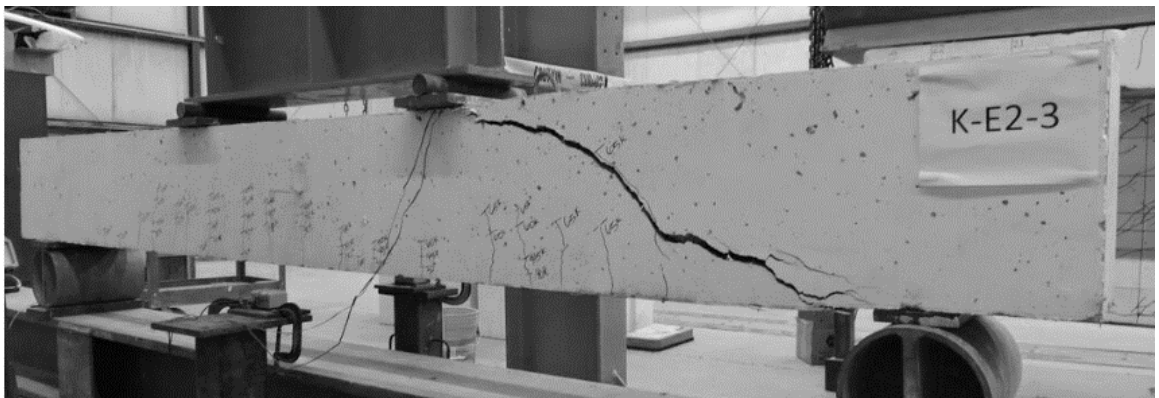


Figure B12 – EBC2-3 shear failure

SHEAR STRENGTH COMPARISONS

The ultimate shear strength data from each beam test is detailed in Table B1.

EBC2 displayed the largest normalized shear strength while CC exhibited the smallest normalized shear strength. All specimens tested exhibited larger normalized shear strengths than the ACI 318 predicted values.

Table B1 – Ultimate shear strength data

Mixture	Beam ID	f'_c	V_{test}	v_{test}	$v_{test}/\sqrt{f'_c}$
CC	CC-1	4750	32.5	178	2.6
	CC-2		29.5	162	2.3
	CC-3		28.2	155	2.2
EBC1	EBC1-1	4440	34.5	189	2.8
	EBC1-2		32.6	179	2.7
	EBC1-3		25.7	141	2.1
EBC2	EBC2-1	4810	30.1	165	2.4
	EBC2-2		35.5	195	2.8
	EBC2-3		34.1	187	2.7

APPENDIX C – STATISTICAL DATA ANALYSIS OF EBC

STATISTICAL DATA ANALYSIS OF EBC

Statistical tests (both parametric and nonparametric) were used to evaluate whether there was any statistically significant difference between the beam shear strengths of the CC and EBC mixtures. The beam shear data was first normalized to account for the effect of compressive strength. The data was normalized by dividing by the square root of the compressive strength.

PARAMETRIC TEST

The paired t-test is a statistical technique used to compare two population means. This test assumes that the difference between pairs are normally distributed. If this assumption is violated, the paired t-test may not be the most powerful test. The hypotheses for the paired t-tests for beam shear strength are as follows:

H_{o1} : The mean of normalized shear strength of the CC beams is equal to that of the EBC1 beams.

H_{o2} : The mean of normalized shear strength of the CC beams is equal to that of the EBC2 beams.

H_{o3} : The mean of normalized shear strength of the EBC1 beams is equal to that of the EBC2 beams.

$H_{a1,2,3}$: Not H_o .

The statistical capabilities of Excel were employed to perform these statistical tests. Table C1 summarizes the results of the paired t-test (p-values at the 0.05 significance level). All the p-values were greater than 0.05, which means the null hypotheses at the 0.05 significance level are confirmed.

NONPARAMETRIC TEST

Unlike the parametric tests, nonparametric tests are referred to as distribution-free tests. These tests have the advantage of requiring no assumption of normality, and they usually compare medians rather than means. The Wilcoxon sign-ranked test is usually identified as a nonparametric alternative to the paired t-test. The hypothesis for this test is the same as those for the paired t-test except median is used instead of mean value. The Wilcoxon sign-ranked test assumes that the distribution of the difference of pairs is symmetrical. This assumption can be checked. If the distribution is normal, it is therefore symmetrical. Results of the Wilcoxon sign-ranked test are summarized in Table C1. All of the p-values were greater than 0.05, which means the null hypotheses at the 0.05 significance level are confirmed.

Table C1 – P-values for statistical tests

Hypothesis	P*	NP**
$V_{(CC)}=V_{(EBC1)}$	0.386	0.175
$V_{(CC)}=V_{(EBC2)}$	0.401	0.175
$V_{(EBC1)}=V_{(EBC2)}$	0.842	0.344

* : parametric test

** : nonparametric test

APPENDIX D – MECHANICAL PROPERTIES OF FR-SCC

MECHANICAL PROPERTIES OF FR-SCC

The following section includes the results and discussion on the compressive strength, tensile splitting strength, and flexural strength of the CC and FR-SCC mixtures.

COMPRESSIVE STRENGTH

Results of the compressive strength tests of the CC, K10, and K15 mixtures at 1, 3, 7, 14, and 28 days are presented in Figure D1. Each data point represents the average of three replicate specimens tested in accordance with ASTM C39 using 4in.x8in. cylindrical specimens. The compressive strength of K10 and K15 were always lower than CC. K15 had similar strength gain over time to K10 until day 14, and then exhibited a major gain in strength.

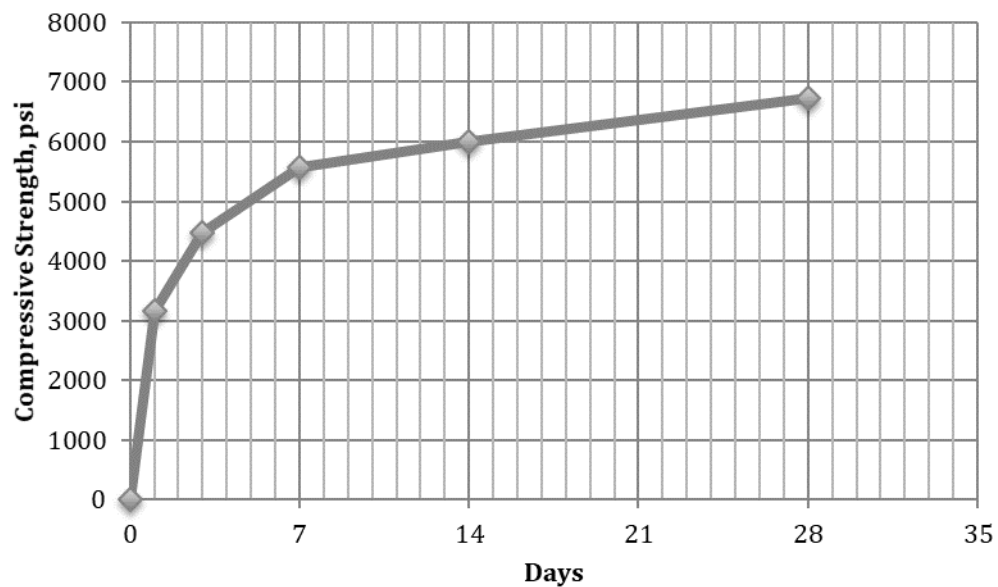


Figure D1 – Development of compressive strength of CC

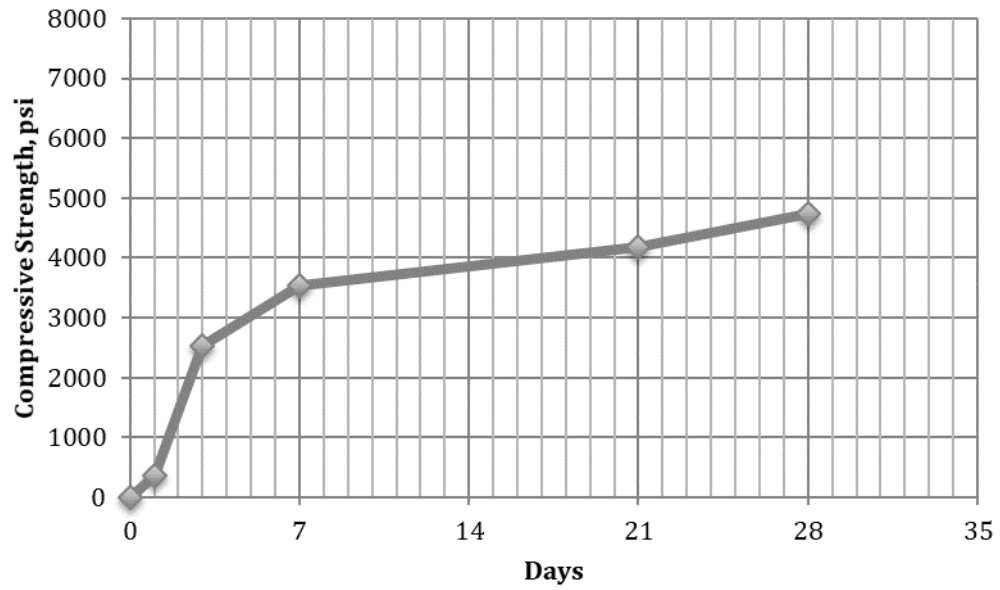


Figure D2 – Development of compressive strength of K10

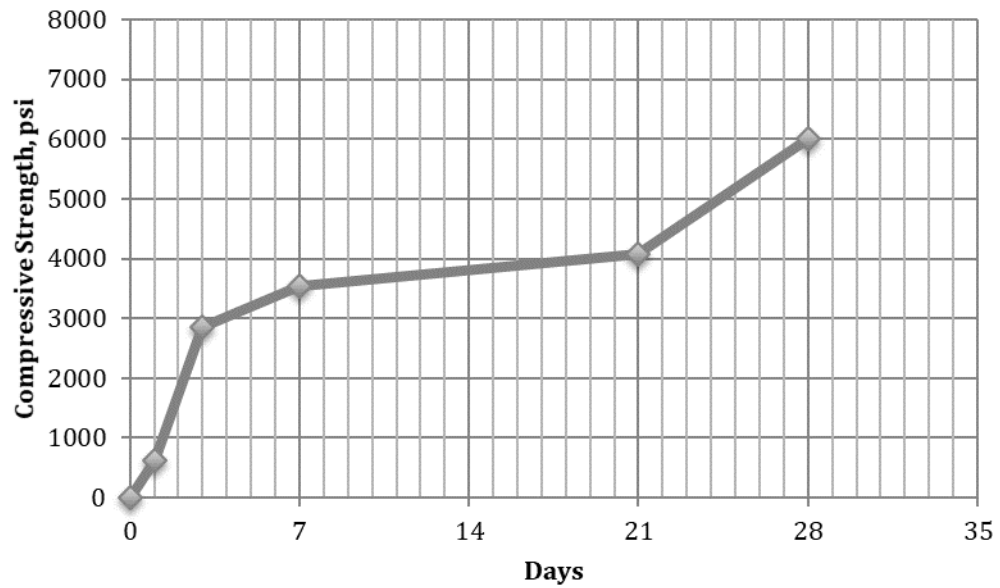


Figure D1 – Development of compressive strength of K15

TENSILE SPLITTING STRENGTH

Results of the splitting tensile strength testing are presented in Table D1. Each data entry represents the average three replicate specimens tested in accordance with

ASTM C496. The values are normalized by dividing by the square root of compressive strength. For all three mixtures, the normalized values fall above the ACI 318 predicted values. K15 exhibited similar normalized strength to CC, and K10 exhibited a lower normalized strength.

Table D1 – Splitting tensile strength of FR-SCC

Mixture	f'_c	f_{ct}	$f_{ct}/\sqrt{f'_c}$
CC	6740	459	6.7
K10	4740	406	5.9
K15	6010	511	6.6

FLEXURAL STRENGTH

Results of the flexural strength testing are presented in Table d2. Three replicate specimens were tested in accordance with ASTM C78. The values are also normalized by dividing by the square root of compressive strength. For all three mixtures, the normalized values fall above the ACI 318 predicted values. Both KFR-SCC mixtures recorded smaller normalized strengths, and K15 recorded the smallest normalized strength.

Table D2 – Flexural strength of FR-SCC

Mixture	Specimen ID	f'_c	f_r	$f_r/\sqrt{f'_c}$
CC	CC-1	6740	689	8.4
	CC-2		777	9.5
	CC-3		694	8.5
K10	K10-1	4740	480	7.0
	K10-2		591	8.6
	K10-3		607	8.8
K15	K15-1	6010	492	6.3
	K15-2		590	7.6
	K15-3		563	7.3

APPENDIX E – BEAM SHEAR TEST DATA OF FR-SCC

BEAM SHEAR TEST DATA OF FR-SCC

LOAD-DEFLECTION DATA

Three beams were tested for each of the three concrete mixtures investigated. All of the beams tested failed in shear. Based on the data collected, none of the longitudinal reinforcement yielded, as was expected. Figures E1 through E3 show the load-deflection plots for each beam. K10 and K15 exhibited similar load-deflection behavior to CC until ultimate load was reached, but they exhibited plasticity at near ultimate loads. Figures E4 through E12 show each beam after failure had been reached.

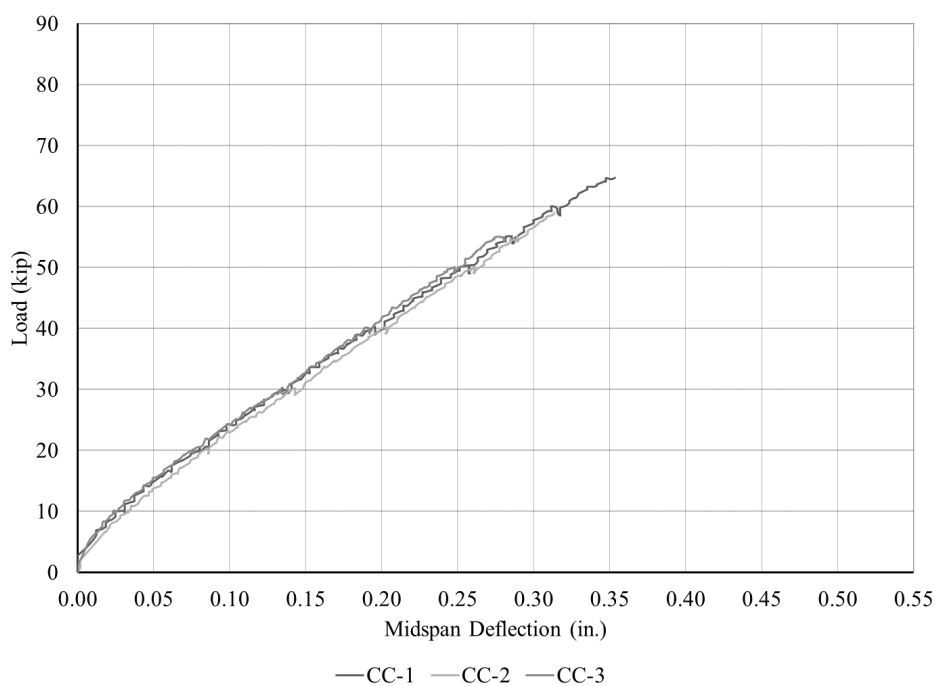


Figure E1 – Control beam load vs deflection plots

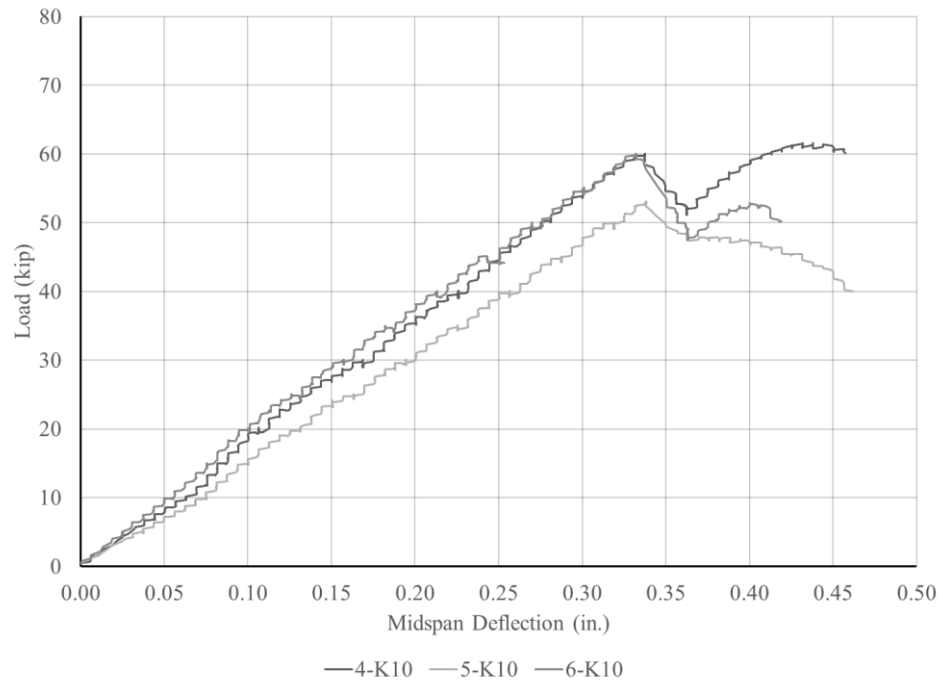


Figure E2 – K10 beam load vs deflection plots

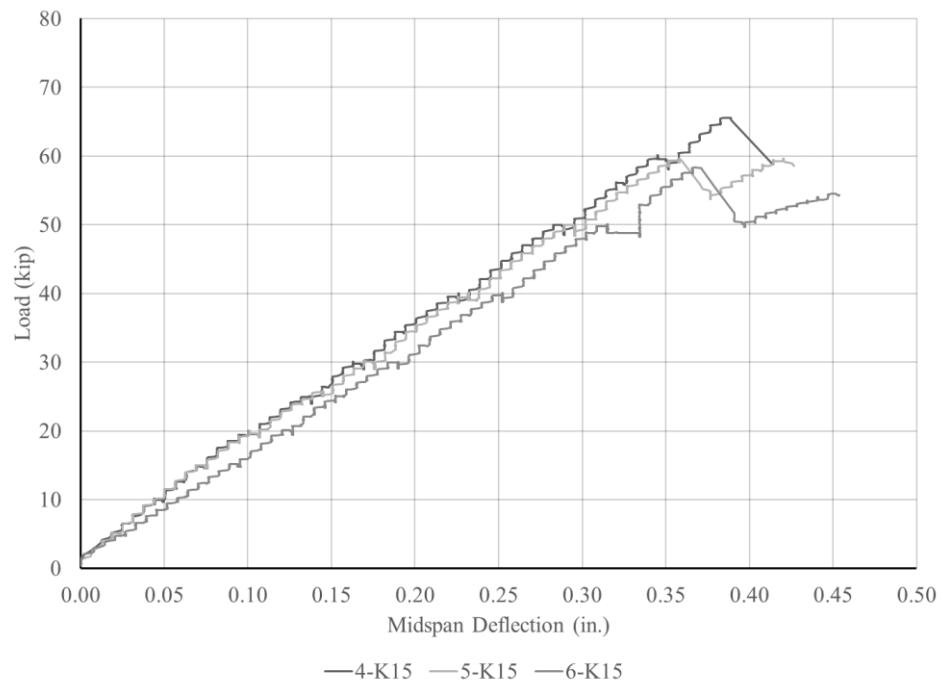


Figure E3 – K15 beam load vs deflection plots

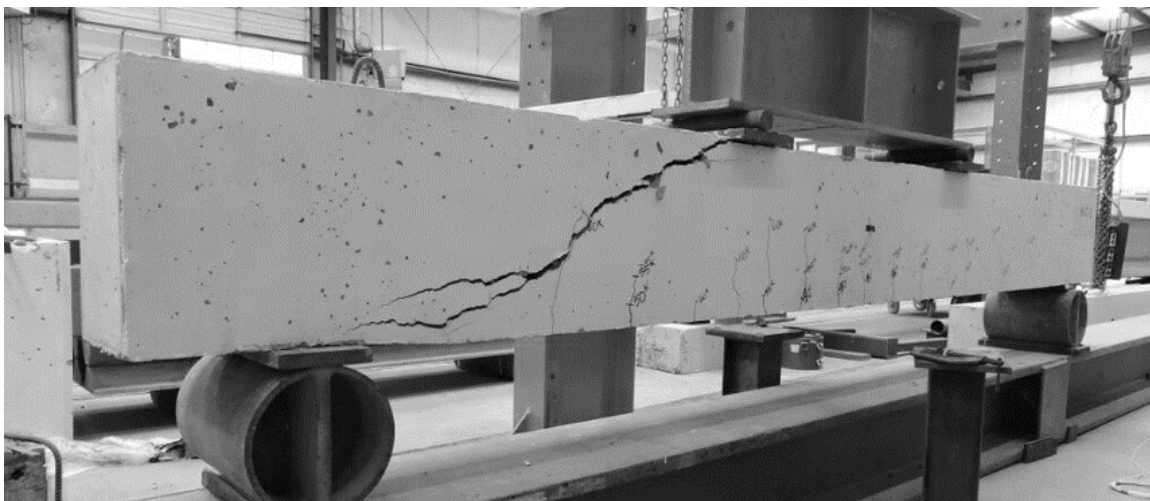


Figure E4 – CC-1 shear failure

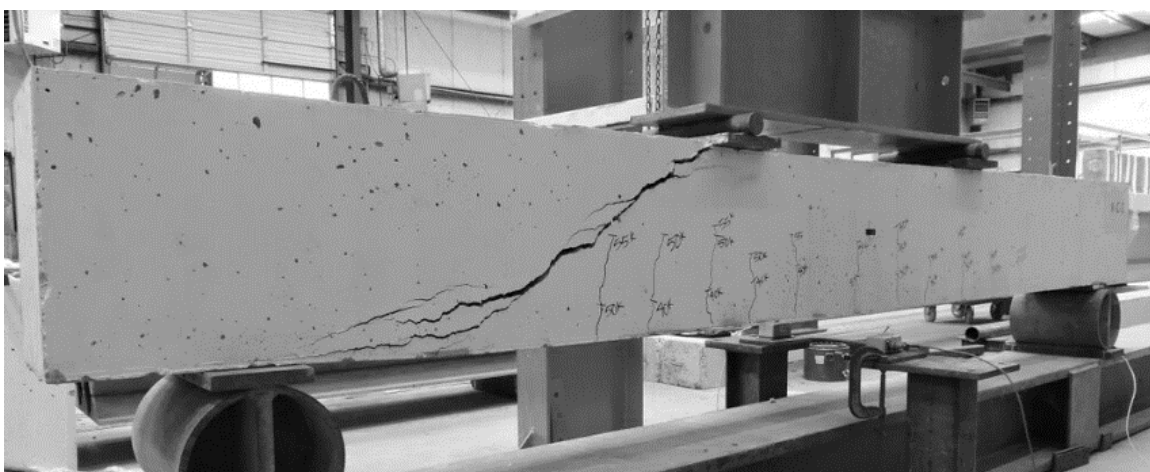


Figure E5 – CC-2 shear failure



Figure E6 – CC-3 shear failure

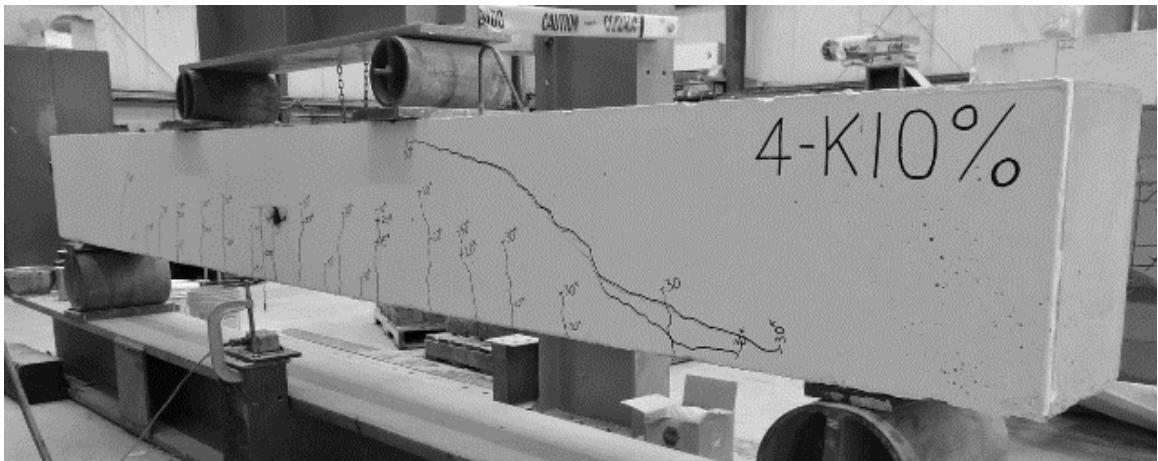


Figure E7 – 4-K10 shear failure

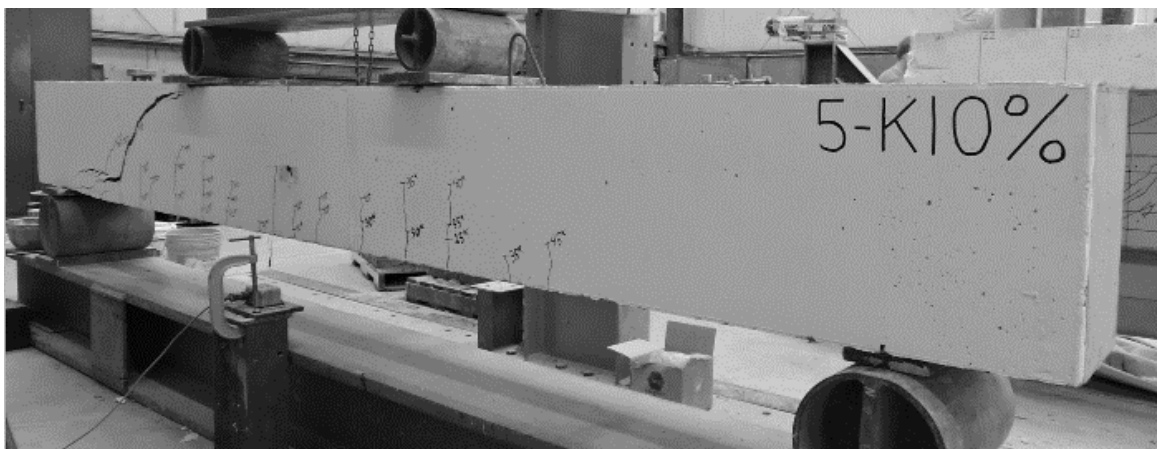


Figure E8 – 5-K10 shear failure

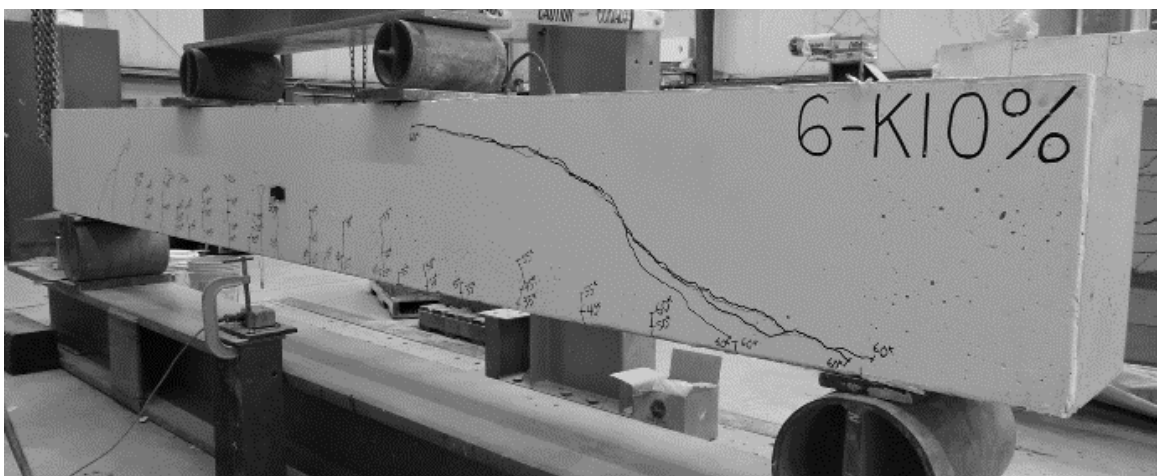


Figure E9 – 6-K10 shear failure

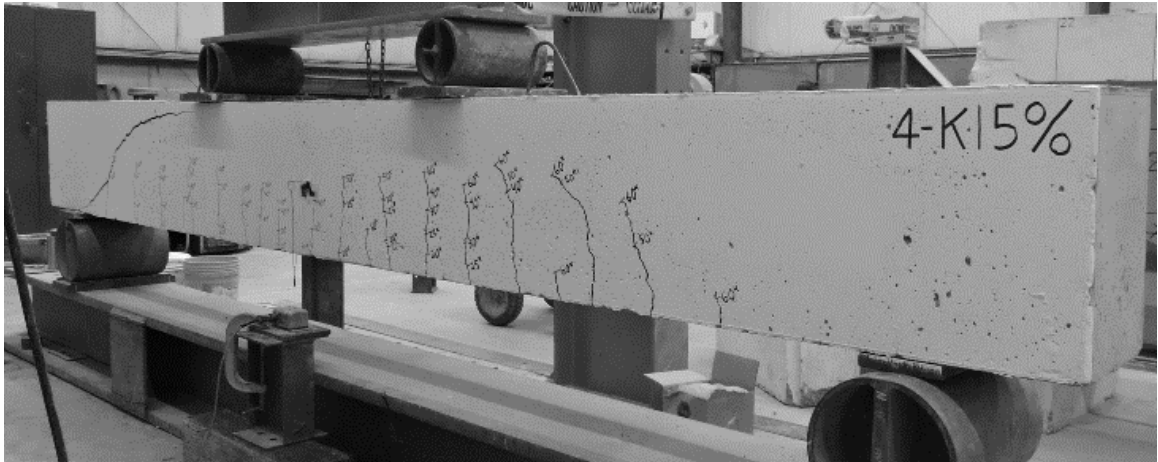


Figure E10 – 4-K15 shear failure

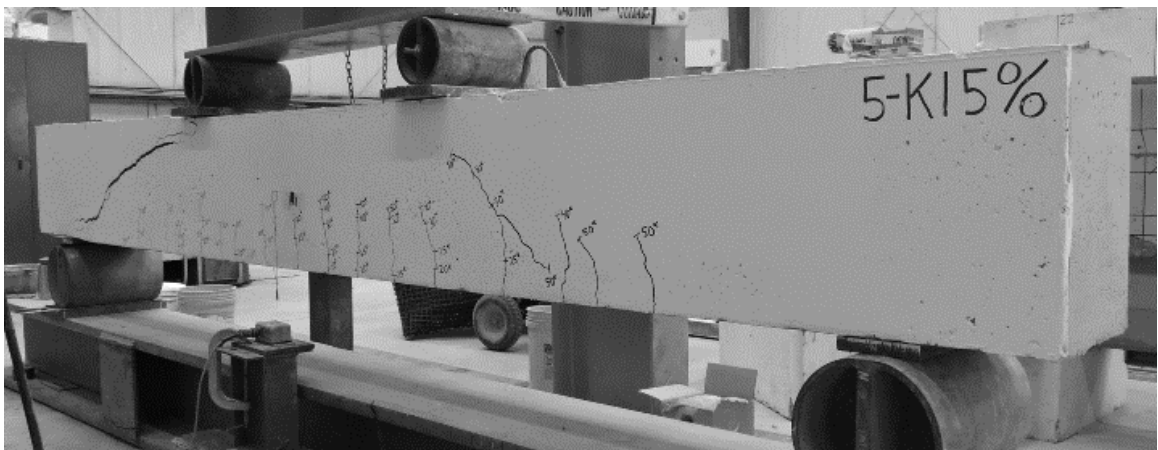


Figure E11 – 5-K15 shear failure

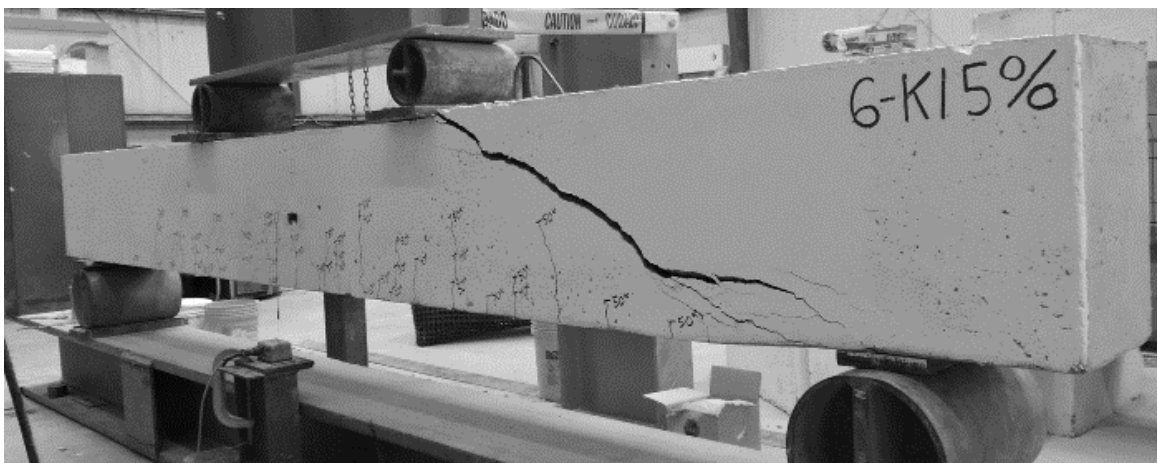


Figure E12 – 6-K15 shear failure

SHEAR STRENGTH COMPARISONS

The ultimate shear strength data from each beam test is detailed in Table E1.

K10 displayed similar normalized shear strength to CC, while K15 exhibited the smallest normalized shear strength. All specimens tested exhibited larger normalized shear strengths than the ACI 318 predicted values.

Table E1 – Ultimate shear strength data

Mixture	Beam ID	f'_c	V_{test}	v_{test}	$v_{test}/\sqrt{f'_c}$
CC	CC-1	4750	32.5	178	2.6
	CC-2		29.5	162	2.3
	CC-3		28.2	155	2.2
K10	4-K10	4460	30.8	169	2.5
	5-K10		26.6	146	2.2
	6-K10		30.0	164	2.5
K15	4-K15	5910	32.8	180	2.3
	5-K15		29.8	163	2.1
	6-K15		29.2	160	2.1

APPENDIX F – STATISTICAL DATA ANALYSIS OF FR-SCC

STATISTICAL DATA ANALYSIS OF FR-SCC

Statistical tests (both parametric and nonparametric) were used to evaluate whether there was any statistically significant difference between the beam shear strengths of the CC and EBC mixtures. The beam shear data was first normalized to account for the effect of compressive strength. The data was normalized by dividing by the square root of the compressive strength.

PARAMETRIC TEST

The paired t-test is a statistical technique used to compare two population means. This test assumes that the difference between pairs are normally distributed. If this assumption is violated, the paired t-test may not be the most powerful test. The hypotheses for the paired t-tests for beam shear strength are as follows:

H_{01} : The mean of normalized shear strength of the CC beams is equal to that of the EBC1 beams.

H_{02} : The mean of normalized shear strength of the CC beams is equal to that of the EBC2 beams.

H_{03} : The mean of normalized shear strength of the EBC1 beams is equal to that of the EBC2 beams.

$H_{a1,2,3}$: Not H_0 .

The statistical capabilities of Excel were employed to perform these statistical tests. Table F1 summarizes the results of the paired t-test (p-values at the 0.05 significance level). The p-values for H_{01} and H_{03} were greater than 0.05, which confirmed the null hypotheses. However, the p-value for H_{02} was smaller than 0.05, which means the null hypothesis was not confirmed.

NONPARAMETRIC TEST

Unlike the parametric tests, nonparametric tests are referred to as distribution-free tests. These tests have the advantage of requiring no assumption of normality, and they usually compare medians rather than means. The Wilcoxon sign-ranked test is usually identified as a nonparametric alternative to the paired t-test. The hypothesis for this test is the same as those for the paired t-test except median is used instead of mean value. The Wilcoxon sign-ranked test assumes that the distribution of the difference of pairs is symmetrical. This assumption can be checked. If the distribution is normal, it is therefore symmetrical. Results of the Wilcoxon sign-ranked test are summarized in Table F1. All of the p-values were greater than 0.05, which means the null hypotheses at the 0.05 significance level are confirmed.

Table F1 – P-values for statistical tests

Hypothesis	P*	NP**
$V_{(CC)}=V_{(K10)}$	0.991	0.894
$V_{(CC)}=V_{(K15)}$	0.011	0.082
$V_{(K10)}=V_{(K15)}$	0.150	0.082

* : parametric test

** : nonparametric test

APPENDIX G – PUSH-OFF TEST DATA OF CC

PUSH-OFF TEST DATA OF CC

The following section includes the results and discussion on the pre-cracking and push off testing of the CC mixtures.

PRE-CRACKING

Results of the pre-cracking step in the push-off test for CC, CC1, and CC2 are presented in Table G1. The specimens were pre-cracked without internal or external reinforcement, as is proposed in the new push-off test method. The apparent tensile strength, the shear force divided by the surface of the failure plane, is presented along with the compressive strengths. The ratio of tensile to compressive strength is also presented. The normalized tensile strength of CC was increased with the addition of micro-fibers, as CC1 was stronger than CC, while it was reduced with the addition of macro-fibers. Without correcting for compressive strength, there were major gains in tensile strength with the addition of micro-fibers, but there was no gain with the addition of macro-fibers. Figures G1 through G12 are photos of the surfaces of the pre-cracked specimens.

Table G1 – Pre-cracking data of CC mixtures

Mixture	Specimen	Apparent Tensile Strength	Compressive Strength	Ratio of Tensile to Compressive
CC	1	281	5500	0.05
	2	359		0.07
	3	384		0.07
CC1	1	530	6680	0.08
	2	441		0.07
	3	468		0.07
CC2	1	577	8250	0.07
	2	398		0.05
	3	454		0.05



Figure G1 – Top view of pre-cracked CC-1



Figure G2 – Side view of pre-cracked CC-1



Figure G3 - Top view of pre-cracked CC-2



Figure G4 - Side view of pre-cracked CC-2

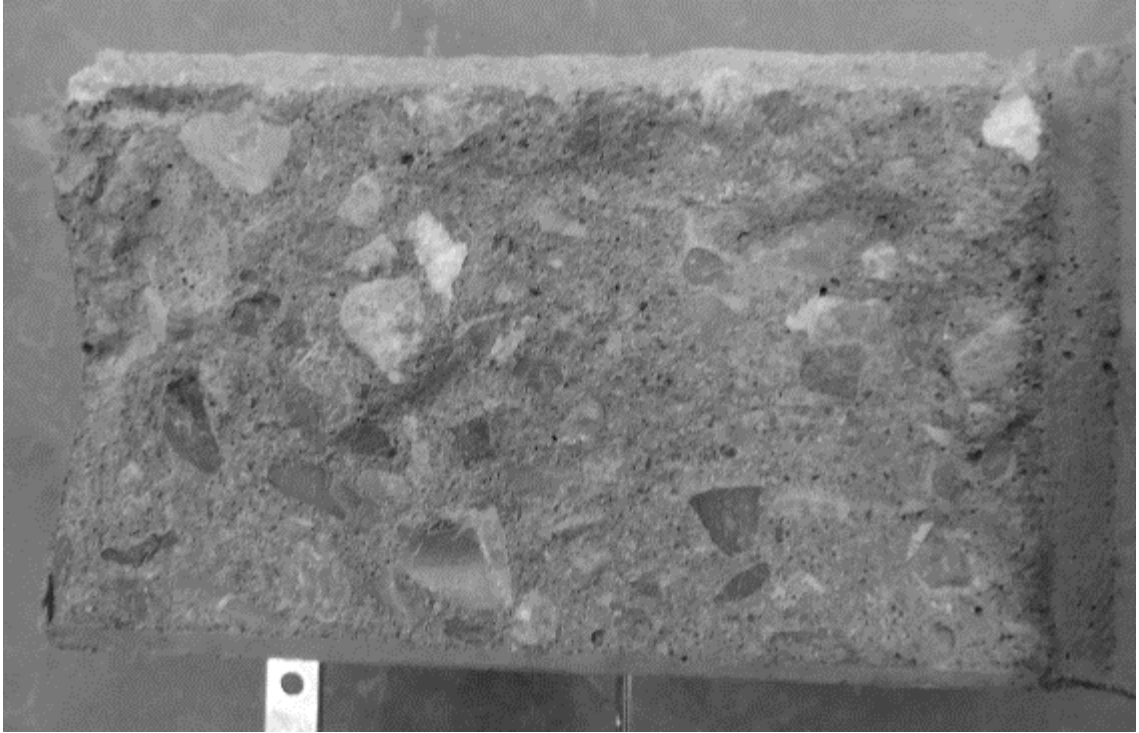


Figure G5 - Top view of pre-cracked CC-3



Figure G6 - Side view of pre-cracked CC-3



Figure G7 – Top view of pre-cracked CC1-1



Figure G8 – Side view of pre-cracked CC1-1



Figure G9 - Top view of pre-cracked CC1-2



Figure G10 - Side view of pre-cracked CC1-2



Figure G11 - Top view of pre-cracked CC1-3



Figure G12 - Side view of pre-cracked CC1-3

PUSH-OFF TEST

Results of the shear stress versus slip and ratio of shear to normal stress versus slip from the push-off test for CC, CC1, and CC2 are presented in Table G2. The specimens were initially restrained with a clamping force between 200 and 300 psi through the use of external reinforcement, and then loaded through the pre-cracked failure plane.

The plots of shear stress versus slip for CC, CC1, and CC2 are presented in Figures G13 through G15. The plots of ratio of shear to normal stress versus slip for CC, CC1, and CC2 are presented in Figures G16 through G18. Figures G19 through G34 are photos of the surfaces of the failed push-off specimens.

Table G2 – Push-off test results of CC mixtures

Concrete Mixture	Peak Shear Strength	Residual Shear Strength			Peak Ratio	Residual Ratio		
		0.10 in.	0.20 in.	0.30 in.		0.025 in.	0.05 in.	0.075 in.
CC	793	757	793	760	2.89	2.57	1.81	1.58
CC1	849	673	793	838	1.93	1.68	1.60	1.44
CC2	780	635	722	766	2.08	1.85	1.53	1.38

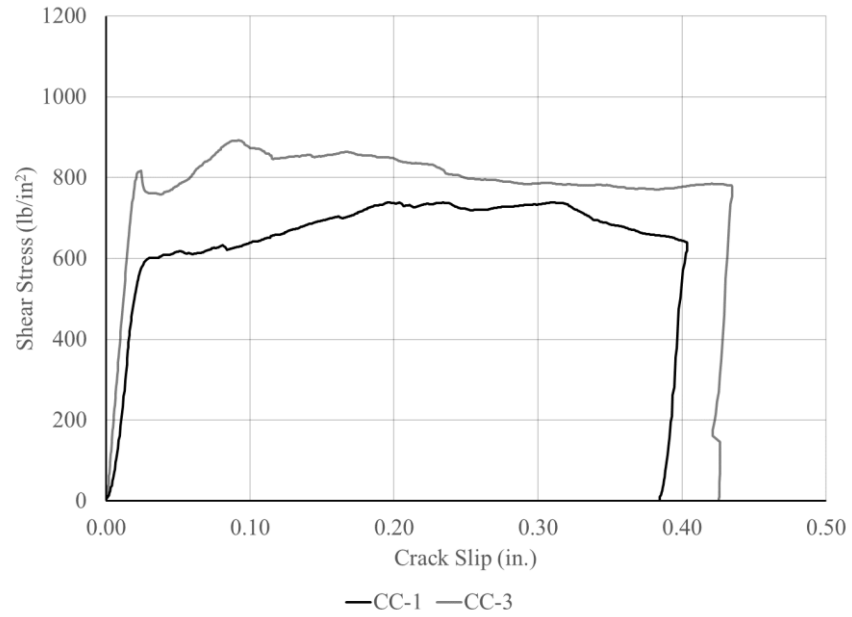


Figure G13 – Shear stress versus slip for CC

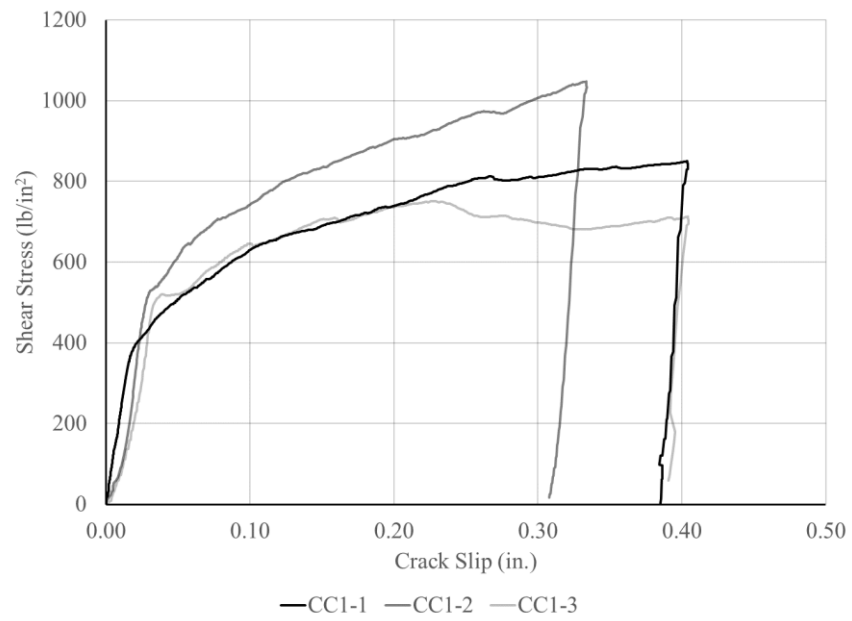


Figure G14 – Shear stress versus slip for CC1

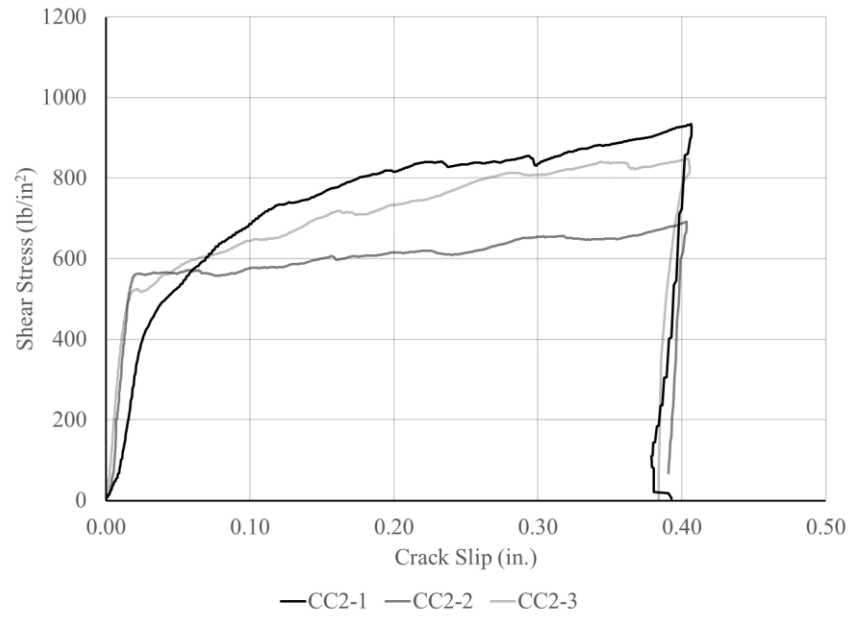


Figure G15 – Shear stress versus slip for CC2

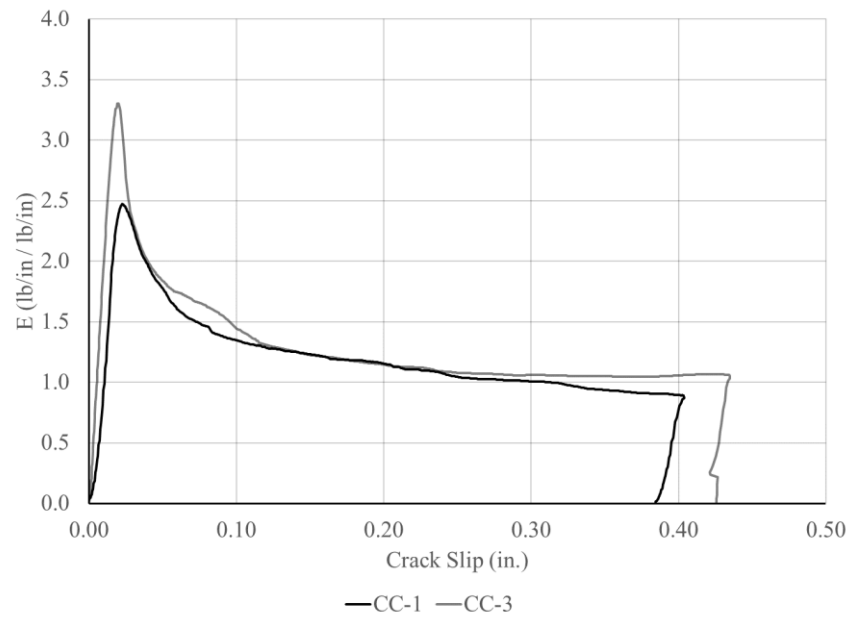


Figure G16 – Ratio versus slip for CC

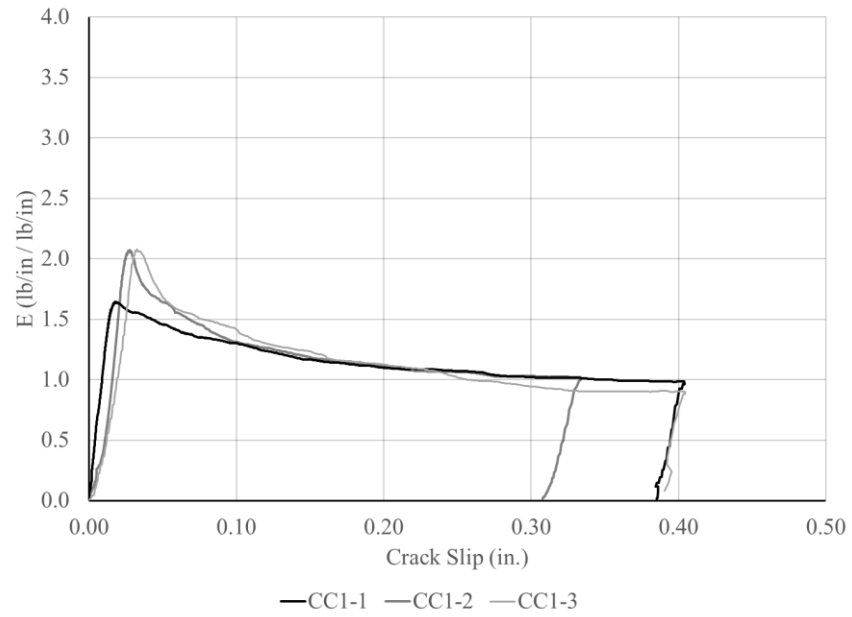


Figure G17 – Ratio versus slip for CC1

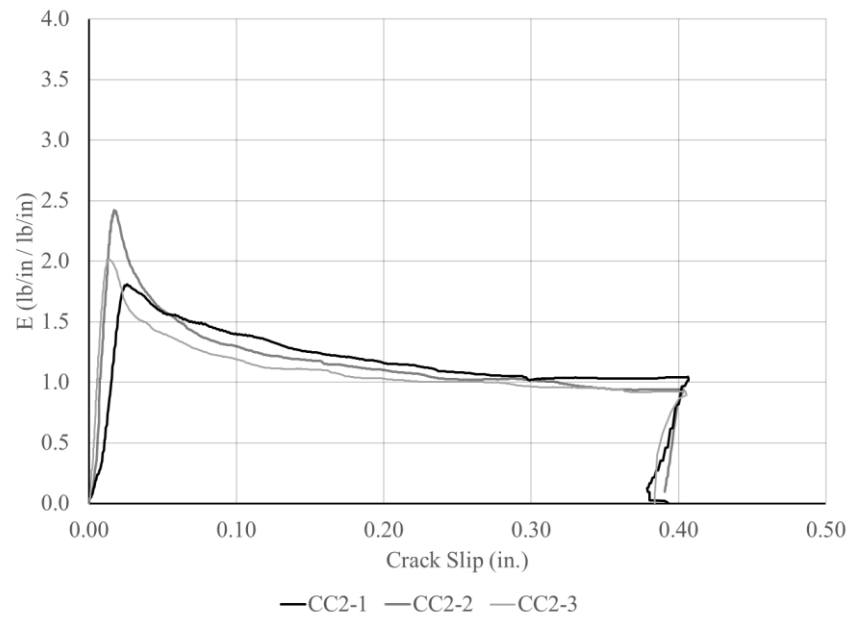


Figure G18 – Ratio versus slip for CC2



Figure G19 - Top view of failed CC-1

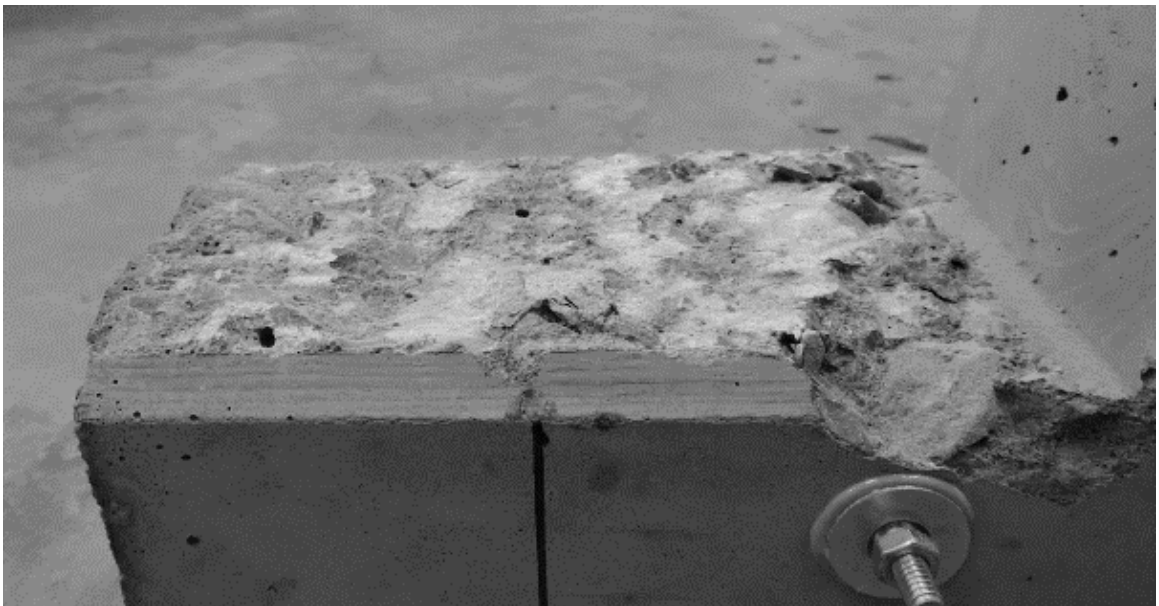


Figure G20 - Side view of failed CC-1



Figure G21 - Top view of failed CC-3

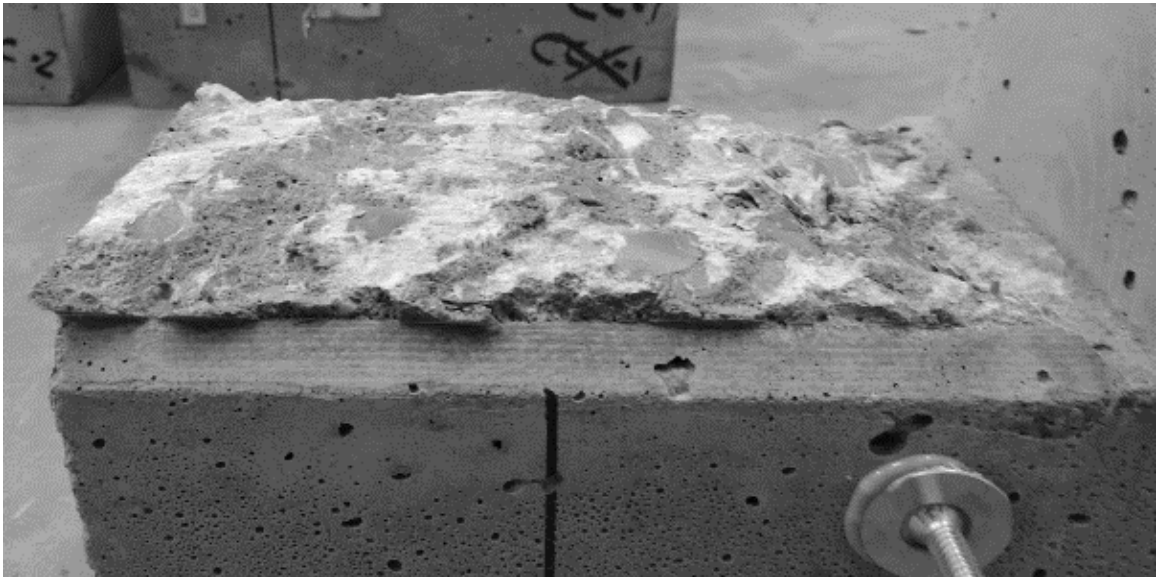


Figure G22 - Side view of failed CC-3



Figure G23 - Top view of failed CC1-1



Figure G24 - Side view of failed CC1-1



Figure G25 - Top view of failed CC1-2

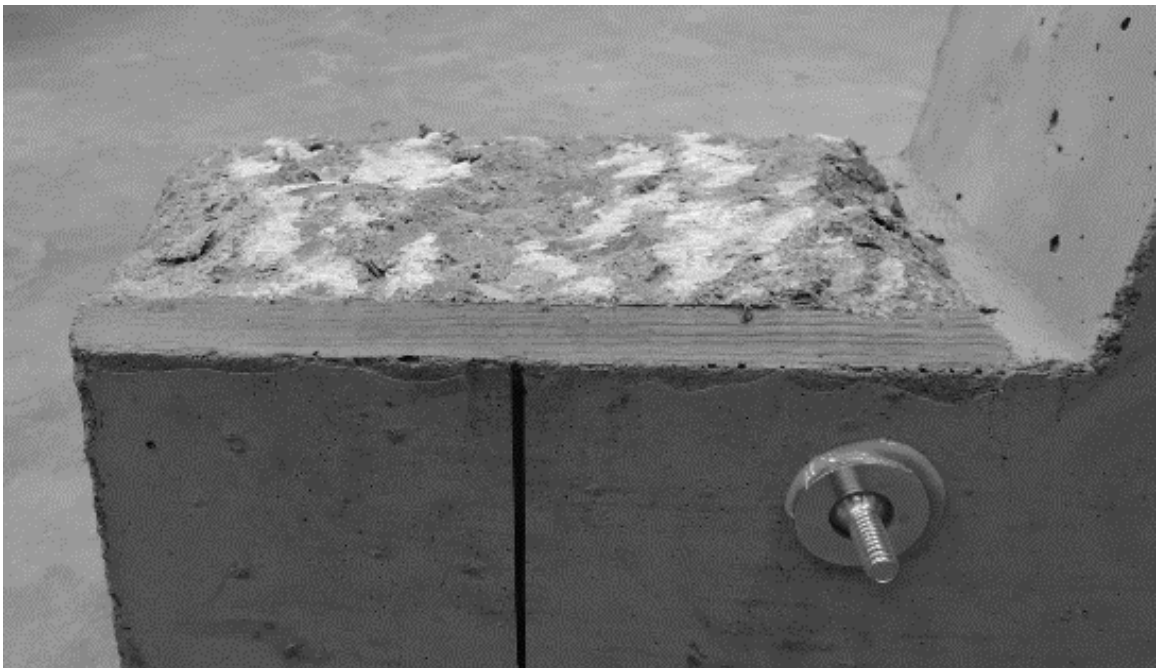


Figure G26 - Side view of failed CC1-2



Figure G27 - Top view of failed CC1-3

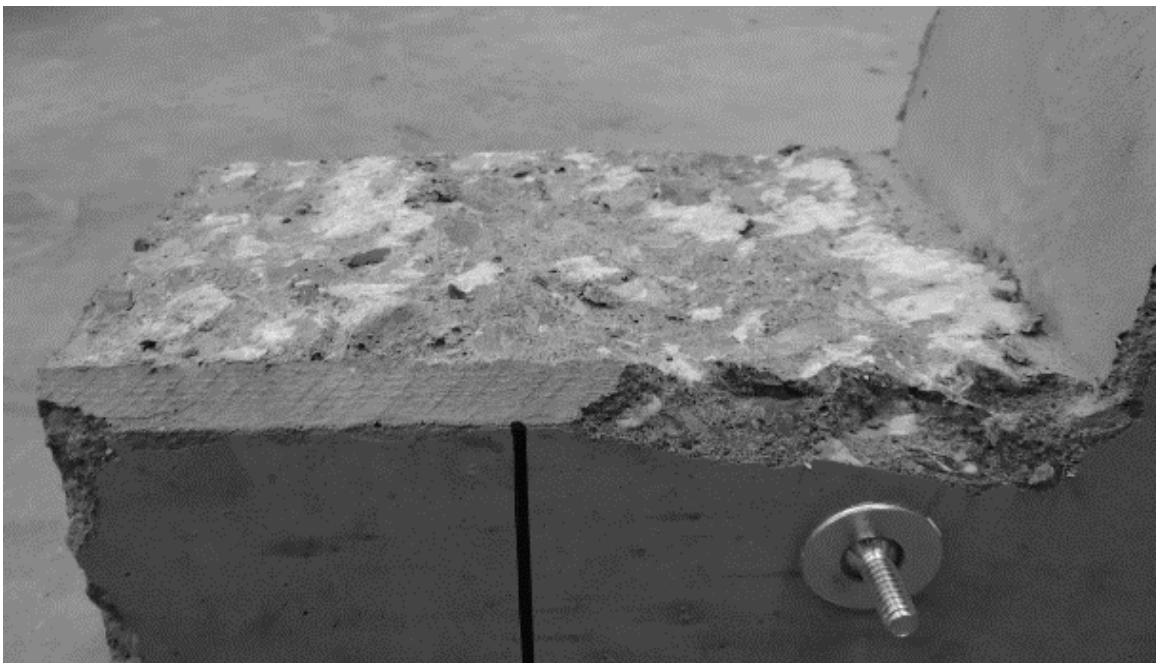


Figure G28 - Side view of failed CC1-3



Figure G29 - Top view of failed CC2-1



Figure G30 - Side view of failed CC2-1



Figure G31 - Top view of failed CC2-2

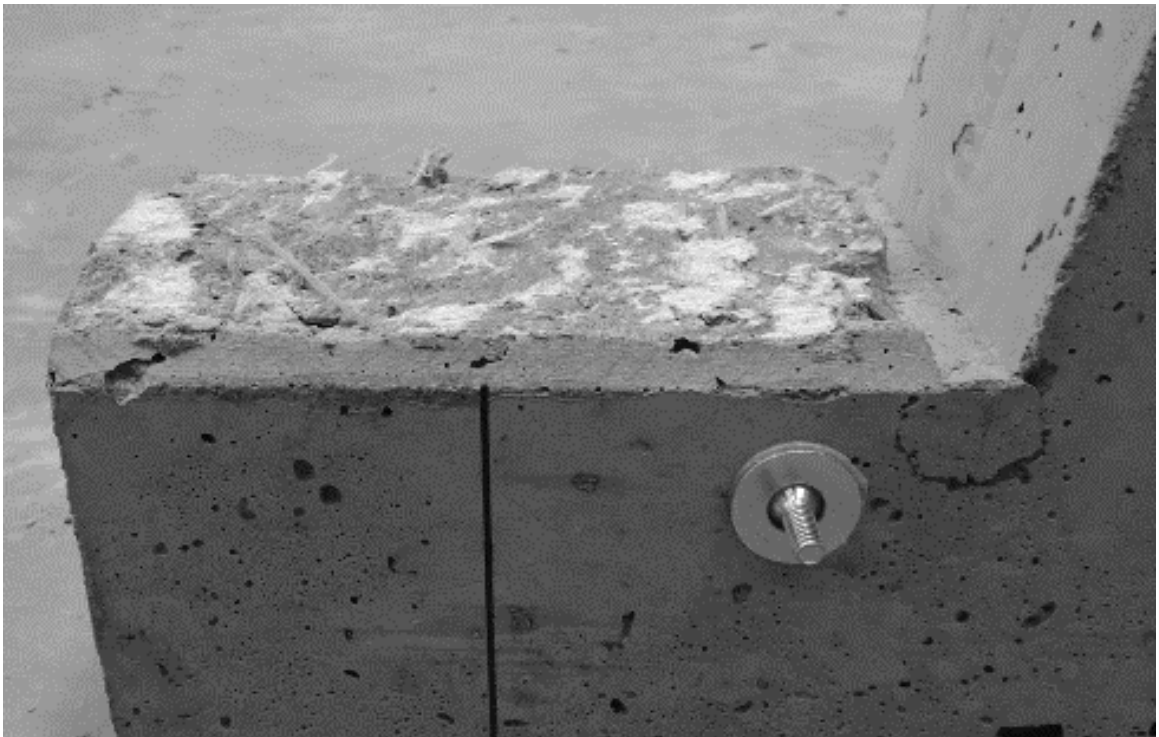


Figure G32 - Side view of failed CC2-2



Figure G33 - Top view of failed CC2-3

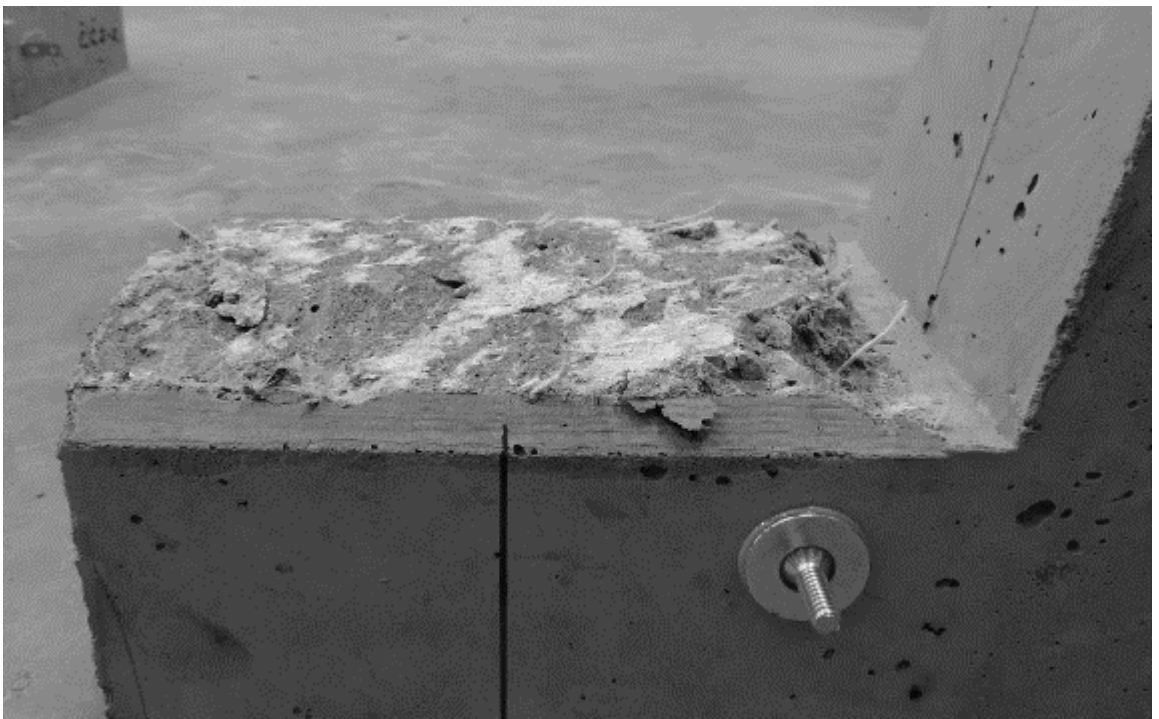


Figure G34 - Side view of failed CC2-3

APPENDIX H – PUSH-FF DATA OF EBC

PUSH-OFF TEST DATA OF EBC

The following section includes the results and discussion on the pre-cracking and push off testing of the EBC mixtures.

PRE-CRACKING

Results of the pre-cracking step in the push-off test for EBC, EBC1, and EBC2 are presented in Table H1. The specimens were pre-cracked without internal or external reinforcement, as is proposed in the new push-off test method. The apparent tensile strength, the shear force divided by the surface of the failure plane, is presented along with the compressive strengths. The ratio of tensile to compressive strength is also presented. The normalized tensile strength of CC was increased with the addition of micro-fibers, as CC1 was stronger than CC, and there was no change with the addition of macro-fibers. Without correcting for compressive strength, there were major gains in tensile strength with the addition of micro-fibers, and again with the addition of macro-fibers. Figures H1 through H10 are photos of the surfaces of the pre-cracked specimens.

Table H1 – Pre-cracking data of EBC mixtures

Mixture	Specimen	Apparent Tensile Strength	Compressive Strength	Ratio of Tensile to Compressive
EBC	1	313	5880	0.05
	2	294		0.05
	3	331		0.06
EBC1	1	351	5950	0.06
	2	346		0.06
	3	296		0.05
EBC2	1	391	6120	0.06
	2	421		0.07
	3	306		0.05



Figure H1 – Top view of pre-cracked EBC-1

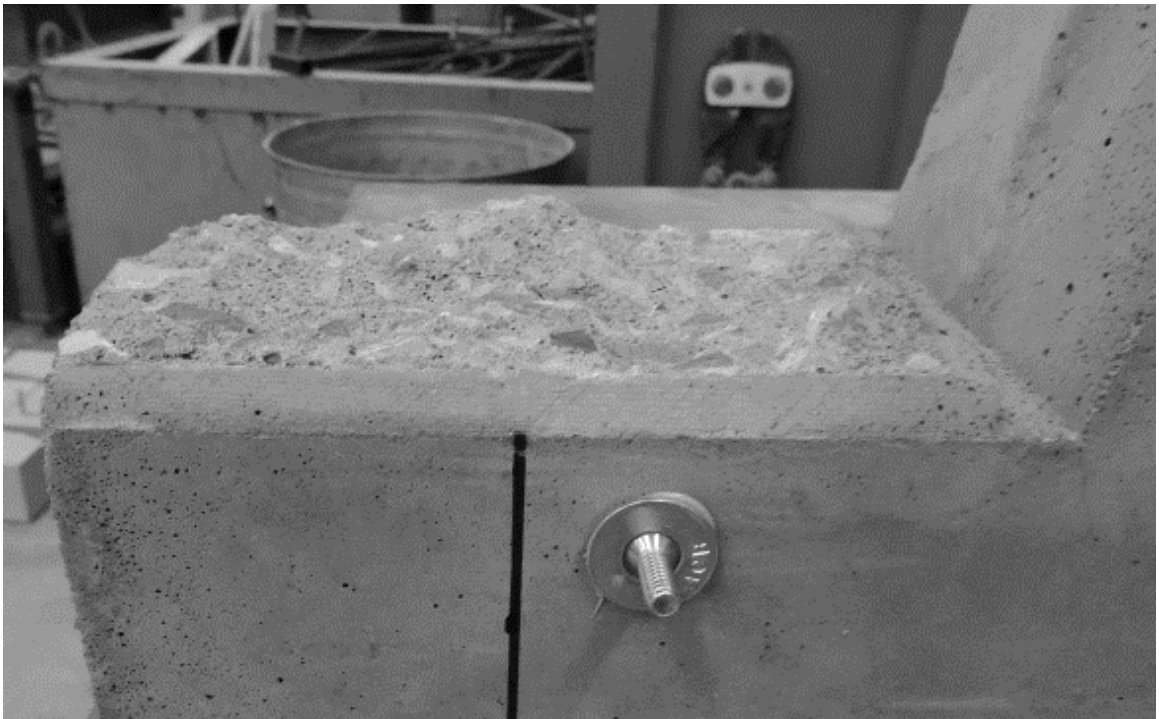


Figure H2 – Side view of pre-cracked EBC-1



Figure H3 - Top view of pre-cracked EBC-2

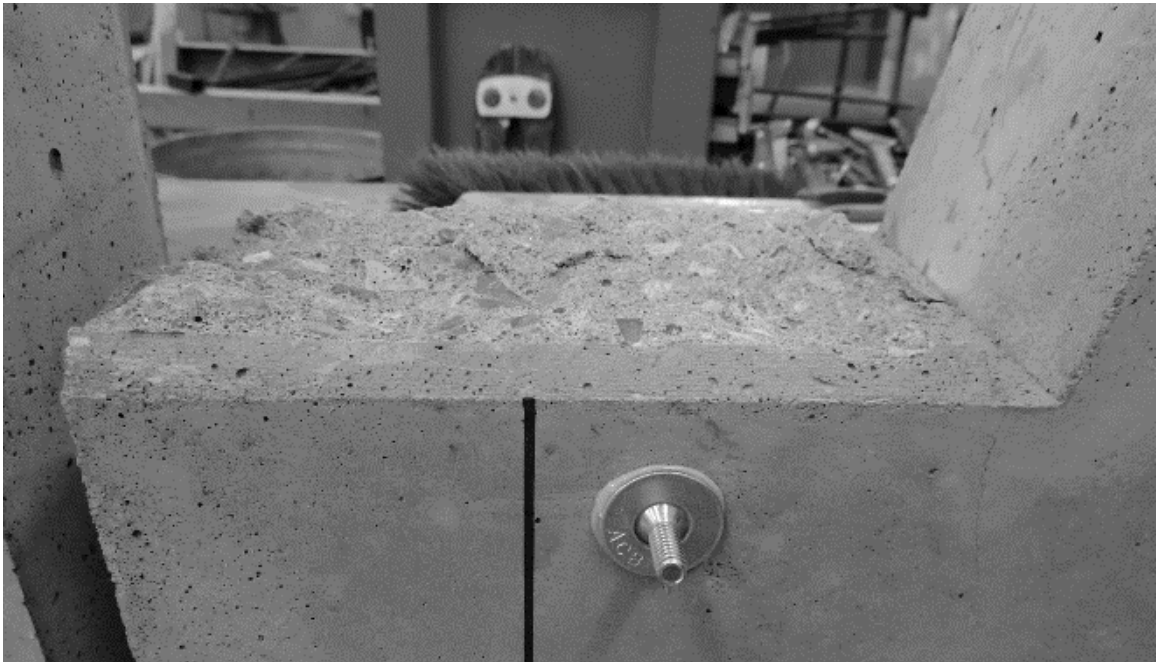


Figure H4 - Side view of pre-cracked EBC-2



Figure H5 - Top view of pre-cracked EBC-3

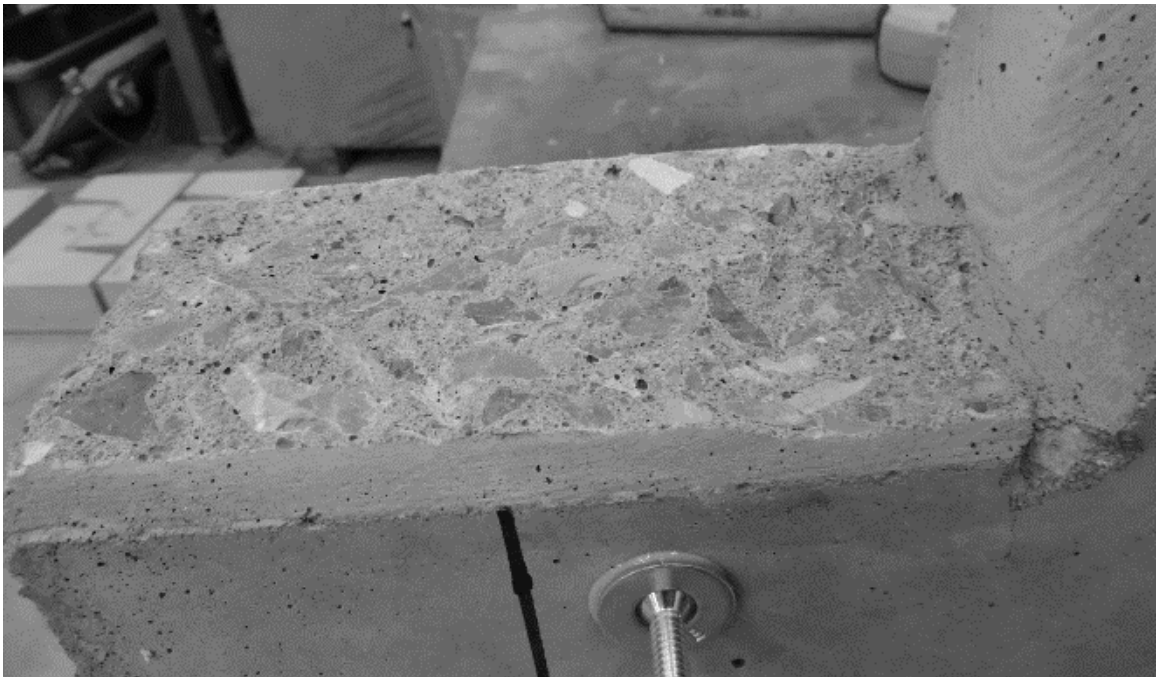


Figure H6 - Side view of pre-cracked EBC-3



Figure H7 – Top view of pre-cracked EBC1-1

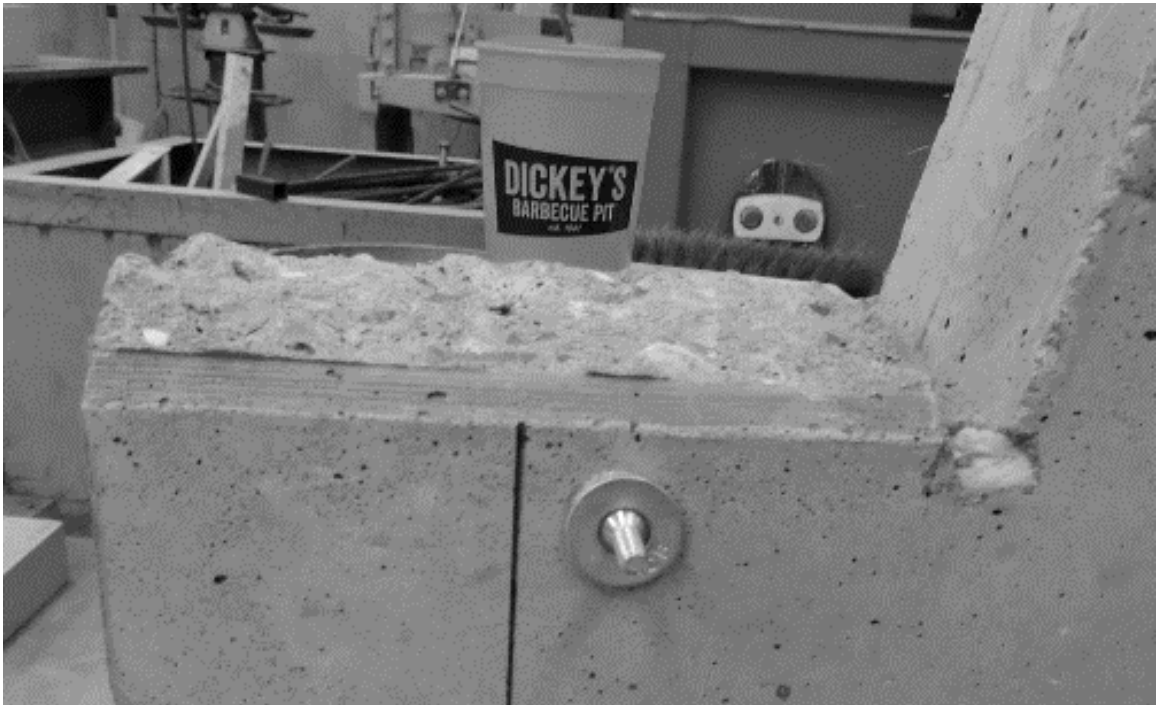


Figure H8 – Side view of pre-cracked EBC1-1



Figure H9 - Top view of pre-cracked EBC1-3



Figure H10 - Side view of pre-cracked EBC1-3

PUSH-OFF TEST

Results of the shear stress versus slip and ratio of shear to normal stress versus slip from the push-off test for EBC, EBC1, and EBC2 are presented in Table H2. The specimens were initially restrained with a clamping force between 200 and 300 psi through the use of external reinforcement, and then loaded through the pre-cracked failure plane.

The plots of shear stress versus slip for EBC, EBC1, and EBC2 are presented in Figures H11 through H13. The plots of ratio of shear to normal stress versus slip for EBC, EBC1, and EBC2 are presented in Figures H14 through H16. Figures H17 through H30 are photos of the surfaces of the failed push-off specimens.

Table H2 – Push-off test results of EBC mixtures

Concrete Mixture	Peak Shear Strength	Residual Shear Strength			Peak Ratio	Residual Ratio		
		0.10 in.	0.20 in.	0.30 in.		0.025 in.	0.05 in.	0.075 in.
EBC	606	598	576	583	3.22	2.37	1.95	1.63
EBC1	742	624	706	737	2.49	2.34	1.66	1.49
EBC2	791	719	791	753	2.98	2.56	1.77	1.58

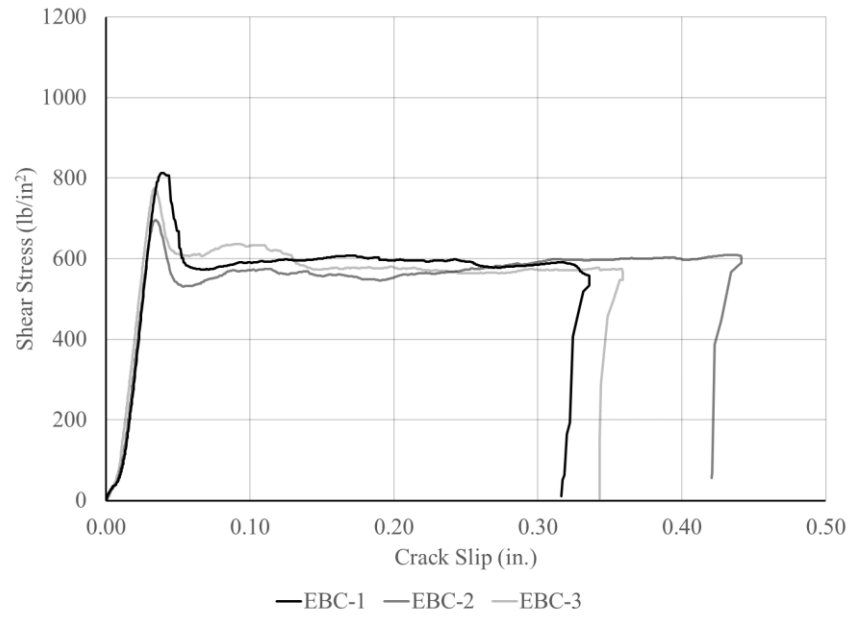


Figure H11 – Shear stress versus slip for EBC

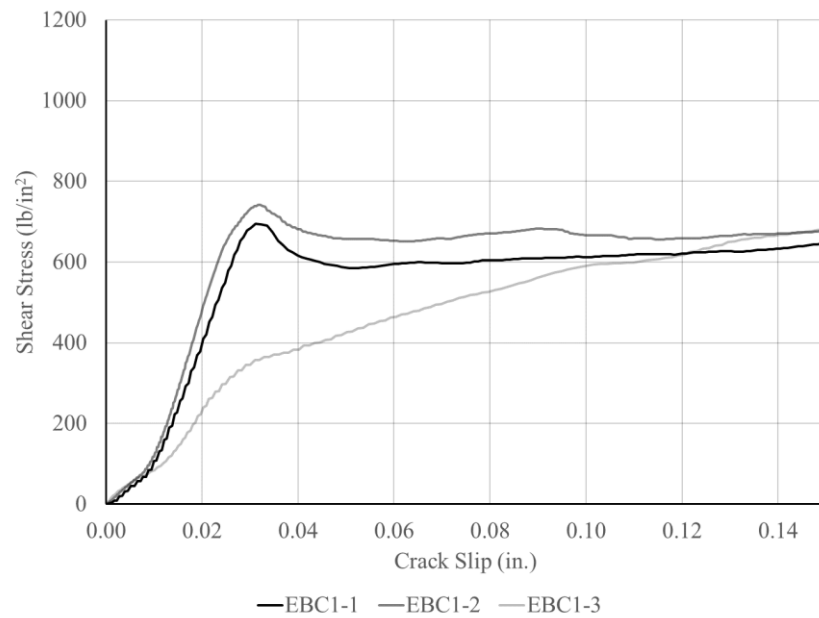


Figure H12 – Shear stress versus slip for EBC1

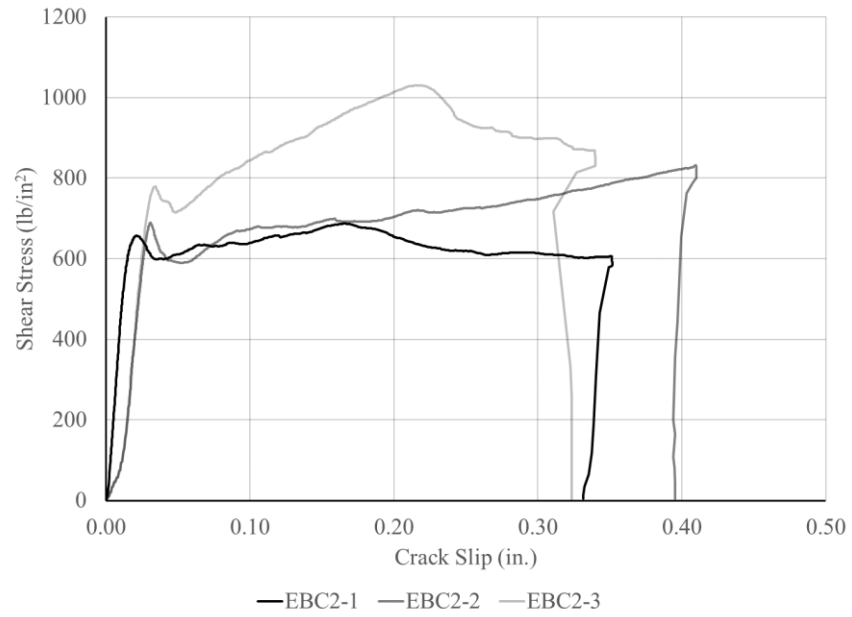


Figure H13 – Shear stress versus slip for EBC2

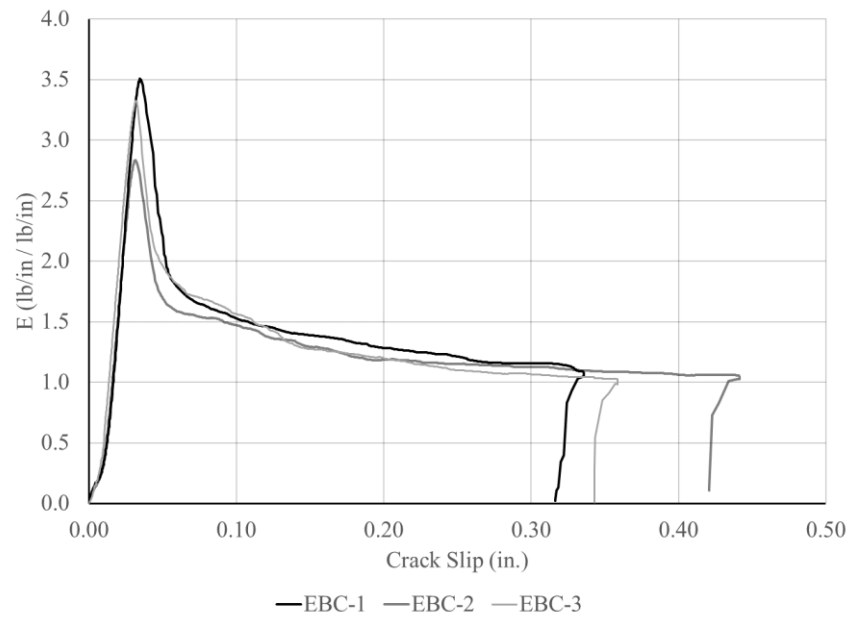


Figure H14 – Ratio versus slip for EBC

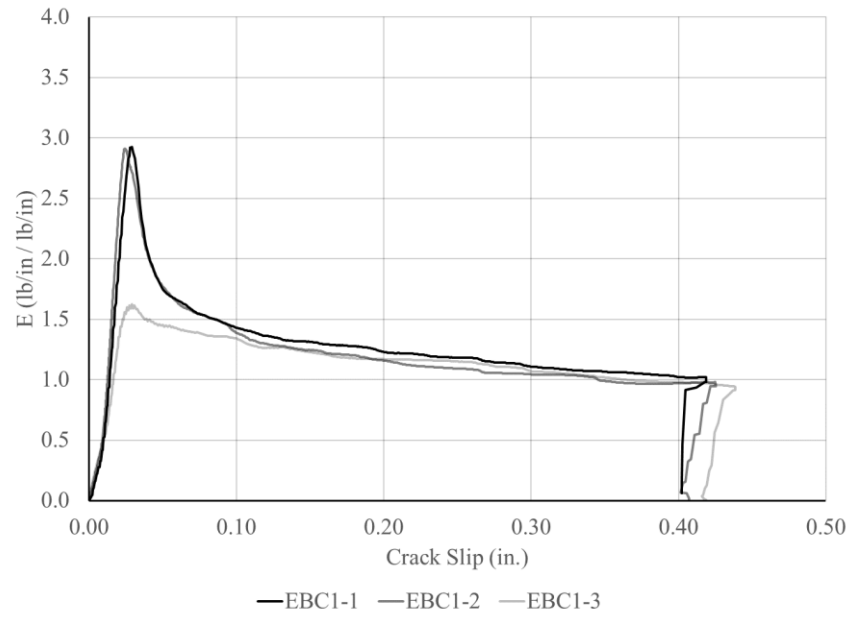


Figure H15 – Ratio versus slip for EBC1

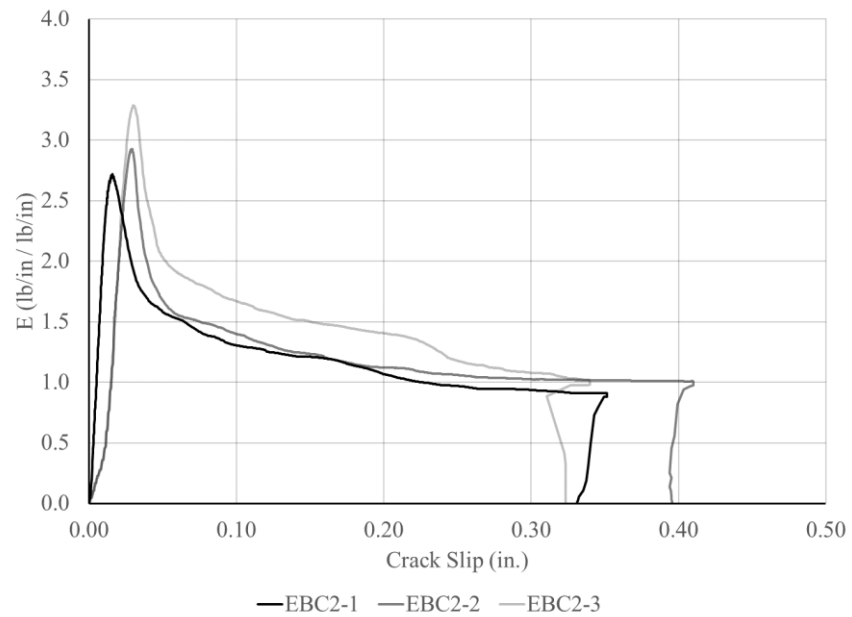


Figure H16 – Ratio versus slip for EBC2



Figure H17 - Top view of failed EBC-1



Figure H18 - Side view of failed EBC-1



Figure H19 - Top view of failed EBC-2

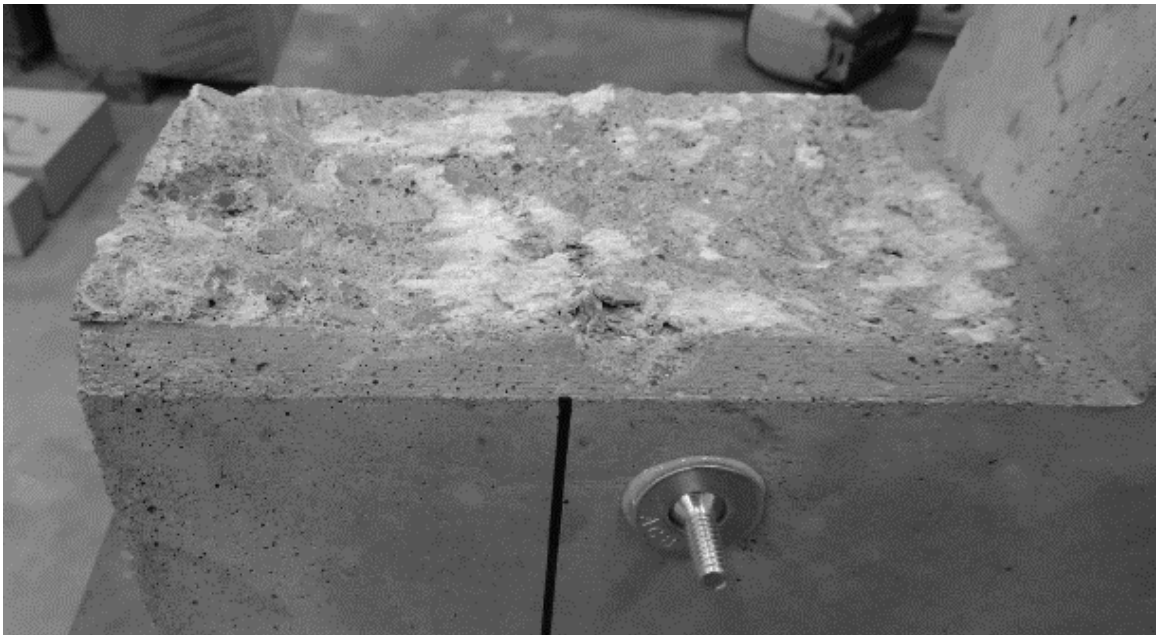


Figure H20 - Side view of failed EBC-2

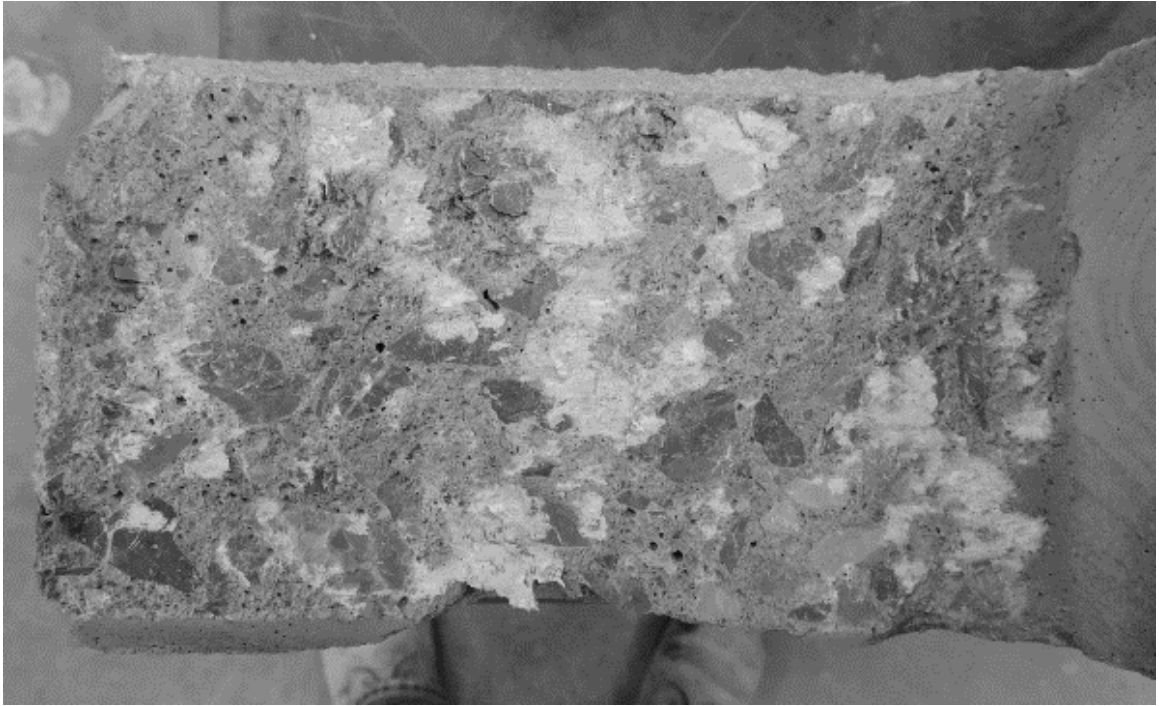


Figure H21 - Top view of failed EBC-3

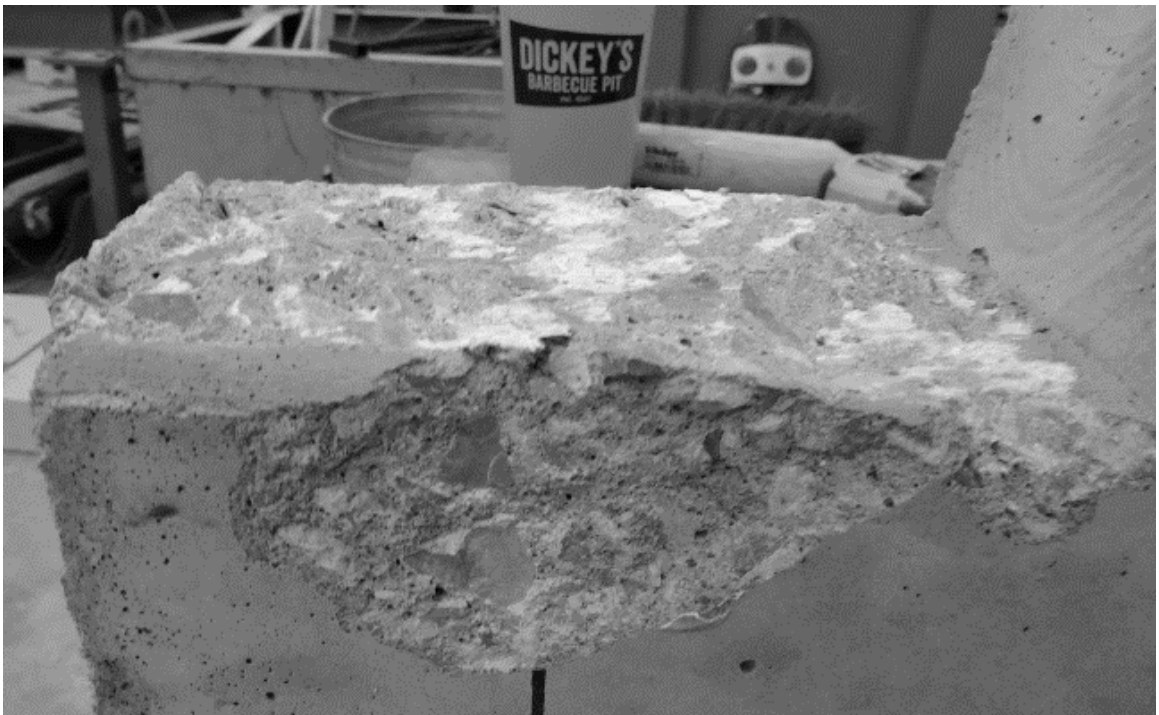


Figure H22 - Side view of failed EBC-3



Figure H23 - Top view of failed EBC1-1



Figure H24 - Side view of failed EBC1-1



Figure H25 - Top view of failed EBC1-2



Figure H26 - Side view of failed EBC1-2



Figure H27 - Top view of failed EBC1-3

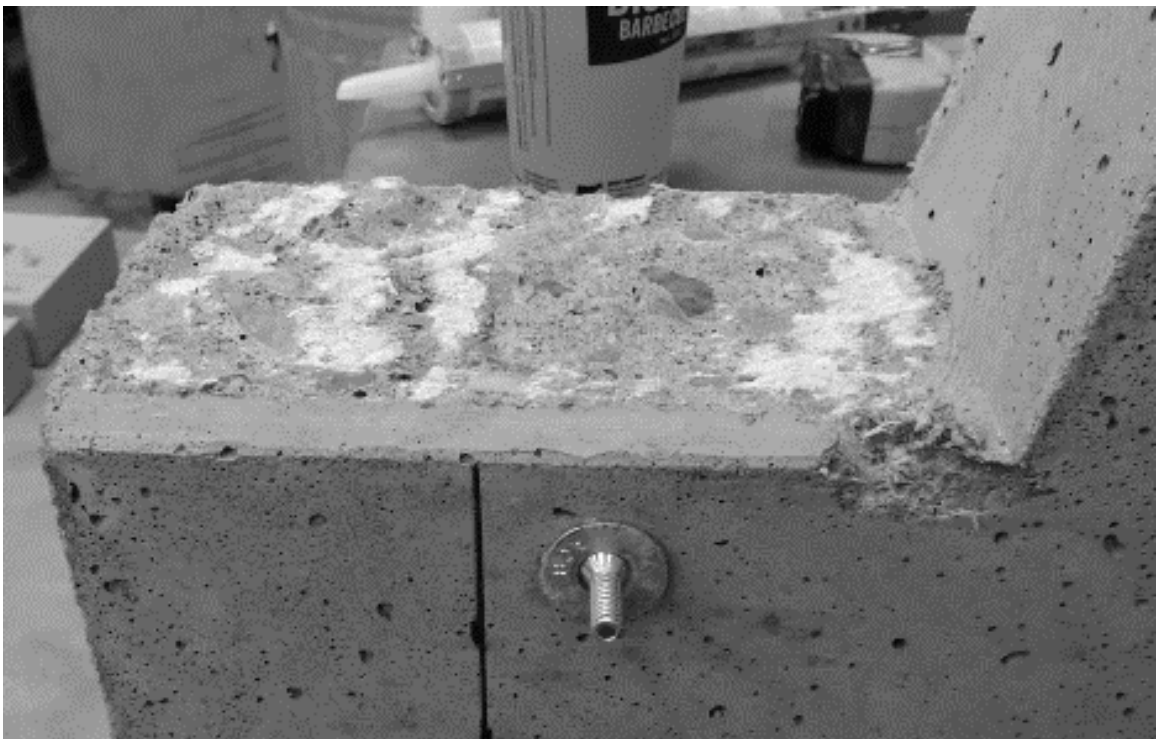


Figure H28 - Side view of failed EBC1-3



Figure H29 - Top view of failed EBC2-1

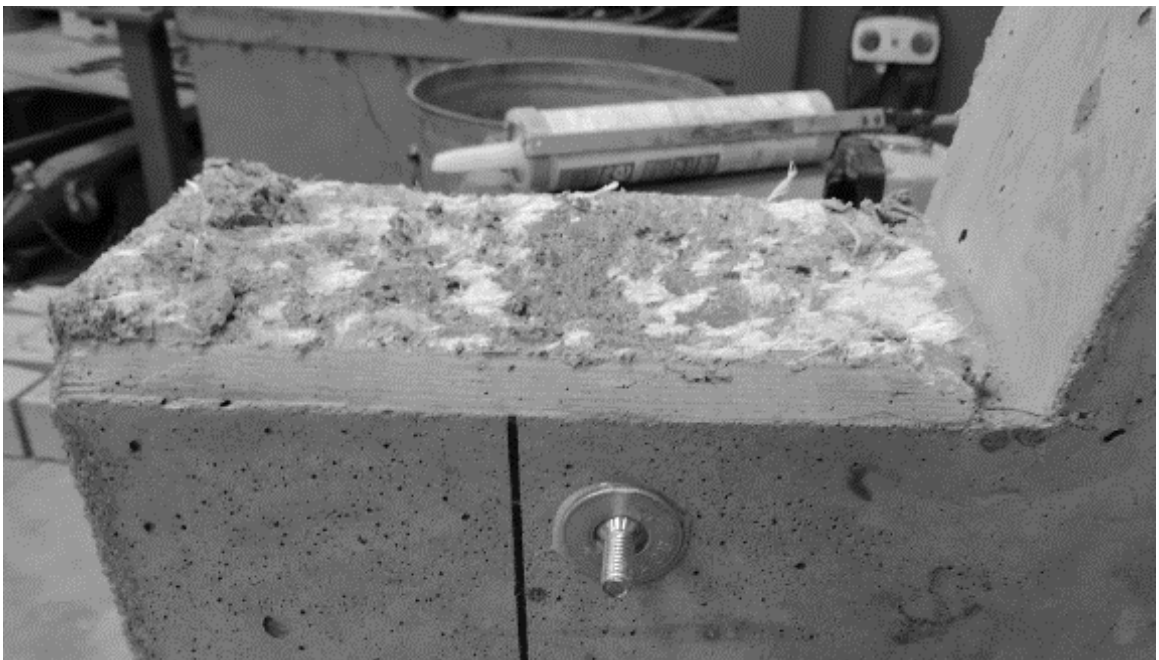


Figure H30 - Side view of failed EBC2-1



Figure H31 - Top view of failed EBC2-2



Figure H32 - Side view of failed EBC2-2



Figure H33 - Top view of failed EBC2-3



Figure H34 - Side view of failed EBC2-3

APPENDIX I – PUSH-OFF DATA OF K15

PUSH-OFF TEST DATA OF K15

The following section includes the results and discussion on the pre-cracking and push off testing of the K15 mixtures.

PRE-CRACKING

Results of the pre-cracking step in the push-off test for K15 and K15F are presented in Table I1. The specimens were pre-cracked without internal or external reinforcement, as is proposed in the new push-off test method. The apparent tensile strength, the shear force divided by the surface of the failure plane, is presented along with the compressive strengths. The ratio of tensile to compressive strength is also presented. The normalized tensile strength of K15 was decreased with the addition of macro-fibers. Without correcting for compressive strength, there was still a major reduction in apparent tensile strength with the addition of macro-fibers. Figures I1 through I4 are photos of the surfaces of the pre-cracked specimens.

Table I1 – Pre-cracking data of K15 mixtures

Mixture	Specimen	Apparent Tensile Strength	Compressive Strength	Ratio of Tensile to Compressive
K15	1	347	5890	0.06
	2	473		0.08
	3	439		0.07
K15F	1	369	7110	0.05
	2	356		0.05
	3	373		0.05



Figure I1 – Top view of pre-cracked K15-2



Figure I2 – Side view of pre-cracked K15-2



Figure I3 - Top view of pre-cracked K15-3



Figure I4 - Side view of pre-cracked K15-3

PUSH-OFF TEST

Results of the shear stress versus slip and ratio of shear to normal stress versus slip from the push-off test for K15 and K15F are presented in Table I2. The specimens were initially restrained with a clamping force between 200 and 300 psi through the use of external reinforcement, and then loaded through the pre-cracked failure plane.

The plots of shear stress versus slip for K15 and K15F are presented in Figures I5 and I6. The plots of ratio of shear to normal stress versus slip for K15 and K15F are presented in Figures I7 and I8. Figures I9 through XXX are photos of the surfaces of the failed push-off specimens.

Table I2 – Push-off test results of K15 mixtures

Concrete Mixture	Peak Shear Strength	Residual Shear Strength			Peak Ratio	Residual Ratio		
		0.10 in.	0.20 in.	0.30 in.		0.025 in.	0.05 in.	0.075 in.
K15	900	802	895	872	3.01	2.66	1.74	1.50
K15F	784	781	736	708	2.81	2.63	1.97	1.73

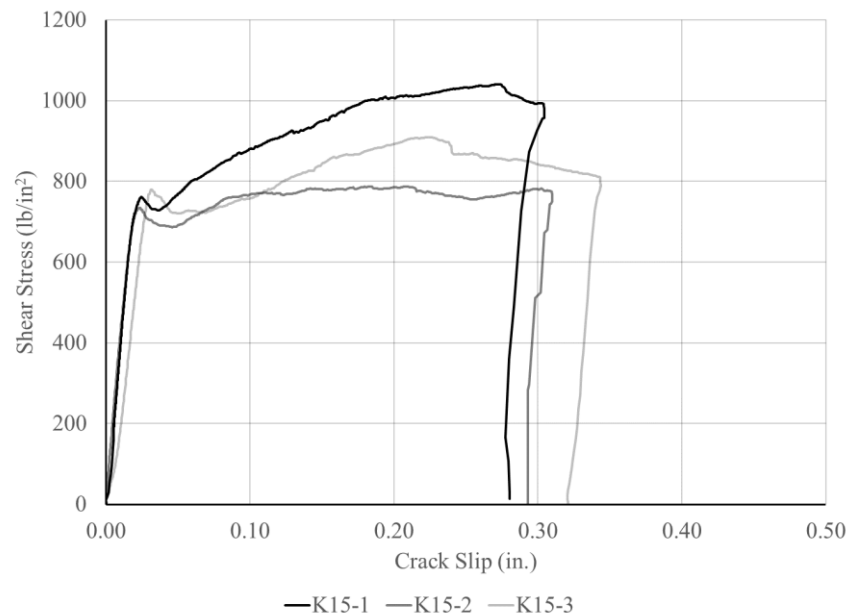


Figure I5 – Shear stress versus slip for K15

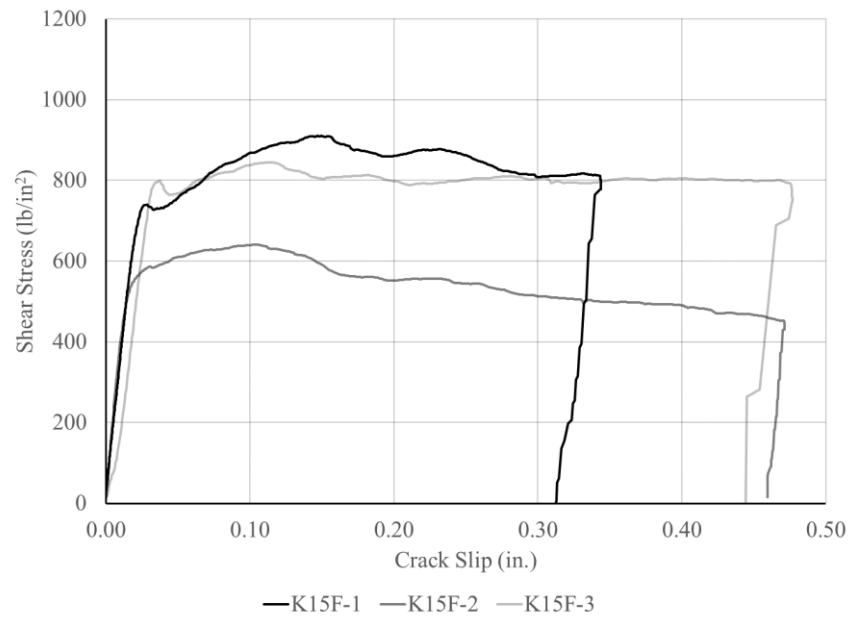


Figure I6 – Shear stress versus slip for K15F

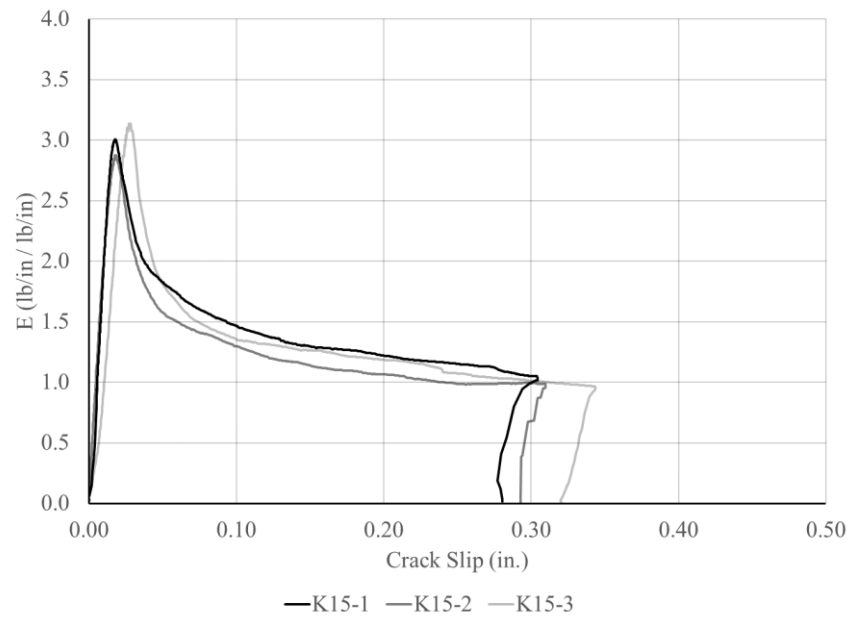


Figure I7 – Ratio versus slip for K15

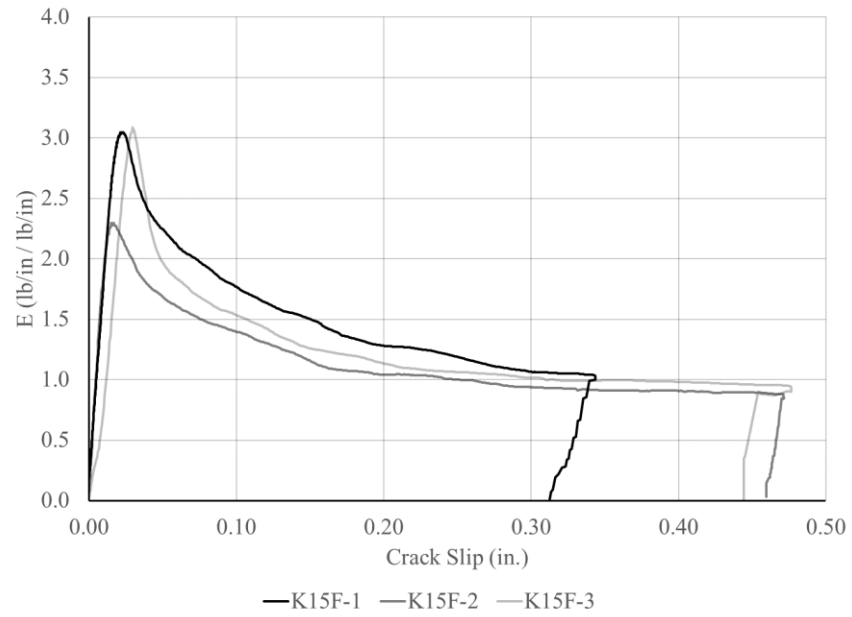


Figure I8 – Ratio versus slip for K15F



Figure I9 - Top view of failed K15-1

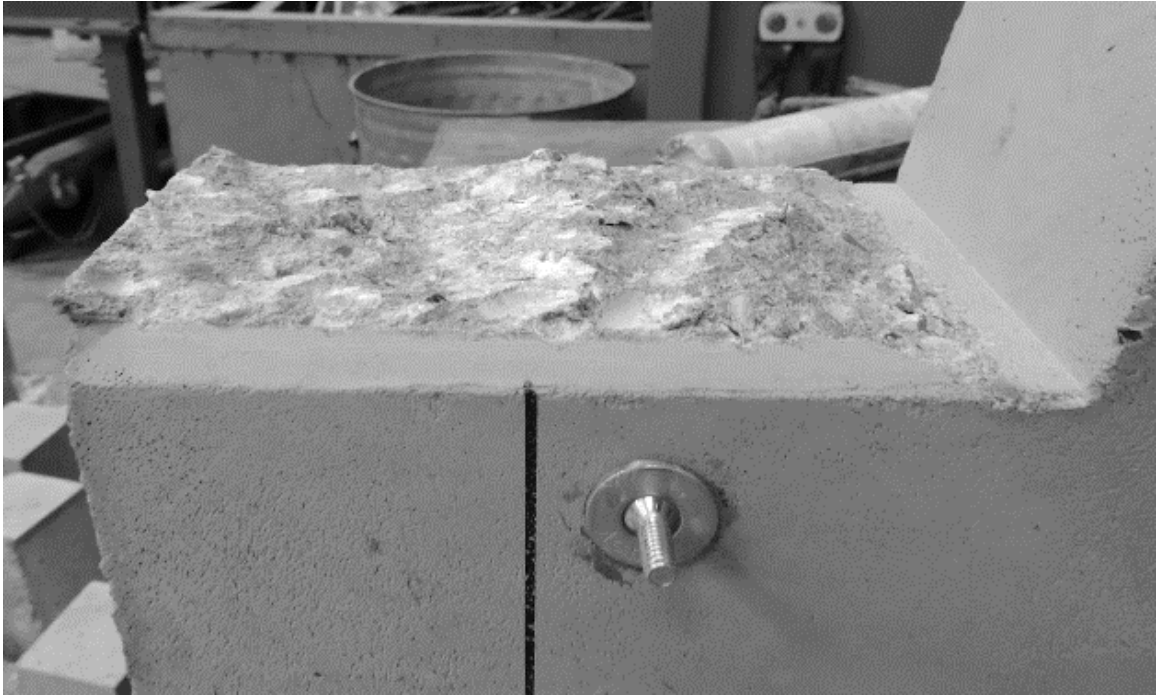


Figure I10 - Side view of failed K15-1



Figure I11 - Top view of failed K15-2



Figure I12 - Side view of failed K15-2



Figure I13 - Top view of failed K15-3



Figure I14 - Side view of failed K15-3



Figure I15 - Top view of failed K15F-1

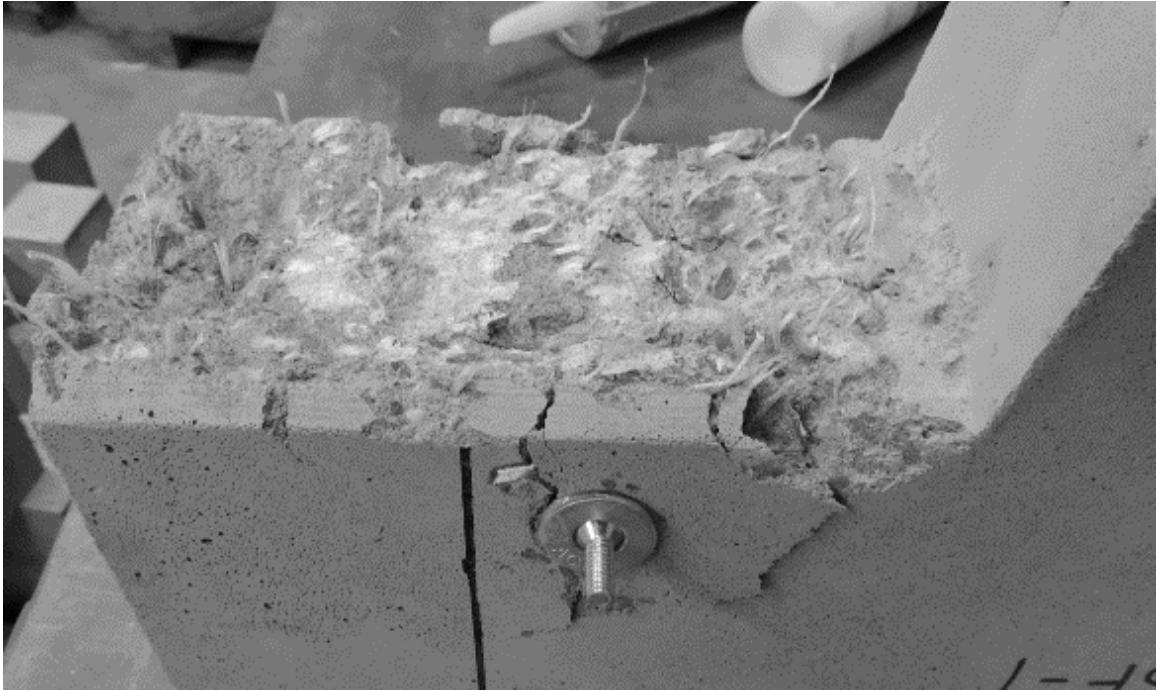


Figure I16 - Side view of failed K15F-1

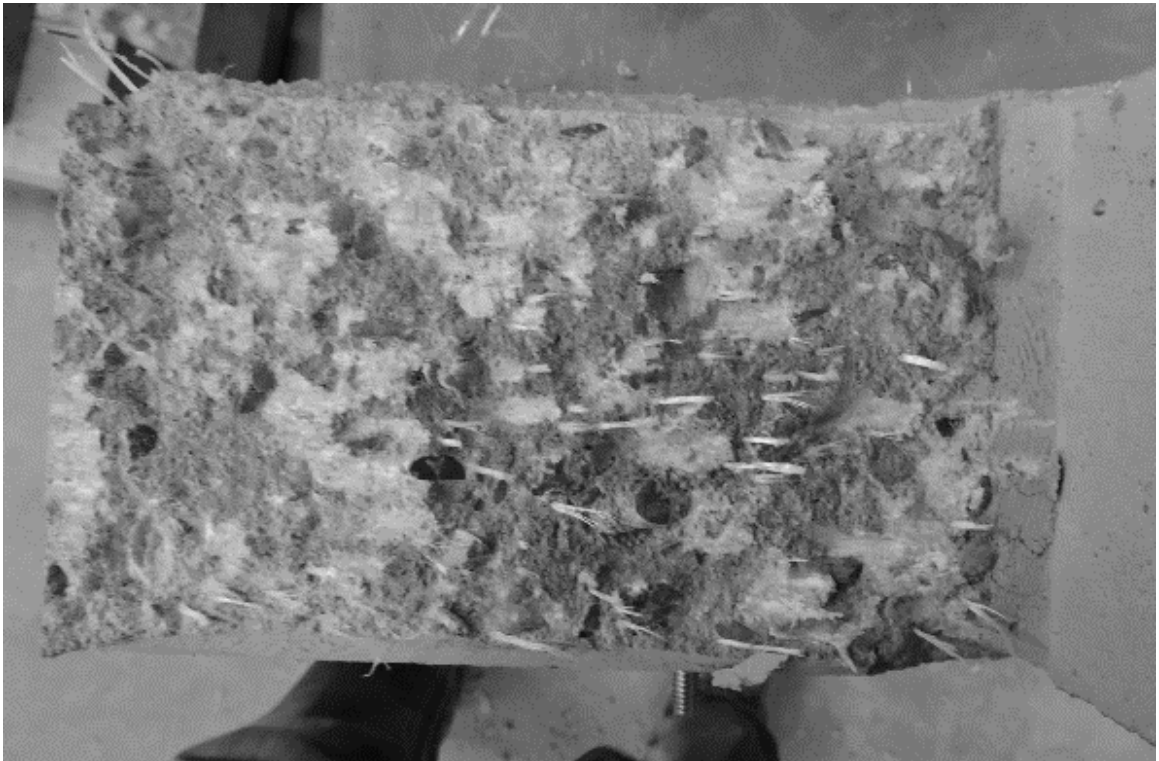


Figure I17 - Top view of failed K15F-2



Figure I18 - Side view of failed K15F-2

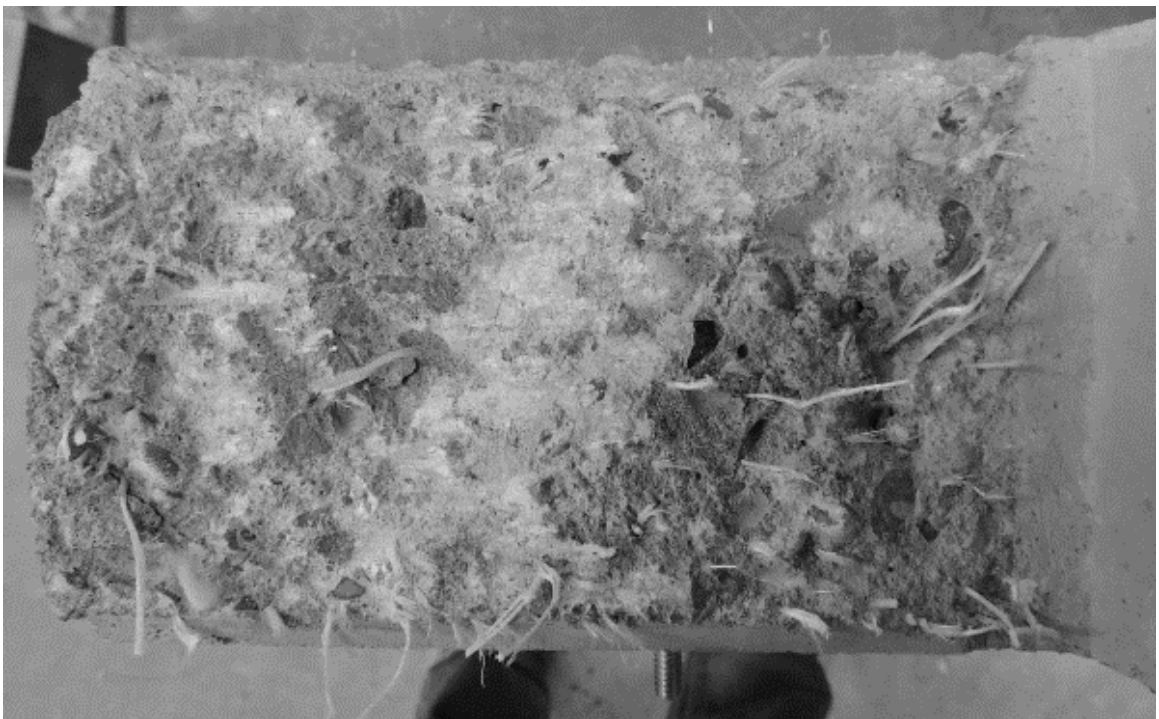


Figure I19 - Top view of failed K15F-3



Figure I20 - Side view of failed K15F-3

**APPENDIX J – SHEAR BEAM REINFORCEMENT, INSTRUMENTATION, &
TEST SETUP**



Figure J1 – Completed rebar cages



Figure J2 – Completed rebar cage

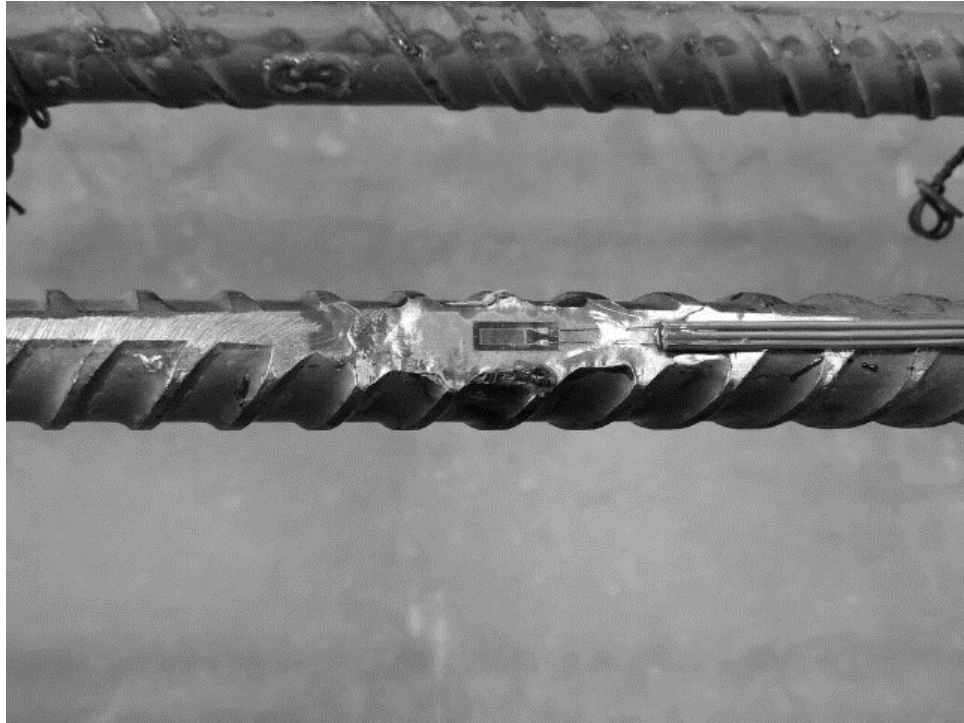


Figure J3 – Strain gauge adhered to longitudinal reinforcement

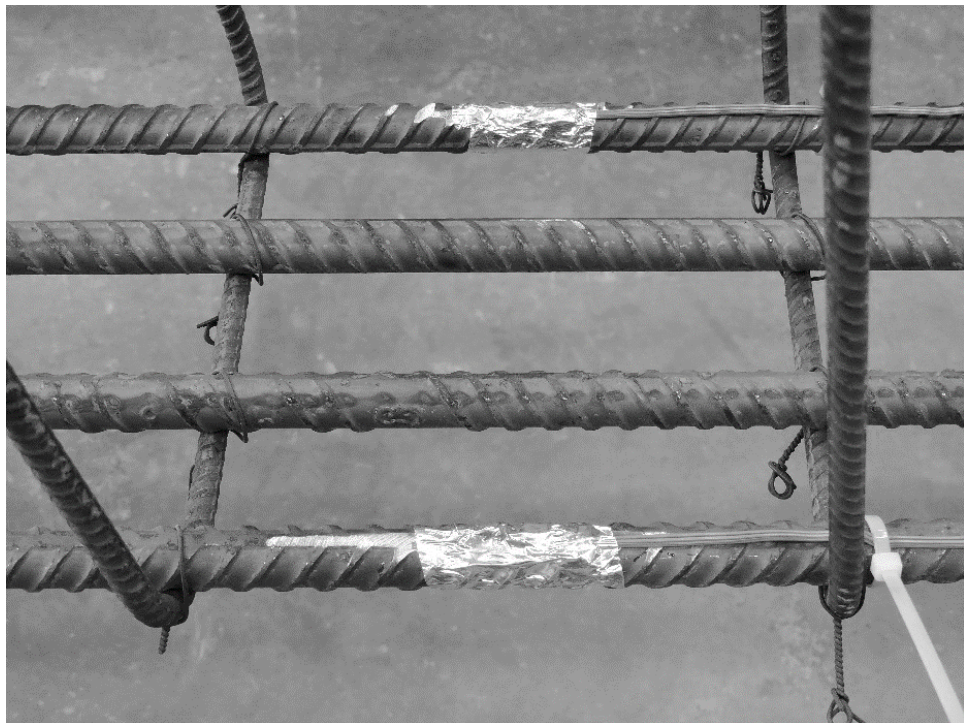


Figure J4 – Completed strain gauge installation



5

Figure J5 – Wire potentiometer setup

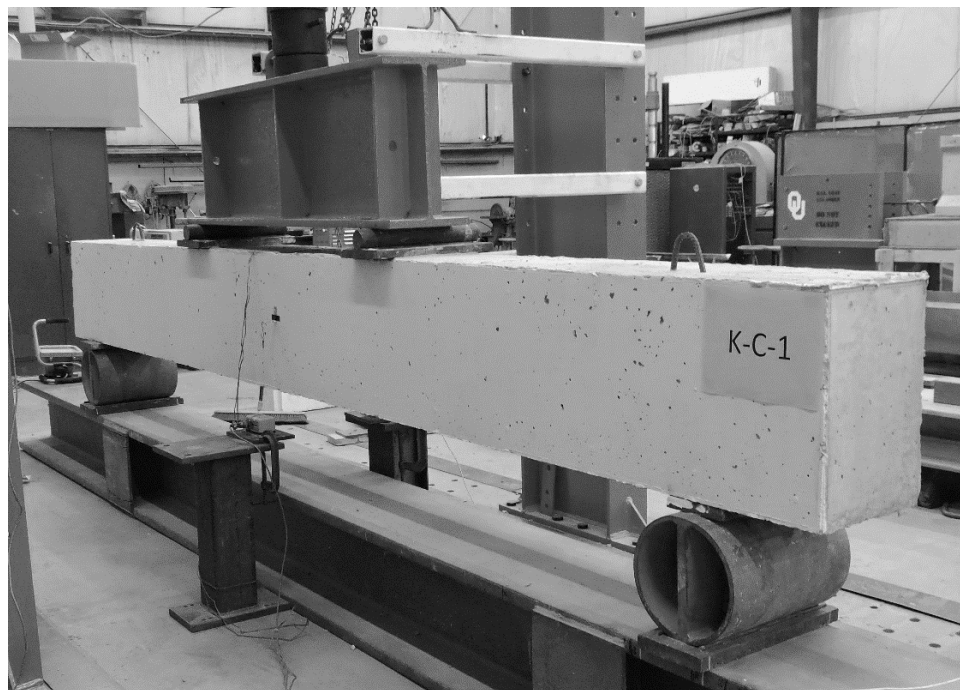


Figure J6 – Simply supported third-point beam setup

APPENDIX K – PUSH-OFF INSTRUMENTATION & TEST SETUP



Figure K1 – Neoprene base pads and wedge for pre-cracking



Figure K2 – Neoprene base pads and wedge for pre-cracking



Figure K3 – Front view of pre-cracking setup

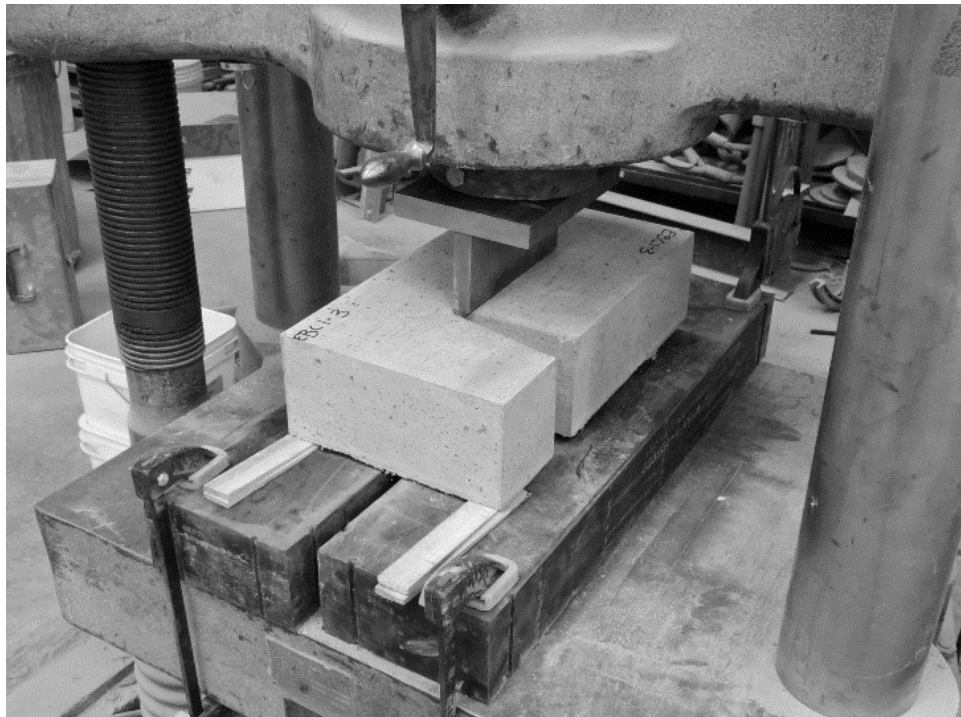


Figure K4 – Pre-cracking setup



Figure K5 – First step in assembling external reinforcement



Figure K6 – Second step in assembling external reinforcement



Figure K7 – Hand tightening external reinforcing nuts



Figure K8 – Pre-stressing the specimen with 200 to 300 psi



Figure K9 – Centering specimen and attaching instrumentation

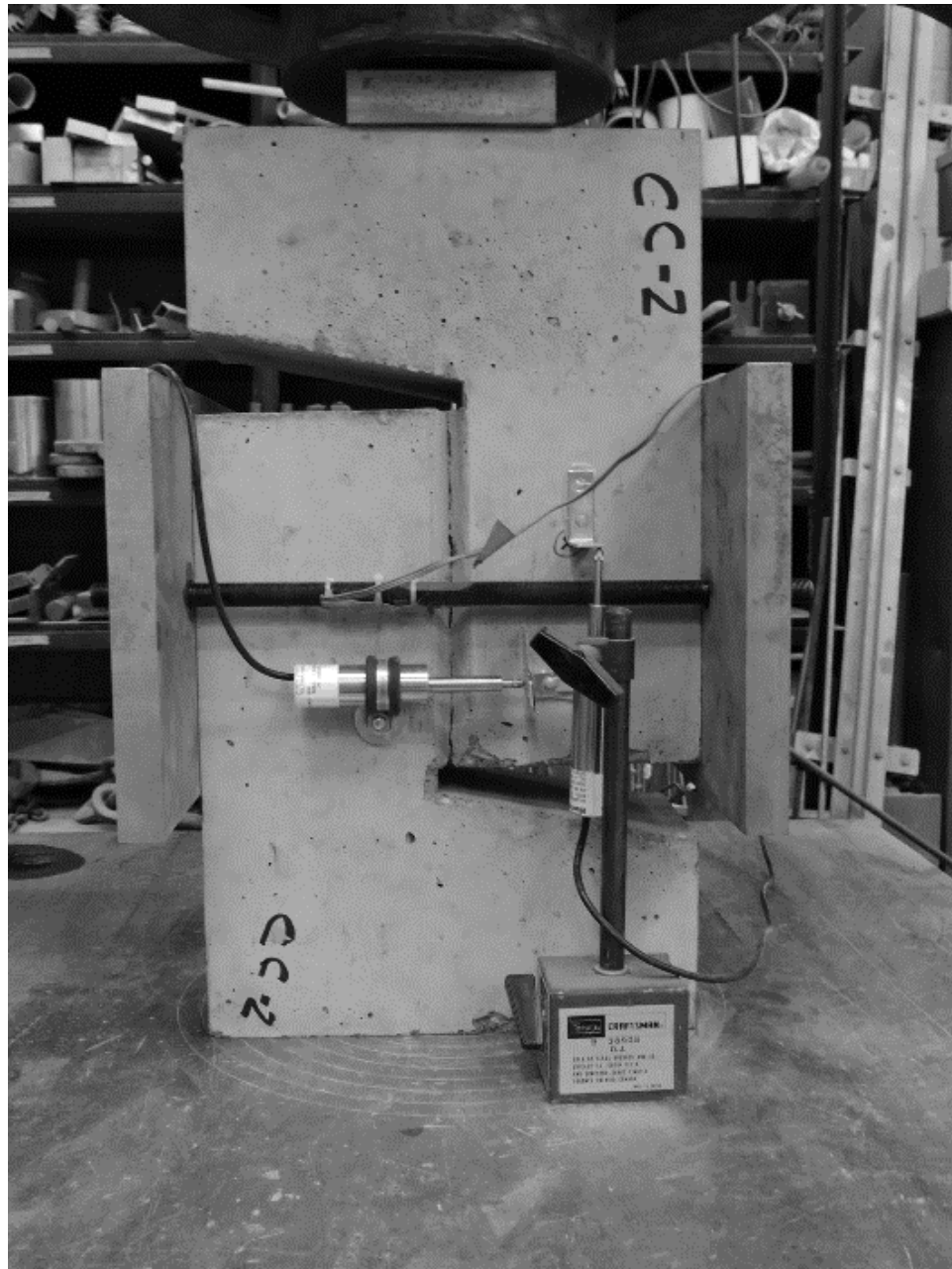


Figure K10 – Push-off test setup and instrumentation

APPENDIX L – CEMENT DATA SHEETS

ASH GROVE CEMENT COMPANY



1801 North Santa Fe
P.O. Box 519
Chanute, KS 66720
Phone: 620-433-3500
Fax: 620-431-3282

LOT # 2633

Type I/II (Low Alkali)

Production Period: April 1 thru April 30, 2016

Date: 5/9/2016

The following information is based on average test data during the production period. The data is typical of cement shipped from the Chanute, Kansas plant. Individual shipments may vary.

STANDARD REQUIREMENTS ASTM C150/C150M-12, Tables 1 and 3

CHEMICAL				PHYSICAL			
Item	A.S.T.M. Test Method	Spec. Limit	Test Result	Item	A.S.T.M. Test Method	Spec. Limit	Test Result
SiO ₂ (%)	C114	A	20.71	Air content of mortar (volume %)	C185	12 max	7
Al ₂ O ₃ (%)	C114	6.0 max	4.08	Fineness (cm ² /g):			
Fe ₂ O ₃ (%)	C114	6.0 max	2.97	Air permeability	C204	2600 min	3971
CaO (%)	C114	A	63.99	Autoclave expansion (%)	C151	0.80 max	0.03
MgO (%)	C114	6.0 max	2.06	Compressive strength (psi)			
SO ₃ (%)	C114	3.0 max	2.92	1 Day	C109	A	2304
Loss on Ignition (%)	C114	3.0 max	2.57	3 Days	C109	1740 min	3788
Na ₂ O (%)	C114	A	0.20	7 Days	C109	2760 min	4631
K ₂ O (%)	C114	A	0.51	Time of setting (minutes)			
Insoluble Residue (%)	C114	0.75 max	0.40	(Vicat)			
CO ₂ (%)	C114	A	1.81	Initial: Not less than	C191	45	124
Limestone (%)	C114	5.0 max	4.6	Not more than		375	124
CaCO ₃ in limestone (%)	C114	70 min	89.82				
Potential compounds (%) ^D							
C ₃ S	C114	A	56				
C ₂ S	C114	A	17				
C ₃ A	C114	8.0 max	6				
C ₄ AF	C114	A	9				
C ₃ S + 4.75 C ₃ A	C114	100 max	85				

OPTIONAL REQUIREMENTS ASTM C150/C150M-12, Tables 2 and 4

CHEMICAL				PHYSICAL			
Item	A.S.T.M. Test Method	Spec. Limit	Test Result	Item	A.S.T.M. Test Method	Spec. Limit	Test Result
C ₃ S + C ₃ A (%)	C114	A		False set (%)	C451	B	88
Equivalent alkalies (%)	C114	0.60	0.53	Heat of hydration (kJ/kg)			
A = Not applicable.				7 days	C186	A	
B = Limit not specified by purchaser, test result provided for information only.							
C = Test results for this period not available.							
D = Adjusted per Annex A1.6 M85							

We certify that the above described cement, at the time of shipment, meets the chemical and physical requirements of ASTM C150/C150M-12 (Types I/II) and AASHTO M85-12 (Type I/II), or (other) _____ specification.

Signature: Marc D. Melton
Title: Chief Chemist

ASH GROVE CEMENT COMPANY



1801 North Santa Fe
P.O. Box 519
Chanute, KS 66720
Phone: 620-433-3500
Fax: 620-431-3282

Type I/II (Low Alkali)

Production Period: April 1 thru April 30, 2016

Date: 5/9/2016

The following information is based on average test data during the production period. The data is typical of cement shipped from the Chanute, Kansas plant. Individual shipments may vary.

Additional Data

Inorganic Processing Addition Data	
Type	Limestone
Amount(%)	4.58
SiO ₂ (%)	5.03
Al ₂ O ₃ (%)	1.47
Fe ₂ O ₃ (%)	1.2
CaO (%)	48.5
SO ₃ (%)	0.06

Base Cement Phase Composition	
C ₃ S	59
C ₂ S	17
C ₃ A	6
C ₄ AF	9

Signature: 
Marc D. Melton
Title: Chief Chemist

ASH GROVE CEMENT COMPANY



1801 North Santa Fe
P.O. Box 519
Chanute, KS 66720
Phone: 620-433-3500
Fax: 620-431-3282

LOT # 2661

Type I/II (Low Alkali)

Production Period: December 1 thru December 31, 2016

Date: 1/9/2017

The following information is based on average test data during the production period. The data is typical of cement shipped from the Chanute, Kansas plant. Individual shipments may vary.

STANDARD REQUIREMENTS ASTM C150/C150M-12, Tables 1 and 3

CHEMICAL				PHYSICAL			
Item	A.S.T.M. Test Method	Spec. Limit	Test Result	Item	A.S.T.M. Test Method	Spec. Limit	Test Result
SiO ₂ (%)	C114	A	20.71	Air content of mortar (volume %)	C185	12 max	6
Al ₂ O ₃ (%)	C114	6.0 max	3.97	Fineness (cm ² /g):			
Fe ₂ O ₃ (%)	C114	6.0 max	3.00	Air permeability	C204	2600 min	3977
CaO (%)	C114	A	64.55	Autoclave expansion (%)	C151	0.80 max	0.04
MgO (%)	C114	6.0 max	1.99	Compressive strength (psi)			
SO ₃ (%)	C114	3.0 max	2.97	1 Day	C109	A	2566
Loss on ignition (%)	C114	3.0 max	2.30	3 Days	C109	1740 min	4124
Na ₂ O (%)	C114	A	0.20	7 Days	C109	2760 min	4940
K ₂ O (%)	C114	A	0.52	Time of setting (minutes)			
Insoluble Residue (%)	C114	0.75 max	0.33	(Vicat)			
CO ₂ (%)	C114	A	1.49	Initial: Not less than	C191	45	117
Limestone (%)	C114	5.0 max	4.5	Not more than		375	117
CaCO ₃ in limestone (%)	C114	70 min	89.82				
Potential compounds (%) ^D							
C ₂ S	C114	A	60				
C ₃ S	C114	A	14				
C ₄ A	C114	8.0 max	5				
C ₄ AF	C114	A	9				
C ₂ S + 4.75 C ₄ A	C114	100 max	84				

OPTIONAL REQUIREMENTS ASTM C150/C150M-12, Tables 2 and 4

CHEMICAL				PHYSICAL			
Item	A.S.T.M. Test Method	Spec. Limit	Test Result	Item	A.S.T.M. Test Method	Spec. Limit	Test Result
C ₂ S + C ₄ A (%)	C114	A		False set (%)	C451	B	89
Equivalent alkalies (%)	C114	0.60	0.55	Heat of hydration (kJ/kg)			
				7 days	C186	A	

A = Not applicable.

B = Limit not specified by purchaser, test result provided for information only.

C = Test results for this period not available.

D = Adjusted per Annex A1.6 M85

We certify that the above described cement, at the time of shipment, meets the chemical and physical requirements of ASTM C150/C150M-12 (Types I/II) and AASHTO M85-12 (Type I/II), or (other) _____ specification.

Signature:

Marc D. Melton

Title: Chief Chemist

ASH GROVE CEMENT COMPANY



1801 North Santa Fe
P.O. Box 519
Chanute, KS 66720
Phone: 620-433-3500
Fax: 620-431-3282

Type I/II (Low Alkali)

Production Period: December 1 thru December 31, 2016

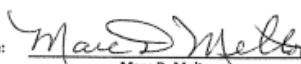
Date: 1/9/2017

The following information is based on average test data during the production period. The data is typical of cement shipped from the Chanute, Kansas plant. Individual shipments may vary.

Additional Data

Inorganic Processing Addition Data	
Type	Limestone
Amount(%)	4.49
SiO ₂ (%)	5.03
Al ₂ O ₃ (%)	1.47
Fe ₂ O ₃ (%)	1.2
CaO (%)	48.5
SO ₃ (%)	0.06

Base Cement Phase Composition	
C ₃ S	63
C ₂ S	14
C ₄ A	6
C ₄ AF	9

Signature: 
Marc D. Melton
Title: Chief Chemist

ASH GROVE CEMENT COMPANY



1801 North Santa Fe
P.O. Box 519
Chanute, KS 66720
Phone: 620-433-3500
Fax: 620-431-3282

LOT # 2673

Type I/II (Low Alkali)

Production Period: April 1 thru April 30, 2017

Date: 5/9/2017

The following information is based on average test data during the production period. The data is typical of cement shipped from the Chanute, Kansas plant. Individual shipments may vary.

STANDARD REQUIREMENTS ASTM C150/C150M-16, Tables 1 and 3

CHEMICAL				PHYSICAL			
Item	A.S.T.M. Test Method	Spec. Limit	Test Result	Item	A.S.T.M. Test Method	Spec. Limit	Test Result
SiO ₂ (%)	C114	A	20.76	Air content of mortar (volume %)	C185	12 max	6
Al ₂ O ₃ (%)	C114	6.0 max	3.77	Fineness (cm ² /g):			
Fe ₂ O ₃ (%)	C114	6.0 max	2.95	Air permeability	C204	2600 min	4064
CaO (%)	C114	A	63.89	Autoclave expansion (%)	C151	0.80 max	0.03
MgO (%)	C114	6.0 max	1.87	Compressive strength (psi)			
SO ₃ (%)	C114	3.0 max	2.92	1 Day	C109	A	2366
Loss on ignition (%)	C114	3.5 max	2.42	3 Days	C109	1740 min	3899
Na ₂ O (%)	C114	A	0.19	7 Days	C109	2760 min	4751
K ₂ O (%)	C114	A	0.49	Time of setting (minutes)			
Insoluble Residue (%)	C114	1.5 max	0.38	(Vicat)			
CO ₂ (%)	C114	A	1.80	Initial: Not less than	C191	45	122
Limestone (%)	C114	5.0 max	4.5	Not more than		375	122
CaCO ₃ in limestone (%)	C114	70 min	89.82	Mortar Bar Expansion	C1038	E, B	0.006
Potential compounds (%) ^D				Specific Gravity	C188	A	3.11
C ₃ S	C114	A	58				
C ₂ S	C114	A	16				
C ₃ A	C114	8.0 max	5				
C ₄ AF	C114	A	9				
C ₃ S + 4.75 C ₃ A	C114	100 max	82				

OPTIONAL REQUIREMENTS ASTM C150/C150M-16, Tables 2 and 4

CHEMICAL				PHYSICAL			
Item	A.S.T.M. Test Method	Spec. Limit	Test Result	Item	A.S.T.M. Test Method	Spec. Limit	Test Result
C ₃ S + C ₃ A (%)	C114	A		False set (%)	C451	B	88
Equivalent alkalies (%)	C114	0.60	0.51	Heat of hydration (kJ/kg)			
A = Not applicable.				7 days	C186	A	

B = Test result provided for information only.

C = Test results for this period not available.

D = Adjusted per Annex A1.6 M85

E = Required only if the SO₃ exceeds 3.0, in which case the expansion shall not exceed 0.020% at 14 days.

We certify that the above described cement, at the time of shipment, meets the chemical and physical requirements of ASTM C150/C150M-12 (Types I/II) and AASHTO M85-12 (Type I/II), or (other) _____ specification.

Signature: Marc D. Melton
Marc D. Melton
Title: Chief Chemist

ASH GROVE CEMENT COMPANY



1801 North Santa Fe
P.O. Box 519
Chanute, KS 66720
Phone: 620-433-3500
Fax: 620-431-3282

Type I/II (Low Alkali)

Production Period: April 1 thru April 30, 2017

Date: 5/9/2017

The following information is based on average test data during the production period. The data is typical of cement shipped from the Chanute, Kansas plant. Individual shipments may vary.

Additional Data

Inorganic Processing Addition Data

Type	Limestone
Amount(%)	4.55
SiO ₂ (%)	5.03
Al ₂ O ₃ (%)	1.47
Fe ₂ O ₃ (%)	1.2
CaO (%)	48.5
SO ₃ (%)	0.06

Base Cement Phase Composition

C ₂ S	60
C ₃ S	16
C ₃ A	5
C ₄ AF	9

Signature:

Marc D. Melton
Title: Chief Chemist

APPENDIX M – FLY ASH DATA SHEETS

Analytical Testing Service Laboratories, Inc.

P.O. Box 1118, Joplin, Missouri 64802
(417) 782-6573

Headwaters Resources
4319 S.National # 127
Springfield, MO 65810-2607
(417)882-0965

May 11, 2016

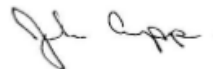
Attn: Kristy Rotramel

Re: 07685 - Jeffrey Fly Ash Sample - 2000 Ton Composite - Unit 1 3/ 19-29 /2016

	AASHTO-M295 Class "C" Requirements	ASTM C-618 Class "C" Requirements	Actual
Fineness (+325 Mesh)	34% Max	34% Max	10.30%
Moisture Content	3% Max	3% Max	0.08%
Density g/cm ³ C188	5% Max	****	2.72
Density Variation	5.0% Max	5.0% Max	1.18%
Loss on Ignition	5% Max	6% Max	0.67%
Soundness	0.8% Max	0.8% Max	0.08%
S.A.I., 7 Days	75% Min	75% Min	105.80%
S.A.I., 28 Days	75% Min	75% Min	111.70%
Water Req. % Control	105% Max	105% Max	94.20%
Silica SiO ₂	****	****	31.86%
Aluminum Oxide Al ₂ O ₃	****	****	20.44%
Ferric Oxide Fe ₂ O ₃	****	****	5.86%
Total	50% Min	50% Min	58.16%
Sulfur Trioxide SO ₃	5% Max	5% Max	2.96%
Calcium Oxide CaO	****	****	28.31%
Magnesium Oxide MgO	****	****	7.21%
Available Alkalies as Na ₂ O	1.50% Max	-----	1.36%

We certify the above was tested in accordance with ASTM C-618 and AASHTO M295.

Analytical Testing Service Laboratories, Inc.



John K. Cupp, Manager

Analytical Testing Service Laboratories, Inc.

P.O. Box 1118, Joplin, Missouri 64802

(417) 782-6573

Headwaters Resources
4319 S.National # 127
Springfield, MO 65810-2807
(417)-827-4413

December 28, 2016

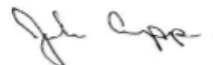
Attn: Kristy Rotramel

Re: 29189 - Jeffrey Fly Ash Sample - 2000 Ton Composite - Unit 3 - 10/27-11/2/2016

	AASHTO-M295 Class "C" <u>Requirements</u>	ASTM C-618 Class "C" <u>Requirements</u>	<u>Actual</u>
Fineness (+325 Mesh)	34% Max	34% Max	14.30%
Moisture Content	3% Max	3% Max	0.09%
Density g/cm ³ C188	5% Max	****	2.89
Density Variation	5.0% Max	5.0% Max	0.30%
Loss on Ignition	5% Max	6% Max	0.80%
Soundness	0.8% Max	0.8% Max	0.06%
S.A.I., 7 Days	75% Min	75% Min	102.80%
S.A.I., 28 Days	75% Min	75% Min	108.60%
Water Req. % Control	105% Max	105% Max	94.20%
Silica SiO ₂	****	****	31.62%
Aluminum Oxide Al ₂ O ₃	****	****	20.79%
Ferric Oxide Fe ₂ O ₃	****	****	5.01%
Total	50% Min	50% Min	57.42%
Sulfur Trioxide SO ₃	5% Max	5% Max	2.66%
Calcium Oxide CaO	****	****	27.89%
Magnesium Oxide MgO	****	****	6.63%
Available Alkalies as Na ₂ O	1.50% Max	-----	1.55%

We certify the above was tested in accordance with ASTM C-618 and AASHTO M295.

Analytical Testing Service Laboratories, Inc.



John K. Cupp, Manager

Analytical Testing Service Laboratories, Inc.
P.O. Box 1118, Joplin, Missouri 64802
(417) 782-6573

Headwaters Resources
P.O. Box 24
St. Mary's, KS 66536
(913)-317-1419

July 14, 2017

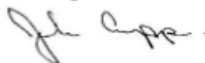
Attn: Ben Franklin

Re: 29779 - Jeffrey Fly Ash Sample - 2000 Ton Composite - Unit 2 - 5/26-6/1/2017

	AASHTO-M295 Class "C" Requirements	ASTM C-618 Class "C" Requirements	Actual
Fineness (+325 Mesh)	34% Max	34% Max	12.00%
Moisture Content	3% Max	3% Max	0.04%
Density g/cm ³ C188	5% Max	****	2.73
Density Variation	5.0% Max	5.0% Max	0.18%
Loss on Ignition	5% Max	6% Max	1.06%
Soundness	0.8% Max	0.8% Max	0.10%
S.A.I., 7 Days	75% Min	75% Min	105.80%
S.A.I., 28 Days	75% Min	75% Min	108.50%
Water Req. % Control	105% Max	105% Max	94.20%
Silica SiO ₂	****	****	32.51%
Aluminum Oxide Al ₂ O ₃	****	****	18.87%
Ferric Oxide Fe ₂ O ₃	****	****	5.58%
Total	50% Min	50% Min	56.96%
Sulfur Trioxide SO ₃	5% Max	5% Max	2.38%
Calcium Oxide CaO	****	****	28.40%
Magnesium Oxide MgO	****	****	8.04%
Available Alkalies as Na ₂ O	1.50% Max	-----	1.33%

We certify the above was tested in accordance with ASTM C-618 and AASHTO M295.

Analytical Testing Service Laboratories, Inc.



John K. Cupp, Manager

APPENDIX N – KOMPONENT® DATA SHEETS

KOMPONENT

Shrinkage-Compensating Additive



KOMPONENT

PRODUCT DATASHEET

DESCRIPTION: KOMPONENT® is an expansive CSA cement-based additive. Mix KOMPONENT with portland cement to produce ASTM C845 Type K Shrinkage-Compensating cement. In concrete mixtures, KOMPONENT compensates for the shrinkage associated with portland cement, improves resistance to sulfate attack, lowers permeability, and prevents slab curling and shrinkage cracking. KOMPONENT has a proven track record of improving concrete durability, providing long-term dimensional stability, saving construction time, and simplifying designs by minimizing or eliminating control joints, waterstops and pour strips.

USES: Use KOMPONENT to make Type K and System-K Shrinkage-Compensating concrete, low shrinkage concrete and non-shrink grouts. Shrinkage-compensating concrete is ideal for industrial slabs, concrete containment structures, post-tensioned and chemically prestressed structures, bridge decks, tilt-up and precast concrete, and any other applications where long-term durability, minimizing or eliminating control joints, and preventing slab curling and shrinkage cracking is desirable.

ENVIRONMENTAL ADVANTAGES: Use KOMPONENT to reduce the carbon footprint and lower environmental impact of a project. Production of KOMPONENT emits far less CO₂ than portland cement. Contact a CTS representative for LEED values and environmental information.

APPLICATION: Use KOMPONENT to replace approximately 15% of the portland cement material in your concrete mixture to make shrinkage-compensating concrete. Actual mix designs vary depending on application, local portland cement, supplementary cementitious materials, admixtures and concrete performance requirements.

Shrinkage-compensating concrete, low shrinkage concrete, and non-shrink grouts made with KOMPONENT are produced by conventional concrete production equipment and installation practices. Refer to CTS Cement's Shrinkage-Compensating Concrete Reference Guide for reinforcement, mixing, placement, finishing and curing considerations. Contact your CTS representative for project support.

BATCHING & MIXING: KOMPONENT is added at the central batch plant and can also be added on site using a CTS Cement approved slurry machine when portable silos or bagged units are used. Typical mix designs use 90 lbs to 100 lbs of Komponent to replace an equivalent weight of portland cement per cubic yard of concrete. Bulk Komponent should be weighed before the portland cement to ensure proper dosage. Bagged Komponent should be added to the mix using a CTS Cement approved slurry machine to ensure complete mixing. For System-K Fiber Reinforced mix designs, K-Fibers are added at a rate of one (1) unit per cubic yard. For batching and mixing instructions, refer to the CTS Shrinkage-Compensating Concrete Reference Guide for details.

WATER/CEMENT RATIO: Based on KOMPONENT's efficient consumption of mix water during hydration, the following water/cement ratios are recommended: Interior placements – 0.45; exterior placements – 0.50; dry shake applications – 0.55. Mix for 5 minutes (minimum) after all components have been added in the truck. Concrete production must comply with ASTM C94/94M except where otherwise stated in CTS Cement's published literature.

CURING: For general applications, seven (7) day wet curing is required. Refer to the CTS Shrinkage-Compensating Concrete Reference Guide for details.

PACKAGING & AVAILABILITY: KOMPONENT® is available in 90-lb (41-kg) polyethylene-lined bags and 2000-lb (909-kg) bulk bags. It is also available in bulk tanker trucks and railcars.

HIGHLIGHTS

Minimizes drying shrinkage cracking

Significantly reduces control joints

*30-40% increased
abrasion resistance*

*Increased durability &
lower permeability*

Improves resistance to sulfate attack

*Protects against
corrosion & deterioration*

Increase slab pour sizes

Prevents slab curling & spalling

CONFORMS TO: ACI 223

*Used to create Type K Cement (ASTM C845)
that is used in Type K and System-K
Shrinkage-Compensating Concrete*

MANUFACTURER:

CTS Cement Manufacturing Corp.
11065 Knott Ave., Suite A
Cypress, CA 90630
Phone: 800-929-3030
Fax: 714-379-8270
www.CTScement.com
info@CTScement.com



PRODUCT CATALOG

SHRINKAGE
COMPENSATING
CEMENT

1

KOMPONENT Shrinkage-Compensating Additive

SHELF LIFE: KOMPONENT has a shelf life of 6 months when stored properly in a dry location, protected from moisture, out of direct sunlight, and in an undamaged package.

USER RESPONSIBILITY: Before using CTS products, read current technical data sheets, bulletins, product labels and safety data sheets at www.CTScement.com. It is the user's responsibility to review instructions and warnings for any CTS products prior to use.

TECHNICAL SUPPORT: CTS Cement provides contractors, engineers, and project owners with professional technical services on any Komponent application. For detailed information on use and applications of Komponent, refer to the CTS Shrinkage Compensating Concrete Reference Guide.

WARNING: DO NOT BREATHE DUST. AVOID CONTACT WITH SKIN AND EYES. Use material in well-ventilated areas only. Exposure to cement dust may irritate eyes, nose, throat, and the upper respiratory system/lungs. Silica exposure by inhalation may result in the development of lung injuries and pulmonary diseases, including silicosis and lung cancer. Seek medical treatment if you experience difficulty breathing while using this product. The use of a NIOSH/MSHA-approved respirator (P-, N- or R-95) is recommended to minimize inhalation of cement dust. Eat and drink only in dust-free areas to avoid ingesting cement dust. Skin contact with dry material or wet mixtures may result in bodily injury ranging from moderate irritation and thickening/cracking of skin to severe skin damage from chemical burns. If irritation or burning occurs, seek medical treatment. Protect eyes with goggles or safety glasses with side shields. Cover skin with protective clothing. Use chemical resistant gloves and waterproof boots. In case of skin contact with cement dust, immediately wash off dust with soap and water to avoid skin damage. In case of skin contact with wet concrete, wash exposed skin areas with cold running water as soon as possible. In case of eye contact with cement dust, flush immediately and repeatedly with clean water and consult a physician. If wet concrete splashes into eyes, rinse eyes with clean water for at least 15 minutes and go to the hospital for further treatment.

PROPOSITION 65 WARNING: This product contains chemicals known to the State of California to cause cancer and birth defects or other reproductive harm.

Please refer to the SDS and www.CTScement.com for additional safety information regarding this material.

LIMITED WARRANTY: CTS CEMENT MANUFACTURING CORP. (CTS) warrants its materials to be of good quality and, at its option, will replace or refund the purchase price of any material proven to be defective within one (1) year from date of purchase. The above remedies shall be the limit of CTS's responsibility. Except for the foregoing, all warranties expressed or implied, including merchantability and fitness for a particular purpose, are excluded. CTS shall not be liable for any consequential, incidental, or special damages arising directly or indirectly from the use of the materials.

PHYSICAL DATA

Type K Shrinkage-Compensating Concrete, low shrinkage concrete, and non-shrink grout can be made using KOMPONENT mixed with local portland cement or on site using pre-blended Type K Cement.

Listed below are typical mix designs using Komponent. For mix designs using pre-blended Type K Cement, refer to the Type K Cement data sheet. For assistance developing project specific mix designs or very low permeability mixes, contact CTS Cement's Technical Service team.

All mixes should be tested in a lab for suitability for the required application.

TYPE K CONCRETE made with KOMPONENT

Portland Cement Type I/II	470 lb
Komponent	90 lb
Fine Aggregate, ASTM C33	1095 lb
Coarse Aggregate, ASTM C33	1800 lb
Water	37 gal
Water Reducer, ASTM C949	24 oz

PERFORMANCE

Slump	5.75 in
Expansion, 7 days	0.045 %
Compressive Strength, 7 days	3400 psi (23.4 MPa)
Compressive Strength, 28 days	4500 psi (31.0 MPa)
Specific Gravity, Komponent	2.87 g/cm ³

NON-SHRINK GROUT made with KOMPONENT

Portland Cement Type I/II	846 lb
Komponent	100 lb
Fine Aggregate ASTM C33	2640 lb
Water	52 gal
Water Reducer, ASTM C949	24 oz

PERFORMANCE

Expansion, 7 days	0.045 %
Compressive Strength, 7 days	4800 psi (33.1 MPa)
Compressive Strength, 28 days	7250 psi (49.6 MPa)
Specific Gravity, Komponent	2.87 g/cm ³



30% post consumer waste recycled fiber

USGBC and related logo is a trademark owned by the U.S. Green Building Council and is used by permission.

CTS Cement Manufacturing Corp. | 11065 Knott Ave., Suite A, Cypress, CA 90630, 800-929-3030 | www.CTScement.com

2

© 2018 CTS Cement Manufacturing Corp. CTS, KOMPONENT, and 201805

APPENDIX O – FIBER DATA SHEETS



We create chemistry

3	03 30 00	Cast-in-Place Concrete
	03 37 13	Shotcrete
	03 40 00	Precast Concrete
	03 70 00	Mass Concrete

MasterFiber® M 100

Monofilament Microsynthetic Fiber

Description

MasterFiber M 100 product is a high-tensile strength, high modulus of elasticity, ultra-thin monofilament homopolymer polypropylene fiber designed to quickly distribute uniformly throughout the concrete matrix. At the engineered dosage level of 0.50 lb/yd³ (0.3 kg/m³) MasterFiber M 100 product outperforms all other plastic shrinkage fiber reinforcements at their typical dosage of 1.0 lb/yd³ (0.6 kg/m³).

Applications

Recommended for use in:

- Residential slabs-on-ground
- Commercial slabs-on-ground
- Stucco
- Dry-packaged cement based products
- Precast products
- Pools and pool decks
- Water tanks
- Shotcrete

Features

- 225 million 0.75 in. (19 mm) fibers in one pound (0.45 kg) of product
- Uniform distribution throughout the concrete matrix
- Excellent finishability

Benefits

- Excellent reduction in plastic shrinkage cracking
- Transforms macro-cracks into micro-cracks
- Measurably reduces plastic settlement
- Measurably reduces the concrete permeability, thus increasing the durability and service life of the concrete
- Performs as an excellent companion in blends with macrosynthetic fibers and steel fibers

Performance Characteristics

Physical Properties

Specific Gravity	0.91
Melting Point	320 °F (160 °C)
Ignition Point	1,094 °F (590 °C)
Absorption	Nil
Alkali Resistance	Excellent
Tensile Strength	70 ksi (480 MPa)
Modulus of Elasticity	1,230 ksi (8.48 GPa)
Available Lengths	0.5 in. (13 mm) and 0.75 in. (19 mm)
Equivalent Diameter	0.00047 in. (12 microns)
Denier	1 dpf

MASTER®
»BUILDERS
SOLUTIONS

Guidelines for Use

Dosage: The recommended dosage of MasterFiber M 100 product is 0.50 lb/yc³ (0.3 kg/m³).

Mixing: Typically no modifications to the mixture proportions are required when the product is used at the engineered dosage of 0.50 lb/yc³ (0.3 kg/m³). MasterFiber M 100 product fibers can be introduced into the mixing system at any time except when the cement is being introduced. Mixing time will vary based on when the fibers are introduced to the mixer. The normal range is 3-5 minutes of mixing with the higher number preferred when the fibers are added after all of the standard ingredients have been introduced and mixed.

Engineering Specifications

MasterFiber M 100 product is a uniquely developed fiber to minimize plastic shrinkage cracking in concrete. With 112.5 million fibers in the engineered dosage of 0.50 lb/yc³ (0.3 kg/m³), MasterFiber M 100 product is capable of reducing plastic shrinkage cracking by approximately 85%. Conventional monofilament polypropylene fibers at 1.0 lb/yc³ (0.6 kg/m³) typically do not achieve 70% reduction in plastic shrinkage cracking.

MasterFiber M 100 product meets the requirements of ASTM C 1116/C 1116M, Section 4.1.3, Type III and Note 2 as well as ICC ES AC308, Section 3.1.1 when used at the engineered dosage of 0.50 lb/yc³ (0.3 kg/m³).

Product Notes

MasterFiber M 100 product is not a replacement for structural steel reinforcement and therefore, should not be used to replace any of the load-carrying steel reinforcement in a concrete element.

Packaging

MasterFiber M 100 product is packaged in pre-weighed 0.50 lb (0.23 kg) and 2.5 lb (1.13 kg) degradable bags to ensure optimum dosing and homogeneous distribution of the product.

Related Documents

Safety Data Sheets: MasterFiber M 100 product

Additional Information

For additional information on MasterFiber M 100 product, contact your local sales representative.

The Admixture Systems business of BASF's Construction Chemicals division is the leading provider of solutions that improve placement, pumping, finishing, appearance and performance characteristics of specialty concrete used in the ready-mixed, precast, manufactured concrete products, underground construction and paving markets. For over 100 years we have offered reliable products and innovative technologies, and through the Master Builders Solutions brand, we are connected globally with experts from many fields to provide sustainable solutions for the construction industry.

Limited Warranty Notice

BASF warrants this product to be free from manufacturing defects and to meet the technical properties on the current Technical Data Guide, if used as directed within shelf life. Satisfactory results depend not only on quality products but also upon many factors beyond our control. BASF MAKES NO OTHER WARRANTY OR GUARANTEE, EXPRESS OR IMPLIED, INCLUDING WARRANTIES OF MERCHANTABILITY OR FITNESS FOR A PARTICULAR PURPOSE WITH RESPECT TO ITS PRODUCTS. The sole and exclusive remedy of Purchaser for any claim concerning this product, including but not limited to, claims alleging breach of warranty, negligence, strict liability or otherwise, is shipment to purchaser of product equal to the amount of product that fails to meet this warranty or refund of the original purchase price of product that fails to meet this warranty, at the sole option of BASF. Any claims concerning this product must be received in writing within one (1) year from the date of shipment and any claims not presented within that period are waived by Purchaser. BASF WILL NOT BE RESPONSIBLE FOR ANY SPECIAL, INCIDENTAL, CONSEQUENTIAL (INCLUDING LOST PROFITS) OR PUNITIVE DAMAGES OF ANY KIND.

Purchaser must determine the suitability of the products for the intended use and assumes all risks and liabilities in connection therewith. This information and all further technical advice are based on BASF's present knowledge and experience. However, BASF assumes no liability for providing such information and advice including the extent to which such information and advice may relate to existing third party intellectual property rights, especially patent rights, nor shall any legal relationship be created by or arise from the provision of such information and advice. BASF reserves the right to make any changes according to technological progress or further developments. The Purchaser of the Product(s) must test the product(s) for suitability for the intended application and purpose before proceeding with a full application of the product(s). Performance of the product described herein should be verified by testing and carried out by qualified experts.

© BASF Corporation 2015 ■ 01/15 ■ OTH-DAT-0423

BASF Corporation
Admixture Systems
www.master-builders-solutions.basf.us

United States
23700 Chagrin Boulevard
Cleveland, Ohio 44122-5544
Tel: 800 629-9990 ■ Fax: 216 839-8821

Canada
1800 Clark Boulevard
Brampton, Ontario L6T 4M7
Tel: 800 387-5882 ■ Fax: 905 792-0651

page 3 of 3

MasterFiber® MAC Matrix

Macrosynthetic Fiber

Description

MasterFiber MAC Matrix product is a macrosynthetic fiber that is manufactured from a proprietary blend of polypropylene resins, and meets the requirements of ASTM C 1116/C 1116M "Standard Specification for Fiber-Reinforced Concrete."

MasterFiber MAC Matrix product also meets the requirements of CSA B66-10 "Design, material, and manufacturing requirements for prefabricated septic tanks and sewage holding tanks."

Applications

Recommended for use in:

- Shotcrete
- Composite metal decks
- Industrial and warehouse floors
- Pavements
- Precast concrete
- Residential and commercial slabs-on-ground
- Precast concrete pipes
- Thin-wall precast
- Tunnel linings
- Wall systems
- Whitetopping/overlays

Features

MasterFiber MAC Matrix product is engineered for use as secondary reinforcement to control shrinkage and temperature cracking, and settlement cracking.

MasterFiber MAC Matrix product was created specifically to replace welded-wire reinforcement and No. 3 and No. 4 (10 mm and 13 mm) reinforcing bars that are typically used as temperature and shrinkage reinforcement.

MasterFiber MAC Matrix product has the following features:

- Excellent flexural performance
- Excellent finishability

Benefits

- Eliminates the need for welded-wire reinforcement (WWR) and small diameter bars used as secondary reinforcement, depending on the application
- Effective tight crack control
- Provides excellent control of settlement cracking
- Improves green strengths and permits earlier stripping of forms with less rejection
- Reduces construction time and overall labor and material costs
- Reduces the effects of handling and transportation stresses
- Increases flexural toughness, impact and shatter resistance

Performance Characteristics

Physical Properties

Specific Gravity	0.91
Melting Point	320 °F (160 °C)
Ignition Point	1094 °F (590 °C)
Absorption	Nil
Alkali Resistance	Excellent
Tensile Strength	85 ksi (585 MPa)
Nominal Length	2.1 in. (54 mm)
Nominal Aspect Ratio	70
Fiber Type	Embossed
Material	100% virgin polypropylene
Chemical Resistance	Excellent

Guidelines for Use

Dosage: The dosage range of MasterFiber MAC Matrix product is 3 to 12 lb/yd³ (1.8 to 7.2 kg/m³). The recommended dosage range for slab-on-ground applications is typically 3 to 5 lb/yd³ (1.8 to 3 kg/m³). For shotcrete, the typical dosage range of MasterFiber MAC Matrix product is 8 to 12 lb/yd³ (4.8 to 7.2 kg/m³).

Mixing: MasterFiber MAC Matrix product should be introduced at the beginning of the mixing cycle, but not at the same time as the cement. For slab-on-ground applications, the entire bag should be dispensed into the mixer to allow for easy handling, while leaving no waste on site. For shotcrete, the bag should be opened so that the fibers can be dispensed directly into the mixer. Three to five minutes of additional mixing will be required to disperse the fibers depending on when the product is added to the mixer. BASF recommends utilizing good concrete mixing practices as outlined in ASTM C 1116/C 1116M.

Engineering Specifications

MasterFiber MAC Matrix product is an option for the replacement of WWR and is an easy-to-use secondary reinforcing system that is rust proof, alkali resistant, and compliant with industry codes when mixed in accordance with ASTM C 1116/C 1116M. MasterFiber MAC Matrix product enhances safety and should be specified for use in applications for:

- Increased flexural toughness
- Reduced rebound
- Increased cohesion
- Increased impact and shatter resistance
- Extended pump life
- Replacement of WWR and other secondary reinforcement
- Improved residual strength
- Improved durability
- Use in areas requiring no metal

MasterFiber MAC Matrix product also conforms to the requirements of CSA B66-10 "Design, material, and manufacturing requirements for prefabricated septic tanks and sewage holding tanks".

Product Notes

Testing has shown that MasterFiber MAC Matrix product can be used as a partial or full replacement for primary/structural steel reinforcement in concrete pipe. The dosage of MasterFiber MAC Matrix product to meet a specified performance level in concrete pipe should be determined in accordance with industry standard procedures. In other applications, MasterFiber MAC Matrix product may also be used as a partial or full replacement for primary/structural steel reinforcement. To explore the use of MasterFiber MAC Matrix product for such purpose, contact the Engineering Department at BASF Corporation in Beachwood, OH.

Placement and Finishing: BASF recommends that the standard practices detailed in ACI 302.1R, ACI 506.1R and ACI 544.3R for placing, finishing and curing concrete be followed when using MasterFiber MAC Matrix product.

Storage and Handling

MasterFiber MAC Matrix product should be stored in a clean, dry area protected from the weather and at temperatures below 140 °F (60 °C). Avoid storing near strong oxidizers and avoid sources of ignition. Use caution when stacking to avoid unstable conditions. Store in a sprinkled warehouse.

Packaging

MasterFiber MAC Matrix product is packaged in a 5 lb (2.3 kg) degradable bag that can be added directly to the mixing system. For shotcrete, the fibers are packaged in 11 lb (5 kg) and 15.4 lb (7 kg) bags which should be opened prior to dispensing the fibers into the mixer.

Related Documents

Safety Data Sheets: MasterFiber MAC Matrix

Additional Information

For additional information on MasterFiber MAC Matrix product, contact your local sales representative

The Admixture Systems business of BASF's Construction Chemicals division is the leading provider of solutions that improve placement, pumping, finishing, appearance and performance characteristics of specialty concrete used in the ready-mixed, precast, manufactured concrete products, underground construction and paving markets. For over 100 years we have offered reliable products and innovative technologies, and through the Master Builders Solutions brand, we are connected globally with experts from many fields to provide sustainable solutions for the construction industry.

Limited Warranty Notice

BASF warrants this product to be free from manufacturing defects and to meet the technical properties on the current Technical Data Guide, if used as directed within shelf life. Satisfactory results depend not only on quality products but also upon many factors beyond our control. BASF MAKES NO OTHER WARRANTY OR GUARANTEE, EXPRESS OR IMPLIED, INCLUDING WARRANTIES OF MERCHANTABILITY OR FITNESS FOR A PARTICULAR PURPOSE WITH RESPECT TO ITS PRODUCTS. The sole and exclusive remedy of Purchaser for any claim concerning this product, including but not limited to, claims alleging breach of warranty, negligence, strict liability or otherwise, is shipment to purchaser of product equal to the amount of product that fails to meet this warranty or refund of the original purchase price of product that fails to meet this warranty, at the sole option of BASF. Any claims concerning this product must be received in writing within one (1) year from the date of shipment and any claims not presented within that period are waived by Purchaser. BASF WILL NOT BE RESPONSIBLE FOR ANY SPECIAL, INCIDENTAL, CONSEQUENTIAL (INCLUDING LOST PROFITS) OR PUNITIVE DAMAGES OF ANY KIND.

Purchaser must determine the suitability of the products for the intended use and assumes all risks and liabilities in connection therewith. This information and all further technical advice are based on BASF's present knowledge and experience. However, BASF assumes no liability for providing such information and advice including the extent to which such information and advice may relate to existing third party intellectual property rights, especially patent rights, nor shall any legal relationship be created by or arise from the provision of such information and advice. BASF reserves the right to make any changes according to technological progress or further developments. The Purchaser of the Product(s) must test the product(s) for suitability for the intended application and purpose before proceeding with a full application of the product(s). Performance of the product described herein should be verified by testing and carried out by qualified experts.



MasterFiber MAC Matrix fiber, as marketed by BASF Corporation, is classified by Underwriters Laboratories Inc. for use in the following fire rated assemblies: UL D700, D800 and D900 Series Designs. Fibers to be added to the concrete mix at a maximum rate of 5.0 lb of fiber for each cubic yard (3.0 kg/m³) of concrete.

© BASF Corporation 2016 ■ 10/16 ■ QTH-DAT-0715

BASF Corporation
Admixture Systems
www.master-builders-solutions.basf.us

United States
23700 Chagrin Boulevard
Cleveland, Ohio 44122-5544
Tel: 800 628-9990 ■ Fax: 216 839-8821

Canada
1800 Clark Boulevard
Brampton, Ontario L6T 4M7
Tel: 800 387-5862 ■ Fax: 905 792-0651

page 3 of 3